Tessa Spano

School of Geography and Planning

University of Sheffield

Tracing the Movement of Sediment Using Multiple Elevated Temperature Infrared Stimulated Luminescence

PhD Thesis

Submitted in accordance with the requirements for the degree of Doctor of Philosophy

February 2025

University of Sheffield

Abstract

The transport of sediment across the Earth shapes both the human and physical world. Sediment transport is both a driver of and responder to landscape evolution over geological time scales, inextricably linked to climate processes and tectonic activity. It is a regulator of biogeochemical cycling, water quality and supply, soil quality and ecosystem health. A quantitative understanding of sediment transport processes is a key to sustainable development, yet current methods for doing so are highly inefficient and often lack the spatial-temporal resolution to account for localised effects. This thesis develops single grain feldspar multiple elevated temperature infrared stimulated luminescence (MET-IRSL) as a tool to address some of these challenges to quantifying the movement of sediment in river systems. It is demonstrated that single grain MET-IRSL is both highly efficient and able to determine localised variability of sediment transport rates and pathways.

This thesis first investigates the process of luminescence signal reduction, known as bleaching, to determine an ideal function with which to model bleaching for grains in a fluvial sediment transport scenario. Optimal methods for measuring MET-IRSL signal and analysing output are developed and tailored to extract transport information. These techniques are applied to three fluvial systems including the Solimões River, the name given to the main strand of the Amazon system. A burial-bleach model is constructed to apply to downstream datasets of MET-IRSL combined signals. Using this model, it is demonstrated that the application of single grain MET-IRSL can produce credible storage times and transport rates for sediments in fluvial systems. Furthermore, this model is adapted to reconstruct the histories of individual grains using parameters derived directly from MET-IRSL measurement. It is shown that single grains can independently contribute bleaching and storage histories to a transport rate that is coherent with the information provided by the combined MET-IRSL signals.

Acknowledgments

I would first like to thank my supervisor Ed Rhodes for his continual support, limitless ideas and enthusiasm, and for always having confidence in me. I will never forget which way to turn the quartz window.

I would also like to thank my second supervisor Jeremy Ely for his encouragement, feedback, and making sure I finished on time.

Thank you to all the people in the department who made the past three years so enjoyable: Helen, Ben, Sammia, Frances, Cari, Jane, Sarah, Darrel, and everyone on the Spain trip team.

To Jess and Liz for their love and positive energy right from the start.

Thank you to my family and friends for their unwavering support.

Thank you to Rosie, for being there through the best and the worst of it.

Thank you to my wife Sarah, for keeping me laughing through the difficult times, for being strong for both of us, and for always believing in me when I didn’t.

Contents

1.0. Chapter 1 Introduction

This chapter first provides a brief overview of the physical basis of luminescence, the broad term for the technique, most commonly used for dating sediments, that this thesis applies and develops to elucidate information on fluvial sediment transport (Section 1.1). The following section discusses the process known as 'bleaching', which is the reduction of luminescence during exposure to light, and its significance for sediment transport applications of luminescence (Section 1.2). The existing literature on using luminescence for sediment transport, specifically luminescence-based sediment transport models is reviewed (Section 1.3). The importance of accurate sediment transport determination and modelling is outlined and briefly discussed to illustrate the wider significance of this work (Section 1.4). The theoretical approach to using multiple-elevated temperature infrared stimulated luminescence (MET-IRSL) to determine sediment transport rates that underpins the work in this thesis is presented (Section 1.5). Finally, this chapter presents the specific aim and objectives of this thesis (Section 1.6).

1.1. The physical basis of luminescence

Luminescence is a phenomenon observed in many minerals including quartz and feldspar. Luminescence signals arise when grains are buried and subject to ionising radiation produced by the decay of common radioactive isotopes within the Earth's crust. Interaction with ionising radiation excites electrons within the crystal, causing a transfer of charge from the valence band to an excited state (Figure 1.1). Following this, some electrons become trapped in states between the valence band and the conduction band which occur at the sites of lattice defects (Rhodes, 2011).

Trapped charge accumulates over time, either until the material is saturated whereby additional trapped charge can no longer accumulate, or it is subject to light or heat, which provides sufficient energy for trapped electrons to become mobile, escape, and transfer to a lower energy level. In the case of stimulation by light, as it escapes, a trapped electron loses its energy through changing state, resulting in photon emission with energy equal or lower to that of the state of the trap. The emission of this photon gives rise to the property termed luminescence. Luminescence techniques are highly sophisticated for the dating of sediments in a wide range of geomorphic and archaeological contexts (e.g. Aitken, 1985; Armitage *et al.* 2019; Bateman *et al.* 2021; Duller, 1995; Huntley *et al.* 1985; Murray and Roberts, 1997; Preusser *et al*. 2008; Rhodes, 2011; Stone *et al.* 2015). The idea behind the use of luminescence as a tool to determine sediment transport dynamics, is that that as grains are transported, this produces a pattern of signal growth and decay (Gray, 2018). This thesis aims to demonstrate that it is the intricacies of this pattern that MET-IRSL specifically has the potential to unlock.

The size of the trapped charge population, that gives rise to a luminescence signal, is proportional to burial time, and the rate at which trapped charge accumulates is proportional to the concentration of radioactive isotopes present in the mineral and its sedimentary environment. Growth of luminescence signal during the burial period is described by the following exponential function (Murray & Wintle 2003):

$$L = I_{max}\left[1 - exp\left(\frac{-t}{D_0}\right)\right] \quad (1.1)$$

where L is intensity of the luminescence signal, t is time, I_{max} is the intensity of the signal at saturation when $t = \infty$, and D_0 is the characteristic saturation dose. The value of D_0 is characteristic of individual aliquots or grains and is subsequently referred to as 'characteristic saturation dose'. The typical form of exponential growth in luminescence signal is shown in Figure 1.1.

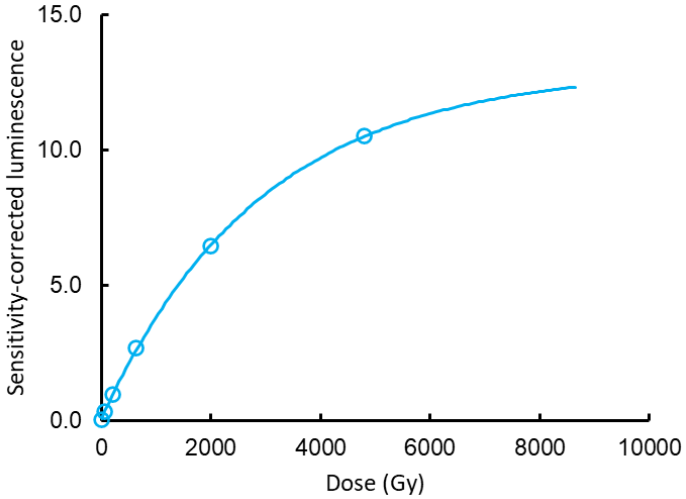

Figure 1.1. *The typical form of exponential growth in luminescence signal with increased dose (Gy).*

Reduction of luminescence signal, a process known as bleaching, is described by the following general order of kinetics equation (Bailiff & Barnet, 1994):

$$I = \frac{I_0}{(1 + at)^b} \quad (1.2)$$

where t is time (s), I_0 is intensity when $t = 0$, I is luminescence intensity as a fraction of I_0, a is a bleachability parameter, which Poolton *et al.,* (2009) state includes information on the initial population of trapped electrons; intensity of excitation source, capture cross-section, which can be thought of as the area of a trap and is used as a measure of how likely it is that a given defect will capture an incident electron (Schroder, 1998), whilst b contains information on the order of the kinetic reaction (Poolton *et al.,* 2009). For clarity, first-order ($b = 1$) would be where the rate of bleaching is

proportional to the concentration of a just single reactant, which in this case is a trapped electron population. The typical form of feldspar IRSL decay is shown in Figure 1.4 in in Section 1.4.

Several variations of the bleaching function applied to simulate the decay of luminescence signals in fluvial systems can be found in the literature (e.g. Gray *et al.,* 2018, Guyez *et al.,* 2023, McGuire & Rhodes 2015a). The various functions have rather different forms, which may impact the use of existing luminescence-based sediment transport models in certain fluvial systems, and potential transport rates derived from luminescence measurements. The significance of accurate reproduction of luminescence signal decay to determining sediment transfer times is discussed further in Section 1.2.1).

1.2. The importance of feldspar IRSL bleaching

1.2.1. What is bleaching?

In luminescence, bleaching is the term given to the reduction of the trapped charge population by light exposure within a crystal (Aitken & Valladas, 1992). Electrons that have been trapped following excitation caused by ionising radiation, are stimulated by a different form of energy such as light. The energised electrons then try to transfer this energy, and in some cases do this by emission of a photon, returning to their ground state. After sufficient exposure to light, a considerable proportion of electron traps are vacated, and the signal is considered reset, or zeroed. However, electrons must travel to specific places to emit their photons, which are called luminescence centres. In feldspars, the distance between a trapped electron and a luminescence centre, and the energy possessed by the electron, can influence the probability of recombination (Huntley, 2006, Huntley & Lamothe, 2001).

There are several 'pathways' an electron can take to travel to a luminescence centre, which require different energies to achieve. In high to low energy order, the possible pathways are as follows: 1) by moving up to the high mobility conduction band where electrons can move around the lattice until they find a luminescence centre, 2) by not quite making it to the conduction band but reaching the slightly lower energy, localised band-tail states just below the conduction band, 3) via multi-step hopping mechanisms from one site to another, 4) by quantum tunnelling, often simply termed 'tunnelling' across energy barriers between different energy levels (Poolton *et al.,* 2002a, b). Poolton *et al.,* (2002a, b) suggest that tunnelling and conduction band tail states are the dominant routes taken by charge that produces IRSL from feldspars. Further, Poolton *et al*., (2009) argue the existence of band tail states ~0.4 eV below the conduction band in feldspars based on low temperature measurements. These data explain the characteristic spectrum at which feldspar luminescence is observed. However, feldspar IRSL measurements are typically made above room temperature, mechanisms of transport and partitioning of charge during blue, green and infrared stimulated feldspar luminescence is successfully modelled by Jain & Ankjærgaard (2011) based on measurements made at 50°C. Jain & Ankjærgaard (2011) conclude that there are two components to the recombination process: a fast component that characterised by excited-state or conduction band transport, and a slow component by band tail transport, during which there is thermal competition between tunnelling from deeper band tail states and the more efficient sub-conduction band tails.

1.2.2. Why is bleaching important?

Understanding the bleaching process is imperative for the development of effective IRSL-based sediment tracing tools. More specifically, to quantify how factors such as dose history, light exposure history, light source wavelength, thermal history, and mineral composition influence feldspar IRSL

decay form and rate will enable improved definition of bleaching parameter space for application of sediment transport models in various fluvial settings. This will enable accurate sediment transport history reconstructions and enhance forecasting potential.

Bleaching in feldspars began to receive significant research attention in the 1980s (e.g. Hüt *et al.,* 1988, Godfrey-Smith et al. 1988) initially due the susceptibility of the IRSL signal to fall victim to anomalous fading. Anomalous fading is the term used to describe the movement of electrons out of thermally stable traps during storage and irradiation to less thermally stable states (Spooner, 1994). In other words, the loss of charge from thermally stable locations that would have contributed to a signal measured in laboratory conditions to locations where it is more likely to recombine with luminescence centres. As a result, without correction, fading of IRSL signals causes age underestimation. The term 'anomalous' is the result of inconsistency with estimated rate of charge loss, based on thermoluminescence studies (Wintle, 1973). Methods to correct for anomalous fading exist and are used as standard procedure for dating feldspars by some protocols (e.g. Huntley & Lamothe, 2001; Auclair *et al*., 2003; Lamothe *et al*., 2003). However, causes of anomalous fading are not well understood.

Thomsen *et al.,* (2011) demonstrated successful reduction of laboratory fading rates by measuring IRSL at an elevated temperature, such as 225°C, after regular IRSL measurement at 50°C. This led to the development of post-IRIR measurement, pioneered by Buylaert *et al.,* (2009), to circumvent some of challenges for IRSL dating that arise due to anomalous fading. Today, many variations of the original Risø-Aarhus post-IRIR protocol and the newer MET-IRSL protocol exist (e.g. Buylaert *et al.,* 2009; Thomsen *et al.,* 2011; Li & Li, 2011, Rhodes, 2015; Fu *et al.*, 2012), with the common goal of isolating an IRSL signal that is less prone to fading thus, optimising feldspar IRSL age estimation. Each post-IRIR and MET-IRSL protocol aims to remove charge from traps that are close to luminescence centres, and therefore considered likely to fade, by simulation at a low temperature, typically 50°C. Taking advantage of the kinetics of feldspar IRSL, the elevated temperature IRSL then stimulates charge in traps that are considered to have remained stable throughout the sample's time in situ.

Post-IRIR and MET-IRSL protocols present a new challenge: higher temperature signals are not so easily reset by light exposure (Buylaert *et al.,* 2012; Murray *et al.,* 2012). This poses as significant challenge for dating sediments in glacial, glacio-fluvial, fluvial, and some marine settings, where sunlight is limited. Effective resetting of a sample in nature is an essential assumption to meet. Issues of partial bleaching can lead to age overestimation (Kars *et al.,* 2014). Robust constraints on the rate at which charge is removed from traps during optical stimulation for IRSL, post-IRIR IRSL, and MET-IRSL are necessary to resolve the trade-off between age overestimation due to partial bleaching, and

age underestimation due to anomalous fading. With this, it is possible to unlock the full potential of feldspar luminescence, to optimise dating procedures, and expand the remit of IRSL as a tool to monitor geophysical processes beyond dating.

Significant research attention has been directed towards anomalous fading of the feldspar IRSL signal. Thus, this study focuses on the determination of different bleaching rates and behaviours. The differential bleaching rates of MET-IRSL signals will be utilised to provide new information on the past and present state of fluvial systems and sediment transport dynamics. The more signals we measure, and bleaching rates we observe, the more accurately we can reconstruct target geomorphic processes and the more predictive power our numerical models will possess. But first, the nature of MET-IRSL bleaching must be properly defined with relevance to the conditions and treatment grains will experience in fluvial transport and storge.

1.3. Luminescence and sediment transport

Many studies have applied luminescence techniques to fluvial sediments. The earliest can be categorised as simple measurements of signal reduction as a function of distance downstream: Gemmel (1985) and Gemmel (1999) document reduction of feldspar TL in a laboratory setting, and feldspar IRSL in the Dora di Ferret in Val d'Aosta in the Italian Alps; Rhodes & Bailey (1997) applied quartz OSL to glaciofluvial sediments in northern Greenland; Stokes *et al.,* (2001) report the reduction of quartz OSL signal for a suite of samples taken over 900 km of the Loire in France.

McGuire & Rhodes (2015a) applied luminescence to extract information on sediment transport using multiple grain MET-IRSL to determine a transit time of 200-800 years over a 65 km reach of the Mojave River, California, USA. They present a simple model using an adaptation of the Eq. 1.2 of Bailiff & Barnett (1994) to simulate the downstream evolution of MET-IRSL signals in the Mojave River.:

$$I = \frac{I_0}{(1+at)^b} + C \tag{1.3}$$

where the additional parameter *C*, represents an unbleachable residual signal. McGuire & Rhodes (2015a) present successful application of Eq. 1.3 to simulate MET-IRSL decay in sunlight conditions at all five measurement temperatures (Figure 1.2) however, they observe significant departure of the model from the data when this function was applied to the fluvial dataset from the Mojave River (Figure 1.3), suggesting Eq. 1.3 may not fully capture the nature of bleaching for grains in fluvial sediment transport.

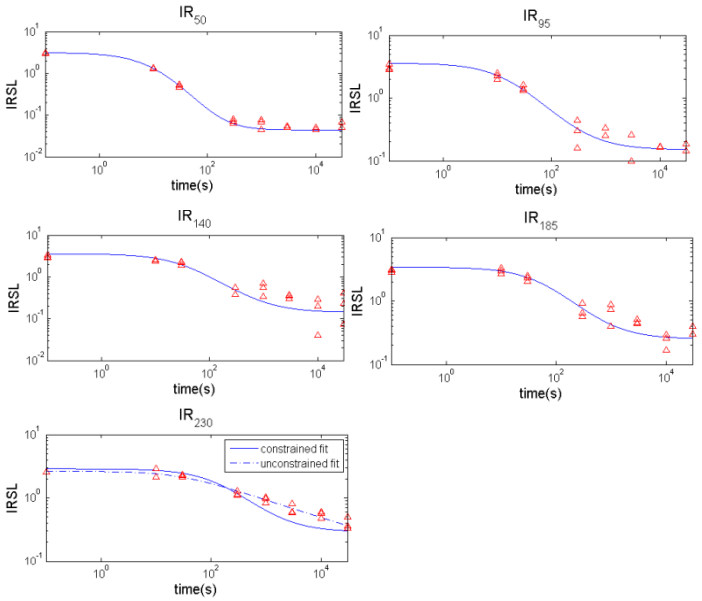

Figure 1.2. *Sunlight bleaching measurements of five MET-IRSL signals fitted with Eq. 1.3 (McGuire & Rhodes, 2015a).*

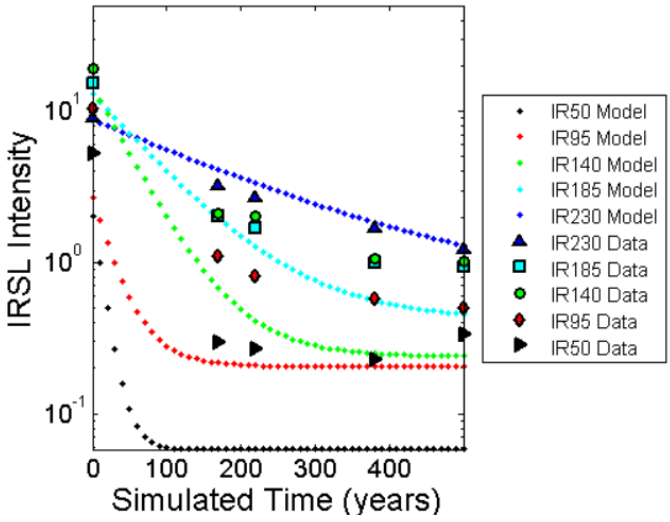

***Figure 1.3**. MET-IRSL signals of samples collected from the active channel of the Mojave River by McGuire & Rhodes (2015a) with their model fitted to the data.*

Gray *et al*., (2017) built on the work of McGuire & Rhodes (2015a; 2015b) to produce a sophisticated sediment transport model based on conservation principles that successfully reproduces the results of McGuire & Rhodes (2015a) and of Stokes *et al.,* (2001). Gray *et al*., (2018) combine field measurements, using a dual signal IRSL approach, with application of the model of Gray *et al*., (2017) to the South River and Difficult Run, Virginia, and Linganore Creek, Maryland, USA. These are more complex fluvial systems where sediment transport lengthscale, virtual velocity and exchange rate are independently known. The model of Gray *et al*., (2017) provides a good fit to field data and independent sediment transport parameters for the South River, but model predictions were not consistent with field data at the other two locations. It is suggested that the steady-state assumptions of the model are violated by the sensitivity of in-channel luminescence to changing landscape dynamics, particularly land use change and subsequent variations in relative source contributions to in-channel sediment flux (Gray *et al.,* 2018).

Rhodes & Leathard (2022) define a new parameter derived from MET-IRSL measurement, using a five-temperature protocol adapted from McGuire & Rhodes (2015a), the 'burial-bleach ratio'. This represents the gradient of a linear fit to the apparent age estimates of each measurement temperature, over 'characteristic bleach time'. The term characteristic bleach time describes a reference time that is typical of a given measurement temperature to bleach to 50%. For example, it could take 24s for the IR_{50} signal to get to 50% of its unbleached signal, whilst the IR_{95} signal may take 90s, and the IR_{140} signal may take 2700s, and so on. It is possible to determine characteristic bleach time for each grain individually, using the bleaching response curve protocol and fitting procedure described in Section 3.3.1, Chapter 3. The burial-bleach ratio can be visualised in Figure 1.4, taken from Rhodes & Leathard (2022).

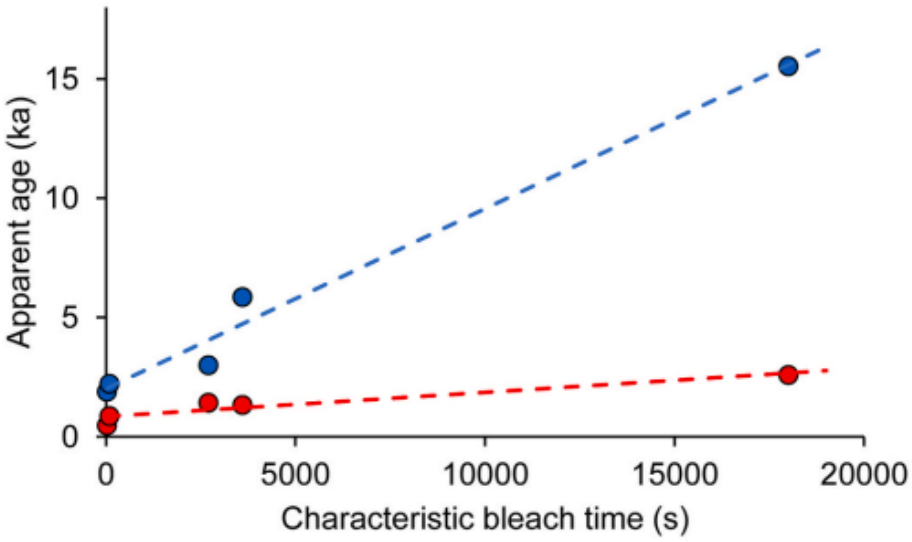

Figure 1.4. *From Rhodes & Leathard (2022). Apparent age of five MET-IRSL signals plotted against their characteristic bleach time for two different samples. Characteristic bleach time is defined as a reference time that is typical of a given measurement temperature to bleach to 50%. The slope of linear fit to these points is the burial-bleach ratio.*

This is a potentially powerful parameter for sediment transport determination that contains information on the extent of past light exposure, relative to time spent in storage. Rhodes & Leathard (2022) demonstrate the similarities between the distributions of burial-bleach ratios and particle size analysis (PSA) data for nine samples. PSA is routinely used for understanding sediment transport dynamics and the depositional environment of sediment, with high frequency of coarse grain sizes representing higher energy transport (Sun *et al.*, 2002). The work of Rhodes & Leathard (2022) provides convincing evidence for a relationship between the availability of coarse grains, and degree of sorting, and higher, or steeper burial-bleach ratios. This indicates the burial-bleach ratio has strong potential to provide information on sediment transport conditions, with steeper burial-bleach ratios reflecting high energy conditions under which coarser material will be transported. This thesis will further explore the use and explanatory power of this parameter for determining sediment transport dynamics for the Allt Dubhaig.

Guyez *et al.*, (2023) use single grain post-IR IRSL ($pIRIR_{50}$ and $pIRIR_{175}$) field measurements from two braided rivers in New Zealand combined with a numerical model to derive virtual velocities and storage times. The model simulates the downstream evolution of the relative proportions of three subgroups of single grain luminescence response. Grains are considered to be either: 1) saturated, 2) partially bleached, 3) bleached. Under partial bleaching conditions, model simulations are able to successfully reproduce the downstream evolution of the three subgroups of luminescence responses in proportions very close to those observed in the field and produce credible virtual velocities and storage times. This work demonstrates that single grain measurements can contribute to an average sediment

transport rate. However, this model does not take account of the variability in bleaching and growth characteristics between grains or samples.

1.4. The importance of accurate determination and modelling of fluvial sediment transport

The rate at which the Earth System transfers sediment from source to sink, and back again, is an indicator of biogeochemical cycling (Respach *et al.,*2021), water quality and supply (Pizzuto *et al.,* 2014), land degradation (Guzman *et al.,* 2013), and ecosystem health. It determines where, when, how much, and the quality of, soil from which we can grow food (Burbank & Anderson 2009, Pizzuto *et al.,* 2014; Wynannts *et al.,* 2021). It is also a primary driver of landscape development: how fast mountains are rising or falling, how our coastlines are changing, where our deserts are expanding and is highlight responsive to tectonic activity (Anderson & Anderson 2010). Fluvial sediment transport specifically is inextricably linked to the carbon capture, transport, export and storage (Hilton & West, 2020), and also the transmission of waterborne diseases (Abia *et al.*, 2017; Craig *et al.*, 2004; Davies *et al.*, 1995; Gardade & Khandeparker, 2007; Perkins *et al.*, 2014).

Yet, current methods for measuring transport rates over long time scales are time consuming and highly inefficient. Fluvial sediment transport rates have been estimated using several techniques including radionuclides (e.g. Walling, 2013), magnetic properties (e.g. Milan & Large, 2014), use of painting and dye tracers (e.g. Hassan & Ergenzinger, 2003), uranium series dating (Dosseto *et al.,* 2006; 2008) and cosmogenic nuclide dating (Wittmann *et al.*, 2015). Many of these techniques are limited. Many of these techniques yield rates that describe average sediment movement or are limited in application to the catchment scale. As a result, these techniques can fail to detect localised variability in transport conditions that could affect the catchment-wide rate. The use of single-grain MET-IRSL to achieve reconstruction of sediment transport and storage histories, potentially for individual grains, has the potential to address these challenges due to its relative efficiency and applicability at small spatial scales.

1.5. A theoretical approach to MET-IRSL based sediment transport tools

This section first briefly outlines reasons for the suitability of feldspar IRSL, and specifically, MET-IRSL as a tool for extracting sediment transport information as opposed to other luminescence techniques, such as quartz OSL or post-IR IRSL. Secondly, this section will outline how knowing about the bleaching and storage times of grains in fluvial systems can provide information on sediment transport times by describing four idealised scenarios.

Feldspar IRSL signals are generally characterised by slower bleaching rates and a higher sensitivity (Sanderson, 1988). This means that whilst some quartz OSL signals are rapidly reset by sunlight exposure feldspar IRSL will contain information on transport and storage history over long timescales. Secondly, MET-IRSL holds such potential for this application owing to the advantages of measuring multiple signals. This allows access to multiple charge populations, which display a range of thermal stabilities and bleaching behaviours (Poolton et al. 2002; Buylaert et al. 2012). The differential bleaching rates of IRSL signals measured at different temperatures can be visualised in Figure 1.5.

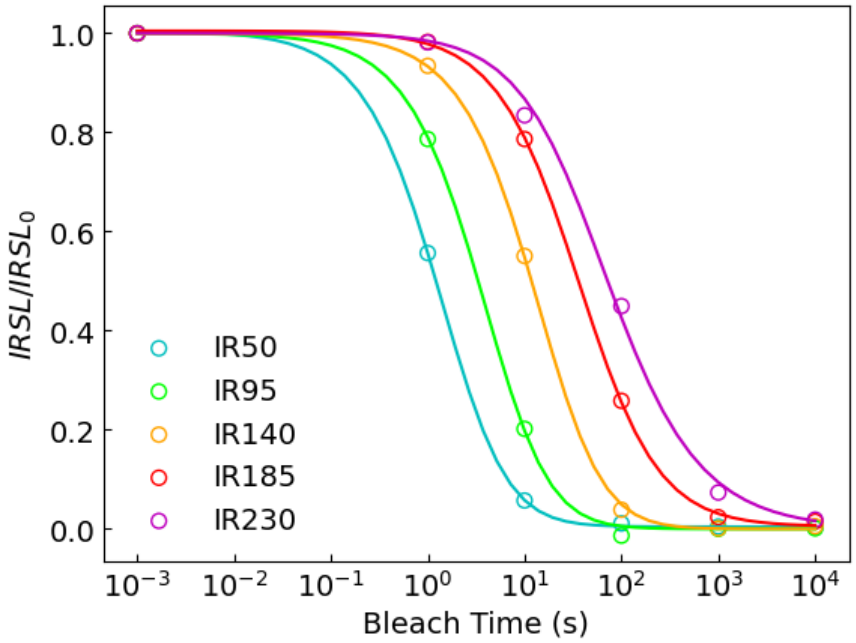

Figure 1.5. *Blue light bleaching measurements and fits of the general order kinetics equation od McGuire & Rhodes (2015a), adapted from Bailiff & Barnett (1994), for IRSL measured at 50˚C, 95˚C, 140˚C, 185˚C and 230˚C. The sample shown here is feldspar standard sample MJ39. Circular points indicate normalised sensitivity corrected luminescence, smooth lines represent modelled signal decay using optimal parameters estimates of a, b, and C.*

As shown in Figure 1.2.1, measurement of feldspar IRSL at higher temperatures allows efficient access to trapped charge that bleaches slowly, whilst lower measurement temperatures allow access to trapped charge that bleaches more quickly (Buylaert *et al.,* 2009). Subsequently, the relative difference between multiple MET-IRSL signals is a function of light exposure history. The apparent age provides information on burial time. In addition, with more signals, it is possible to determine bleaching and burial times deeper into the history of an individual grain. This thesis demonstrates how this physical attribute of feldspar MET-IRSL can be utilised to provide information on transport and storage history in fluvial systems and propose methods for deriving sediment transfer times.

The significance of bleaching and burial information for determining sediment transport rates can be understood by conceptualising the journey of a grain, or group of grains, through four simple idealised models that each represent a fluvial system with a distinct style of sediment transport:

1) Exclusive bleaching. In this scenario, a grain enters the system and is in constant transport until it exits the system. In transit, this grain is exposed to light which causes the continuous reduction of its trapped charge population, at a rate proportional to Equation 1.2. This is analogous with 'flume-like' behaviour and could perhaps be observed as grains pass through a river channel that has undergone extensive modification such that its banks and bed are constructed of a highly erosion-resistant material. This produces a pattern of uninterrupted decay of the luminescence signal of a grain as it moves through this system (Figure 1.6).

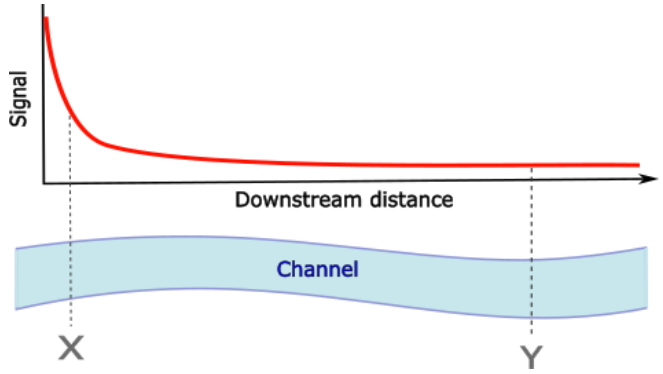

Figure 1.6. *Conceptual model of an idealised channel whereby as grains are transported through the system (left to right), they are subject to light exposure. This causes the continuous reduction of the trapped charge population as it moves downstream. The red line represents the hypothesised IRSL signal of grains as they move through the channel in these conditions. This model assumes time-space equivalence, whereby the signal of grains at location marked 'X' is equivalent to the signal of grains at location 'Y' when they passed location 'X'.*

To determine the transit time of a grain that has travelled through this system, it is necessary to adopt an assumption of time-space equivalence, whereby the signal of a grain at location X is equivalent to the signal of grains at location Y when they passed location X (Figure 1.2.2). Here, the transit time of grains is simply *t* in Equation 1.2.

2) Exclusive growth. On entering this system, a grain is not exposed to sufficient light for the bleaching process to occur. As the grain travels downstream, low light conditions continue to prevent signal reduction. For the signal to grow, the grain must enter storage, however when it is once again transported, it remains in low light conditions. In this scenario, the luminescence signal of a grain will increase with downstream distance (Figure 1.7).

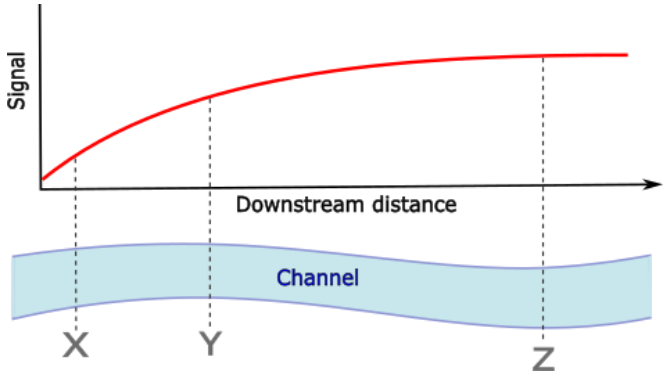

Figure 1.7*. Conceptual model of an idealised channel whereby as grains are transported through the system (left to right), they enter storage at various times and are not subject to light exposure. This causes the continuous growth of the trapped charge population as it moves downstream. The red line represents the hypothesised IRSL signal of grains as they move through the channel in these conditions. The transit time of this grain between locations X and Z is related to the apparent ages of grains at location X subtracted from the apparent ages at location Z (Figure 1.7). The same approach could be used to estimate transit times between locations X and Y, and Y and Z.*

Applying the principle of time-space equivalency, the transit time of this grain between locations X and Z is related to the apparent ages of grains at location X subtracted from the apparent ages at location Z (Figure 1.7). The same approach could be used to estimate transit times between locations X and Y, and Y and Z. These conditions may be observed close to the bed of an extremely deep, sediment laden channel.

3) Bleaching and burial, dominated by bleaching. This represents a combination of model 1) and 2) whereby as a grain travels along the channel, it is exposed to light during transport. Grains in this system also spend time in storage before they exit. However, the amount of time spent in transport and exposed to light is sufficient to cause an overall decrease in IRSL signal with downstream distance (Figure 1.8).

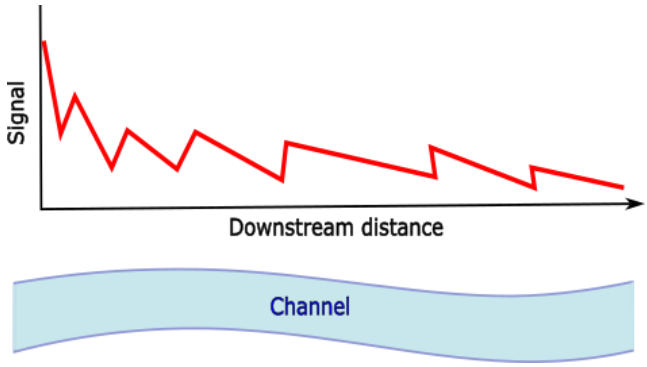

Figure 1.8. *Conceptual model of an idealised channel whereby as grains are transported through the system (left to right), they are subject to both storage and light exposure, but the amount of time exposed to light is sufficient, relative to the time spent in storage, to cause an overall decrease in IRSL signal with downstream distance.*

In this model, the transit time of grains relates to characteristic storage time and the number of transport-storage cycles grains are subject to during their time in this system, which can be constrained using the relative difference between MET-IRSL signals caused by light exposure. This is because, although bleaching during the time grains spend in transport dominates signal behaviour, it is negligible relative to the time grains spend in storage.

4) Bleaching and burial, dominated by burial. This also represents a combination of model 1) and 2), but here light exposure between periods of storage is insufficient to cause a decrease in luminescence signal with downstream distance. Overall, luminescence signal increases with downstream distance but periods of increase are interspersed with signal reduction (Figure 1.9).

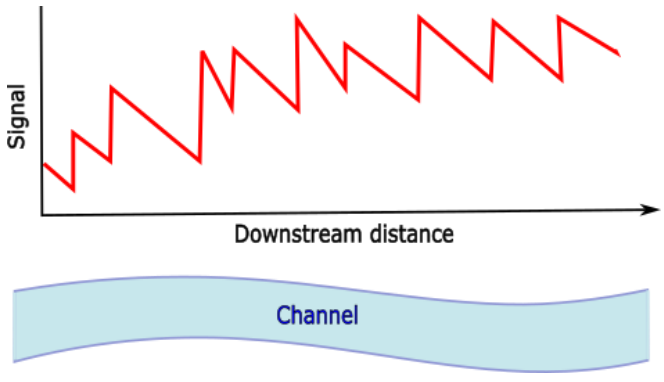

Figure 1.9. *Conceptual model of an idealised channel whereby as grains are transported through the system (left to right), they are subject to both storage and light exposure, but the amount of time exposed to light is insufficient, relative to the time spent in storage, to cause an overall decrease in IRSL signal with downstream distance.*

To estimate sediment transport rates for grains in systems such as this, it is possible to calculate total time spent in transit by estimating the average time spent in storage and degree of age reduction by light with multiple IRSL signals with different bleaching rates.

In this thesis, the principles illustrated by conceptualising these four distinct styles of system functioning are applied to further the development of MET-IRSL as a tool for extracting detailed information on fluvial sediment transport, for both bulk signals and individual grains. It should be noted that these highly idealised models do not account for the influence of variables external to the active channel on the IRSL signal of the in-channel sediment flux and assumes that all bleaching occurs during transport. One such variable is lateral input of sediment (via bed and bank erosion, or extreme events such as landslides). This thesis uses the simple models depicted in depicted Figures 1.6-1.9 as a jumping off point from which to design approaches to dealing this complexity.

1.6. Bleaching and growth parameters

The table below lists and defines bleaching (Eq. 1.3) and growth (Eq. 1.1) parameters commonly referred to in this thesis for reference.

Table 1.1. *Bleaching and growth parameters and their definitions.*

Parameter	**Definition**
Growth	
Characteristic saturation dose, D_0	The radiation dose necessary to raise the signal from 0 to 1-1/e, which is ~ 63% of the fully saturated signal.
Maximum intensity, I_{max}	The intensity of the signal at saturation i.e. infinite time.
Bleaching	
Bleachability, a	Includes information on the initial population of trapped electrons; intensity of excitation source, capture cross-section.
Order, b	contains information on the order of how the kinetic 'reaction' proceeds.
Residual, C	A non-bleachable component of the signal.
Initial intensity, I_0	The intensity of the signal at zero time – time being seconds of light exposure

1.7. Aim and objectives

The aim of this thesis is to develop MET-IRSL as a tool for extracting fluvial sediment transport information including storage times and transport rates at spatial scales ranging from system-scale to localised reaches.

Objective 1: Investigate feldspar MET-IRSL bleaching to determine an ideal function with which to model the bleaching process for grains in fluvial transport.

Objective 1 is achieved through a series of laboratory experiments designed to produce knowledge that is of particular significance to the development of MET-IRSL as a tool for determining fluvial sediment transport dynamics. These experiments broadly aim to answer two questions: 1) How do factors that affect bleaching rate need to be accounted for in fluvial transport scenarios? 2) Can length of past light exposure be accurately recovered?

A burial-bleach model is constructed using an improved bleaching function to simulate the MET-IRSL signal behaviour of grains when subject to cyclical bleaching and burial.

Objective 2: Develop optimal methods for analysing MET-IRSL data to determine fluvial sediment transport dynamics and assess the success of the burial-bleach model.

Samples are collected from the active channel of the Allt Dubhaig, a small gravel bed river in Perthshire, Scotland. This dataset is used as a training ground to fully explore the vast quantity of data produced by MET-IRSL measurements and devise analysis techniques that can be used to obtain an array of different information on sediment transport histories, styles, and rates, and storage duration. The degree to which the burial-bleach model is successful at reproducing downstream MET-IRSL signals observed in the Allt Dubhaig is assessed.

Objective 3: Test and apply methods developed in achieving Objective 2 to elucidate sediment transport information for more complex systems with multiple potential lateral inputs.

Techniques developed through achieving Objective 2 are applied to a dataset from the Solimões River, the main strand of the Amazon system, Brazil and a dataset from the Santa Clara River in southern California. The burial-bleach model is applied to assess its utility for characterising lateral input.

Objective 4: Reconstruct transport histories using single grains to identify multiple pathways of transport within a single sample.

The burial-bleach model is adapted for application to individual grains to assess the potential of single grains measured using MET-IRSL to provide independent storage and transport information.

2.0. Chapter 2 Methods

This chapter details the standard methods and procedures used to produce the results presented in this thesis. Chapters 3, 4 and 5 each contain sections detailing the specific methods used to collect samples and produce the results presented that are not included here.

2.1. Sample preparation

The details of sample preparation described below is for samples from the Allt Dubhaig, this preparation was carried out by the author of this thesis. Samples from the Solimões River were prepared in São Paulo, as in Sawakuchi *et al.* (2017). Samples from the Santa Clara River were prepared in Los Angeles, as in McGuire & Rhodes (2015a). All presented in this thesis are listed in Table 2.4 in Section 2.6 of this chapter.

Samples were prepared in red light at the University of Sheffield Luminescence Dating Laboratory. After tubes were opened ~ 1 cm was scraped off each end (more in the presence of a lot of coarse grains) to remove grains that may have been subject to light exposure during collection and transport of the sample. This part of each sample was weighed and then placed in the oven over night to remove any moisture. Once dry, the samples were weighed once more to calculate moisture content. Approximately two thirds of the remaining sample were put into glass beakers and stored in the oven over night to remove any moisture before dry sieving.

Samples were passed through a 250 µm and 125 µm sieve to obtain the desired fraction for this stage of preparation of 125-250 µm. Hydrogen chloride (HCl) was added to the 125-250 µm fraction (just enough to cover the sample) to remove any carbonates. Samples were left until it was no longer possible to hear a reaction taking place. HCl was then poured off and samples were rinsed. Next, samples were treated with hydrogen peroxide (H_2O_2) in the same manner to remove organic material and left over night. After rinsing of H_2O_2, samples were stored in the oven to dry. Once dry, samples were passed through 212 µm, 180 µm and 125 µm sieves to isolate the 180-212 µm fraction for measurement. It was considered optimal to measure the 180-212 µm fraction because the feldspar grains were often elongate, this grain size is less likely to protrude out of the 300 µm holes in the disc (Section 2.2.4). Further, it is more straight forward to empty discs of grains of this size, and issues of multiple grains in a single hole were rare.

The 180-212 µm fraction was put into test tubes to which 40 ml of sodium polytungstate (NaPT) with a density of 2.58 g cm^{-3} was added to separate the feldspar grains. NaPT is a low-viscosity heavy liquid, and at this density, allows feldspar grains float to the top on the liquid, and any quartz of other minerals sink. The floating feldspar grains were then carefully poured off into a Buchner funnel lined

with filter paper and the liquid drained using a vacuum filter. Once drained, samples were stored in an oven to remove moisture.

2.2. Sample measurement

2.2.1. Luminescence reader

All of the IRSL measurements presented in this thesis were performed using the Risø TL-DA-20 DASH luminescence reader shown in Figure 2.1 at the University of Sheffield Luminescence Dating Laboratory. Filters BG3 and BG39 (blue filter pack) were used for IRSL measurements, and 7.5mm of Hoya U340 when exposing samples to blue or green LEDs. Single grain IRSL measurements were made using a 150 mW 830 nm infrared laser filtered through an RG-780 filter to minimise resonance at 415 nm. This reader is fitted with an EMD-9107 PMT tube (photomultiplier) and clusters of LEDs for stimulation at different wavelengths: two clusters of Epitex SMBB470-1100-TINA-RS for blue light, two clusters of SMBB525-1100-TINA-RS for green light, and three clusters of SMBB870-1100-TINA-RS for infrared.

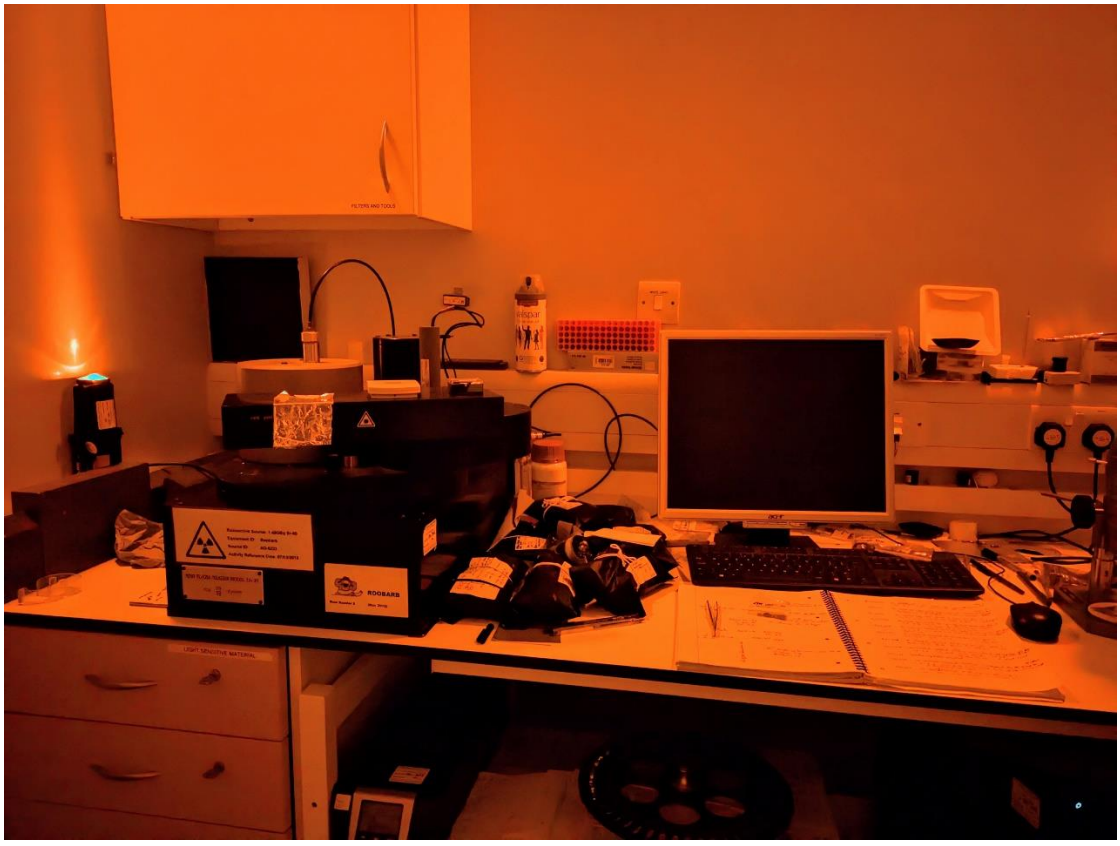

Figure 2.1. *The Risø TL/OSL Reader Model DA-20 used to make the IRSL measurements presented in this thesis*

2.2.2. IRSL measurement

Three types of IRSL measurement were used to produce the data in this thesis:

1) multiple grain (MG) MET-IRSL at multiple elevated temperatures.

2) short shine MG IRSL measured at 50°C.

3) single grain (SG) MET-IRSL at multiple elevated temperatures.

Measurements of type 1), 2) and 3) were made in a series of experiments presented in Chapter 3, whereas fluvial samples presented in Chapters 4 and 5 were measured using 3). A summary of all the samples measured for this thesis can be found in Section 2.6.

2.2.3. MET-IRSL protocols

METx

The METx protocol builds upon the five temperature MET-IRSL protocol of McGuire & Rhodes (2015a) used to determine a virtual velocity for sediments of the Mojave River, southern California. The protocol of McGuire & Rhodes (2015a) is visualised in Table 2.1 below. The METx protocol differs from the MET-IRSL protocol of McGuire & Rhodes (2015a) in two key ways:

1) a warm bleach at 250˚C for 100s is administered prior to the test dose

2) a larger test dose of 20 grays (Gy), increased from 8 Gy, is used.

These changes were made, following the recommendations of Colarossi *et al.* (2018) with the intention of producing exponential growth rather than the exponential plus linear growth that was commonly observed using the original protocol of McGuire & Rhodes (2015a). This is in part because it is challenging to convert intensity into fraction of saturation with a non-saturating exponential, and also because it was expected that a larger signal would yield more single grain results. Further, discussed by Colarossi *et al.* (2018), with exponential growth there is less likely to be carry over of charge between SAR cycles and a larger test dose is thought to reduce sensitivity change between cycles.

Table 2.1. *The METx protocol. Key adaptations from the MET-IRSL protocol of McGuire & Rhodes (2015a) are highlighted in bold. Doses used for regenerations were 20 Gy, 5 Gy, 60 Gy, 200 Gy, 480 Gy and 0 Gy. The 20 Gy dose was repeated for the recycling test.*

Natural or beta dose
Preheat 60s 250°C 5°Cs^{-1}
IRSL 50°C 2.5s 90% power
IRSL 95°C 2.5s 90% power
IRSL 140°C 2.5s 90% power
IRSL 185°C 2.5s 90% power
IRSL 230°C 2.5s 90% power
IRSL warm bleach 250°C 400s 90%
Beta test dose **20 Gy**
Preheat 60s 250°C 5°Cs^{-1}
IRSL 50°C 2.5s 90% power
IRSL 95°C 2.5s 90% power
IRSL 140°C 2.5s 90% power
IRSL 185°C 2.5s 90% power
IRSL 230°C 2.5s 90% power
IRSL hot bleach 290°C 400s 90%

The METx protocol was primarily used to measure single grains for samples from the Solimões River, Brazil and the Santa Clara River, southern California. This protocol was also used in several of the bleaching experiments outlined in Chapter 3.

ILT-3ET

A protocol that stimulates IRSL at three elevated temperatures (3ET) was developed, termed 'Improved Low Temperature' 3ET (ILT-3ET). The details of the ILT-3ET protocol are displayed in Table 2.2. ILT-3ET builds upon the original 3ET approach of Ivester *et al.,* (2022), and principles from the five-temperature protocol of McGuire & Rhodes (2015a). The ILT-3ET protocol is optimised for the measurement of burial periods on timescales much shorter than those targeted by conventional IRSL dating. For this reason, the ILT-3ET protocol stimulates IRSL using the first three measurement temperatures of the METx approach: 50°C, 95°C, and 140°C, which is permitted by a lower preheat of 170°C. This protocol was also designed to minimise thermal transfer (Rhodes, 2000) and provide exponential signal growth (Colarossi *et al.,* 2018).

Table 2.2. *The ILT-3ET protocol. Key adaptations from the MET-IRSL protocol of McGuire & Rhodes (2015a) are highlighted in bold. Doses used for regeneration were 20 Gy, 5 Gy, 60 Gy, 130 Gy, 200 Gy and 0 Gy. The 20 Gy dose was repeated for the recycling test. This is similar to the protocol of Ivester et al. (2022) but with a lower preheat and measurement temperatures, plus the addition of a warm bleach.*

Natural or beta dose
Preheat 60s 170°C 5°Cs^{-1}
IRSL 50°C 2.5s 90% power
IRSL 95°C 2.5s 90% power
IRSL 140°C 2.5s 90% power
IRSL Warm bleach 160°C 400s 90%
Beta test dose 20 Gy
IRSL 50°C 2.5s 90% power
IRSL 95°C 2.5s 90% power
IRSL 140°C 2.5s 90% power
IRSL hot bleach 290°C 100s 90%

The ILT-3ET protocol was predominantly used to measure fluvial and glacial sediments from the alluvial section of Allt Dubhaig, Scotland. This protocol was also used in several of the bleaching experiments outlined in Chapter 3.

2.2.4. Discs

Grains are held by, or mounted on, discs to be placed into the luminescence reader for IRSL measurement. Three types of discs were used:

- Single grain measurements: regular single grain discs manufactured by Risø (Bøtter-Jensen *et al.,* 2000). These are composed of anodised aluminium and have 10 x 10 300 µm holes. Build up and backscatter effects gives these discs an internal beta dose rate 9% higher than standard aluminium discs.
- Oxford aluminium multiple grain discs (0.997cm diameter).
- Stainless steel multiple grain discs. These receive a dose rate 22% higher than aluminium discs, also due to build up and backscatter.

2.2.5. Equivalent dose measurement

The goal of making luminescence measurements is to estimate the amount of radiation to which a sample is exposed in nature, this is referred to as equivalent dose (D_e). The rate at which the sample received radiation is also measured by either quantifying the concentrations of radioactive isotopes in the sample (laboratory analysis) or directly measuring the counts of emitted radiation (in the field). These measurements are used to calculate the amount of radiation to which a sample was exposed each year, which is referred to as the environmental dose rate (Duller, 2008). The apparent age of a sample is estimated using the equivalent dose and the environmental dose rate in the following equation (Duller *et al.,* 2008):

$$Age\ (years) = \frac{equivalent\ dose\ (Gy)}{dose\ rate\ (Gy\ yr^{-1})} \tag{2.1}$$

The luminescence reader records photon counts during IRSL stimulation, measured in counts per second (c/s), which is also referred to as luminescence intensity. Stimulation time is divided into a user defined number of intervals called channels. Counts per channel are recorded and the sum of these gives rise to the signal. A background subtraction is carried out to calculate the luminescence response to a given or natural dose. The single aliquot regenerative dose (SAR) procedure of Murray & Wintle, (2000) is used to estimate the amount of radiation grains were exposed to in situ since the event being dated, the equivalent dose. The 'regenerative' approach of SAR is such that initially, luminescence intensity as a product of the dose to which a sample was exposed in nature is measured. Following this, luminescence response is regenerated and measured by administering known doses of beta radiation over a series of cycles (Table 2.3). The regenerated responses are used to construct a dose response curve, also referred to as a growth curve (Figure 2.2). Dose response curves with fitted with the exponential function described by Eq. 1.1 (Murray & Wintle 2003).

To estimate equivalent dose, the sensitivity corrected luminescence response to the natural dose is interpolated on to the dose response curve (indicated by the red lines in Figure 2.2), which is 230 Gy in Figure 2.2. Measurement of the luminescence response to one of the regenerative doses is repeated as a recycling test, in line with routine SAR protocol (20 Gy in the METx protocol detailed in Section 2.2.3). In this thesis equivalent dose estimation was carried out using the Analyst software package (Duller, 2015).

Table 2.2 also shows additional steps that comprise the typical SAR protocol used in this thesis, these are:

1) preheat (ii) – the sample is heated prior to measurement of luminescence intensity in order to remove any unstable charge (Duller, 2008),

2) test dose (iv) – the number of photons emitted per unit radiation varies between samples and individual grains. Thus, the luminescence response to a fixed dose, the test dose, is measured in each SAR cycle. This is used to calibrate the luminescence responses in step iii) of Table 2.2), to account for variability in sensitivity,

3) hot bleach (vii), this is to reset the signal and reduce the effect of charge trapped in response to the dose from the previous cycle carrying over to the next.

Table 2.3 *Basic elements of the single aliquot regenerative dose procedure of Murray & Wintle (2000). Note the luminescence responses to natural and regenerative doses is L_x, and the luminescence response to the test dose is T_x.*

	Cycle 1	**Cycle 2**	**Cycle 3…**
i)	Radiation exposure in nature	Regenerative dose	Regenerative dose
ii)	Preheat	Preheat	Preheat
iii)	Measurement of luminescence intensity (L_n)	Measurement of luminescence intensity (L_1)	Measurement of luminescence intensity (L_2)
iv)	Test dose	Test dose	Test dose
v)	Preheat	Preheat	Preheat
vi)	Measurement of luminescence intensity (T_n)	Measurement of luminescence intensity (T_1)	Measurement of luminescence intensity (T_2)
vii)	Hot bleach	Hot bleach	Hot bleach

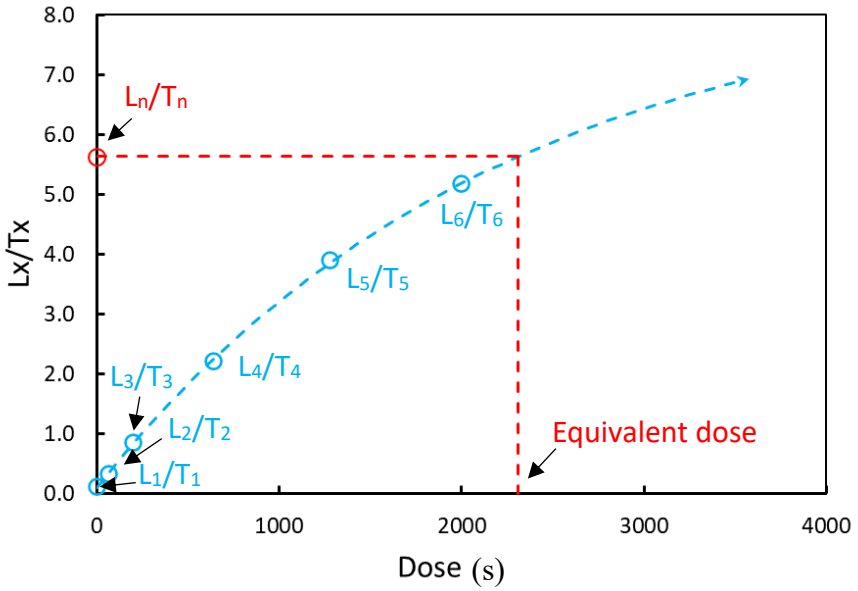

Figure 2.2. *Example of a fitted dose response curve using Eq.1.1 and equivalent dose estimation. Displayed here is the super synthetic aliquot IR_{140} response of sample 22181, from the active channel of the Allt Dubhaig, Scotland). L_n/T_n indicates sensitivity-corrected luminescence response to the natural dose, plotted at zero regenerative dose (x-axis), L_x/T_x is the sensitivity-corrected luminescence response to the laboratory administered regenerative doses.*

2.3. Bleaching measurements

Detailed descriptions of bleaching measurements and protocols can be found in Chapter 3, however here it is noted that most of the bleaching studies in this thesis were concerned with understanding the luminescence response of grains in subaqueous conditions. Blue light was selected as a proxy for the bleaching in these conditions based on the results of bleaching measurements made in a solar simulator. These showed that bleaching of METx signals in the solar simulator proceeds at a faster rate than our blue light measurements indicate (Section 3.3.1, Chapter 3). It is has been documented that light intensity decreases with increasing depth under water (Berger and Lauternauer 1987, Berger 1990; Sanderson et al. 2007), and dominantly green to amber light is transmitted at depth (Berger, 1990). Therefore, it appeared reasonable that blue light bleaching would approximate the bleaching of METx signals by sunlight in sub aqueous conditions. The results of bleaching measurements using a solar simulator are displayed in Figure 2.3.

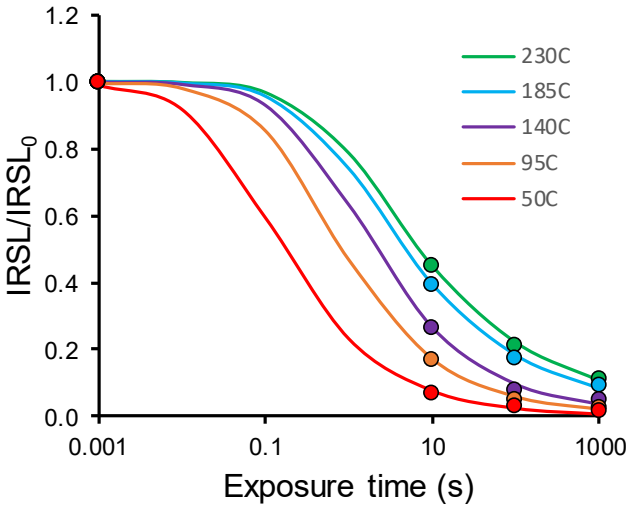

Figure 2.3. *Bleaching of orthoclase feldspar standard sample MJ39 in a solar simulator. Exposure times were 10, 100, 1000s. MET-IRSL responses to these exposure times are fitted by the bleaching function of Bailiff & Barnett (1994)*

2.4. Data processing and analysis

The following section describes the range of ways in which single grain METx signals are presented and analysed in this thesis, each of which are found in different contexts within Chapters 3, 4 and 5. These are summaried in Table 2.3. Where relavent, specific methods are described in the following chapters.

***Table 2.4**. Summary of methods used to present MET-IRSL signal in different manners.*

Signal	**Method**	**Software**
Sensitivity corrected luminescence (L_x/T_x)	Dose response (L_x) divided by test dose response (T_x). Dose response is calculated by summing measured counts per channel during stimulation following regenerative dose. Test dose response is calculated in the same manner following the test dose.	Analyst, Python
Super synthetic alquot apparent age (Sum all grains)	Sum of L_x and T_x of all grains of that sample (usually 200 grain positions representing two discs). Calculate summed L_x/T_x. Equivalent dose is estimated using the method shown in Figure 2.2. Age calculated as shown in Eq. 2.1.	Analyst, Excel
Single grain apparent age	Equivalent dose estimated for each individual grain using the method shown in Section 2.2.3. Age calculated as shown in Eq 2.1.	Analyst, Python
Mean apparent age	An unweighted average of all relevant single grain apparent ages.	Analyst, Python
Minimum plateau age	Method described by Ivester *et al.* (2022) and Rhodes &	Analyst, Python (Python code from Ivester, pers comms, was

	Leathard (2022). Grains with consistent equivalent dose estimate across two or more measurement temperature are identified. The discreet minimum dose model of Rhodes (2015) is applied for estimating final equivalent dose and subsequently age.	adapted for five temperature MET-IRSL)
Fraction of saturation	Luminescence intensity divdided by I_{max} (I_{max} the maximum intensity parameter from the exponential growth function (Eq. 1.1), intensity at infinite dose)	Analyst, Python
Burial-bleach ratio	Method of Rhodes & Leathard (2022), which is described in Section 1.3, Chapter 1.	Analyst, Python

2.5. Samples

A table of all samples presented in this thesis with lab code, geomorphic context, and location is shown below (Table 2.4).

Table 2.5. *The samples presented in their thesis, with lab codes, geomorphic contexts, and locations.*

Lab code	Geomorphic context	Location
20164	Fluvial terrace	Kekerengu, New Zealand
19121	Fluvial sediment	Los Angeles, California
MJ39	Rock sample	UCLA laboratory standard
22094	Rock sample	San Gabriel mountains, California
18031	Fluvial channel	Allt Dubhaig, Scotland
18032	Fluvial channel	Allt Dubhaig, Scotland
18033	Fluvial channel	Allt Dubhaig, Scotland
18034	Fluvial channel	Allt Dubhaig, Scotland
22177	Scree apron	Allt Dubhaig, Scotland
22178	Moraine	Allt Dubhaig, Scotland
22179	Moraine	Allt Dubhaig, Scotland
22180	Fluvial channel	Allt Dubhaig, Scotland
22181	Fluvial channel	Allt Dubhaig, Scotland
22182	Fluvial channel	Allt Dubhaig, Scotland
22183	Fluvial channel	Allt Dubhaig, Scotland
22184	Fluvial channel	Allt Dubhaig, Scotland
22185	Fluvial channel	Allt Dubhaig, Scotland
22186	Fluvial channel	Allt Dubhaig, Scotland
22187	Fluvial channel	Allt Dubhaig, Scotland
22188	Fluvial channel	Allt Dubhaig, Scotland
22189	Fluvial channel	Allt Dubhaig, Scotland
22190	Fluvial channel	Allt Dubhaig, Scotland
22191	Fluvial channel	Allt Dubhaig, Scotland
L0609	Fluvial channel	Solimões River, Brazil
L0611	Fluvial channel	Solimões River, Brazil
L0612	Fluvial channel	Solimões River, Brazil
L0613	Fluvial channel	Solimões River, Brazil
L0614	Fluvial channel	Solimões River, Brazil
L0615	Fluvial channel	Solimões River, Brazil
L0616	Fluvial channel	Solimões River, Brazil
L0617	Fluvial channel	Solimões River, Brazil

L0618	Fluvial channel	Solimões River, Brazil
L0619	Fluvial channel	Solimões River, Brazil
L0620	Fluvial channel	Solimões River, Brazil
L0621	Fluvial channel	Solimões River, Brazil
J0344	Fluvial channel	Santa Clara River, California
J0345	Fluvial channel	Santa Clara River, California
J0346	Fluvial channel	Santa Clara River, California
J0347	Fluvial channel	Santa Clara River, California
J0349	Fluvial channel	Santa Clara River, California
J0350	Fluvial channel	Santa Clara River, California
J0352	Fluvial channel	Santa Clara River, California

3.0. Chapter 3 Understanding feldspar IRSL bleaching for MET-IRSL-based sediment transport models

3.1. Introduction

This Chapter presents a series of IRSL bleaching experiments tailored to produce knowledge that is of particular significance to the development of MET-IRSL as a tool for determining fluvial sediment transport dynamics. Experiments broadly aim to answer two questions: 1) How do factors that affect bleaching rate need to be accounted for in the development of luminescence-based sediment transport tools? 2) Can length of past light exposure be accurately recovered? By answering these questions there is potential for detailed reconstruction of sediment transport histories for fluvial systems and assessing likelihoods of different scenarios and constraint of IRSL-based sediment transport models. There is also significant potential benefits for other applications of IRSL to determine pre-depositional history, such as palaeophotometry, a proxy for variable transport conditions through time developed by Rhodes & Leathard (2022).

This Chapter will first review the literature on bleaching (Section 3.2), then outline experiment design, results and interpretation (Section 3.3), discuss results and new frameworks for analysis of IRSL bleaching behaviour (3.4), and conclude the findings of this Chapter (Section 3.5).

3.2. Background

This section provides an overview of the current research concerned with felspar IRSL bleaching dynamics, highlighting progress made to date and gaps in knowledge it may be beneficial to address in order to enhance the utility of MET-IRSL as a sediment tracing tool.

3.2.1. State of the art

It is known that the feldspar IRSL signal bleaching more slowly than the fast component of the quartz OSL signal in full sunlight (Buylaert *et al*., 2012; Murray *et al.*, 2012), and much faster than the TL signal (Godfrey-Smith *et al.*, 1988) (Figure 3.1).

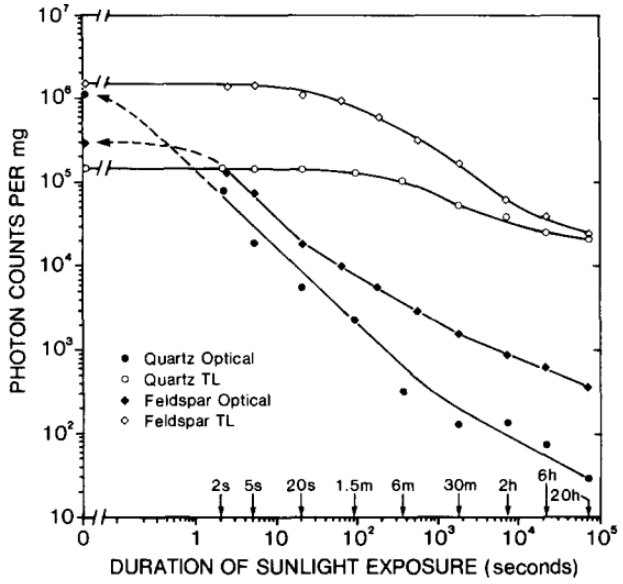

Figure 3.1. *Response of thermoluminescence and OSL of quartz and feldspar to sun light exposure. Note the break in the x-axis. From Godfrey-Smith et al., (1988).*

It is also known that energy of the stimulation source significantly affects feldspar IRSL bleaching rate. Jain & Ankjærgaard (2011) state this dependency is likely related to the depth below the conduction band occupied by the trapped charge. Kars *et al.,* (2014) tentatively report a depth of ~2.5 eV for IR-sensitive traps of potassium-rich feldspar, and ~2.1 eV for sodium-rich feldspar. The efficiency with which charge in IR-sensitive traps is transferred to the excited state increases with decreasing wavelength Jain & Ankjærgaard (2011). For light in the visible range, the excited state is the conduction band. It is considered that stimulation at wavelengths much below the green range (~2.36 eV), very minimal excitation occurs. For infrared light (~1.4 eV), resonance between charge in IR-sensitive traps and photons travelling in the infrared range causes sub-conduction band excitation, resulting in recombination either via tunnelling or band tail states Jain & Ankjærgaard (2011).

Relevant to this study, is the effect of sunlight attenuation by water in fluvial settings. Several studies have measured what happens to the solar spectrum with increasing depth in turbid water (Berger and Lauternauer 1987, Berger 1990; Sanderson et al. 2007), and report two main effects: 1) light intensity decreases with increasing depth, causing a reduction in bleaching rate and 2) the preferential reduction of the high energy part of the spectrum means that dominantly green to amber light is transmitted at depth (Berger, 1990) – as mentioned at the start of this paragraph, what this means for bleaching rates is unclear.

It is known that in post-IRIR and MET-IRSL higher temperature signals bleach more slowly than low temperature signals (Poolton et al. 2002; Buylaert et al. 2012). Fu *et al.,* (2012) present a low-temperature MET-IRSL protocol where IRSL is stimulated at five temperatures (50, 80, 110, 140, 170) and the bleachability of each signal is tested (Figure 3.2). Their findings are consistent with those of Poolton *et al.,* (2002) and Buylaert *et al.*, (2012) for this five elevated temperature protocol. Stimulation of IRSL signals at high temperatures can cause issues of thermal transfer to arise, whereby charge is transported from non-IR-sensitive traps to IR-sensitive traps due to thermal excitation. Here, preheat temperature is pivotal for minimising this effect. The effects preheat temperature on feldspar IRSL bleaching form and rate is discussed further in the following section.

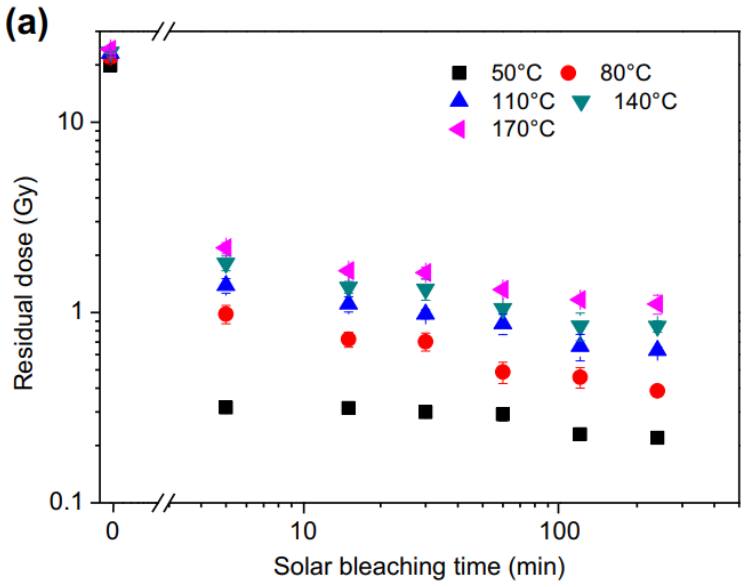

Figure 3.2*. Response of five MET-IRSL signals solar bleaching. Note the break in the x-axis. From Fu et al., (2012).*

McGuire and Rhodes (2015a) measure bleaching rates of MET-IRSL signals using a protocol adapted from Li and Li (2011), stimulating IRSL at 50°C, 95°C, 140°C, 185°C, 230°C. Here, a general order kinetics equation (Eq. 1.1, Chapter 1) is fit to MET-IRSL response to increasing sunlight exposure. The fitted parameters are used to forward model cyclical bleaching and growth to MET-IRSL signals

observed in samples from a longitudinal profile of the Mojave River (Figure 3.3). The model provides a reasonable fit for the IR230 signal only, possibly due to the characteristic flow dynamics of an ephemeral river limiting the light exposure of grains, to which the lower temperature signals will be more sensitive (McGuire & Rhodes, 2015a). However, it should be considered that more robust simulation of the MET-IRSL bleaching process could also improve model accuracy.

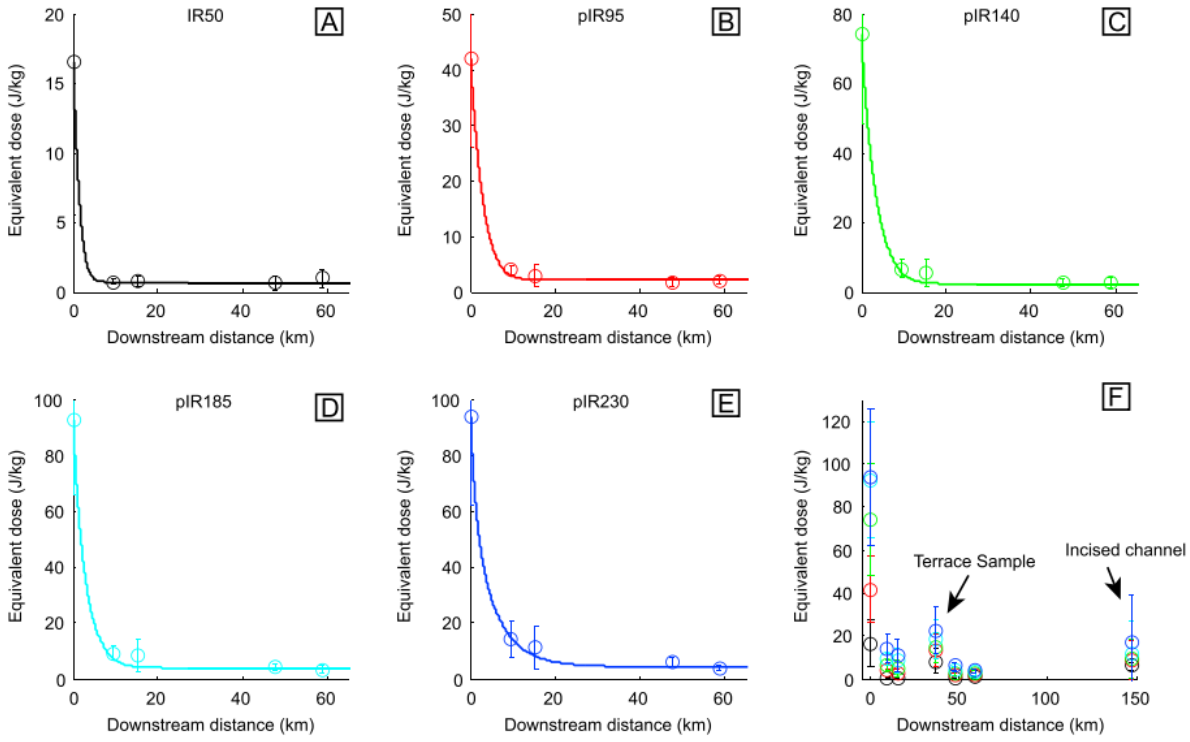

Figure 3.3. *Downstream MET-IRSL data of McGuire & Rhodes (2015a) fitted with the model of Gray et al. (2018) Circular points are field data from the Mojave River, published by McGuire & Rhodes (2015a). Solid lines are fits to the data using a model constructed by Gray et al., (2017).* ***A)*** *IR_{50} equivalent dose plotted with downstream distance and model fit.* ***B)*** *IR_{50} equivalent dose plotted with downstream distance and model fit.* ***C)*** *IR_{50} equivalent dose plotted with downstream distance and model fit.* ***D)*** *IR_{50} equivalent plotted with downstream distance dose and model fit.* ***E)*** *IR_{50} equivalent dose plotted with downstream distance and model fit.* ***F)*** *Equivalent dose from all signals plotted with downstream distance. From Gray et al., (2017).*

A single grain bleaching study from Smedley *et al.,* (2015) showed that bleaching rate does vary between grains of the same sample for post-IRIR. Smedley *et al.,* (2015) demonstrate for three samples (two from aeolian settings and one from glaciofluvial) that despite intra-sample variability of bleachability, there is minimal impact on natural equivalent dose. Smedley *et al.,* (2015) demonstrate clear variability in bleaching rate between grains from this sample. For this sample, they also report bleach rate does not exert dominant control on single grain equivalent dose distributions. Subsequently, Smedley *et al.,* (2015) suggest instead that light exposure history characteristic of

contrasting geomorphic settings has a primary control on natural equivalent dose distributions, in their particular context.

A study by Rhodes *et al.* (2024), of which the author of this thesis is a co-author, presents data to demonstrate the potential of single grain bleach recovery for constraining the exposure and burial history of individual grains. They show how a known light exposure time can be accurately recovered, using the general order kinetics equation of Bailiff & Barnett (1994), by weighting the recovered light exposure times of individual grains by their errors. The concept of an 'equilibrium' and 'non-equilibrium' bleach is introduced, whereby it is demonstrated that MET-IRSL bleaching rate is a function of prior light exposure, providing the signal has not been saturated of zeroed. The form of MET-IRSL decay under different light sources is also explored. Finally, they present a burial-bleach model that accounts for changes in bleaching rate as a result of prior light exposure. This model uses parameter estimates from direct observations, and demonstrates the potential to simulate MET-IRSL signal bleaching and growth for successive cycles of transport and storage. The author of this thesis was involved in the design of the experiments presented in this study, and is responsible for constructing the burial-bleach model using Python. Thus, some of the experiments and the burial-bleach model development of Rhodes *et al.* (2024) are presented in Section 3.4.

3.2.2. Challenges remaining

Key to the successful use of post-IRIR for sediment age estimation is understanding whether high temperature signals (pIRIR) indeed have an unbleachable component. Substantial effort has been made to determine whether there is a need to subtract a residual to account an unbleachable component for accurate equivalent dose determination, and how to quantify this value.

Buylaert *et al.,* (2012) suggest that ~ 4 ± 2 Gy should be subtracted from the pIRIR290 signal, regardless of natural dose.

Zhang *et al.,* (2015a) observe 'no unbleachable residual dose', which they describe as less than 10 Gy after 4 hours of bleaching for IR50 and pIR225. They estimate that natural doses of samples used in this study ranged from ~30 Gy to ~1200 Gy. They did observe a positive relationship between residual doses and natural doses measured.

Kars *et al.,* (2014) put samples in a solar simulator for a series of exposure times from 1 hour to 11 days to record bleaching of IRSL signals measured at 50°C, 90°C, 125°C, 150°C and 175°C. They observed a continuous decrease in luminescence intensity for all signals over the duration of the experiment.

With similar observations, Colarossi *et al.,* (2015) reports a monotonic reduction in pIRIR225 and pIRIR290 signals after 14 days (336 hours) of exposure in a solar simulator, which suggests an unbleachable component of pIRIR may not exist.

Yi *et al.,* (2016, 2018) report a very hard to bleach residual pIRIR290 signal after ~ 300 hours of exposure in a solar simulator. They continued measurements for ~1900 hours.

Zhang *et al.,* (2023) approach to the question of an unbleachable component is to try and quantify length of light exposure prior to the most recent burial. They use a 'predicted' an 'observed' residual dose to estimate degree of bleaching (Figure 3.4). In Figure 3.4, predicted residual dose is calculated as the fading-corrected D_e for each pIRIR temperature minus the quartz OSL D_e (black diamonds). Observed residual dose is the D_e calculated after various exposure times in a solar simulator (coloured points).

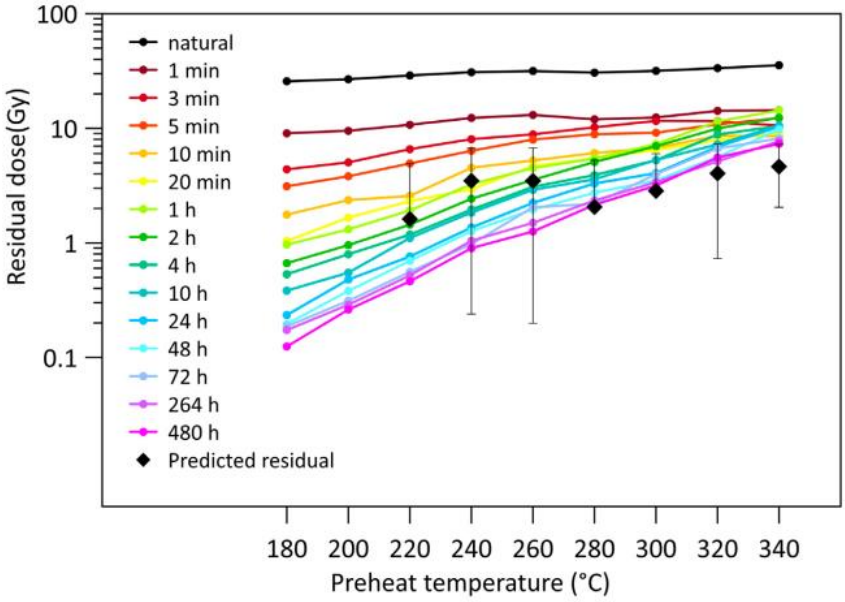

Figure 3.4. *Residual doses of seven MET-IRSL signals from Zhang et al., (2023). Residual doses are represented by preheat temperature on the x-axis. Black diamonds are 'predicted residual dose' for each measurement temperature, which is the fading-corrected equivalent dose minus the quartz OSL equivalent dose. Coloured points are observed residual doses after various exposure times in a solar simulator.*

Zhang *et al*., (2023) assumed a normal distribution for the standardised difference between the observed and predicted residual doses, and the sums of the squared differences (SOSD) to follow a Chi-squared distribution. Bleaching degree was calculated as the area beneath the upper tail of the Chi-squared distribution when x = SOSD for each pIRIR temperature. Here is a diagram I made for my own understanding, which I will leave here for my own benefit (Figure 3.5).

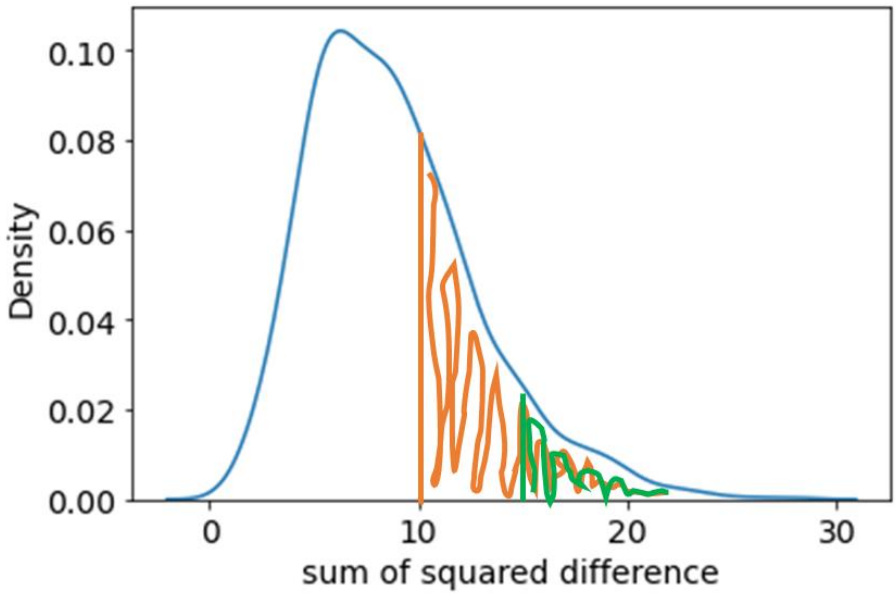

Figure 3.5. *Schematic representation of the method of Zhang et al., (2023) for calculating extent of bleaching prior to the most recent burial – the event of interest. The blue line is a probability density function for the distribution for the sum of the squared differences between observed and predicted residual doses (see text for an explanation of how observed and predicted residual dose is calculated). Orange shaded area is degree of bleaching when x = 10 Gy^2; green shaded area is degree of bleaching when x = 15 Gy^2. This method assumes that pIRIR residual doses become more the similar to each other with increasing light exposure.*

Using this method, the degree of bleaching prior to burial of a loess sample with a quartz age of 6.3 ± 0.4 ka (Zhang *et al*., 2015a; Zhang *et al*., 2015b), which they fairly assume to be well-bleached prior to burial, was estimated as 264 hours in a solar simulator (x = >95% in Figure 5). This is equivalent to ~83 days in nature. The authors note that this is a plausible result, since Nottenbaum *et al*., (2015) provide evidence to suggest the loess sample from this study had been subject to suspension during dust storm events, and long-distance transport by westerlies. One caveat is that the recovered value cannot be validated or invalidated (Zhang *et al*., 2023). However, there exist several drawbacks to this approach: it is dependent on accurate dose rate measurements and g-value measurement, and perhaps most significantly, availability of reliable age control. In addition, transport-deposition cycles that may have left their signature within the recovered bleach value, are not accounted for.

An additional notable observation from Zhang *et al*., (2023) is that the increase in residual dose with increasing measurement temperature and preheat temperature, which is in line with studies mentioned in the previous section and others e.g. (e.g., Li and Li, 2011; Lowick et al., 2012; Kars et al., 2014; Colarossi et al., 2015; McGuire & Rhodes, 2015a; Reimann et al., 2015), and the decrease in bleaching rate with increasing measurement temperature and also preheat temperature. Yet, it is also

noteworthy that bleaching rate was calculated using a power law decay function, which results in a different form of decay to the function of Bailiff & Barnett (1994) (Figure 3.6).

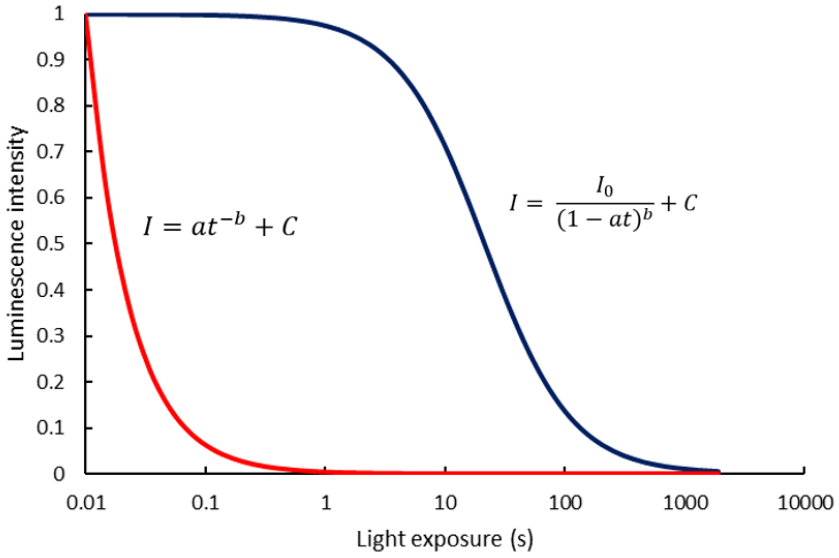

Figure 3.6. *Comparison of bleaching functions used by Zhang et al., (2023) (red line), and McGuire & Rhodes (2015a) (blue line).*

There are two clear elements of feldspar IRSL bleaching behaviour that would benefit from further study: 1) factors that affect bleaching rate and 2) light exposure recovery. To address the aim of this study, we must ask two questions related to the bleaching process: 1) What are the dominant controls on bleaching rates for grains in fluvial systems, and how do bleaching rates vary? 2) What is the optimal method for accurate quantification of light exposure prior to deposition? This chapter addresses these questions through a series of experiments combined with numerical modelling. The aim of this is to have a robust understanding of the bleaching process, and what we need to know about it to achieve the effective application of MET-IRSL for tracing past and present movement of sediment in fluvial systems.

3.3. Methods

Detailed descriptions of standard methods for sample preparation, IRSL measurement and MET-IRSL protocols can be found in Chapter 2.

3.3.1. Bleaching parameter estimation

Much like growth response curve determination, bleach response curves were measured using a SAR procedure with cycles of irradiation, light exposure, followed by a preheat, MET-IRSL measurement, then a hot bleach to reset the signal at the end of each cycle. Note the importance of fully resetting the signal with a hot bleach prior to commencing any bleach curve measurements. Three styles of bleach response curves were measured in this series of experiments, with varying measurement duration. In order of long to short duration:

1) the 'half order of magnitude' (HOM) bleach curve with light exposure times of 0.1, 0.32, 1, 3.2, 10, 32, 100, 320, 1000, 3200, 10000, 100000s

2) 'the full order of magnitude' (FOM) bleach curve with light exposure times of 0.1, 1.0, 10, 100, 1000, 10000, 100000s

3) the quick bleach (QB) curve with light exposure times of 1.0, 100, 10000s. Choice of irradiation time prior to light exposure varied according to expected sensitivity of the sample.

An example of a METx FOM bleach response curve protocol is shown in Table 3.1.

Table 3.1. *A full order of magnitude METx bleach response curve*

1	2	3	4	5	6	7	8
Natural	Beta dose **Blue bleach 0.1s 51°C**	Beta dose **Blue bleach 1.0s 51°C**	Beta dose **Blue bleach 10.0s 51°C**	Beta dose **Blue bleach 100s 51°C**	Beta dose **Blue bleach 1000s 51°C**	Beta dose **Blue bleach 10000s 51°C**	Beta dose **Blue bleach 100000s 51°C**
Preheat 60s 250°C 5°Cs^{-1}	Preheat 60s 250°C 5°Cs^{-1}	Preheat 60s 250°C 5°Cs^{-1}	Preheat 60s 250°C 5°Cs^{-1}	Preheat 60s 250°C 5°Cs^{-1}	Preheat 60s 250°C 5°Cs^{-1}	Preheat 60s 250°C 5°Cs^{-1}	Preheat 60s 250°C 5°Cs^{-1}
IRSL 50°C 2.5s 90% power	IRSL 50°C 2.5s 90% power	IRSL 50°C 2.5s 90% power	IRSL 50°C 2.5s 90% power	IRSL 50°C 2.5s 90% power	IRSL 50°C 2.5s 90% power	IRSL 50°C 2.5s 90% power	IRSL 50°C 2.5s 90% power
IRSL 95°C 2.5s 90% power	IRSL 95°C 2.5s 90% power	IRSL 95°C 2.5s 90% power	IRSL 95°C 2.5s 90% power	IRSL 95°C 2.5s 90% power	IRSL 95°C 2.5s 90% power	IRSL 95°C 2.5s 90% power	IRSL 95°C 2.5s 90% power
IRSL 140°C 2.5s 90% power	IRSL 140°C 2.5s 90% power	IRSL 140°C 2.5s 90% power	IRSL 140°C 2.5s 90% power	IRSL 140°C 2.5s 90% power	IRSL 140°C 2.5s 90% power	IRSL 140°C 2.5s 90% power	IRSL 140°C 2.5s 90% power
IRSL 185°C 2.5s 90% power	IRSL 185°C 2.5s 90% power	IRSL 185°C 2.5s 90% power	IRSL 185°C 2.5s 90% power	IRSL 185°C 2.5s 90% power	IRSL 185°C 2.5s 90% power	IRSL 185°C 2.5s 90% power	IRSL 185°C 2.5s 90% power
IRSL 230°C 2.5s 90% power	IRSL 230°C 2.5s 90% power	IRSL 230°C 2.5s 90% power	IRSL 230°C 2.5s 90% power	IRSL 230°C 2.5s 90% power	IRSL 230°C 2.5s 90% power	IRSL 230°C 2.5s 90% power	IRSL 230°C 2.5s 90% power
IRSL warm bleach 250°C 400s 90%	IRSL warm bleach 250°C 400s 90%	IRSL warm bleach 250°C 400s 90%	IRSL warm bleach 250°C 400s 90%	IRSL warm bleach 250°C 400s 90%	IRSL wam bleach 250°C 400s 90%	IRSL warm bleach 250°C 400s 90%	IRSL warm bleach 250°C 400s 90%
Beta test dose 20 Gy	Beta test dose 20 Gy	Beta test dose 20 Gy	Beta test dose 20 Gy	Beta test dose 20 Gy	Beta test dose 20 Gy	Beta test dose 20 Gy	Beta test dose 20 Gy
Preheat 60s 250°C 5°Cs^{-1}	Preheat 60s 250°C 5°Cs^{-1}	Preheat 60s 250°C 5°Cs^{-1}	Preheat 60s 250°C 5°Cs^{-1}	Preheat 60s 250°C 5°Cs^{-1}	Preheat 60s 250°C 5°Cs^{-1}	Preheat 60s 250°C 5°Cs^{-1}	Preheat 60s 250°C 5°Cs^{-1}
IRSL 50°C 2.5s 90% power	IRSL 50°C 2.5s 90% power	IRSL 50°C 2.5s 90% power	IRSL 50°C 2.5s 90% power	IRSL 50°C 2.5s 90% power	IRSL 50°C 2.5s 90% power	IRSL 50°C 2.5s 90% power	IRSL 50°C 2.5s 90% power
IRSL 95°C 2.5s 90% power	IRSL 95°C 2.5s 90% power	IRSL 95°C 2.5s 90% power	IRSL 95°C 2.5s 90% power	IRSL 95°C 2.5s 90% power	IRSL 95°C 2.5s 90% power	IRSL 95°C 2.5s 90% power	IRSL 95°C 2.5s 90% power
IRSL 140°C 2.5s 90% power	IRSL 140°C 2.5s 90% power	IRSL 140°C 2.5s 90% power	IRSL 140°C 2.5s 90% power	IRSL 140°C 2.5s 90% power	IRSL 140°C 2.5s 90% power	IRSL 140°C 2.5s 90% power	IRSL 140°C 2.5s 90% power
IRSL 185°C 2.5s 90% power	IRSL 185°C 2.5s 90% power	IRSL 185°C 2.5s 90% power	IRSL 185°C 2.5s 90% power	IRSL 185°C 2.5s 90% power	IRSL 185°C 2.5s 90% power	IRSL 185°C 2.5s 90% power	IRSL 185°C 2.5s 90% power
IRSL 230°C 2.5s 90% power	IRSL 230°C 2.5s 90% power	IRSL 230°C 2.5s 90% power	IRSL 230°C 2.5s 90% power	IRSL 230°C 2.5s 90% power	IRSL 230°C 2.5s 90% power	IRSL 230°C 2.5s 90% power	IRSL 230°C 2.5s 90% power
IRSL hot bleach 290°C 100s 90%	IRSL hot bleach 290°C 100s 90%	IRSL hot bleach 290°C 100s 90%	IRSL hot bleach 290°C 100s 90%	IRSL hot bleach 290°C 100s 90%	IRSL hot bleach 290°C 100s 90%	IRSL hot bleach 290°C 100s 90%	IRSL hot bleach 290°C 100s 90%

MET-IRSL signals were corrected for sensitivity using the test dose responses to calculate L_x/T_x. The sensitivity corrected signals were then normalised to a fraction of the unbleached signal (column 1 in Table 3.1). Normalised signals were plotted over a bleach time (s) on a log scale as the x-axis. Figure 1 shows bleaching response curve measurements using an ILT-3ET-IRSL protocol (Figure 3.1). Details of the ILT-3ET-IRSL protocol can be found in Section 2.2.3, Chapter 2.

Eq. 1.3 was fit to bleaching response data using the in-built Python function scipy.optimise.curve_fit, which performs least squares minimisation using the Levenberg-Marquardt algorithm to find optimised values for parameters *a, b* and *C*. Data was normalised to the value of initial unbleached IRSL response, there is a small amount of variation in fitted values of initial IRSL, but this has a minor effect. The approximate covariance of the optimal values is estimated, and the square root of the diagonals used to compute the standard deviation to calculate uncertainty. This produces fitted bleach curves (Figure 3.7) and parameter estimates with their uncertainties (Table 3.2).

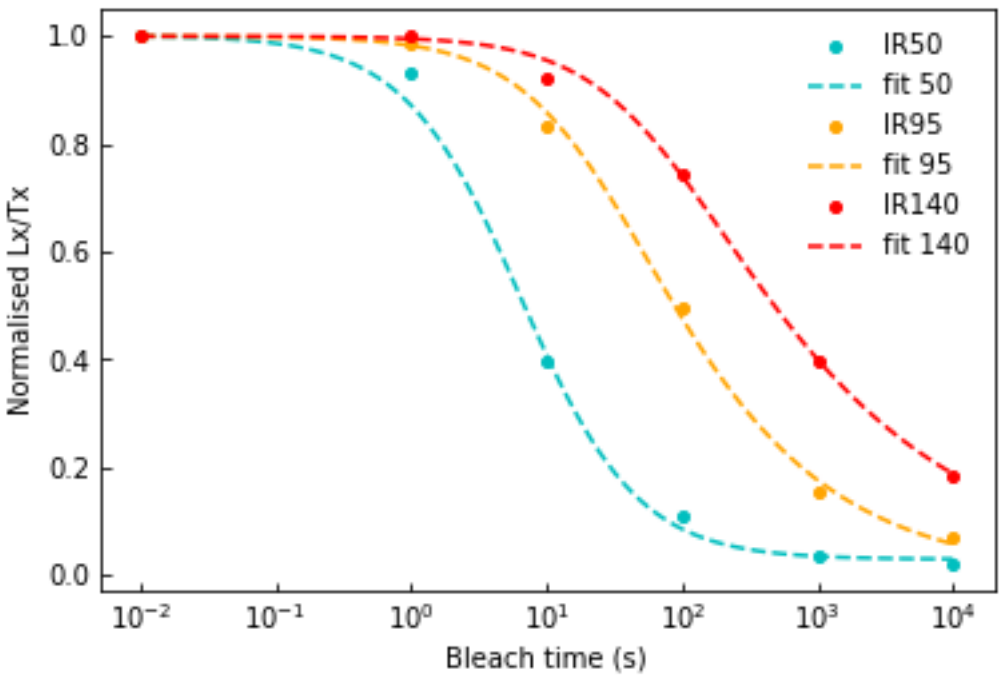

Figure 3.7. *Circular points are full order of magnitude (FOM) ILT-3ET bleach response curve measurements. Measurements were made on sample 22183 from the active channel of the Allt Dubhaig, Perthshire, Scotland. IRSL signal was measured at 50°C, 95°C and 140°C following 0.1, 1, 10, 100, 1000 and 10,000s of blue light exposure. Blue points represent the response of the IR_{50}; orange points are the response of the IR_{95}; red points are the response of the IR_{140}. Dashed lines are the bleaching function of Poolton et al., (2009) fitted to the data using the in-built Python function scipy.optimise.curve_fit, which performs least squares minimisation using the Levenberg-Marquardt algorithm.*

Table 3.2. *Fitted bleaching parameters and their 1-sigma uncertanty for sample 22183.*

Temperature (°C)	*a*	*σa*	*b*	*σb*	C	*σC*
50	0.15	0.08	1.03	0.35	0.03	0.02
95	0.04	0.01	0.47	0.06	< -0.01	0.02
140	0.01	< 0.01	0.33	0.03	-0.01	0.01

3.4. Results

The following series of bleaching experiments was tailored to fill in some of the gaps in our knowledge and observations of the bleaching process for feldspar MET-IRSL. The experiments fall into two categories: 1) exploring the factors affecting bleaching rate and 2) light exposure recovery. The first half of this section will report and discuss results from experiments designed to explore controls on bleaching that may be of particular importance to sediment tracing applications of MET-IRSL. The second half will explore optimal procedures for light exposure recovery for single grains. Each subsection will outline the design, protocols, results of each experiment with some interpretation.

3.4.1. Factors that affect bleaching rate

3.4.1.1. Testing the dependency of bleaching rate on fraction of saturation

To understand the luminescence behaviour of grains that undergo cyclical transport and burial on their journey from source to sink an experiment was designed to investigate how bleaching rate may respond to different doses. Bleaching curves were measured following variable laboratory-administered doses to simulate variable storage times grains experience, as they are transported through the geomorphic environment. Other studies have investigated the relationship between prior dose and residual D_e after a fixed bleach time in a solar simulator (e.g. Sohbati *et al.,* 2012; Smedley *et al.,* 2015). However, the effect on prior dose on bleaching rate is less well-documented. For this reason, the following experiment measures bleaching rates through fitting Eq. 1.3 to the luminescence response of each METx signal to explore the behaviour of fitted bleaching parameters to investigate any variation in decay form with increasing prior dose.

Experimental design

Two MG aliquots were constructed using one sample from the Winterholme fluvial terrace close to the village of Kekerengu in New Zealand (lab code 20164). A single aliquot was constructed using a sample from the Puente Hills Thrust Fault System in Pico Rivera, a suburb of Los Angeles, California (lab code 19121). Both aliquots were given a dose of ~706 Gy and IRSL subsequently measured using the METa protocol after 0, 1, 10, 100, 1000 and 10,000 seconds of blue light

bleaching at 50°C and 90% diode power. The signal used was between 6s and 25s with a background from between 226s and 245s subtracted. This measurement procedure was repeated for doses of ~177 Gy and ~78 Gy to put grains at different fractions of saturation. The data were corrected for any sensitivity change in the usual manner for SAR protocol.

Results and interpretation

The blue LED bleach curves measured following different doses are displayed in Figure 3.8 for the five measurement temperatures. In agreement with previous studies, (e.g. Buylaert et al. 2012; Murray et al. 2012), bleaching rate slows with increasing measurement temperature for both sample 19121 (Figure 3.8a) and 20164 (Figure 3.8b), as illustrated by the later 'roll offs' in Figure 3.8. The term 'roll-off' is herein used to describe the stage of decay where the signal is below two sigma from unity. For example, for 19121 at the IR50 roll off occurs before one second of light exposure, whereas the IR230 roll off begins at ~10 seconds of light exposure. It is also observed that remaining signal after the maximum bleach time increases with increasing measurement temperature for both samples (Figure 3.8, Table 3.3, 3.4). For example, looking at sample 19121 shown in Figure 3.8, after 706 Gy irradiation and 10 000s of blue light exposure, the IR50 signal is ~1.2% of its initial intensity, whereas the IR230 is ~16% (Table 3.8). Inspection of Table 3.3 and Table 3.4 reveals no systematic variation in estimates of *a* and *b*, or remaining signal based on the size of the dose administered prior to bleaching response curve measurement for either of the samples measured in this experiment.

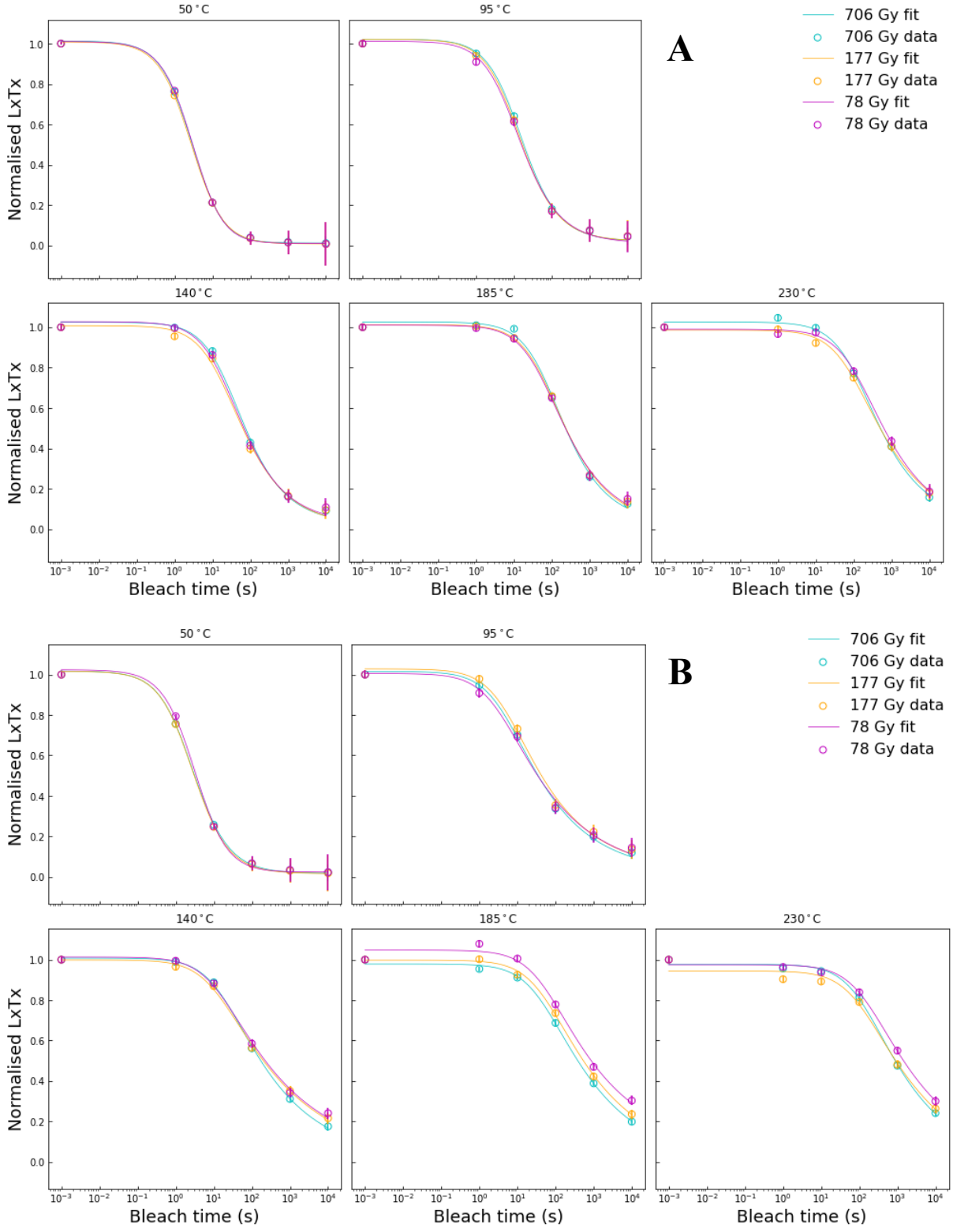

Figure 3.8. Bleaching form following variable dose. ***A)*** *Bleach response curve measurements and fits for sample 19121, from close to the Pico Rivera fault, California for the five METx signals. Bleach response curves were measured following 706, 177 and 78 Gy to test for a dependency of bleaching rate on the size of prior dose.* ***B)*** *Bleach response curve measurements and fits for sample 20164, from Kekerengu, New Zealand for the five METx signals. Bleach response curves were measured following 706, 177 and 78 Gy to test for a dependency of bleaching rate on the size of prior dose. Errors displayed in* ***A)*** *and* ***B)*** *are derived from counting statistics.*

Table 3.3. *Estimates of bleaching parameters a, b and C for the five METx temperatures for sample 19121 from Pico Rivera, California. Bleach response curves were measured following 706, 177 and 78 Gy to test for a dependency of bleaching rate on the size of prior dose. Fractional uncertainties ranged from >0.01 to 0.4, with a small amount greater than 1 for estimates of C.*

	706 Gy			**177 Gy**			**78 Gy**		
Temperature (°C)	*a*	*b*	*C*	*a*	*b*	*C*	*a*	*b*	*C*
50	0.279	1.193	0.013	0.336	1.071	0.009	0.258	1.234	0.013
95	0.091	0.760	0.022	0.106	0.728	0.021	0.130	0.645	0.022
140	0.040	0.534	0.025	0.061	0.448	0.008	0.051	0.496	0.025
185	0.014	0.517	0.026	0.017	0.442	0.012	0.020	0.413	0.026
230	0.009	0.427	0.025	0.013	0.330	-0.014	0.009	0.359	0.025

Table 3.4. *Estimates of bleaching parameters a and b and C for the five METx temperatures for sample 20164 from Kekerengu, New Zealand. Bleach response curves were measured following 706, 177 and 78 Gy to test for a dependency of bleaching rate on the size of prior dose. Fractional uncertainties ranged from >0.01 to 0.6, with a small amount greater than 1 for estimates of C.*

	706 Gy			**177 Gy**			**78 Gy**		
Temperature (°C)	*a*	*b*	*C*	*a*	*b*	*C*	*a*	*b*	*C*
50	0.451	0.821	0.017	0.427	0.866	0.016	0.283	1.079	0.023
95	0.249	0.319	0.06	0.218	0.321	0.028	0.357	0.273	0.005
140	0.065	0.283	0.008	0.101	0.225	-0.002	0.096	0.231	0.013
185	0.027	0.269	-0.021	0.023	0.265	-0.002	0.283	1.079	0.047
230	0.009	0.301	-0.023	0.011	0.244	-0.056	0.008	0.255	-0.025

This observation does not conflict with those of Sohbati *et al.,* (2012) or Smedley *et al.,* (2015), but indicates that although grains exposed to larger doses will exhibit larger remaining doses after a given light exposure time, the rate at which trapped charge will reach say 50% of its pre-light exposure population does not show significant variation according to prior dose in these samples. The invariable bleaching rates at each measurement temperature observed in this experiment suggest that the size of the trapped charge population neither increases nor decreases the probability

of recombination during light exposure for these samples. In this case, these data suggest that the process of trap population during irradiation is not systematic in the spatial dimension.

In the physical model of Jain & Ankjærgaard (2011), the probability of a trapped electron recombining with a luminescence centre during bleaching is suggested to be a function of distance, with the very closest luminescence centres used up by anomalous fading, and after this, electrons will preferentially recombine with the next closest luminescence centres (Section 3.2.3). Thus, the largely invariable bleaching rates at each measurement temperature observed in this experiment can be explained by the random nature of trap population when grains are exposed to ionising radiation. When traps are populated randomly during irradiation, this produces equal probability of trapped charge recombining with a luminescence centre during light exposure, regardless of the size of the trapped charge population.

3.4.1.2. Testing the dependency of bleaching rate on prior light exposure

Following the previous experiment, a second experiment was designed to explore the relationship between bleaching rate and prior light exposure. As the bleaching decay shape is not self-similar over the course of decay, in contrast to the exponential decay of the quartz OSL fast component (Jain *et al.,* 2005), it should be expected that prior light exposure makes a difference to subsequent bleaching rate. This effect would need to be accounted for in the design of accurate sediment transport models and reconstruction of transport histories.

Experimental design

Using the same MG discs and in a similar manner to Experiment 3.4.1.1, bleaching curves were measured following 10s and 32s of light exposure. At the start of each of the following cycles, samples 19121 and 20164 were subject to 177 Gy of irradiation followed by 10s of blue light bleaching 50°C and 90% diode power. After this treatment, IRSL was measured using the METx protocol after 0, 1, 10, 100, 1000 and 10000s of blue light bleaching at 50°C and 90% diode power. The signal used was between 6s and 25s with a background from between 226s and 245s subtracted.

Results and interpretation

METx IRSL response at different temperature was measured following each treatment and bleaching curves were constructed. These are displayed in Figure 3.9, fitted bleaching parameter values are shown in Table 3.5 and 3.6 for MG discs of samples 19121 and 20164 respectively. The same fitting procedure described in Experiment 3.4.1.1 was applied to these measurements. Here, once again we observe the well-documented dependency of bleaching rate on measurement

temperature (e.g. Poolton *et al.,* 2002; Buylaert *et al.*, 2012; Sohbati *et al.,* 2012; McGuire & Rhodes 2015a; 2015b; Smedley *et al.,* 2015; Zhang *et al.,* 2023). We also observe a marked decrease in bleaching rate for the IR50 and IR95 with increasing prior light exposure, and for the IR140 for sample 20164. This effect becomes less pronounced with increasing measurement temperature, likely due to expected slower bleaching rates. We also observe a consistent decrease in the fitted bleachability parameter, *a,* at all measurement temperatures, which suggests a decrease in bleaching rate with increasing light exposure for the higher measurement temperatures, but the effect is sufficiently small for these light exposure times that it is not clearly illustrated in Figure 3.9.

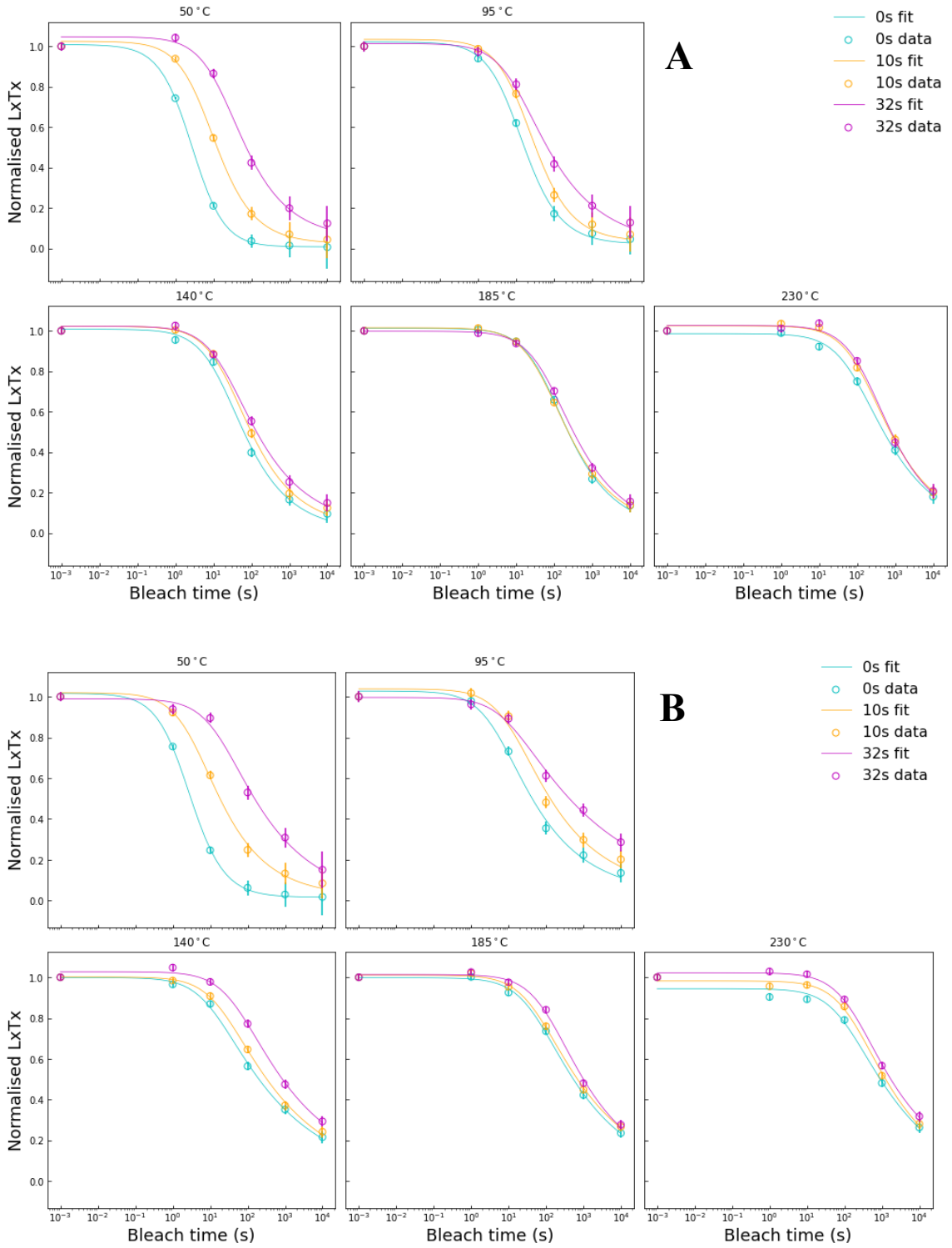

Figure 3.9. *Bleaching form after variable lengths of prior light exposure.* ***A)*** *Bleach response curve measurements and fits for sample 19121, from close to the Pico Rivera fault, California for the five METx signals. Bleach response curves were measured following 0s, 10s, and 32s to test for a dependency of bleaching rate on the size of prior dose.* ***B)*** *Bleach response curve measurements and fits for sample 20164, from Kekerengu, New Zealand for the five METx signals. Bleach response curves were measured following 706, 177 and 78 Gy to test for a dependency of bleaching rate on the size of prior dose. Errors displayed in* ***A)*** *and* ***B)*** *are derived from counting statistics.*

Table 3.5. *Estimates of bleaching parameters a , b and C for the five METx temperatures for sample 20164 from Pico Rivera, California. Bleach response curves were measured following 0, 10 and 32s of prior light exposure to test for a dependency of bleaching rate on prior light exposure. Fractional uncertainties ranged from >0.1 to 0.8 for most fits. All estimates of a and b have fractional uncertainties below 0.5, and a small number of estimates for C are close to, or greater than 1 for the 32s treatment.*

	0s			**10s**			**32s**		
Temperature (°C)	*a*	*b*	*C*	*a*	*b*	*C*	*a*	*b*	*C*
50	0.336	1.071	0.009	0.168	0.652	0.025	0.062	0.462	0.047
95	0.106	0.728	0.021	0.063	0.681	0.034	0.107	0.344	0.013
140	0.061	0.448	0.008	0.045	0.433	0.022	0.052	0.354	0.023
185	0.017	0.442	0.012	0.021	0.406	0.015	0.016	0.381	-0.002
230	0.013	0.330	-0.014	0.007	0.395	0.025	0.006	0.434	0.026

Table 3.6. *Estimates of bleaching parameters* a , b *and C for the five METx temperatures for sample 20164 from Kekerengu, New Zealand. Bleach response curves were measured following 0, 10 and 32s of prior light exposure to test for a dependency of bleaching rate on prior light exposure. Fractional uncertainties ranged from >0.1 to 0.7 for most fits. All estimates of* a *and* b *have fractional uncertainties below 0.5, and a small number of estimates for C are close to, or greater than 1 for the 32s treatment.*

	0s			**10s**			**32s**		
Temperature (°C)	*a*	*b*	*C*	*a*	*b*	*C*	*a*	*b*	*C*
50	0.427	0.866	0.016	0.278	0.405	0.019	0.062	0.286	-0.011
95	0.218	0.321	0.028	0.092	0.301	0.038	0.117	0.175	-0.004
140	0.101	0.225	-0.002	0.056	0.235	0.001	0.023	0.247	0.027
185	0.023	0.265	-0.002	0.022	0.257	0.011	0.010	0.300	0.014
230	0.011	0.244	-0.056	0.007	0.293	-0.018	0.006	0.296	0.022

The reduction in bleaching rate with increasing partial bleaching extent is expected to be related to the changing radial density of luminescence centres caused by removal of trapped charge. As previously mentioned, according to the model of Jain & Ankjærgaard (2011) (Section 3.2.3), the probability of trapped charge moving to a luminescence centre during the bleaching process has a predictable relationship with distance. In this view, trapped charge is transported to the most proximal recombination centres during an event of light exposure. As a result, charge must travel

greater distances as the duration of light exposure increases. These data are consistent with this element of Jain & Ankjærgaard's (2011) model, and suggests bleaching rate during a given light exposure event will vary as a function of the extent of prior bleaching.

3.4.1.3. Single grain bleaching as a function of past light exposure

This experiment was designed to further explore the effect of prior light exposure on bleaching rate of the higher temperature signals using longer prior bleaching times. Single grains were measured to determine the variability of this effect between grains. Here, decay rate was measured following 10, 32, 100, 320, 1000 and 3200s of blue light exposure.

Experimental design

Bleaching curves constructed following 177 Gy irradiation in Experiment 3.4.1.1 were treated as a measure of bleaching rate at 0s of light exposure. A sample with lab code 22183 from the active channel of Allt Dubhaig, Scotland was subject to 177 Gy of irradiation followed by 10s of blue light bleaching 51°C and 90% diode power. After this treatment, IRSL was measured using the METx protocol after 0, 1, 10, 100, 1000 and 10,000s of blue light bleaching at 50°C and 90% diode power. This procedure was repeated for 32, 100, 320 and 1000 seconds of initial blue light bleaching prior to bleaching curve measurements.

Results and interpretation

The decays of individual grains for each MET-IRSL signal are shown in Figure 3.10. The reduction in decay rate with increasing prior light exposure is observable at for the IR185 and IR230 signal, as well as the lower temperature METx signals, for the longer light exposure times of 100, 320, and 1000 seconds.

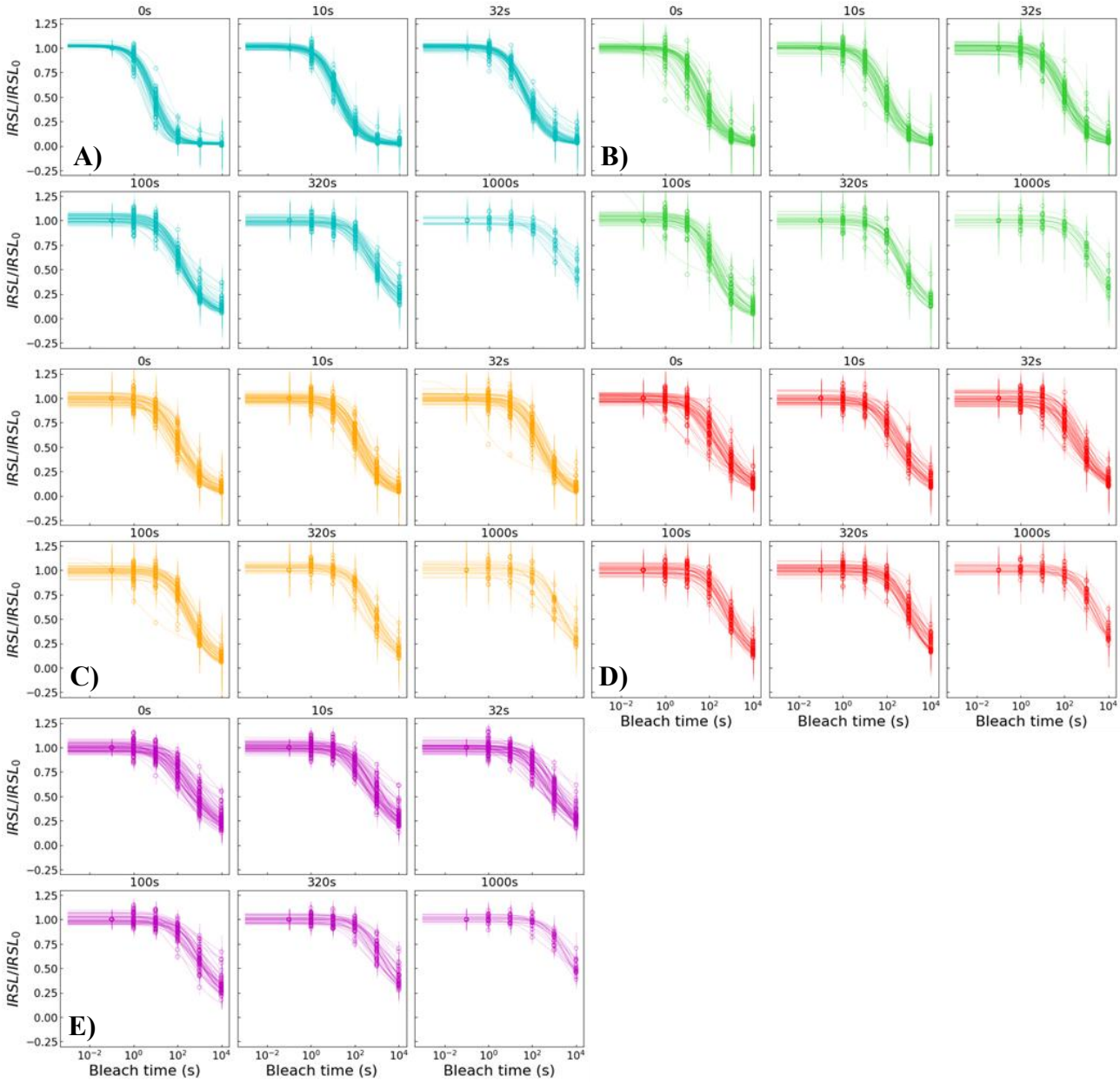

Figure 3.10. *Single grain METx bleach response curve measurements for two 100 grain discs of sample with lab code 22183. All grains with fractional measurement errors below 50% are shown here.* ***A)*** *IR50 (blue),* ***B)*** *IR95 (green),* ***C)*** *IR140 (orange),* ***D)*** *IR185 (red),* ***E)*** *IR230 (purple). In* ***A-E****, each of the six subplots contain signal response and fit for individual grains after different lengths of prior light exposure. Prior light exposure times were 0, 10, 32, 100, 320 and 1000 seconds.*

For the IR185 and IR230, a reduction in bleaching rate is clearly observable after 1000s of prior light exposure. This is further illustrated by the notable decrease in estimated values of parameter *b*, shown in Figure 3.11 below.

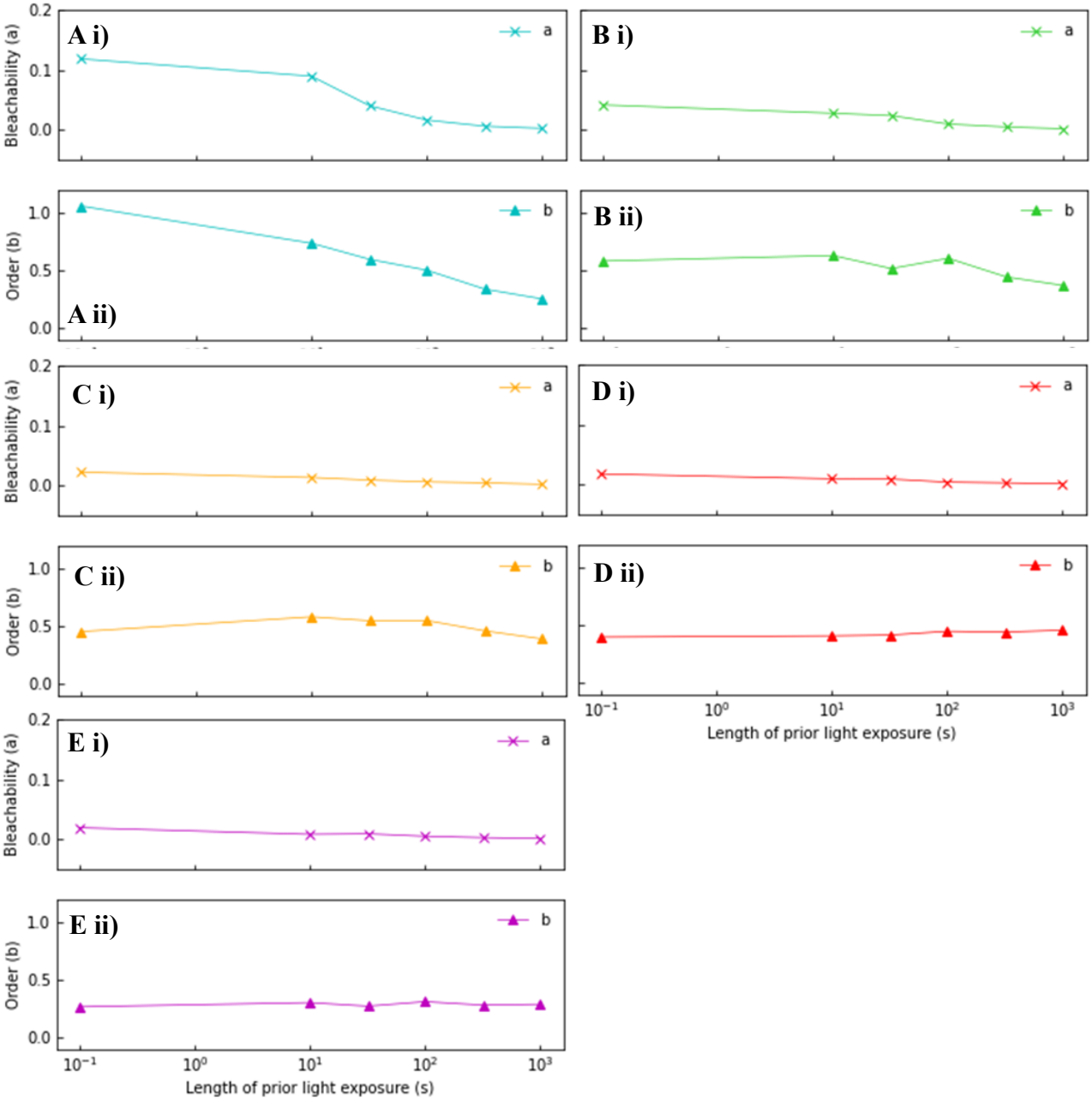

Figure 3.11. *Median a and b calculated from the single grain fits shown in* ***Figure 3.10.*** *for sample with lab code 22183, plotted with length of light exposure prior to bleach response curve measurement.* ***A)*** *IR50 (blue),* ***B)*** *IR95 (green),* ***C)*** *IR140 (orange),* ***D)*** *IR185 (red),* ***E)*** *IR230 (purple). Subplots* ***i)*** *display a plotted with length of prior light exposure, subplots* ***ii)*** *display b plotted with length of prior light exposure.*

For the IR50 and IR140, a reduction in both *a* and *b* with increasing prior light exposure are observed. For the higher temperature signals, there is a slight reduction in *a* with increasing light exposure, but very little variability in estimates of *b*. According to Poolton *et al*., (2009), *a* contains information on the luminescence properties of a material that affect bleachability. The results presented here suggest it is possible *a* also contains information on light exposure history, and that we may be able to determine prior light exposure for individual grains.

3.4.1.4. Testing the dependency of bleaching rate on light source wavelength

A brief introductory outline and discussion of the following experiment can be found in Rhodes *et al.,* (2024). To explore bleaching rate dependency on wavelength of bleaching light source, multiple grain aliquots were constructed from laboratory standard samples. An orthoclase sample called MJ39 was used to explore the effects on K-feldspar (Lawson *et al.,* 2015; Daniels *et al.,* 2016). Based on the findings of Berger (1990), that predominantly green and amber light is transmitted a depth under water, the dependency and direction of the relationship between bleaching rate and source wavelength (λ) is of significance for understanding IRSL behaviour in grains that have spent time in marine or fluvial systems.

Experimental design

Two MG grain aliquots of sample MJ39 were prepared in light conditions. For this reason, a METx hot bleach was first administered followed by a dose of ~144 Gy. The METx protocol was used with 90% optical power, with MET-IRSL measurements adjusted to 24s, signal used was 0.6-2.5s minus 22.5-24.6s. This was repeated with exposure times of 1, 10, 100, 1000, 10000s using blue, green, and IR diodes (wavelength emission at 470 nm, 525 nm and 870 nm respectively) at 50°C, 90% power prior to METx measurement. The resultant signals were corrected for sensitivity with a test dose response.

Results and interpretation

Bleach response curves fitted to data are shown in Figure 3.12, and estimates of *a*, *b*, and *C* are shown in Table 3.7. Figure 3.12 shows that the higher frequency blue light reduces METx signals at a considerably faster rate than green and IR, reducing even the hardest to bleach 230°C signal to a few percent of its initial response (Figure 3.12). Green light bleaching is much slower for this sample, with greater differences in decay rate between METx signals (approximately an order of magnitude compared to half an order of magnitude for blue light) (Figure 3.12). Infrared bleaching appears to be more efficient that green light for the IR50 and IR95, especially in the early stages of decay. However, IR is much less efficient than blue and green light for the higher temperature signals (Figure 3.12). For example, after 10,000s of IR exposure, the IR230 signal reaches only ~70% of its initial intensity, whereas for 10 000s of blue and green light exposure, the IR230 reaches ~10% and 50% respectively.

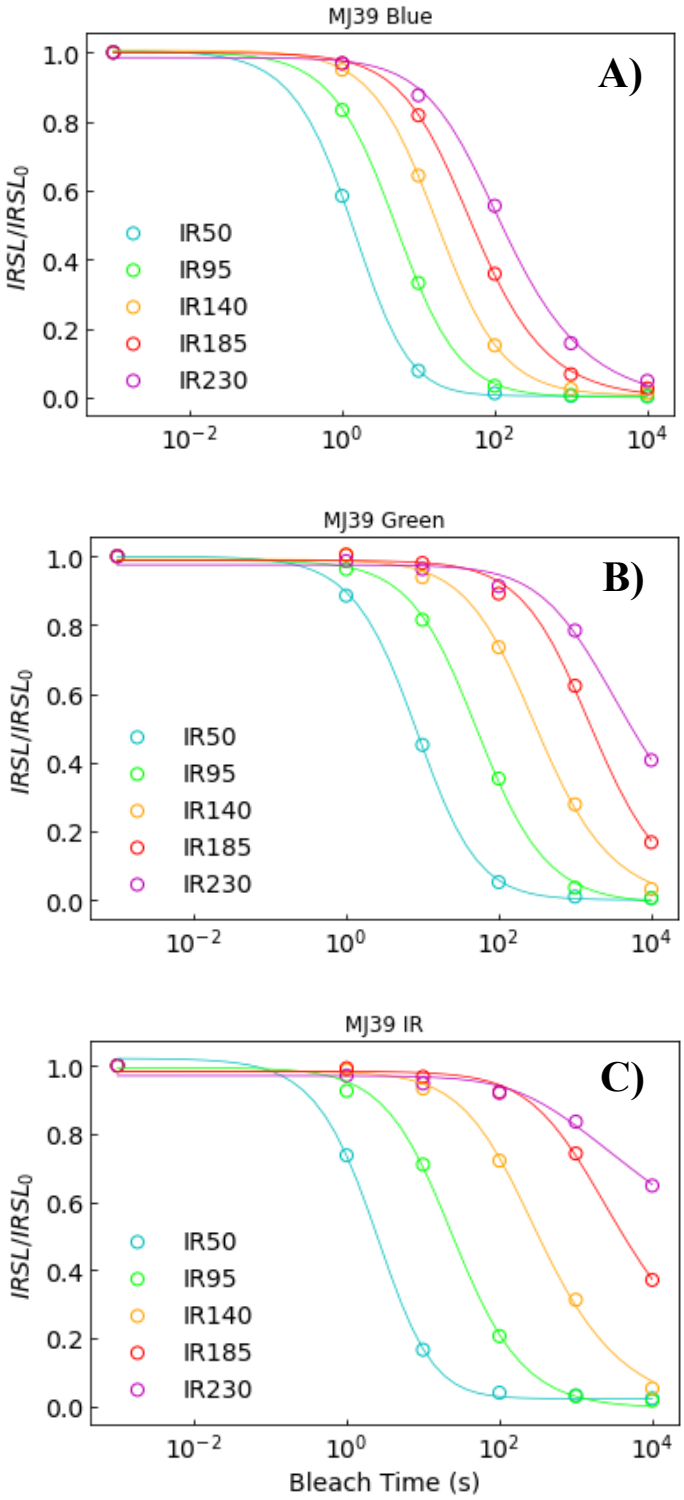

Figure 3.12. *Full order of magnitude bleach response curve measurements and fits for sample MJ39 for all five METx signals.* ***A)*** *Blue light bleaching.* ***B)*** *Green light bleaching.* ***C)*** *Infrared bleaching.* *Note the unbleached signal (time=0) is plotted at 0.001.*

Table 3.7*. Estimates of METx bleaching parameters a , b and C for sample MJ39 for blue, green, and infrared light exposure*

	Blue			**Green**			**IR**		
Temperature (°C)	*a*	*b*	*C*	*a*	*b*	*C*	*a*	*b*	*C*
50	0.404	1.609	0.004	0.168	0.091	-0.001	0.239	1.573	0.021
95	0.174	1.109	>0.001	0.063	0.022	-0.012	0.049	0.861	-0.006
140	0.056	1.016	0.005	0.045	0.005	-0.010	0.007	0.574	-0.017
185	0.031	0.736	-0.002	0.021	>0.001	-0.012	0.001	0.375	-0.017
230	0.018	0.573	-0.02	0.007	>0.001	-0.025	0.003	0.109	-0.030

The relative increase in efficiency of IR bleaching for the lower temperature signals is attributed to the effect of resonance between electrons in IR-sensitive traps and photons travelling in the IR range (Hütt *et al.,* 1988). From these results, it is possible to expect a reduction in bleaching rate for all five METx signals in subaqueous conditions, due to the preferential transmission of the green and amber ranges.

3.4.1.5. Testing dependency of bleaching rate on prior light exposure for bleaching at different wavelengths

This experiment explores the effect of prior light exposure on bleaching rates for different wavelengths of bleaching source. Based on the results of experiment 3.4.1.1.2 and 3.1.4.4, this is an important effect to constrain for the construction of accurate luminescence-based sediment transport models and sediment tracing tools. Like the previous experiment, an introductory discussion of this experiment is described in Rhodes *et al.,* (2024).

Methods

Short shine IR50 measurements were made on a MG disc from sample 22094 from the Lowe intrusion in the San Gabriel Mountains, California. First, the signal was reset using a METx hot bleach, then a dose of 8Gy was applied, followed by a preheat of 170 ◦C for 60s. Alternating measurements of 0.1s IR50 short shines (90% illumination power) and 1.0s blue LED exposures (90% illumination, 50 ◦C) were made for 20 cycles. The procedure was repeated, but with a 10s blue bleach after the 8Gy dose, and prior to the preheat and first 0.1s IR50 short shine. This was to put the sample in a partially bleached state. This entire process was repeated but with replacing the 10.0s of blue light bleaching with 10.0s of green light bleaching and 10.0s of IR bleaching. All

SSIR50 measurements were corrected for the loss of signal from the short shines themselves, although this is a minor effect.

Results and interpretation

The unbleached responses of the SSIR50 shows a similar effect to that observed in Experiment 3.4.1.4, with increasing bleaching rate with decreasing wavelength of the light source (Figure 3.13, black data points). A slower initial unbleached decay of the SSIR50 for green light bleaching compared to IR bleaching was observed, much like in experiment 3.4.1.4.

For blue, green and IR bleaching there is a notable decrease in the bleaching rate of the SSIR50 signal after 10s of prior light exposure. The grey data points in Figure 3.13 are the unbleached data (lighter colours) shifted up the x-axis by 10 units (s) to simulate prior light exposure; note the similarity to the partially bleached data that really was partially bleached for 10s. The impact of prior blue light exposure on subsequent decay rate is much more pronounced than that of green light or IR. The form of the green SSIR50 decay is much closer to the form of the IR decay than the blue, which is also what we observe in Experiment 3.4.1.4. This suggests that blue light is very efficient at using up close luminescence centres with just 10s of exposure, altering the radial density to reduce the bleachability of the material, whereas the lower energy green and infrared light do not alter the radial density of luminescence centres quite so significantly after 10s of exposure, thereby the probability of recombination remains closer to that of the material in an unbleached state.

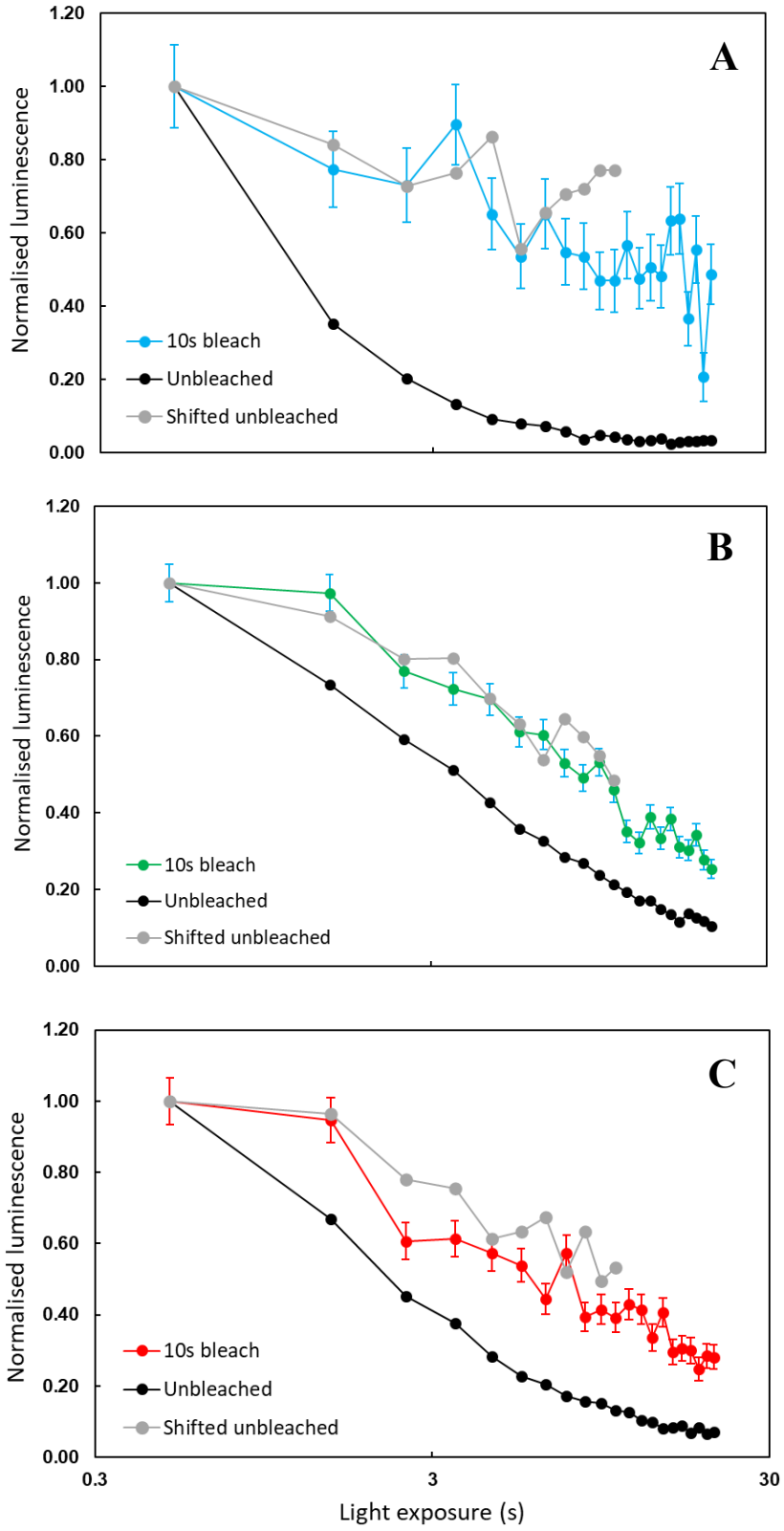

Figure 3.13. *Alternating measurements of 0.1s IR50 short shines (90% power) and 1.0s blue LED exposures (90% power, 50 ◦C) for 20 cycles using sample 22093 from the Lowe intrusion in the San Gabriel Mountains, California. Each data point represents the short shine IR50 response. Black markers represent unbleached short shines, grey markers represent the unbleached data shifted by 10s, coloured markers represent short shine signals with 10s of prior bleaching.* ***A)*** *Blue light bleaching.* ***B)*** *Green light bleaching.* ***C)*** *Infrared bleaching.*

3.1.4.6. Estimating degree of thermal transfer from light insensitive traps to light-sensitive traps for different preheat temperatures

To have a robust understanding of bleaching in nature, it is necessary to quantitatively constrain the degree of control exerted by protocol effects, notably preheat temperature, on bleaching rates measured in the laboratory. Other studies report decreasing decay rate with increasing preheat and measurement temperature (e.g. Zhang *et al.,* 2023; Li and Li, 2011; Lowick et al., 2012; Colarossi et al., 2015; Reimann et al., 2015). Zhang *et al.* (2023) suggest that this effect is at least in part due to thermal transfer of charge to traps targeted by the measurement temperature from traps that are not of interest. If this effect is real, it must be quantified to understand its impact on measurements made using SAR protocol, since this suggests there is a possibility of an 'artificial' signal contribution from prior SAR cycles to the signal of subsequent cycles in addition to the given dose.

An additional dilemma presented here for sediment transport applications of IRSL is such that it is not possible to measure the luminescence behaviour of grains as would occur in nature, without subjecting those grains to a series of laboratory treatments, such as preheats, hot bleaches, and repeated irradiation, which can alter the signal measured.

Methods

A series of short shine IR50 (SSIR50) measurements at 90% diode power for 0.1s were made on MG aliquots for sample 22093 the Lowe intrusion in the San Gabriel mountains, California. These measurements were made following a hot bleach and ~177 Gy irradiation. Each cycle was comprised of 14 short shine measurements with a 40s measurement of IRSL decay followed by a hot bleach at 290˚C for 400 seconds at 90% power to reset the signal. After the first measurement, aliquots were subject to a 60s 250°C preheat every 2nd short shine. Each cycle was paired with another identical cycle apart from the addition of blue light bleaching between short shine measurements. SSIR50 was measured following blue LED exposure at 0.32, 1.0, 3.2, 10, 32 s at 90% optical power. This was repeated using a 150°C and zero preheat. Two pairs of cycles were measured for each preheat temperature, or lack thereof. Fractional loss as a result of the short shine measurement itself was calculated at each step and data was adjusted to ensure the loss of signal following light exposure was not overestimated. This protocol is slightly unusual, so is probably better understood by looking at Table 3.8.

Table 3.8. *Full protocol for Experiment 3.4.6.1 designed to estimate the degree of thermal transfer from light insensitive traps to light-sensitive traps for different preheat temperatures.*

250°C preheat				150°C preheat				Zero preheat			
1	**2**	**3**	**4**	**5**	**6**	**7**	**8**	**9**	**10**	**11**	**12**
Beta dose	Beta dose	Beta dose	Beta dose	Beta dose	Beta dose	Beta dose	Beta dose	Beta dose	Beta dose	Beta dose	Beta dose
IRSL 50°C 0.1s 90%	IRSL 50°C 0.1s 90%	IRSL 50°C 0.1s 90%	IRSL 50°C 0.1s 90%	IRSL 50°C 0.1s 90%	IRSL 50°C 0.1s 90%	IRSL 50°C 0.1s 90%	IRSL 50°C 0.1s 90%	IRSL 50°C 0.1s 90%	IRSL 50°C 0.1s 90%	IRSL 50°C 0.1s 90%	IRSL 50°C 0.1s 90%
Preheat 60s 250°C 5°Cs^{-1}	Preheat 60s 250°C 5°Cs^{-1}	Preheat 60s 250°C 5°Cs^{-1}	Preheat 60s 250°C 5°Cs^{-1}	Preheat 60s 150°C 5°Cs^{-1}	Preheat 60s 150°C 5°Cs^{-1}	Preheat 60s 150°C 5°Cs^{-1}	Preheat 60s 150°C 5°Cs^{-1}				
IRSL 50°C 0.1s 90%	IRSL 50°C 0.1s 90%	IRSL 50°C 0.1s 90%	IRSL 50°C 0.1s 90%	IRSL 50°C 0.1s 90%	IRSL 50°C 0.1s 90%	IRSL 50°C 0.1s 90%	IRSL 50°C 0.1s 90%	IRSL 50°C 0.1s 90%	IRSL 50°C 0.1s 90%	IRSL 50°C 0.1s 90%	IRSL 50°C 0.1s 90%
	Blue bleach 0.1s 51°C		**Blue bleach 0.1s 51°C**		**Blue bleach 0.1s 51°C**		**Blue bleach 0.1s 51°C**		**Blue bleach 0.1s 51°C**		**Blue bleach 0.1s 51°C**
IRSL 50°C 0.1s 90%	IRSL 50°C 0.1s 90%	IRSL 50°C 0.1s 90%	IRSL 50°C 0.1s 90%	IRSL 50°C 0.1s 90%	IRSL 50°C 0.1s 90%	IRSL 50°C 0.1s 90%	IRSL 50°C 0.1s 90%	IRSL 50°C 0.1s 90%	IRSL 50°C 0.1s 90%	IRSL 50°C 0.1s 90%	IRSL 50°C 0.1s 90%
Preheat 60s 250°C 5°Cs^{-1}	Preheat 60s 250°C 5°Cs^{-1}	Preheat 60s 250°C 5°Cs^{-1}	Preheat 60s 250°C 5°Cs^{-1}	Preheat 60s 150°C 5°Cs^{-1}	Preheat 60s 150°C 5°Cs^{-1}	Preheat 60s 150°C 5°Cs^{-1}	Preheat 60s 150°C 5°Cs^{-1}				
IRSL 50°C 0.1s 90%	IRSL 50°C 0.1s 90%	IRSL 50°C 0.1s 90%	IRSL 50°C 0.1s 90%	IRSL 50°C 0.1s 90%	IRSL 50°C 0.1s 90%	IRSL 50°C 0.1s 90%	IRSL 50°C 0.1s 90%	IRSL 50°C 0.1s 90%	IRSL 50°C 0.1s 90%	IRSL 50°C 0.1s 90%	IRSL 50°C 0.1s 90%
	Blue bleach 0.32s 51°C		**Blue bleach 0.32s 51°C**		**Blue bleach 0.32s 51°C**		**Blue bleach 0.32s 51°C**		**Blue bleach 0.32s 51°C**		**Blue bleach 0.32s 51°C**
IRSL 50°C 0.1s 90%	IRSL 50°C 0.1s 90%	IRSL 50°C 0.1s 90%	IRSL 50°C 0.1s 90%	IRSL 50°C 0.1s 90%	IRSL 50°C 0.1s 90%	IRSL 50°C 0.1s 90%	IRSL 50°C 0.1s 90%	IRSL 50°C 0.1s 90%	IRSL 50°C 0.1s 90%	IRSL 50°C 0.1s 90%	IRSL 50°C 0.1s 90%
Preheat 60s 250°C 5°Cs^{-1}	Preheat 60s 250°C 5°Cs^{-1}	Preheat 60s 250°C 5°Cs^{-1}	Preheat 60s 250°C 5°Cs^{-1}	Preheat 60s 150°C 5°Cs^{-1}	Preheat 60s 150°C 5°Cs^{-1}	Preheat 60s 150°C 5°Cs^{-1}	Preheat 60s 150°C 5°Cs^{-1}				
IRSL 50°C 0.1s 90%	IRSL 50°C 0.1s 90%	IRSL 50°C 0.1s 90%	IRSL 50°C 0.1s 90%	IRSL 50°C 0.1s 90%	IRSL 50°C 0.1s 90%	IRSL 50°C 0.1s 90%	IRSL 50°C 0.1s 90%	IRSL 50°C 0.1s 90%	IRSL 50°C 0.1s 90%	IRSL 50°C 0.1s 90%	IRSL 50°C 0.1s 90%
	Blue bleach 1.0s 51°C		**Blue bleach 1.0s 51°C**		**Blue bleach 1.0s 51°C**		**Blue bleach 1.0s 51°C**		**Blue bleach 1.0s 51°C**		**Blue bleach 1.0s 51°C**
IRSL 50°C 0.1s 90%	IRSL 50°C 0.1s 90%	IRSL 50°C 0.1s 90%	IRSL 50°C 0.1s 90%	IRSL 50°C 0.1s 90%	IRSL 50°C 0.1s 90%	IRSL 50°C 0.1s 90%	IRSL 50°C 0.1s 90%	IRSL 50°C 0.1s 90%	IRSL 50°C 0.1s 90%	IRSL 50°C 0.1s 90%	IRSL 50°C 0.1s 90%
Preheat 60s 250°C 5°Cs^{-1}	Preheat 60s 250°C 5°Cs^{-1}	Preheat 60s 250°C 5°Cs^{-1}	Preheat 60s 250°C 5°Cs^{-1}	Preheat 60s 150°C 5°Cs^{-1}	Preheat 60s 150°C 5°Cs^{-1}	Preheat 60s 150°C 5°Cs^{-1}	Preheat 60s 150°C 5°Cs^{-1}				
IRSL 50°C 0.1s 90%	IRSL 50°C 0.1s 90%	IRSL 50°C 0.1s 90%	IRSL 50°C 0.1s 90%	IRSL 50°C 0.1s 90%	IRSL 50°C 0.1s 90%	IRSL 50°C 0.1s 90%	IRSL 50°C 0.1s 90%	IRSL 50°C 0.1s 90%	IRSL 50°C 0.1s 90%	IRSL 50°C 0.1s 90%	IRSL 50°C 0.1s 90%
	Blue bleach 3.2s 51°C		**Blue bleach 3.2s 51°C**		**Blue bleach 3.2s 51°C**		**Blue bleach 3.2s 51°C**		**Blue bleach 3.2s 51°C**		**Blue bleach 3.2s 51°C**
IRSL 50°C 0.1s 90%	IRSL 50°C 0.1s 90%	IRSL 50°C 0.1s 90%	IRSL 50°C 0.1s 90%	IRSL 50°C 0.1s 90%	IRSL 50°C 0.1s 90%	IRSL 50°C 0.1s 90%	IRSL 50°C 0.1s 90%	IRSL 50°C 0.1s 90%	IRSL 50°C 0.1s 90%	IRSL 50°C 0.1s 90%	IRSL 50°C 0.1s 90%
Preheat 60s 250°C 5°Cs^{-1}	Preheat 60s 250°C 5°Cs^{-1}	Preheat 60s 250°C 5°Cs^{-1}	Preheat 60s 250°C 5°Cs^{-1}	Preheat 60s 150°C 5°Cs^{-1}	Preheat 60s 150°C 5°Cs^{-1}	Preheat 60s 150°C 5°Cs^{-1}	Preheat 60s 150°C 5°Cs^{-1}				
IRSL 50°C 0.1s 90%	IRSL 50°C 0.1s 90%	IRSL 50°C 0.1s 90%	IRSL 50°C 0.1s 90%	IRSL 50°C 0.1s 90%	IRSL 50°C 0.1s 90%	IRSL 50°C 0.1s 90%	IRSL 50°C 0.1s 90%	IRSL 50°C 0.1s 90%	IRSL 50°C 0.1s 90%	IRSL 50°C 0.1s 90%	IRSL 50°C 0.1s 90%
	Blue bleach 10s 51°C		**Blue bleach 10s 51°C**		**Blue bleach 10s 51°C**		**Blue bleach 10s 51°C**		**Blue bleach 10s 51°C**		**Blue bleach 10s 51°C**
IRSL 50°C 0.1s 90%	IRSL 50°C 0.1s 90%	IRSL 50°C 0.1s 90%	IRSL 50°C 0.1s 90%	IRSL 50°C 0.1s 90%	IRSL 50°C 0.1s 90%	IRSL 50°C 0.1s 90%	IRSL 50°C 0.1s 90%	IRSL 50°C 0.1s 90%	IRSL 50°C 0.1s 90%	IRSL 50°C 0.1s 90%	IRSL 50°C 0.1s 90%
Preheat 60s 250°C 5°Cs^{-1}	Preheat 60s 250°C 5°Cs^{-1}	Preheat 60s 250°C 5°Cs^{-1}	Preheat 60s 250°C 5°Cs^{-1}	Preheat 60s 150°C 5°Cs^{-1}	Preheat 60s 150°C 5°Cs^{-1}	Preheat 60s 150°C 5°Cs^{-1}	Preheat 60s 150°C 5°Cs^{-1}				

IRSL 50°C 0.1s 90%	IRSL 50°C 0.1s 90%	IRSL 50°C 0.1s 90%	IRSL 50°C 0.1s 90%	IRSL 50°C 0.1s 90%	IRSL 50°C 0.1s 90%	IRSL 50°C 0.1s 90%	IRSL 50°C 0.1s 90%	IRSL 50°C 0.1s 90%	IRSL 50°C 0.1s 90%	IRSL 50°C 0.1s 90%	IRSL 50°C 0.1s 90%
	Blue bleach 32s 51°C		**Blue bleach 32s 51°C**		**Blue bleach 32s 51°C**		**Blue bleach 32s 51°C**		**Blue bleach 32s 51°C**		**Blue bleach 32s 51°C**
IRSL 50°C 0.1s 90%	IRSL 50°C 0.1s 90%	IRSL 50°C 0.1s 90%	IRSL 50°C 0.1s 90%	IRSL 50°C 0.1s 90%	IRSL 50°C 0.1s 90%	IRSL 50°C 0.1s 90%	IRSL 50°C 0.1s 90%	IRSL 50°C 0.1s 90%	IRSL 50°C 0.1s 90%	IRSL 50°C 0.1s 90%	IRSL 50°C 0.1s 90%
Preheat 60s 250°C 5°Cs^{-1}	Preheat 60s 250°C 5°Cs^{-1}	Preheat 60s 250°C 5°Cs^{-1}	Preheat 60s 250°C 5°Cs^{-1}	Preheat 60s 150°C 5°Cs^{-1}	Preheat 60s 150°C 5°Cs^{-1}	Preheat 60s 150°C 5°Cs^{-1}	Preheat 60s 150°C 5°Cs^{-1}				
IRSL 50°C 0.1s 90%	IRSL 50°C 0.1s 90%	IRSL 50°C 0.1s 90%	IRSL 50°C 0.1s 90%	IRSL 50°C 0.1s 90%	IRSL 50°C 0.1s 90%	IRSL 50°C 0.1s 90%	IRSL 50°C 0.1s 90%	IRSL 50°C 0.1s 90%	IRSL 50°C 0.1s 90%	IRSL 50°C 0.1s 90%	IRSL 50°C 0.1s 90%
IRSL hot bleach 290°C 40s 90%	IRSL hot bleach 290°C 40s 90%	IRSL hot bleach 290°C 40s 90%	IRSL hot bleach 290°C 40s 90%	IRSL hot bleach 290°C 40s 90%	IRSL hot bleach 290°C 40s 90%	IRSL hot bleach 290°C 40s 90%	IRSL hot bleach 290°C 40s 90%	IRSL hot bleach 290°C 40s 90%	IRSL hot bleach 290°C 40s 90%	IRSL hot bleach 290°C 40s 90%	IRSL hot bleach 290°C 40s 90%

Results and interpretation

Bleaching rates measured with following different preheats temperatures do not exhibit significant variation (Figure 3.14). Thermal transfer of charge during the preheat does not significantly affect the percentage of IR50 signal lost through blue light bleaching for this sample (Figure 3.14).

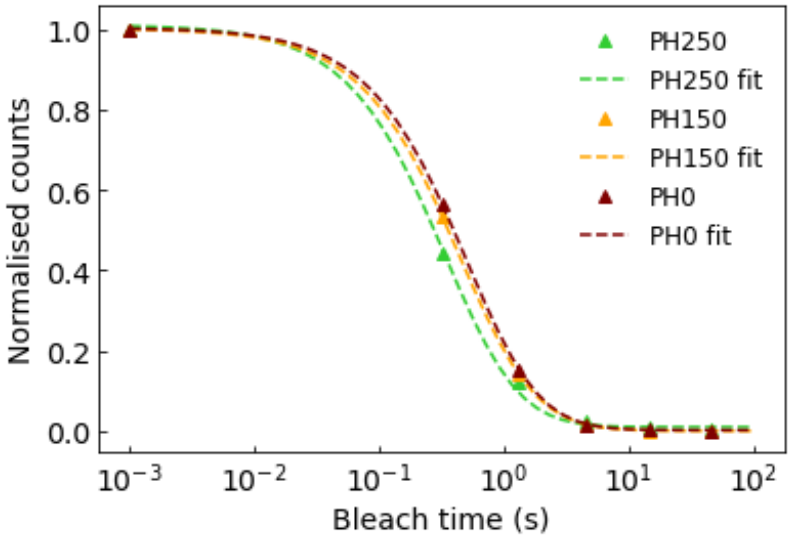

Figure 3.14. *IR50 short shine blue light bleaching measurements following different preheat temperatures with fits using the bleaching function of Bailiff & Barnett (1994).*

The results of experiment 3.4.1.2 and the charge transport model of Jain & Ankjærgaard (2011) suggests that increasing preheat temperatures may remove unstable trapped charge at increasing radial distance from luminescence centres, or at unstable depths below the conduction band. However, for the IR50 signal, different preheat temperatures do not produce significant variation in bleaching rate. Whether thermal transfer affects IRSL decay rate at higher measurements is difficult to test with short shine measurements due to the need for longer prior bleaching times of these signals. This remains an important question to answer in future work.

3.4.2. Light exposure recovery

This experiment aims to explore what are the optimal techniques for reconstructing light exposure history to inform the design of IRSL-based tools to infer past and present sediment transport dynamics in the natural environment. Specifically, the following experiments aim to demonstrate the utility of single grain measurements for estimating past light exposure through bleach recovery by providing the opportunity to assess the range of individual values. First, as outlined by Rhodes *et al.* (2024), consider a single grain the smallest possible unit of burial and bleaching history. Different parts of the grain may have different luminescence properties such as density of traps or recombination centres, but the entire grain shares the same dose, light exposure, and thermal history. Much like characteristics relating to growth and sensitivity, a high degree of variation in bleaching properties is observed between grains from the same sample (Figure 3.15 for a METx example and Figure 3.16 for a ILT-3ET example). Based on experiment results, the following section proposes an approach to quantify and utilise this variability to recover length of past light exposure and to improve the accuracy of IRSL-based sediment transport models. An additional benefit of single grain measurements for sediment transport applications is the potential to reconstruct multiple light exposure histories within a single sample, which could reflect the range of lateral inputs and the various pathways grains take on as they pass through a given system.

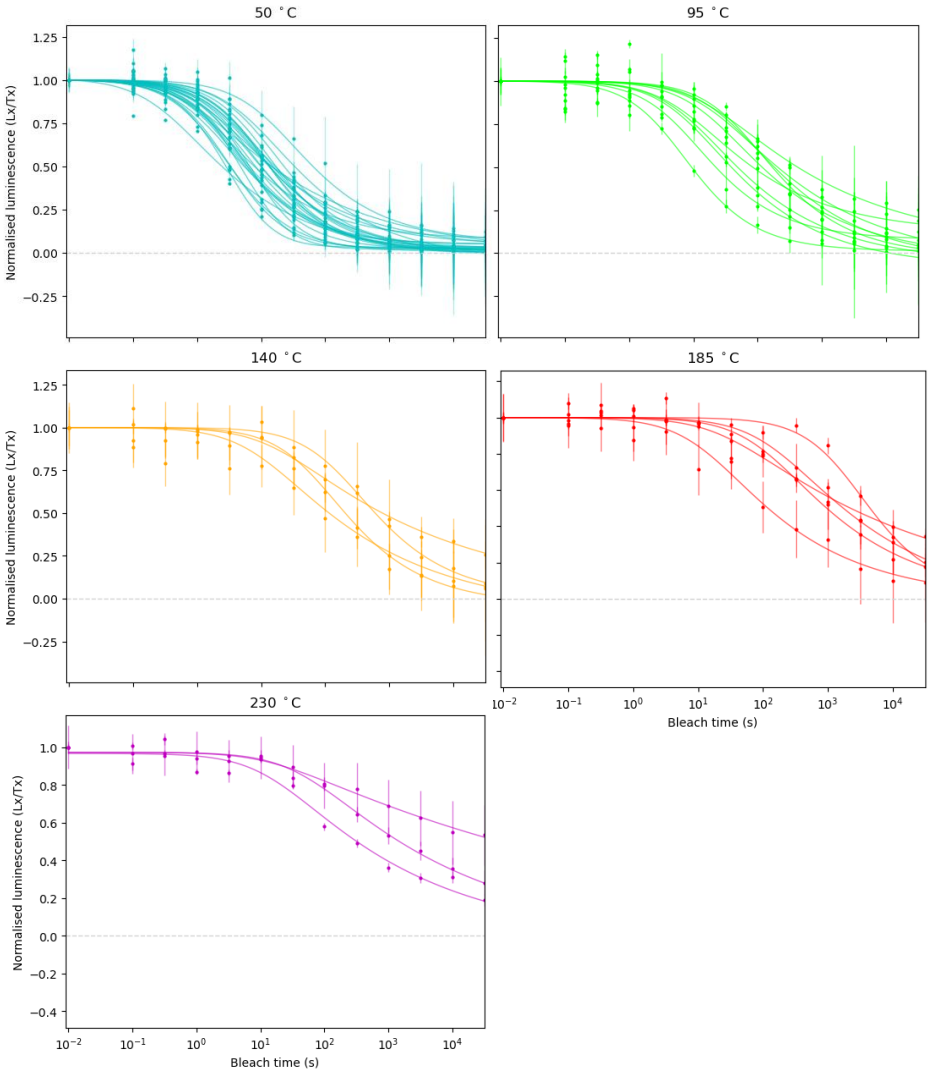

Figure 3.15. *METx bleaching measurements and fits of two discs of sample L0620 from the Solimões River. IRSL intensity was measured after 0.1, 0.32, 1.0, 3.2, 10, 32, 100, 3200, 10,000, and 100,000 seconds of blue light exposure. Fitting was performed to normalised intensity using a Levenberg-Marquardt algorithm to find optimised parameter values. All fits shown here returned parameter estimates with a fractional uncertainty below 0.5. Note the high degree of variability in bleaching characteristics between grains.*

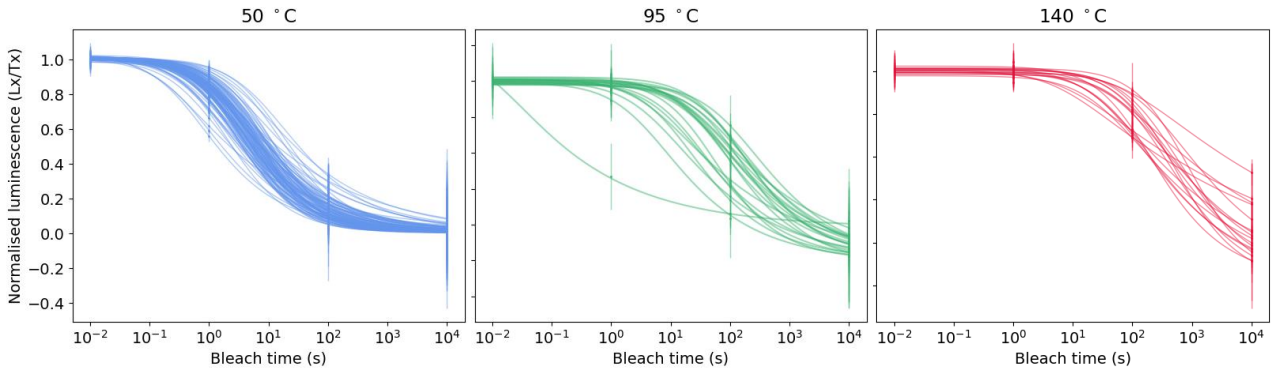

Figure 3.16. *ILT-3ET bleaching measurements and fits of two discs of sample 22183 from the Allt Dubhaig. IRSL intensity was measured after three blue light exposure times, which were 1.0, 100, and 10,000 seconds. The high number of results demonstrates the efficacy of measuring just three points to construct a bleach response curve. Fitting was performed to normalised intensity using a Levenberg-Marquardt algorithm to find optimised parameter values. All fits shown here returned parameter estimates with a fractional uncertainty below 0.5. Note the high degree of variability in bleaching characteristics between grains.*

Here, optimal methods for recovering a known bleach time given the signals and fitted parameters are assessed for individual grains using Eq. 1.3 in terms of t (Eq. 2.1).

$$t = \frac{1}{a}\left[\frac{\mathrm{I}_0}{I - C}\right]^{\frac{1}{b}} - 1 \tag{2.1}$$

where t is time, I is intensity, I_0 is intensity when $t = 0$, a is a bleachability parameter, b is the order of the kinetic reaction, and C is the non-bleachable component.

Methods

Two discs of single grans from sample 22183 taken from the active channel of the Allt Dubhaig were measured using the ILT-3ET protocol to determine growth parameters and blue light bleaching parameters using the method outlined in Section 3.3.1. The measurements and results of these fits are shown above in Figure 3.16. This protocol measured just three point growth curves and three point bleaching response curves; this shortened protocol saves a significant amount of machine time, and the bleach fits in Figure 3.16 demonstrate this is highly effective. Next, the grains were reset with a hot bleach and then given a dose of 51Gy followed by measurement of ILT-3ET response to this dose. This step was then repeated with 34s of blue light exposure after the 51Gy dose and prior to the preheat.

Only grains with a fractional measurement uncertainty below 0.5 and fractional uncertainties on fitted values of a and b below 0.5 were included in bleach time recovery procedure. The 34s bleach time was then recovered using the bleached signal as a fraction of the unbleached signal using three different approaches (A-C):

A. Calculating an unweighted average *a*, *b,* and *C* value using the fitted *a*, *b,* and *C* values from all grains. For each grain, substituting these average values in Eq. 2.1, where *I* is the measured intensity after 32s blue light exposure as a fraction of the unbleached signal to return *t* for each grain. An unweighted average is calculated using *t* values estimated for all grains.
B. Inserting the individually fitted *a*, *b,* and *C* values for each grain into Eq. 2.1, where *I* is the measured intensity after 32s blue light exposure as a fraction of the unbleached signal to return *t* for each grain. An unweighted average is calculated using *t* values estimated for all grains.
C. Inserting the individually fitted *a*, *b,* and *C* values for each grain into Eq. 2.1, where *I* is the measured intensity after 32s blue light exposure as a fraction of the unbleached signal to return *t* for each grain, in the same manner as approach B. Calculate a weighted average by weight each value of *t* by its uncertainty.

For approach B and C, uncertainties on *t* are calculated through propagation of measurement error uncertainty and parameter estimate uncertainty.

Results and interpretation

Each row of subplots in Figure 3.17 corresponds to a different measurement temperature (row X, Y and Z are IR50, IR95 and IR140 respectively). The left column (1) shows histograms of the sensitivity corrected IRSL response to a dose of 51 Gy (dark blue data in Figure 3.17) and 51 Gy followed by 34 seconds of blue light bleaching (light blue data in Figure 3.17). The middle and right column show recovered light exposure times, *t* using Eq. 2.1, where I_0 is the measured intensity after 32s blue light exposure as a fraction of the unbleached signal (the light blue data in Column 1 divided by the dark blue data in column (1). The middle column (2) shows histograms of recovered *t* values using unweighted average parameter values for each grain (approach A), with unweighted average *t* indicated by the blue dashed line, and the known bleach time of 34 seconds indicated by the red dashed line. The right column (3) shows results of approach B and C. Pink histograms show recovered light exposure times, *t* using the individual bleaching parameter estimates fitted for each grain. The red dashed line indicates the known light exposure time of 34 seconds, the blue dashed line indicates an unweighted average of the pink *t* values (approach B), the black dashed line indicate a weighted average of the pink *t* values, where the estimate of *t* for each grain is weighted by its uncertainty. The high dispersion visible in column (3) relative to column (2), is a product of using each grain's individual bleaching parameter values, which for some grains have low precision compared to the higher precision average values used for the recovered *t* values in column (2). Recovered *t* values estimated using approaches A-C (indicated by the dashed lines in Figure 3.17 are summarised in Table 3.9.

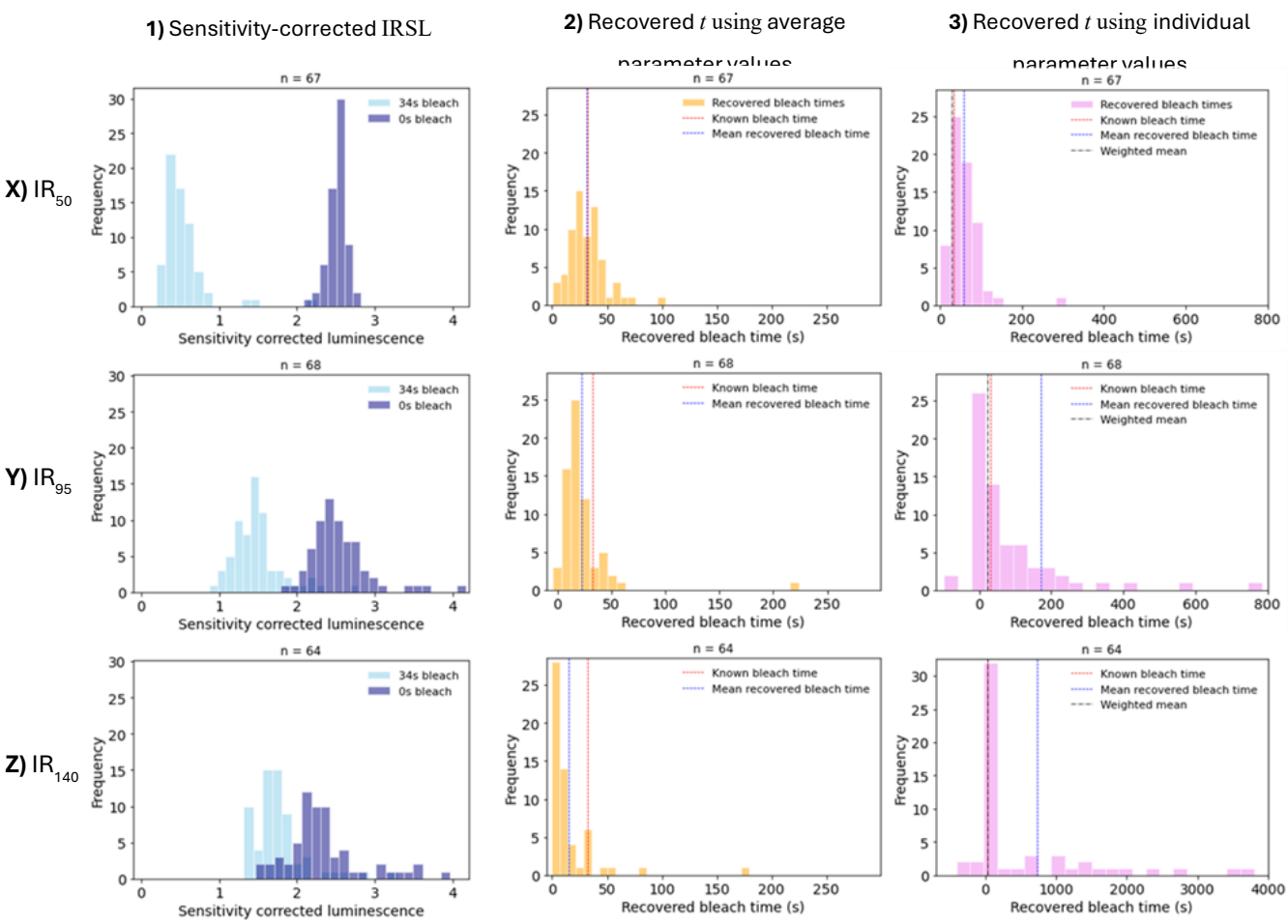

Figure 3.17. *Results from bleach recovery experiment. Column (1) shows histograms of the sensitivity corrected IRSL response to a dose of 51 Gy (dark blue) and 51 Gy followed by 34 seconds of blue light bleaching (light blue). Column (2) shows histograms of recovered t values using unweighted average parameter values for each grain (approach A), with unweighted average t indicated by the blue dashed line, and the known bleach time of 34 seconds indicated by the red dashed line. Column (3) shows results of approach B and C. Pink histograms show recovered light exposure times, t using the individual bleaching parameter estimates fitted for each grain. The red dashed line indicates the known light exposure time of 34 seconds, the blue dashed line indicates an unweighted average of the pink t values (approach B), the black dashed line indicate a weighted average of the pink t values, where the estimate of t for each grain is weighted by its uncertainty.*

Table 3.9. *Recovered t values using approaches **A-C** of a known light exposure time of 32s for each of the three ILT-3ET measurement temperatures. Approach **A** calculates an unweighted average recovered t using the same unweighted average bleaching parameter estimates for each grain. Approach **B** calculates an unweighted average t using individually fitted bleaching parameter estimates for each grain. Approach **C** calculates an average t weighted by the errors on individually recovered t, also using individually fitted parameter estimates for each grain in the same manner as approach **B**.*

Measurement temperature (˚C)	**A:** Unweighted *t* (s) [average bleaching parameters]	**B:** Unweighted *t* (s) [individual bleaching parameters]	**C:** Weighted *t* (s) [individual bleaching parameters]
50	31.46 ± 17.0	58.7 ± 40.39	29.4 ± 1.6
95	22.3 ± 27.7	172.22 ± 774.06	22.0 ± 1.4
140	15.31± 26.25	727.42 ± 1723.82	32.5 ± 2.1

Inspection of Figure 3.17 reveals that estimating past light exposure using approach C, where the individual bleaching parameter values of each grain are weighted by their uncertainties, provides the more accurate result for the IR50 and the IR140 (proximity of the black dashed line to the red dashed line in Figure). For the IR95, the approach A yields a recovered bleach time closer to the known value of 32 seconds by 0.3s, however the uncertainties on this value are much larger than those using approach C (Table 3.9). Approach A and B appear to produce a systematic departure from the known bleach time (red dashed line in Figure) with increasing measurement temperature, likely due to associated sensitivity decrease. It appears that this effect is mitigated by decreasing the weight of less sensitive grains with large parameter estimate errors and increasing the weight of brighter grains with higher parameter estimate precision. This approach (C) also produces values closer to the known recovered bleach time than using average parameter estimates.

The results from this experiment also clearly demonstrate the wide variability of bleaching characteristics between grains that have a shared, known dose and light exposure history. For this sample, and in the case of grains having a shared history, these results suggest that the optimal way to deal with this variability is to apply an approach to light exposure recovery whereby grains are weighted by their uncertainties. In this experiment, grains were weighted by the uncertainties on their recovered *t* value, which are calculated through propagation of measurement error uncertainty and parameter estimate uncertainty.

3.5. Discussion

3.5.1. Factors that affect bleaching rate

3.5.1.1. Dose and light exposure history

The set of experiments presented in this chapter investigated factors that affect MET-IRSL bleaching rate, specifically the dependency on dose history, prior light exposure history, preheat temperature and bleaching source wavelength. These variables were chosen for their particular importance for the development of IRSL-based sediment transport models and sediment tracing tools. Constraining bleaching response to prior dose and prior light exposure is essential to understanding the growth and decay of luminescence signals as grains are cyclically buried and transported on their passage through the geomorphic environment. It is also important to understand MET-IRSL bleaching response to different wavelengths of light due to the effects of light attenuation by water.

The results of experiments 3.4.1.1 and 3.4.1.2 demonstrate no systematic variation in MET-IRSL bleaching rates with prior dose, but notable variation in MET-IRSL bleaching rates with prior light exposure. A reduction in bleaching rate with increased light exposure is observed in experiment 3.4.1.2. It is assumed this is providing the signal has not been saturated or reset. This magnitude of this effect appears to decrease with increasing measurement temperature due to low bleachability of high temperature IRSL signals. According to Huntley (2006), the reduction in bleaching rate as a function of prior light exposure can be explained by the relationship between on the radial density of luminescence centres and probability of recombination. This relationship is approximated in Figure 3.18 .

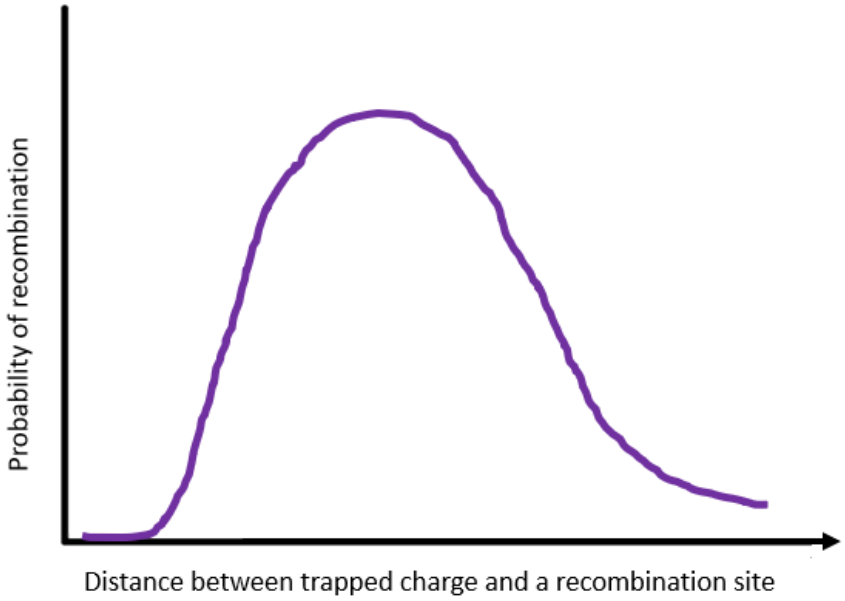

Figure 3.18. *Schematic approximation of the relationship between recombination probability and distance between trapped charge and a recombination site.*

Huntley (2006) predicts that once the very closest luminescence centres are randomly filled by electrons that faded during storage, trapped charge then preferentially recombines with the next closest luminescence centres, and so on. It should be noted that Huntley's (2006) model predicts the movement of trapped charge in feldspar IRSL occurs via tunnelling. Some studies have found that the rate of trap population during irradiation is proportional to the dose rate and associated luminescence centres are distributed randomly (Jain *et al.,* 2015; Pagonis *et al.,* 2016). As a result, there is potential that during cyclical irradiation and light exposure, random population of traps during irradiation does not alter detrapping probability, but the probability of recombination is reduced with increasing light exposure as the average distance between trapped charge and luminescence centres increases, if applying Huntley's (2006) model. This could explain observations of reduced decay rate with increasing prior light exposure, but no systematic variation with prior dose.

The reason it is thought that during excitation, excited-state tunnelling is the dominant mechanism of charge transport between traps and recombination centres in feldspar IRSL, is in part because studies show the wave function of the excitation state is wider than that of the ground state, allowing the wave function to tunnel through the energy barrier between a trapped electron and its nearest luminescence centre (Jain *et al.,* 2015). This mechanism is dependent on the distance between traps and luminescence centres, with traps at a greater distance from luminescence centres characterised by greater stability (Jain *et al.,* 2015). Hence, in Huntley's (2006) model, charge trapped at these more stable locations has a lower probability of recombination. The distance-dependent excited-state tunnelling probability is given by Huntley (2006):

$$P(r') = P_0 \exp\left(-p'^{-\frac{1}{3}} r'\right) \quad (2.2)$$

where r' is dimensionless distance between a trapped electron and a luminescence centre; P_0 is the probability of an attempt to tunnel over time (s^{-1}) and p' is dimensionless density of luminescence centres. According to this model, the results of experiment 3.4.1.1 and 3.4.1.2 suggest that the effect of repeated light exposure may cause systematic departure of p' from p'_{max}, which produces variation in $P(r')$ for feldspar IRSL decay. The physical model of Jain & Ankjærgaard (2011) successfully predicts that, for ground-state tunnelling (fading), there is an exponential decrease in tunnelling probability with increasing distance, which means that electrons with far away holes have a greater probability of retrapping or transport via band-tail states. An exciting direction for future work could be to explore whether the mechanism for and mode of charge transport during feldspar IRSL decay can be predicted in a similar way. The ability to predict charge transport pathways and the reduction in bleaching rate as a result of prior light exposure has the potential to significantly enhance the accuracy and detail with which the movement of sediment in fluvial systems can be forecast.

The effect of prior light exposure on bleaching rate has important implications for the success of IRSL-based sediment transport models. The following section (Section 3.5.1.2) introduces a burial-bleach model that accounts for this effect in forward modelling cyclical growth and decay of MET-IRSL signals using parameter estimates from direct measurements. Further, in Chapters 4 and 5, this model is applied to fluvial datasets in attempt to reconstruct transport-storage cycles based on observed MET-IRSL signals. The term 'non-equilibrium bleaching' is introduced to describe the occurrence of IRSL decay at a reduced rate due to prior light exposure. Subsequently, the term 'equilibrium bleaching' is introduced to describe IRSL decay following saturation or resetting of the signal. These terms will be used notionally throughout this thesis to describe bleaching conditions. All bleaching measurements presented in this chapter are equilibrium bleaches. This is because in all cases, a hot bleach precedes each SAR-style cycle to reset the signal (Table 3.1). In an idealised fluvial system with cyclical storage and transport, such as those illustrated in Figures 1.6 and 1.7, Chapter 1) almost all bleaching a grain is subject to during its time in the main channel will be non-equilibrium bleaching providing the signals of this grain have not been saturated or reset. Thus, there is potential for the identification of non-equilibrium ratios of MET-IRSL signals to provide a powerful tool for determining sediment transport dynamics. The degree of departure from equilibrium ratios can be used to constrain a range of different possible storage and transport times for an individual grain or group of grains. For an idealised sample, the more MET-IRSL signals measured, the more defined these constraints will be for interpreting more complex transport and storage scenarios.

3.5.1.2. Burial bleach model development

A numerical model of growth and decay was built to reconstruct possible grain histories, based on knowledge of bleaching behaviour gained in Experiments 3.4.1.1 and 3.4.1.2. This model can simulate MET-IRSL signal behaviour (fraction of saturation, N/n) of individual grains or multiple grain aliquots at three or five elevated temperatures over *n* cycles of bleaching and growth. Growth and bleaching parameters are derived directly from measurements, by fitting the single saturating exponential of Murray & Wintle (2003) (Eq. 1.1) and the bleaching function of Bailiff and Barnett (1994) (Eq. 1.3) respectively. Required input parameters include D_0 (yrs) and I_{max} (N/n, kept at 1.0) for growth (Eq. 1.1), *a* and *b* for bleaching, with the option to include the additional residual bleaching parameter, *C* (Eq. 1.3). The model also uses the parameters 'bleaching acceleration' and 'burial acceleration'. These are simply factors by which simulated bleaching and burial times can be multiplied to simulate increasing or decreasing bleaching and burial with each cycle.

In the model, regardless of initial fraction of saturation, I_{max} the first simulated bleach is an equilibrium bleach. Subsequent simulated bleaches, following (non-saturating) growth, are non-equilibrium bleaches. However, the newly acquired trapped charge that arises each time growth is simulated (some fraction of the total trapped charge population), will exhibits equilibrium bleaching behaviour. Thus, it is necessary to model the decay of bleached and unbleached trapped charge populations as separate components. The number of components it is necessary to model comprises of the number of burial-bleach cycles the user wishes to simulate.

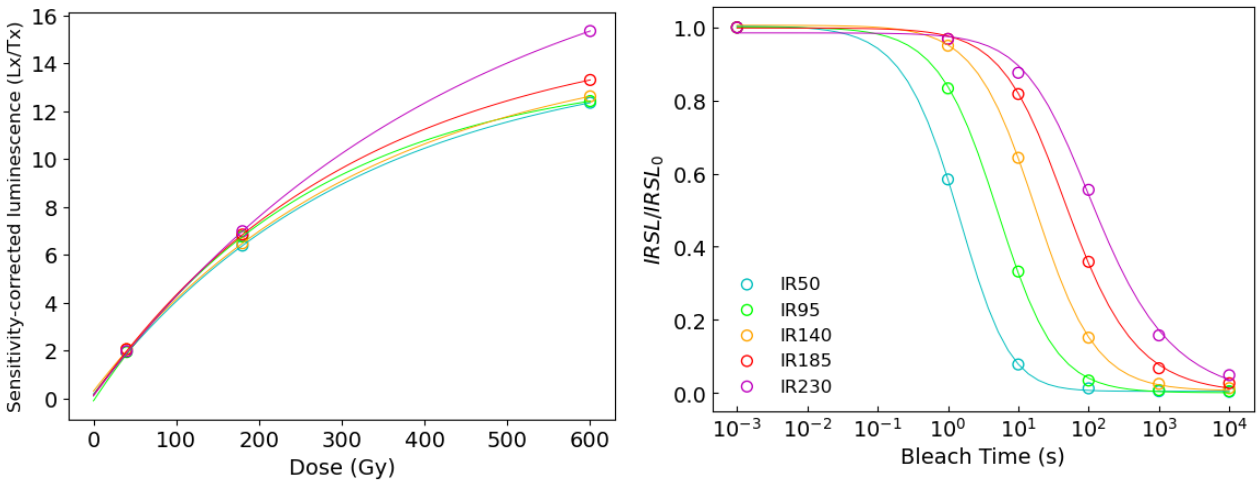

Figure 3.19. *METx bleaching and growth measurements and fits for sample MJ39. Optimal parameter estimates returned by these fits were input to the burial-bleach model.*

Table 3.10. *METx bleaching and growth parameter estimates from measurements of sample MJ39 input to the burial-bleach model. Fractional uncertainty on all parameters apart from C were less than or equal to 0.50.*

Measurement temperature (˚C)	***a***	***b***	***C***	**D_0 (s)**
50	0.40	1.61	<0.01	3177
95	0.17	1.11	<0.01	2671
140	0.06	1.02	0.006	3301
185	0.03	0.74	<-0.01	3177
230	0.02	0.57	-0.02	4390

Figure 3.20a and Figure 3.20b shows METx signals simulated over 10 and 50 cycles respectively. Each cycle is comprised of 60s bleaching and 500 years of burial. Input bleaching and growth parameters estimated from direct measurements of sample MJ39. Bleaching parameters were determined using blue light bleaching with the measurement procedure as outline in Experiment 3.4.1.4. Growth parameters were estimated using the procedure described in Section 2.2.5. Bleaching and growth data and fits are shown in Figure, parameter estimates are shown in Table.

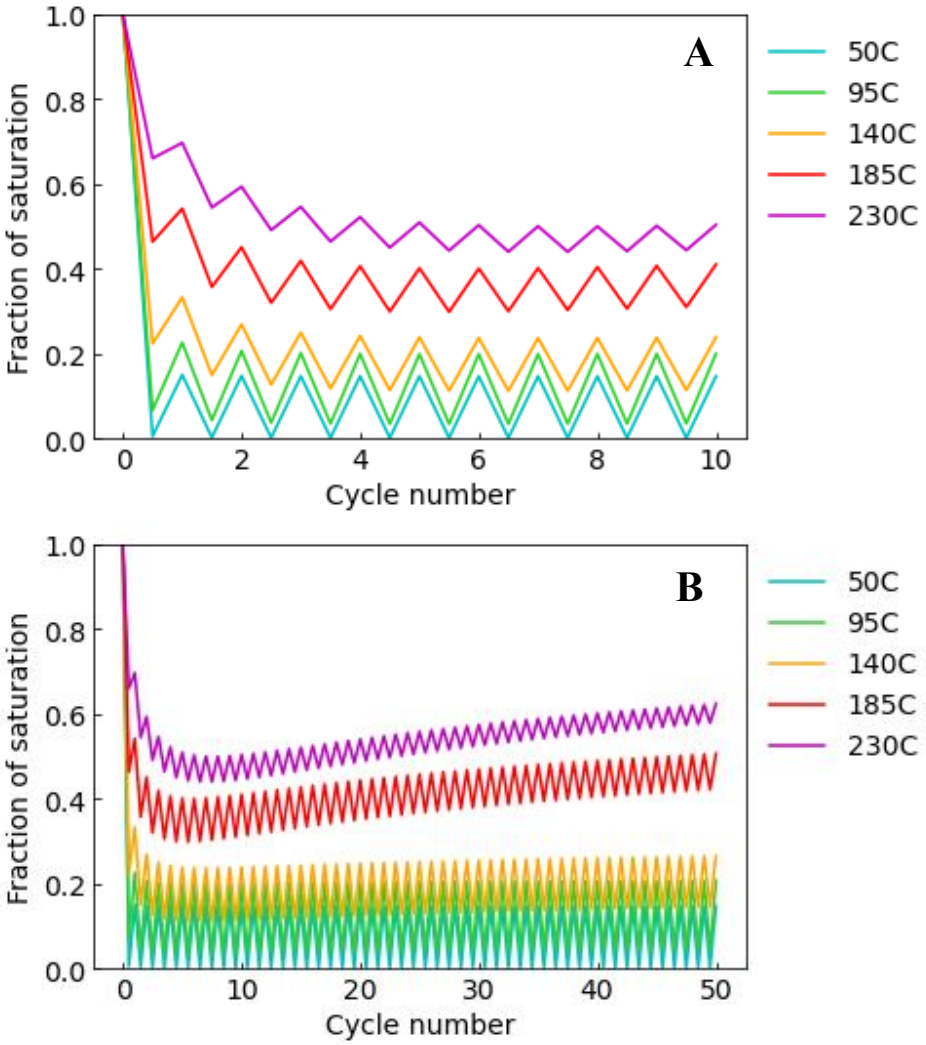

Figure 3.20. *A forward model of cyclical MET-IRSL bleaching and burial that accounts for the observed reduction in decay rate as a function of prior light exposure. Each cycle is comprised of 60s of bleaching and 500 years of burial. Bleaching and growth parameters input to the model were derived directly from measurement of feldspar standard sample MJ39.* ***A)*** *Bleaching and burial simulated over 10 cycles.* ***B)*** *Bleaching and burial simulated over 50 cycles.*

This model can be fit to fluvial datasets to reconstruct the range of possible sediment transport and storage scenarios for multiple grain and single grain measurements, which will be demonstrated in the following chapters of this thesis. This model uses the growth and bleaching functions. used by McGuire & Rhodes (2015a). However, a key way in which it differs from this previous model is with the ability to predict the reduction in bleaching rate in subsequent cycles as a function of light exposure in the previous cycle, and all other cycles up until a given point. Accounting for this effect also build on the model of Gray *et al.* (2018). The burial-bleach model shown here also builds on the model of Gray *et al.* (2018) by allowing IRSL decay to proceed with the inclusion of the residual parameter, *C,* and by simultaneously simulating the growth and decay of five MET-IRSL signals. Gray *et al.* (2018) also apply volumetric principles to simulate the downstream evolution in-channel luminescence as a result of deposition and entrainment, as well as bleaching. Gray *et al.* (2018) observe significant success of their model predicting downstream change in signal at one study site, but see deviation of the model from the data at others due to the break down of some key assumptions. Specifically, when there is perturbation to the signals of grains in the main channel, assumed to be caused by lateral input of sediment with luminescence properties different to those of the main channel flux. At this stage, the burial-bleach model presented here does not yet simulate lateral input of material with different luminescence properties. However, in Chapter 5 of this thesis, the model presented here is applied to a dataset from the Santa Clara River, California where significant perturbation to MET-IRSL signals is observe in attempt to characterise lateral input. In the future, an modelling approach that combines the volumetric approximations of deposition and entrainment of Gray *et al.* (2018), with equilibrium and non-equilibrium MET-IRSL bleaching behaviour reported here to actually simulate lateral input of sediment represents an exciting direction for future work.

3.5.1.3. Wavelength

Results from experiments 3.4.1.4 and 3.4.1.5 demonstrate that blue light is significantly more efficient at bleaching MET-IRSL signals than green and infrared sources. This is in support of the hypothesis that the rate of detrapping increases with decreasing wavelengths of light, at least up to the blue range of the electromagnetic spectrum (Jain & Ankjærgaard, 2011). It appears reasonable to account for a reduction in MET-IRSL bleaching rate in subaqueous conditions, through the use of bleaching parameters estimated from blue light bleaching measurements for simulations of bleaching during fluvial sediment transport. Figure 3.21 displays the variability of bleaching parameter *a* and *b* and their standard deviation with photon energy (eV) of the stimulating light source.

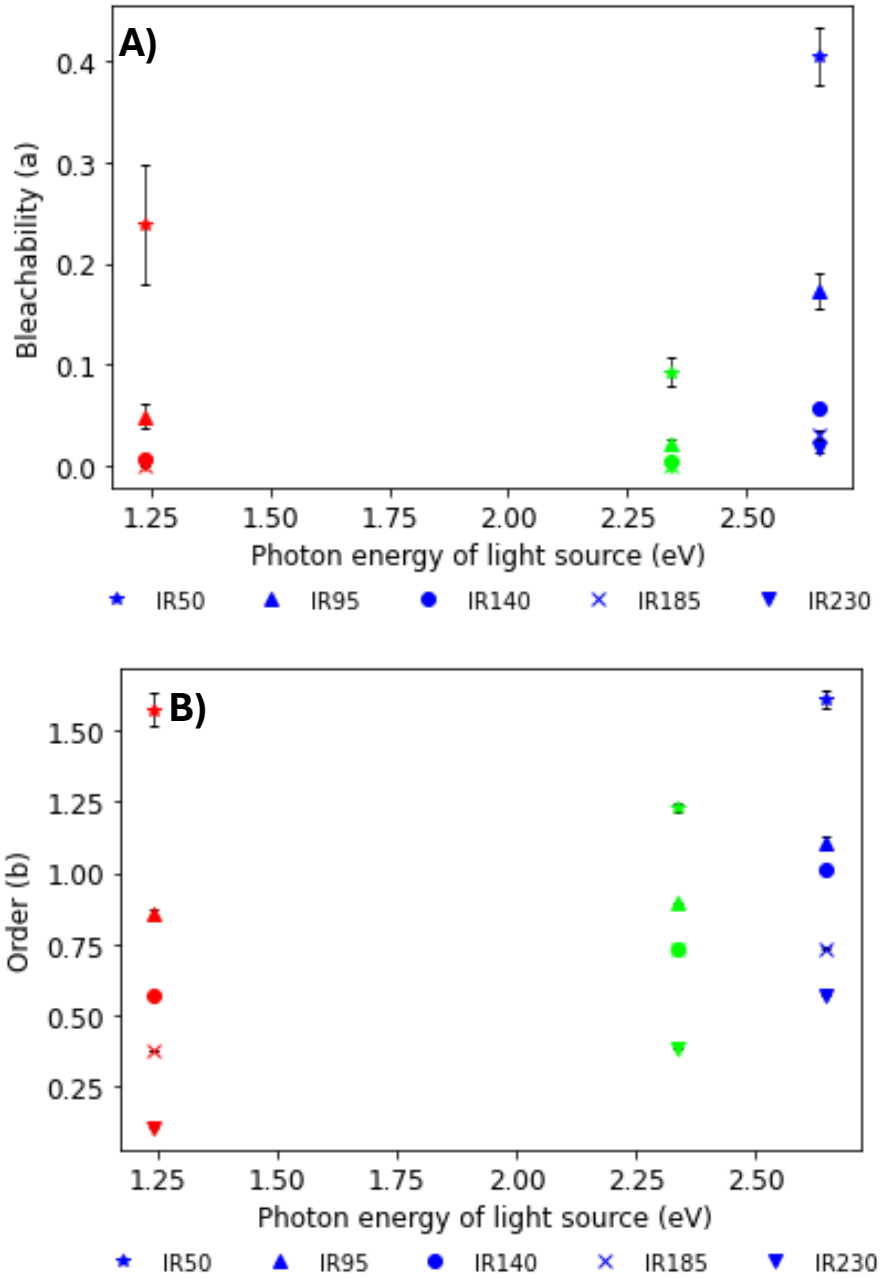

Figure 3.21. *Bleaching parameters estimated using the bleaching function of Bailiff & Barnet (1994) to bleaching measurements of feldspar standard sample MJ39 using blue green and infrared light against photon energy of the bleaching light source for each METx measurement temperature.* ***A)*** *Estimated values for parameter a, which contains information on the initial population of trapped electrons; intensity of excitation source, capture cross-section (Poolton et al., 2009) plotted against photon energy of bleaching light source.* ***B)*** *Estimated values for parameter b, which contains information on the order of the kinetic reaction (Poolton et al., 2009) plotted against photon energy of bleaching light source*

Figure 3.21 shows that fits of Eq. 1.3 to higher energy blue light bleaching measurements produce larger estimates of *a*, which includes information on the initial population of trapped electrons; intensity of excitation source, capture cross-section (Poolton *et al.*, 2009), than those of lower energy green light. Fitting of Eq. 1.3. to IR bleaching measurements produces elevated estimates of *a* for the

IR50 and IR95 relative to green light. In the IR range, the faster bleach rates can be explained by resonance between photons transmitted in the IR range, and electrons in IR-sensitive traps, which has been well-documented since 1980s by (Hütt *et al.* ,1988). Estimated values for *b* however display a positive relationship with increasing photon energy for all METx temperatures.

3.5.2. Light exposure recovery

Bleach recovery experiment 3.4.2 demonstrates a known equilibrium bleach time of 32s can recovered using the parameter estimates from a fitted bleach response curve using Eq. 2.1 for individual grains, where *I* is the measured intensity after 32s blue light exposure as a fraction of the unbleached signal of each grain. In this experiment, using sample 22183 two approaches were reasonably successful. Table 3.9 displaying the results of experiment 3.4.2 is inserted below as Table 3.11 for the convenience of the reader. The first, approach A, which uses average bleaching parameter values calculated from grains that provided individual parameter estimates with less than 50% fractional uncertainty produced recovered light exposure times in agreement with the known time of 32s within their uncertainties. It is acknowledged that these uncertainties are large and exceed the recovered value for the IR95 and IR140 (Table 3.11). These uncertainties may be a product of the large amount of noise introduced to the system when using single grains. Approach C, where the individual bleaching parameter values for each grain were weighted by their uncertainties to calculate a weighted mean recovered light exposure time also produced recovered values in agreement with the known value of 32s for the IR50 and the IR140 signal. The recovered value calculated using the IR95 signal was ~10s below the known value (Table 3.11). The uncertainties on light exposure times are surprisingly small compared to those of approach A. It is possible that these uncertainty values are underestimates and that these calculations perhaps require the incorporation of overdispersion. Inspection of Figure 3.16 in reveals irregular behaviour from one more sensitive grain, which decays at a significantly quicker rate than the majority of the population. This may also contribute to the ~10s underestimate of the IR95 signal.

Table 3.11. *Recovered t values using approaches **A-C** of a known light exposure time of 32s for each of the three ILT-3ET measurement temperatures. Approach **A** calculates an unweighted average recovered t using the same unweighted average bleaching parameter estimates for each grain. Approach **B** calculates an unweighted average t using individually fitted bleaching parameter estimates for each grain. Approach **C** calculates an average t weighted by the errors on individually recovered t, also using individually fitted parameter estimates for each grain in the same manner as approach **B**.*

Measurement temperature (˚C)	**A:** Unweighted *t* (s) [average bleaching parameters]	**B:** Unweighted *t* (s) [individual bleaching parameters]	**C:** Weighted *t* (s) [individual bleaching parameters]
50	31.46 ± 17.0	58.7 ± 40.39	29.4 ± 1.6
95	22.3 ± 27.7	172.22 ± 774.06	22.0 ± 1.4
140	15.31± 26.25	727.42 ± 1723.82	32.5 ± 2.1

Recovered values for different MET-IRSL temperatures are in agreement, using approach A and for the IR50 and IR140 signal using approach C, which is a promising result for the potential of the use of single grain measurements to construct a consistent light exposure history, despite wide variability in bleaching characteristics. The reasonable success of light exposure recover using approaches A and C, suggests perhaps a combined approach whereby for the brightest grains with low bleaching parameter uncertainties their individually fitted parameters are used in light exposure recovery, but for dimmer grains with large bleaching parameter uncertainties, average parameter values are used. With this initial success, combined with identification of equilibrium and non-equilibrium bleaching behaviour through quantifying MET-IRSL signal ratios, the wide-ranging insight single grains measurements have the potential to offer to determination of sediment transport dynamics is further explored in the following chapters of this thesis. This includes the detection of subpopulations of grains within a single sample that have shared histories and single grain virtual velocity estimates.

3.6. Conclusions

The series of experiments that comprise this chapter have contributed to understanding of the IRSL bleaching process; the knowledge contributed is of particular importance for the development of IRSL-based sediment tracing tools and sediment transport reconstructions and is also useful in validating sediment dating procedures using MET-IRSL approaches. A dependency of IRSL decay rate on length of prior light exposure, providing IRSL signals have not been saturated or zeroed between light exposure events, has been identified at all METx measurement temperatures. The bleaching behaviour of grains in this state is here termed ‘non-equilibrium bleaching’, whereas bleaching of saturated, or reset and subsequently dosed signals, is termed ‘equilibrium bleaching’. This highlights the potential to

obtain detailed information on bleaching and burial history, for multiple grains and single grains, through quantification of the degree of disequilibrium observed in the ratios of MET-IRSL signals, which is further explored in the following chapters of this thesis.

The dependency of IRSL bleaching rate on the wavelength of stimulating light source is documented for blue, green and IR, and agrees with previous studies (e.g. Duller & Bøtter-Jensen, 1993; Jain & Ankjærgaard, 2011). In addition, equilibrium and non-equilibrium bleaching behaviour was identified for blue, green and IR bleaching (experiment 3.4.1.5).

Successful light exposure recovery was demonstrated using single grain measurements using average bleaching parameter estimates and the individual parameter estimates of each grain.

A numerical model to simulate cyclical equilibrium and non-equilibrium bleaching, and burial was presented. Similar modelling approaches of McGuire & Rhodes (2015a), Gray *et al.* (2018) and Guyez *et al.* (2023) demonstrate success in a steady-state system with equilibrium bleaching conditions but do not account for the reduction in bleaching rate as a function of prior light exposure documented here for MET-IRSL decay stimulated by blue, green and IR light (Experiments 3.4.1.2, 3.4.1.3, 3.4.1.5). This effect is expected to be significant MET-IRSL decay in some sediments in fluvial systems due to the cyclical nature of storage and transport. The burial-bleach model presented in Section 3.5.1 of this chapter takes account of this effect and has the potential to accurately reproduce the burial and bleaching histories of grains in systems that are not in equilibrium conditions, which is assessed in Chapter 4 and Chapter 5.

4.0. Chapter 4 Allt Dubhaig: A training ground for the development of MET-IRSL as a tool to extract information on fluvial sediment transport

4.1. Introduction

This Chapter aims to present the vast quantity of data produced by MET-IRSL measurements, and the analysis techniques that can be used to obtain an array of different information on sediment transport histories, styles, and rates, as well as storage duration and environments in fluvial systems. The Allt Dubhaig, Scotland, is used as a training ground to explore the power of MET-IRSL. Chapter 3 provided new insight MET-IRSL bleaching dependency on prior light exposure and introduced the concept of equilibrium and non-equilibrium bleaching. Subsequently, a burial-bleach model that simulates MET-IRSL signals over cyclical burial and light exposure, and accounts for a reduction in bleaching rate as a function of past light exposure was presented. Chapter 3 also demonstrated successful single grain light exposure recovery using bleaching parameter values derived directly from measurements. In this chapter, these new insights and procedures are applied to elucidate sediment transport information, including average storage times and virtual velocity.

4.2. Background

4.2.1. The Allt Dubhaig, Perthshire, Scotland

The Allt Dubhaig is a small gravel-bed stream that flows through a glacially deepened valley in the central Scottish Highlands (Ferguson & Ashworth, 1991) (Figure 4.1). The alluvial section, which will be the focus of this Chapter and has been the focus of a number of previous studies (e.g. Ferguson & Ashworth, 1991; Hoey & Ferguson, 1994, Ferguson & Wathen, 1998; Ferguson *et al*., 2002; Hodge *et al*., 2011), flows SSE from the confluence of its eastern and western tributaries and extends for approximately 3.5 km until it meets the River Gary at Dalnaspidal Lodge. Hills on either side of the valley are lined with hummocky moraines that are thought to be formed by outlet glaciers fed by plateau icecaps during the Younger Dryas ~13.5 – 11.7 ka (Sissons, 1974). Ferguson & Ashworth (1991) interpret the valley floor to be comprised of early Holocene sediments. The Allt Dubhaig mobilises sediments in its modern channel; the stream migrates laterally across its floodplain, it adjusts its geometry. Photographs of this site taken during sample collection for this study in 2022 are shown in Figure 4.2-4.4. Details of sampling locations and strategy are outlined in Section 4.3.1; photographs are shown here to illustrate the geomorphic setting of the site.

Figure 4.1. *Location of the Allt Dubhaig in the Scottish Highlands. For context, the locations of Perth and Edinburgh are included.*

Figure 4.2. *Photograph taken looking SSE from the west bank of the Allt Dubhaig in the upstream segment of the alluvial reach.*

Figure 4.3. *Photograph taken from the east bank in the upstream section of the alluvial reach, looking south down the glacial valley through which the Allt Dubhaig flows*

Figure 4.4. *Photograph of the middle section of the alluvial reach of the Allt Dubhaig, taken from ~12m up the side of a moraine that lines the eastern valley wall, looking southwest.*

The Allt Dubhaig was selected as a study site for the following reasons: 1) previous studies have documented various fluvial and geomorphic processes at this site (e.g. Ferguson & Ashworth, 1991; Hoey & Ferguson, 1994, Ferguson & Wathen, 1998; Ferguson *et al*., 2002; Hodge *et al*., 2011); 2) minimal lateral input of water and sediment from tributaries or valley sides reported by Ferguson *et al*., (1996) provides reason to expect somewhat flume-like behaviour, which makes for an appropriate training ground to explore the utility of MET-IRSL for the determination of sediment transport dynamics, since conditions in the Allt Dubhaig appears closely resemble an idealised natural channel. This provides opportunity for determination of MET-IRSL signal behaviour with reduced complexity of inputs; 3) preliminary MET-IRSL results from four samples collected from the active channel by Ed Rhodes and Rebecca Hodge in 2018 showed encouraging downstream trends; 4) MET-IRSL has the potential to compliment other techniques for sediment tracing and determination of fluvial system behaviour.

Several previous studies of the Allt Dubhaig document sediment transport information. Ferguson & Ashworth (1991) report a significant reduction in channel slope, from 0.02˚ to 0.00015˚, over a 3 km reach of the stream, which is attributed to strong local base level control by an alluvial fan in the lower reaches. This decline in slope causes rapid downstream fining of the gravel bed load, and a subsequent abrupt shift to a sand bed. Further, Ferguson & Ashworth (1991) also identify gradual changes in the channel morphology with downstream distance over the 3 km study reach as follows: '1) near braided, 2) meandering with active point-bar chutes, 3) meandering with active outer-bank thalweg, 4) stable equiwidth sinuous.' (Ferguson & Ashworth, 1991, p65). For reference, key morphological characteristics of each distinct reach are summarised in Table 4.1, some of which will be discussed in relation to insights provided by MET-IRSL measurements and analysis in the discussion section of this chapter.

Table 4.1 *Geomorphological features identified by Ferguson & Ashworth (1991) in what the authors define as distinct sections of the Allt Dubhaig.*

Distance (m)	Key features
0.2	• Low sinuosity • Pools and riffles • Moderately divided
0.6	• Low relief medial bars • Moderately divided
0.8	• Increased sinuosity • Less divided • More meandering
1.1	• Closer to classic meandering • Single channel • Large gravel point bar
2.0	• Narrower • Less visible gravel • Straight reaches separated by sharp bends
2.5	• Almost straight reach between two bends • Outer bank thalweg

In gravel bed rivers, sediment movement in the short term is dominated by controls on particle entrainment (relative size and shear stress), whereas over longer timescales transport is affected by depositional dynamics (Ashworth, 1987). Ferguson & Hoey (2002) provide insight into the importance of burial and exchange of sediments in depositional environments over long timescales for the Allt Dubhaig. They observed the burial of surface-seeded tracers into long-term storage as a result of vertical mixing of the bedload, which produces a long-term trend of decreasing gravel mobility, with virtual velocities of mixed-sized tracers ~50% lower over an 8-year period compared with over 2 years.

Downstream fining of bed material is a common characteristic of gravel bed rivers. Ferguson *et al*., (2006) demonstrate that the rapid downstream fining observed in the Allt Dubhaig by Ferguson & Ashworth (1991) is not associated with changes in discharge and associated abrasion rates, but with changing channel morphology (specifically, decline in slope angle), which indicates that sorting is the dominant driver of downstream reduction in particle size. Further, the rate of downstream fining is successfully simulated using a numerical sorting model. The authors go on to argue that, at least to first order, the Allt Dubhaig is in approximate equilibrium. Ferguson *et al*., (2006) explain that this relates to the tendency of a river to reduce downstream bed load transport rates, which can take place on much shorter timescales than the necessary aggradation to otherwise reach equilibrium.

A comprehensive tracer study conducted by Hodge *et al*., (2011) also provides evidence of size-selective transport, with a strong dependency of transport distance on particle size in the Allt Dubhaig.

However, Hodge *et al*., (2011) argue that, in gravel-bed rivers, this in fact throws into question whether such systems are in long term equilibrium, since a dominance of sorting over abrasion suggests the accumulation of larger particle sizes in the river. Thus, there exist questions surrounding the system state of the Allt Dubhaig.

This Chapter demonstrates how MET-IRSL can provide detailed insight into the transport conditions of the Allt Dubhaig. Single grain and multiple grain MET-IRSL are used as complementary techniques. Multiple grain measurements can provide a robust indication of average system behaviour. With single grain measurements, there is potential to extract information that may be masked by multiple grain signals that are often dominated by just a few bright grains (Rhodes, 2015). By interrogating each grain individually, it is possible to construct a profile of different possible transport scenarios and assess likelihoods of different grain histories.

4.3. Methods

4.3.1. Study site and sampling strategy

The ~ 3.5 km alluvial stretch of the Allt Dubhaig flows NNW-SSE almost parallel to the A9 road approximately 10 km south of Dalwhinnie and ~ 70 km northwest of Perth (Figure 4.5).

The author of this thesis and Ed Rhodes collected 13 fluvial samples from the active channel to access grains that store information on sediment transport (Lab codes: 22180-93). Based on the form of feldspar IRSL decay and expected flume-like behaviour of the Allt Dubhaig, it was anticipated that in-channel IRSL signals would exhibit an initial rapid reduction as grains are subject to transport, followed by a long tail as bleaching rate slows with increasing light exposure. For this reason, fluvial samples were spaced in a logarithmic fashion to capture the expected pattern of decay. In addition, marked on Figure 4.5 are four fluvial samples collected by Ed Rhdoes and Rebecca Hodge in 2018, indicated by '*'.

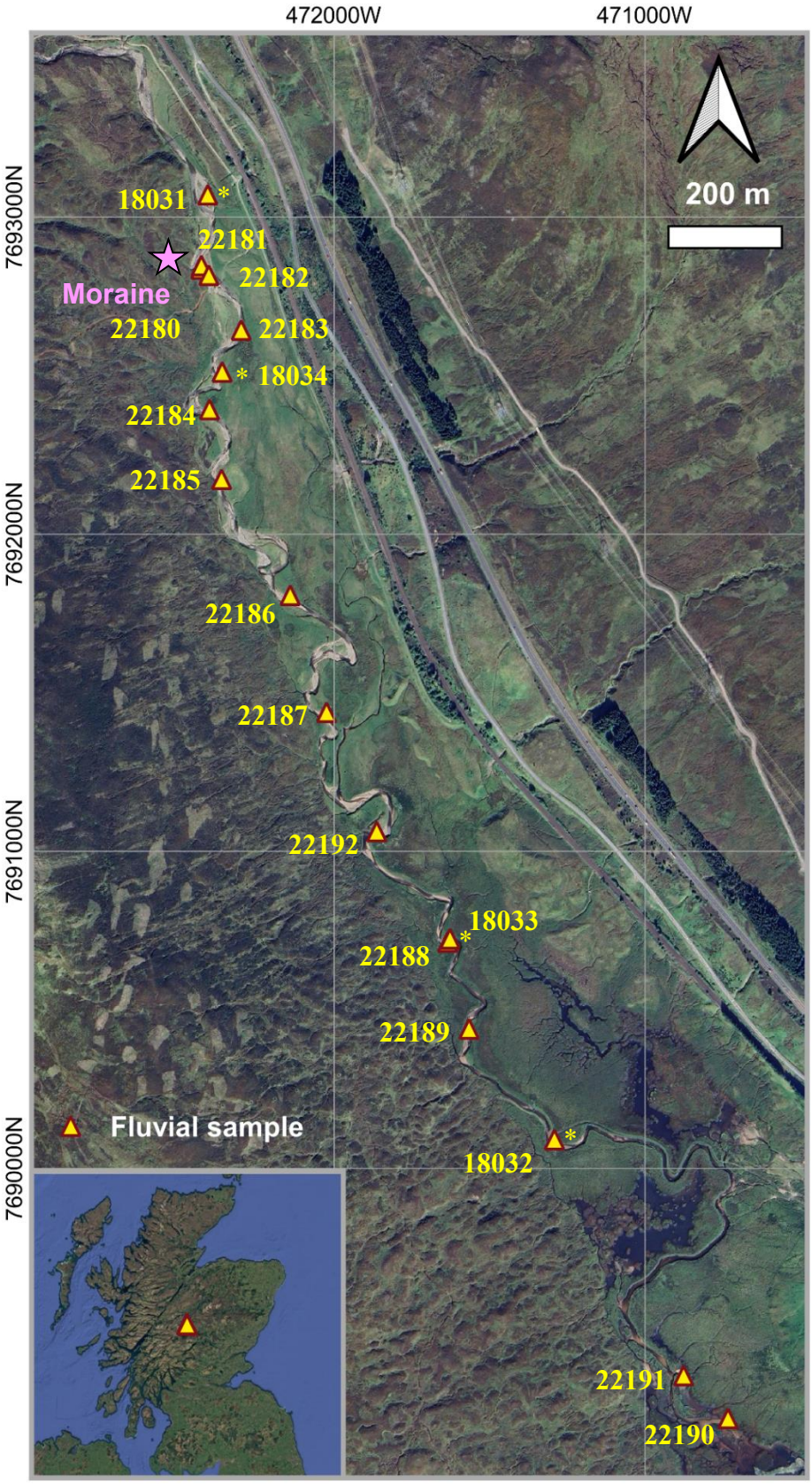

***Figure 4.5**. Locations of samples collected along the Allt Dubhaig and their lab codes. The 13 samples without '*' were collected by Ed Rhodes and the author of this Thesis in 2022. The four locations with '*' were collected by Ed Rhodes and Rebecca Hodge in 2018.*

Three samples were collected from a moraine exposure (herein referred to as ‘the moraine’) cut into by the stream, located in the northern reach of the alluvial stretch (Lab codes: 22177-9) (Figure 4.3.2). This was to determine the luminescence characteristics of what was thought to be a significant contributor of sediment to the active channel. Here, three key stratigraphic features of the moraine were identified and sampled from. From bottom to top, there were: glacial till (22178), a scree apron (22179), and what is potentially a post glacial erosion channel near the top of the exposure (Figure 4.6). A gamma spectrometer was used to measure the environmental dose rate at this location, this is done by directly measuring the counts of emitted gamma radiation.

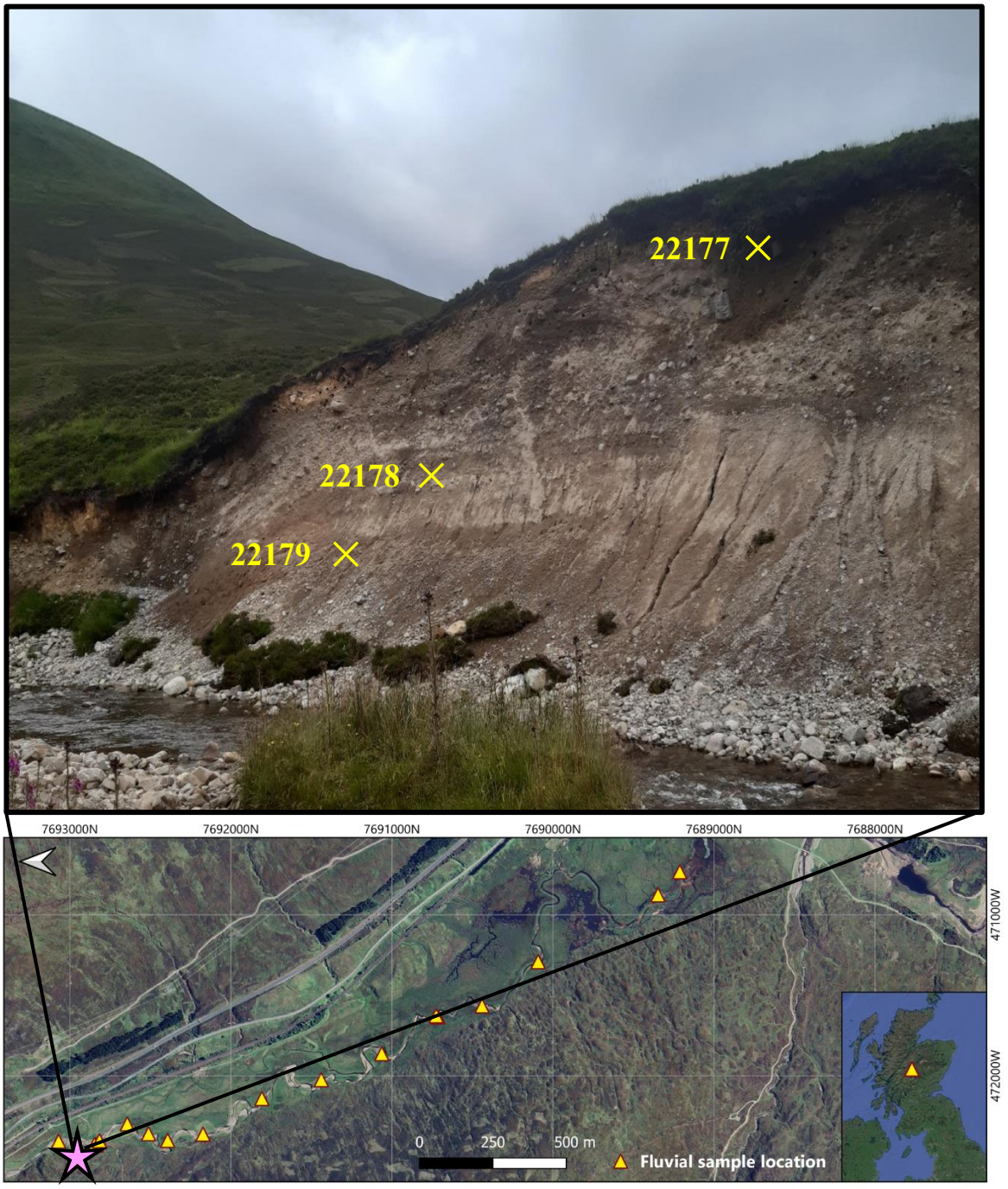

Figure 4.6. *In the top panel, locations of three samples taken from the moraine on the west bank of the Allt Dubhaig indicated by the yellow crosses. Sample 22177 (top), 22178 (till) and 22179 (scree apron) were taken from ~5m, ~2m, ~1m.*

4.3.4. Sample measurement

Equivalent dose estimations for all samples were made using a single grain ILT-3ET. A more detailed description of the ILT-3ET protocol, and a discussion of the reasons for applying it can be found in Section 2.2.2.1 in Chapter 2. For reference, the ILT-3ET protocol is summarised here in Table 4.2.

Table 4.2*. The ILT-3ET protocol used to measure growth curves for the entire suite of 17 fluvial samples and three moraine samples*

Beta dose or natural
Preheat 60s 170°C 5°Cs^{-1}
IRSL 50°C 2.5s 90% power
IRSL 95°C 2.5s 90% power
IRSL 140°C 2.5s 90% power
IRSL warm bleach 160°C 400s 90%
Beta test dose 20 Gys
IRSL 50°C 2.5s 90% power
IRSL 95°C 2.5s 90% power
IRSL 140°C 2.5s 90% power
IRSL hot bleach 180°C 400s 90%

Bleach response curves were measured and fitted for four samples using the 'half order of magnitude' (HOM) or 'full order of magnitude' (FOM) styles, and the fitting procedures described in detail in Section 3.3.1, Chapter 3. Bleaching measurements were made to explore trends in bleaching parameter variability, amongst single grains, with downstream distance, with a view to determine optimal parameter ranges to input MET-IRSL-based sediment transport models. All measurements presented in this chapter are of single grains. Two discs of approximately 100 grains were measured for each sample

4.4. Results

An advantage of feldspar luminescence as a sediment transport technique is that there are multiple ways to express IRSL signal, from which we can learn different things. This also allows us to assess optimal methods for expressing and visualising MET-IRSL data for sediment transport applications.

The first section (Section 4.3.1) presents ages from the three samples collected from the moraine because these samples were collected to act as a proxy for the initial state of grains that enter the Allt Dubhaig at the beginning of the alluvial reach. In this way, the stories of many of the grains presented in this chapter start here. Section 4.4.2 presents average MET signals for the 17 fluvial samples expressed in different manners. Section 4.3.3 explores what can be contributed by distributions of single grain apparent ages, sensitivities and burial-bleach ratios to building a story of sediment transport and storage.

4.4.1. Moraine samples

Plateau ages calculated using the ILT-3ET protocol and the plateau method of Ivester *et al.* (2022) are presented in Figure 4.7 Sample 22177 taken from near the top of the exposure gives an age of 8.4 ± 1.5 ka; sample 22178 taken from glacial till gives an age of 14.9 ± 2.6 ka; and sample 22179 taken from a scree apron at the base of the exposure gives an age of 0.89 ± 0.18 ka. These ages are interpreted in Section 4.5.1.

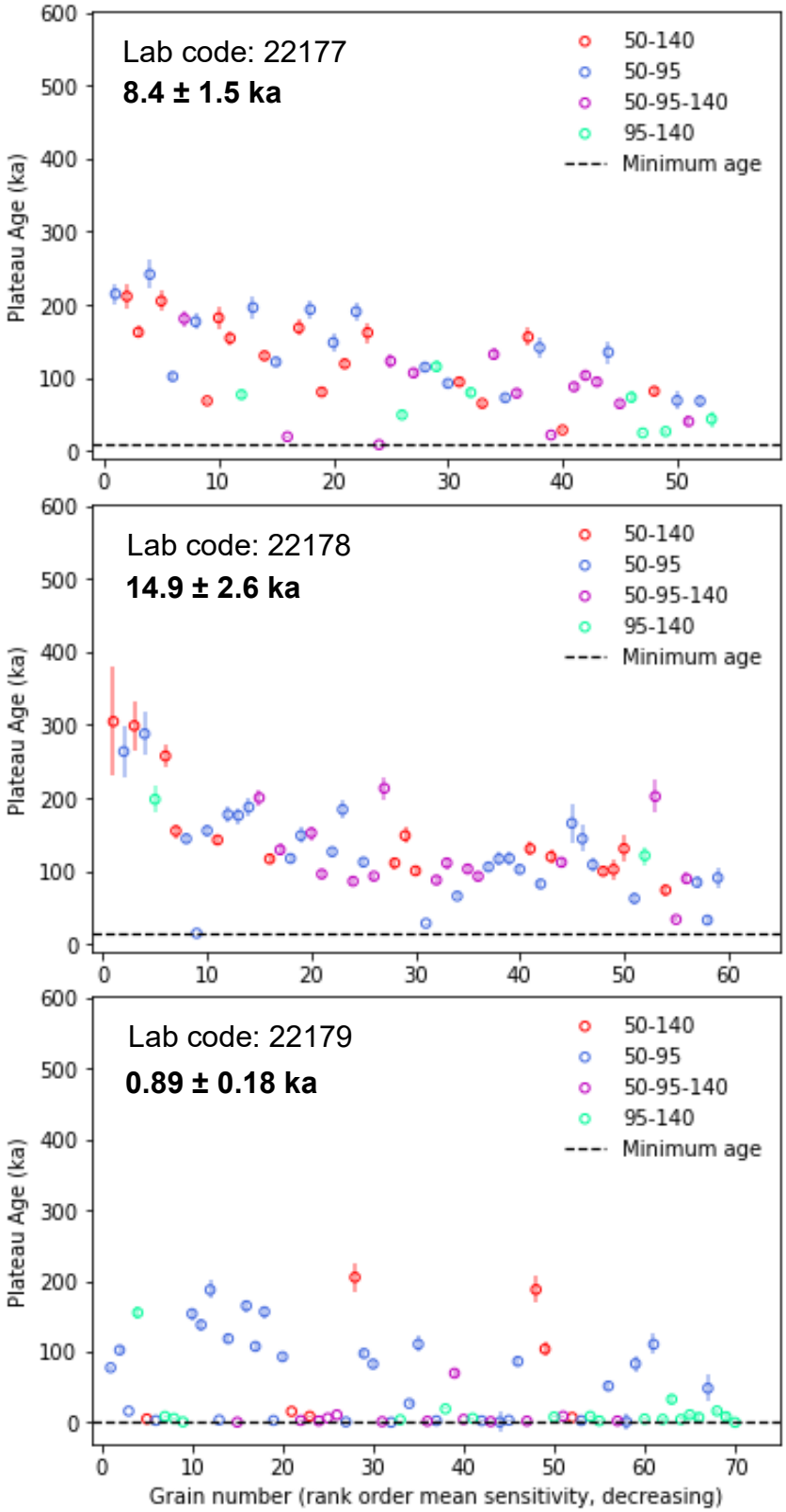

Figure 4.7. *Plateau ages of for the three moraine samples; samples 22177 (upper), 22178 (middle), and 22179 (lower). Coloured points indicate plateau age and plateau type (the ILT-3ET signals of which it is comprised) for individual grains. Minimum age calculated from plateau ages is represented by the black dashed line and is in bold type below the lab code.*

4.4.2. Downstream MET-IRSL signal profiles

Preliminary inspection of single grain ILT-3ET apparent ages combined into super synthetic aliquots apparent ages (SSAs) in Figure 4.8 and Table 4.3 reveals a general pattern of decrease in apparent age with downstream distance for all three measurement temperatures. However, the rate at which decrease proceeds varies along the length of the stream, and periods of signal increase are observed in the downstream sections (Figure 4.8. The SSA apparent age is comprised of all grains that provided an equivalent dose estimate for all three temperatures, however these did not necessarily form a plateau.

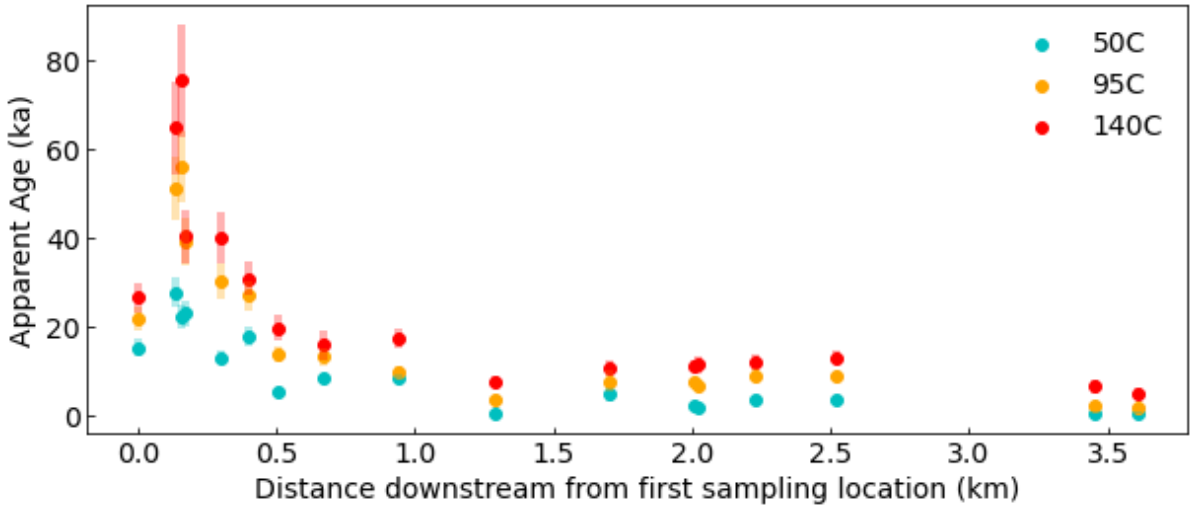

Figure 4.8. *Super synthetic aliquot apparent age plotted with downstream distance. The IR_{50} signal is plotted in blue, IR_{95} is plotted in orange and IR_{140} is plotted red*

Table 4.3 *Summary of super synthetic aliquot apparent ages with their errors and downstream distance for each fluvial sample.*

Lab code	Distance (km)	IR50 (ka)	IR95 (ka)	IR140 (ka)
18031	0	15.5 ± 1.9	21.9 ± 2.7	26.6 ± 3.2
22181	0.14	27.9 ± 3.4	51.3 ± 7.1	64.8 ± 10.4
22180	0.16	22.4 ± 2.7	56.2 ± 7.9	75.7 ± 12.6
22182	0.17	23.1 ± 2.8	39.3 ± 5.3	40.4 ± 6.0
22183	0.3	13.1 ± 1.6	30.3 ± 4.0	40.2 ± 5.9
18034	0.4	17.9 ± 2.2	27.2 ± 3.3	31.1 ± 3.8
22184	0.51	5.4 ± 0.6	14.0 ± 1.8	20.0 ± 3.0
22185	0.67	8.5 ± 1.2	13.3 ± 2.2	16.0 ± 3.2
22186	0.94	8.5 ± 1.2	10.2 ± 1.3	17.5 ± 2.4
22187	1.29	0.8 ± 0.3	3.6 ± 0.4	7.70 ± 1.3
22192	1.7	5.0 ± 1.6	7.9 ± 2.3	10.9 ± 1.9
18033	2.01	2.3 ± 0.6	7.6 ± 0.9	11.3 ± 1.4
22188	2.02	2.1 ± 0.3	7.0 ± 1.3	11.6 ± 2.1
22189	2.23	3.9 ± 0.5	9.3 ± 1.4	12.0 ± 1.8
18032	2.52	3.6 ± 0.6	9.0 ± 1.1	13.2 ± 1.6
22191	3.45	0.8 ± 0.3	2.2 ± 0.8	6.6 ± 1.4
22190	3.61	0.8 ± 0.2	1.8 ± 0.7	5.1 ± 1.2

The second sample at 0.14 km downstream from the most upstream sample location displays a significant increase in apparent age, particularly the IR_{95} and IR_{140} signals, from ~22 – 51 ka and ~27 – 64 ka respectively. The IR_{50} also increases at this location, but this is much less pronounced than the higher temperature signals. At the third location at 0.16 km downstream, the IR_{95} and IR_{140} signals appear increase yet again but their uncertainties overlap with those of the second location. Moving downstream, all three signals begin a rapid monotonic decrease over a short distance of ~0.5 km, apart from the IR_{50} signal, with a small increase at ~0.3 km and another after ~0.5 km. Following this, between 0.67 and 0.94 km downstream from the most upstream sample, we observe a slight increase in signal for the IR_{140} and the IR_{50}. Notably, we observe another, general trend of increase across all three temperatures between 1.29 and 2.52 km. Following this, at the two most downstream locations we see a reduction in apparent age for all three signals.

Figure 4.9 (below) compares downstream signal profiles expressed as SSA fraction of saturation (Figure 4.9) and plateau ages (Figure 4.9).

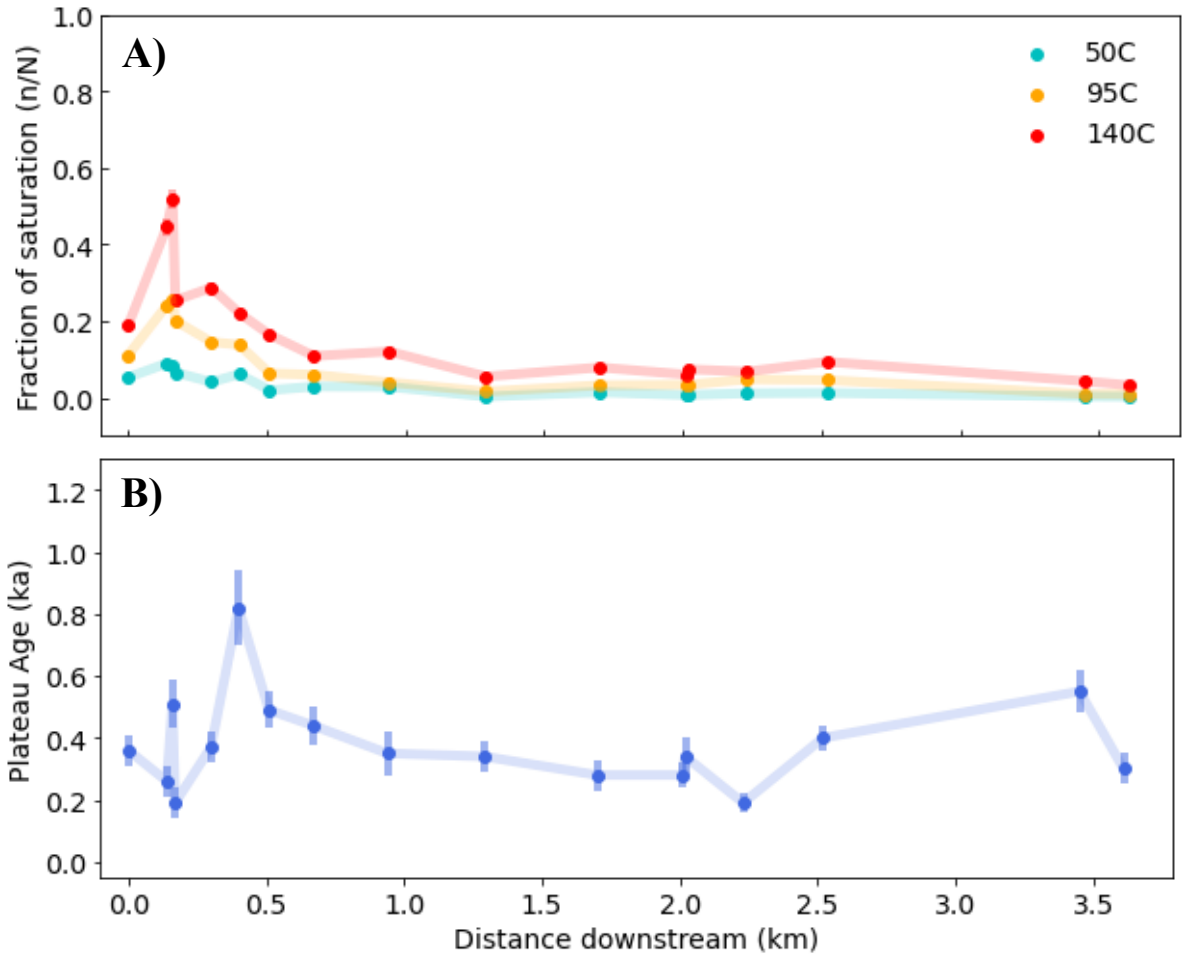

Figure 4.9 *Downstream profiles of fraction of saturation and minimum age in the Allt Dubhaig.* ***A)*** *Super synthetic aliquot fraction of saturation plotted with downstream distance for the IR_{50} (blue), IR_{95} (orange) and IR_{140} signal (red).* ***B)*** *Minimum age calculated using the plateau method of Ivester et al. (2022) plotted with downstream distance.*

Perhaps the most striking difference between the downstream evolution of IRSL signals derived from SSAs, and those derived from single grain plateau ages, is that the early peak in age is less pronounced for the plateau age downstream profile; it is dwarfed by a much larger peak at 0.4 km. It is also observed downstream age reduction in plateau age up until ~ 2 km, followed by a significant increase. Reasons for these differences will be discussed in Section 4.5.2, yet it highlights the potential for additional insight provided through variation of IRSL signal expression.

Figure 4.10 displays the apparent ages for each individual grain with a fractional uncertainty below 0.5 for all three measurement temperatures. In general, the IR_{50} ages (Figure 4.10a) are much younger than those of the IR_{95} and IR_{140} signals (Figure 4.10b and Figure 4.10c respectively), which is expected due to the lower bleachability of IRSL measured at elevated temperatures (Buylaert et al. 2012). This is also what is observed in downstream profiles of SSA and plateau ages. There is increasing variability of single grain apparent ages with increasing measurement temperature. Note the low variability of apparent ages for the two most downstream samples. There is also low variability of

apparent ages at 1.29 km downstream, after the phase of rapid signal reduction and prior to the first phase of signal increase. Following this, there is an increase in signal variability over the next ~ 1 km.

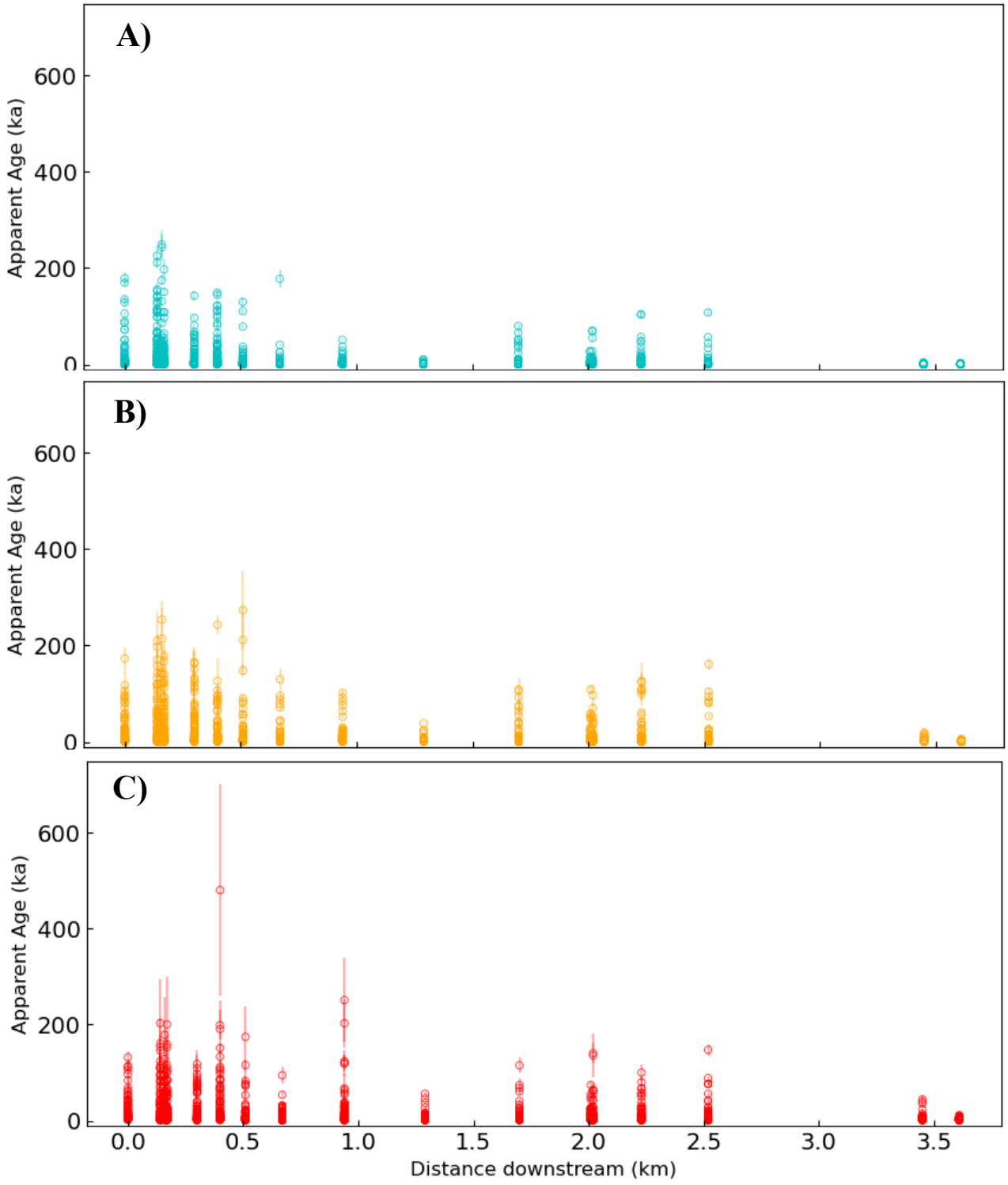

Figure 4.10 *Single grain apparent age estimates and their associated errors plotted with downstream distance for the* ***A)*** IR_{50}, ***B)*** IR_{95} *and* ***C)*** IR_{140}.

Downstream profiles of MET-IRSL signals provide the first indication that the Allt Dubhaig may not behave as 'flume-like' as initially expected. Increases in average signals (Figure 4.8, Figure 4.9) and changing intra-sample variability of single grain ages (Figure 4.10) suggest more complex sediment

transport dynamics, that may include lateral input of new material or grains coming out of storage in the section of the Allt Dubhaig.

4.4.3. Single grains: insights from distribution characteristics

This section presents downstream trends in luminescence characteristics for individual grains for each of the three MET-IRSL signals. Distributions of apparent ages, sensitivity, and the parameter 'burial-bleach ratio' of Rhodes & Leathard (2022) are used to explore the range of information these parameters provide on sediment transport in the Allt Dubhaig. Figure 4.11 displays distributions of $\log_{10}$ ILT-3ET apparent age estimates at each sampling location downstream for all grains with fractional uncertainty on the measured equivalent dose below 0.5.

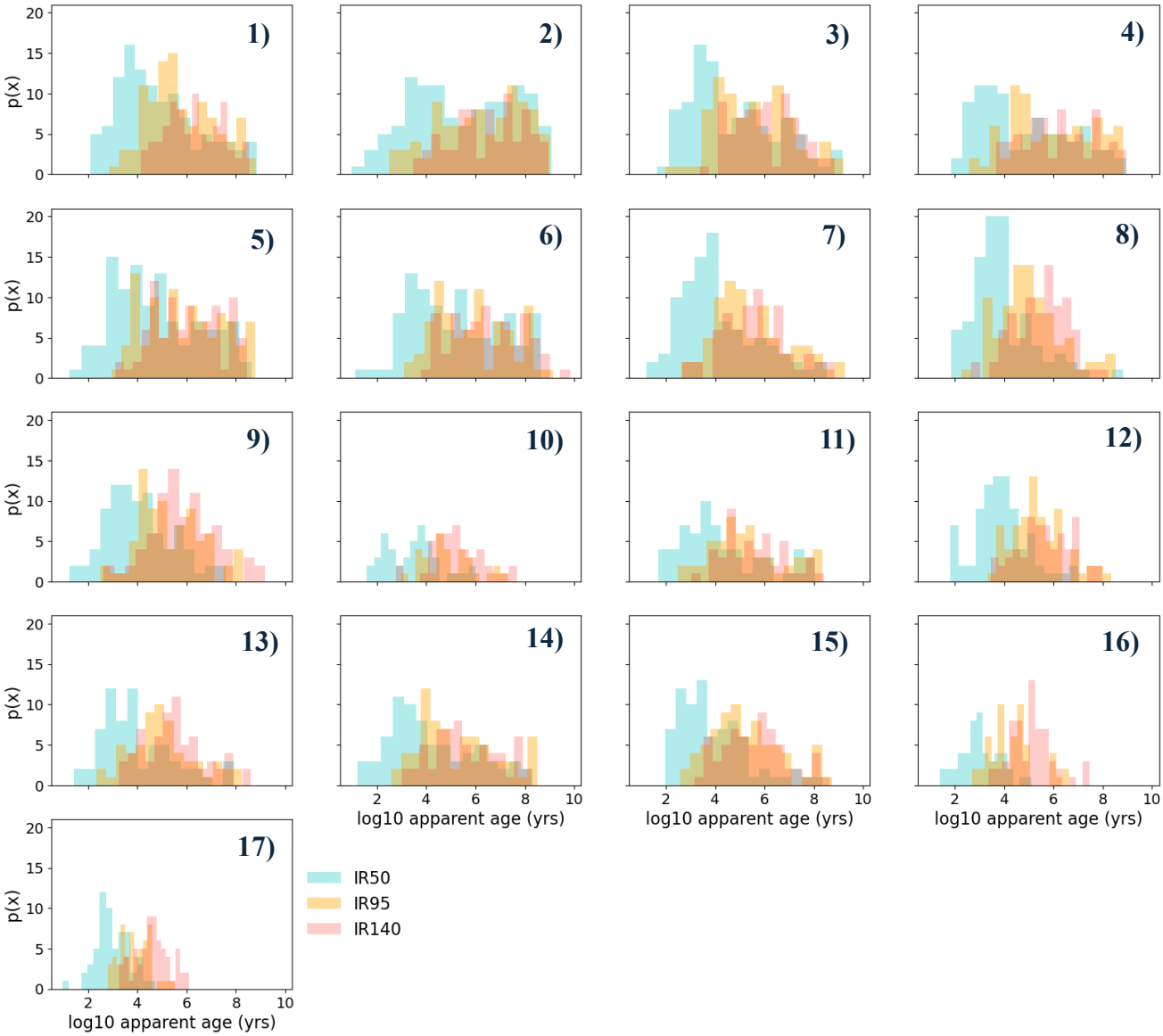

Figure 4.11. *Distributions of single grain $\log_{10}$ apparent age estimates (years). Histograms for the IR_{50}, IR_{95}, and IR_{140} for each sample are overlapping to illustrate the variable location and shape of the distribution of each measurement temperature. The numbers on the top right corner of each plot represents the relative location of the sample downstream.*

At all locations we observe overlapping distributions, but with clear increasing frequency of older ages with increasing measurement temperature. This is what would be expected based on the work of Poolton *et al.*, (2002) and Buylaert *et al.*, (2012), which is discussed in Section 1.2 and Section 3.2. It is also observed that the distributions become narrower with downstream distance, which is most pronounced for the IR_{140} data, and increasing frequency of younger ages are observed. However, further interrogation of downstream age distributions is required to construct a transport story from these data; further analysis is included in Section 4.5.3.4.

Figure 4.12 shows distributions of test signal response for each sampling location. Here, grains have a higher sensitivity when measured with IR_{50} and sensitivity decreases with increasing measurement temperature. Note that the location of the medians of IR_{95} and the IR_{140} data appear more similar to each other than to that of the IR_{50}. There are also similar downstream trends to those of the age distributions in Figure 4.4.5; with the range of sensitivities decreasing with downstream distance.

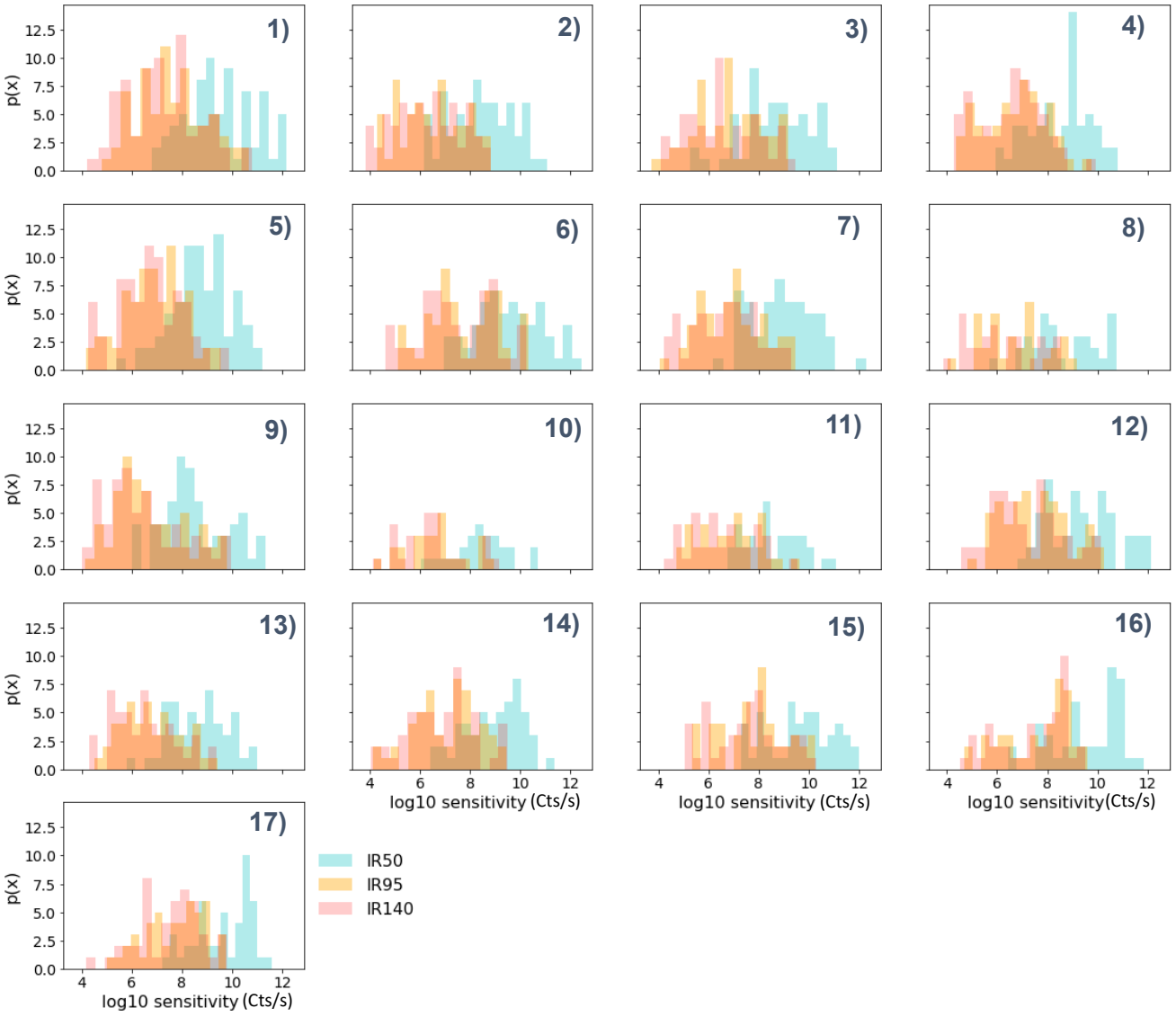

Figure 4.12 *Distributions of single grain log_{10} sensitivity in counts per second. Histograms for the IR_{50}, $IR_{9}5$, and IR_{140} for each sample are overlapping to illustrate the variable location and shape of the distribution of each measurement temperature. The numbers on the top right corner of each plot represents the relative location of the sample downstream.*

Distributions of burial-bleach ratios (Rhodes & Leathard, 2022) reveal clear downstream trends (Figure 4.13). In Figure 4.13 distributions become narrower with downstream distance. There also appears to be a higher frequency of lower burial-bleach ratios, which suggests decreasing burial relative to light exposure. That downstream trends in burial-bleach ratio distributions are observed is a promising finding for the utility of this parameter to reflect sediment transport dynamics, specifically related to the storage times of grains and the light exposure they are subject to in transit.

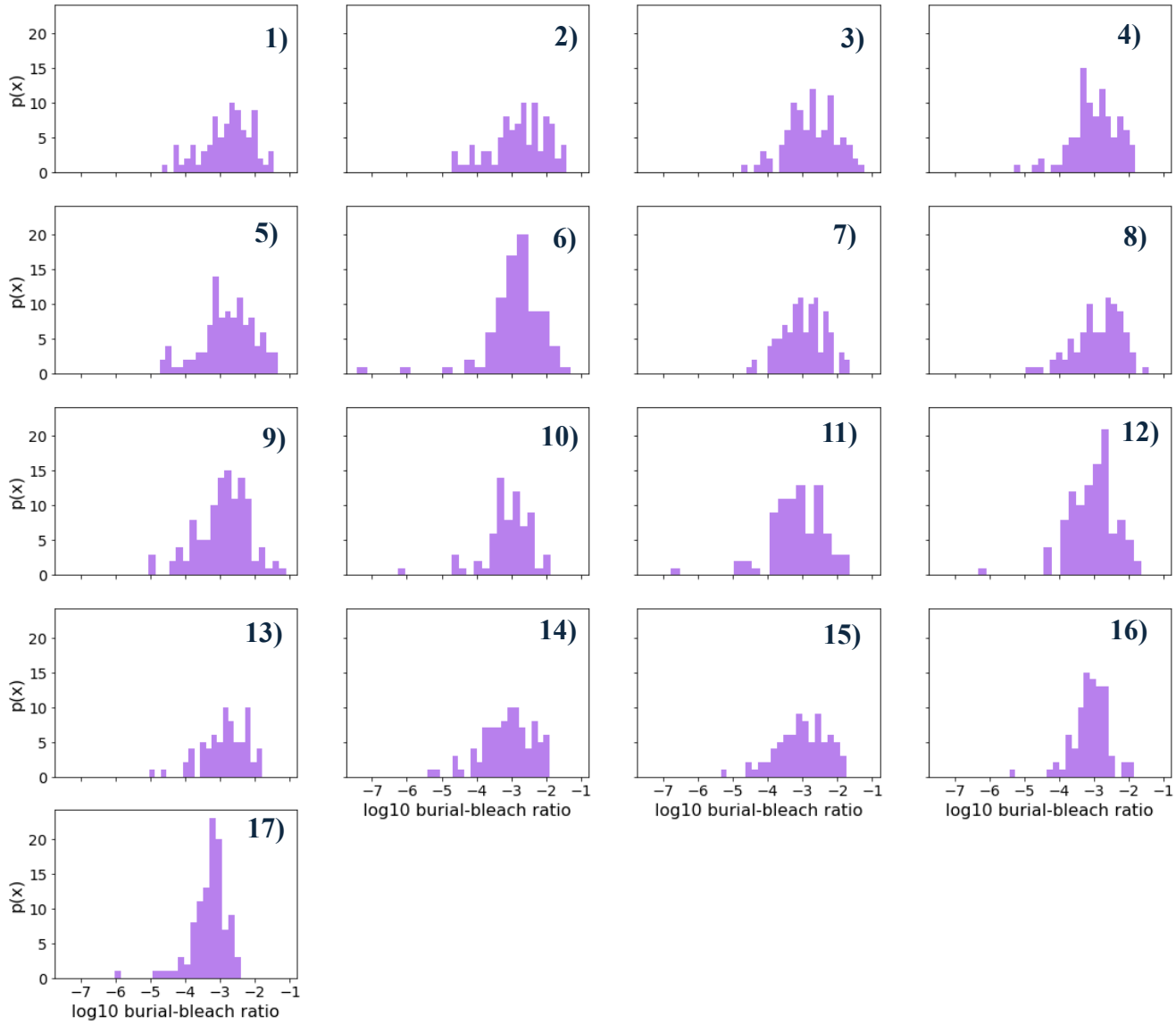

Figure 4.13. *Distributions of single grain log_{10} burial-bleach ratios calculated using the approach of Rhodes & Leathard (2022). The numbers on the top right corner of each plot represents the relative location of the sample downstream.*

Figure 4.14 shows burial-bleach ratios derived from super synthetic aliquots over downstream distance. Higher burial-bleach ratios indicate storage dominates over bleaching in determining the luminescence characteristics of the in-channel sediment flux, whereas lower values indicate the dominance of light exposure (Rhodes & Leathard, 2022). However, the large uncertainties on the burial-bleach ratios of the combined signals of the upstream samples (Figure 4.14, below), do not allow for confident assessment of downstream burial-bleach ratio variability and whether this relates to a real change in transport dynamics. In fact, it appears this profile may even suggest a system average burial-bleach ratio. This has been tentatively indicated in Figure 4.14 to be somewhere around 0.002. If other rivers display a consistent value similar to what is illustrated in Figure 4.14 below, what this means could be an interesting concept to explore, since it is possible this relates to steady-state system behaviour or state of equilibrium, for example.

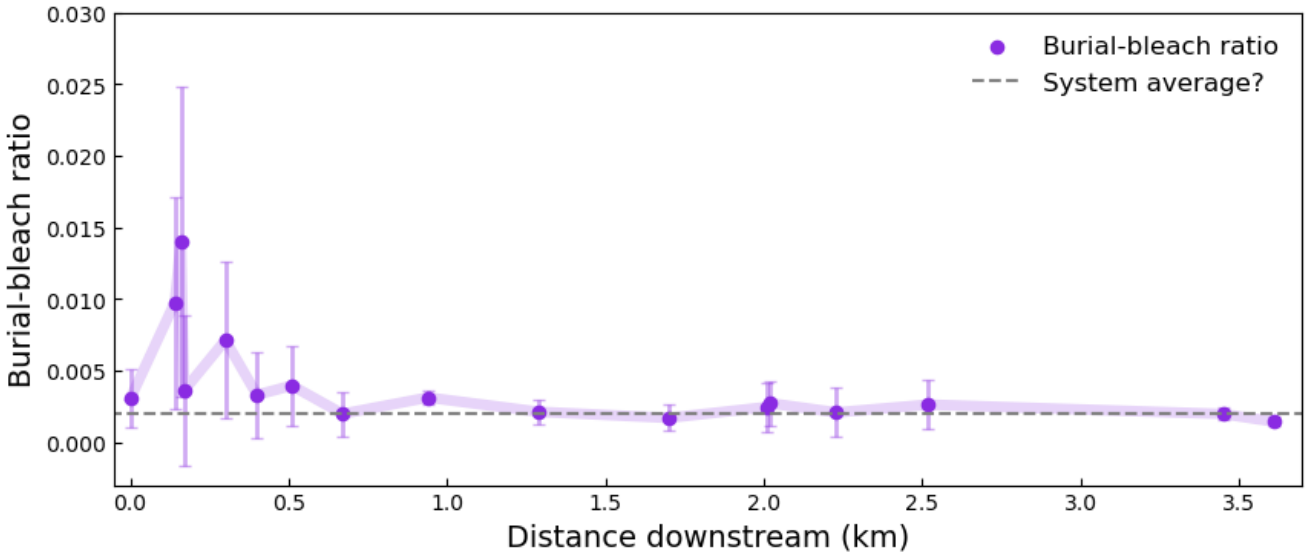

Figure 4.14. *Super synthetic aliquot burial-bleach ratios using the approach of Rhodes & Leathard (2022) plotted against downstream distance. Note the grey dashed line is drawn as a potential average burial-bleach ratio of 0.002 that is characteristic of the transport regime of the Allt Dubhaig. This has not been calculated, it is a suggestion and possibly interesting concept to explore if this type of pattern is observed in other rivers.*

4.4.4. Downstream plateau ages

The plateau ages and plateau types of a subset of nine samples are inspected in close detail. The locations of these samples are shown in Figure 4.15. The nine samples were selected to obtain representative spatial coverage of the study site: four from the upper reach, three from the middle reach, and two from the lower reach. Figure 4.16 displays samples 18031, 22181, 22180 and 22183, Figure 4.17 displays samples 22187, 22188, 22189, 22191, and 22190. The relative locations of these samples are displayed in each subplot. The plateau ages for individual grains within these nine samples are shown in Figure 4.16 and Figure 4.17. The type of plateau is also shown, which refers to the measurement temperatures contribute to a given plateau age. The range of plateau ages and plateau types has the potential to provide insight into the range of possible storage and transport histories for these grains.

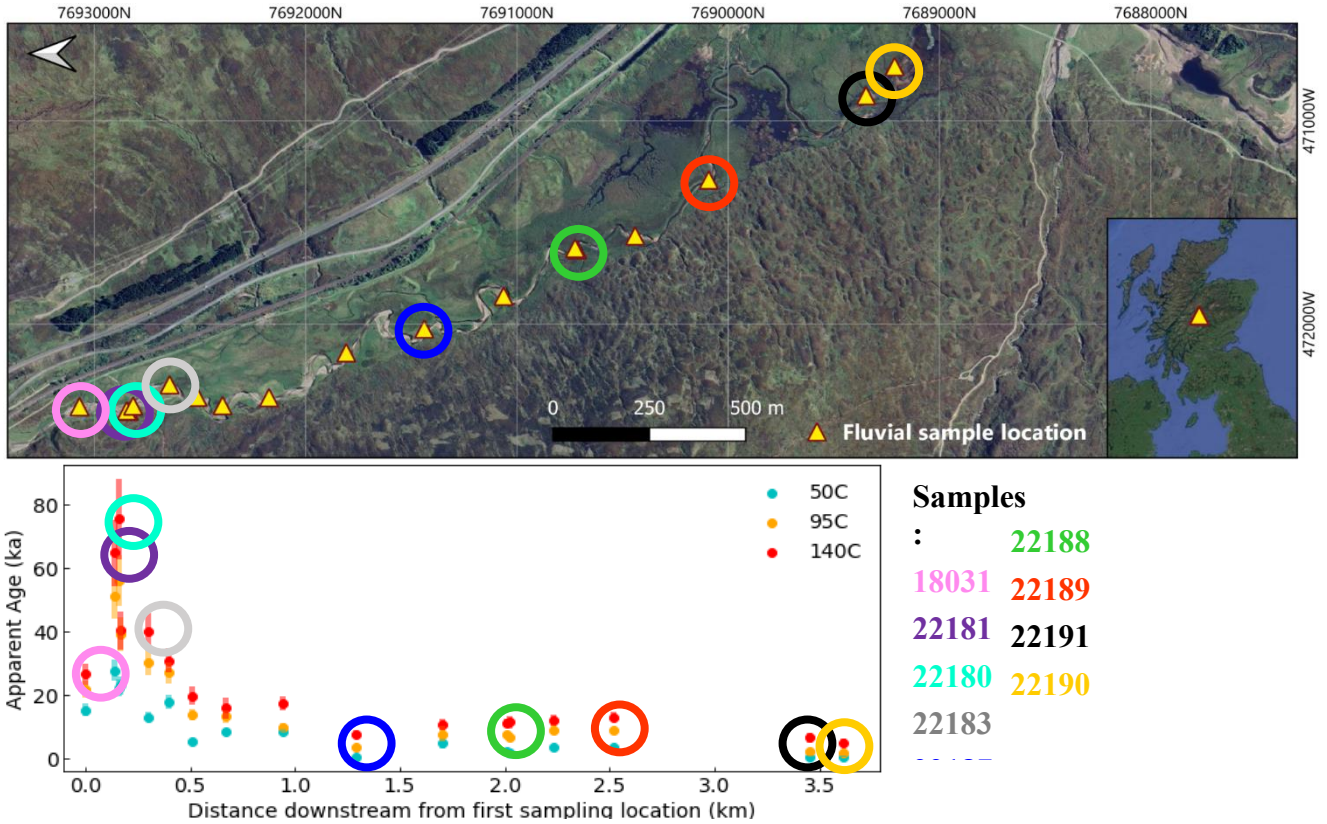

***Figure 4.15**. The top panel highlights the locations of the nine samples for which plateau ages were calculated with coloured circles. The lab codes of these samples are listed in the corresponding colour to the right of the bottom panel. The bottom panel highlights the super synthetic aliquot apparent age estimates for these samples.*

In Figure 4.16, sample 18031 (1) is ~ 100 m upstream of the moraine and has a minimum single grain plateau age of 0.36 ± 0.05 ka. The majority of grains likely share this history; a few grains display older ages with a the oldest > 100 ka. Moving downstream, sample 22181 (2) has a plateau age of 0.26 ± 0.05 ka, yet we observe many older grains. This sample was taken from the active channel just immediately downstream of the moraine. Further, the scatter of its plateau ages (Figure 4.16) closely resembles the pattern shown in sample 22178 from glacial till in the moraine exposure (Figure 4.16) which was taken from exposed glacial till in the moraine, however they appear to be 'shifted younger'. Similarly, the scatter of plateau ages of the next sample downstream, also share remnants of a declining base, but with fewer grains older grains, yet has a minimum age of 0.51 ± 0.8 ka. Continuing to move downstream, sample 22183 has a minimum age of 0.19 ± 0.05 ka, and a small group of grains with ages ranging from 25 ka to 75 ka.

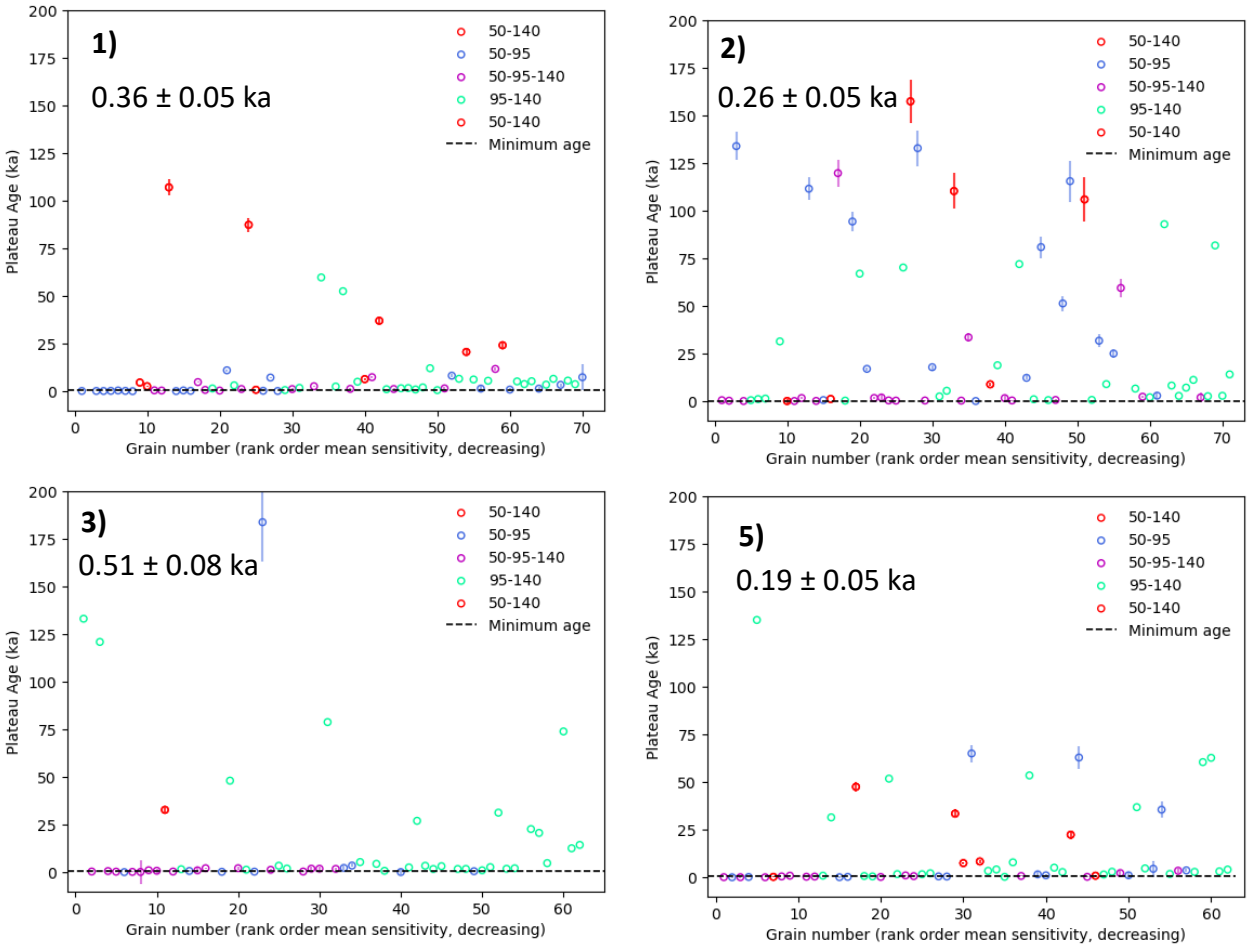

Figure 4.16. *Single grain plateau ages for a subset of samples 18031, 22181, 22180 and 22183. Coloured points indicate plateau age and type for individual grains. Minimum age calculated from plateau ages is shown on each subplot and is indicated by the black dashed line. The bold numbers on each subplot represent the relative locations of these samples*

In the middle reach are samples 22187 (10), 22188 (12) and 22189 (14) (Figure 4.16). Here, there is less variability but a small number of older grains in samples 22188 (12) and 22189 (14). There is also a downstream reduction in minimum ages of 0.34 ± 0.05 ka, 0.28 ± 0.04 ka, and 0.19 ± 0.03 ka for these three samples. The two most downstream samples, 22191 and 22190, have minimum ages of 0.55 ± 0.07 ka and 0.3 ± 0.05 ka respectively (Figure 4.17). This increase in the lower reach it not observed in downstream profiles using any other method of IRSL signal expression (Figure 4.8, Figure 4.9, Figure 4.10).

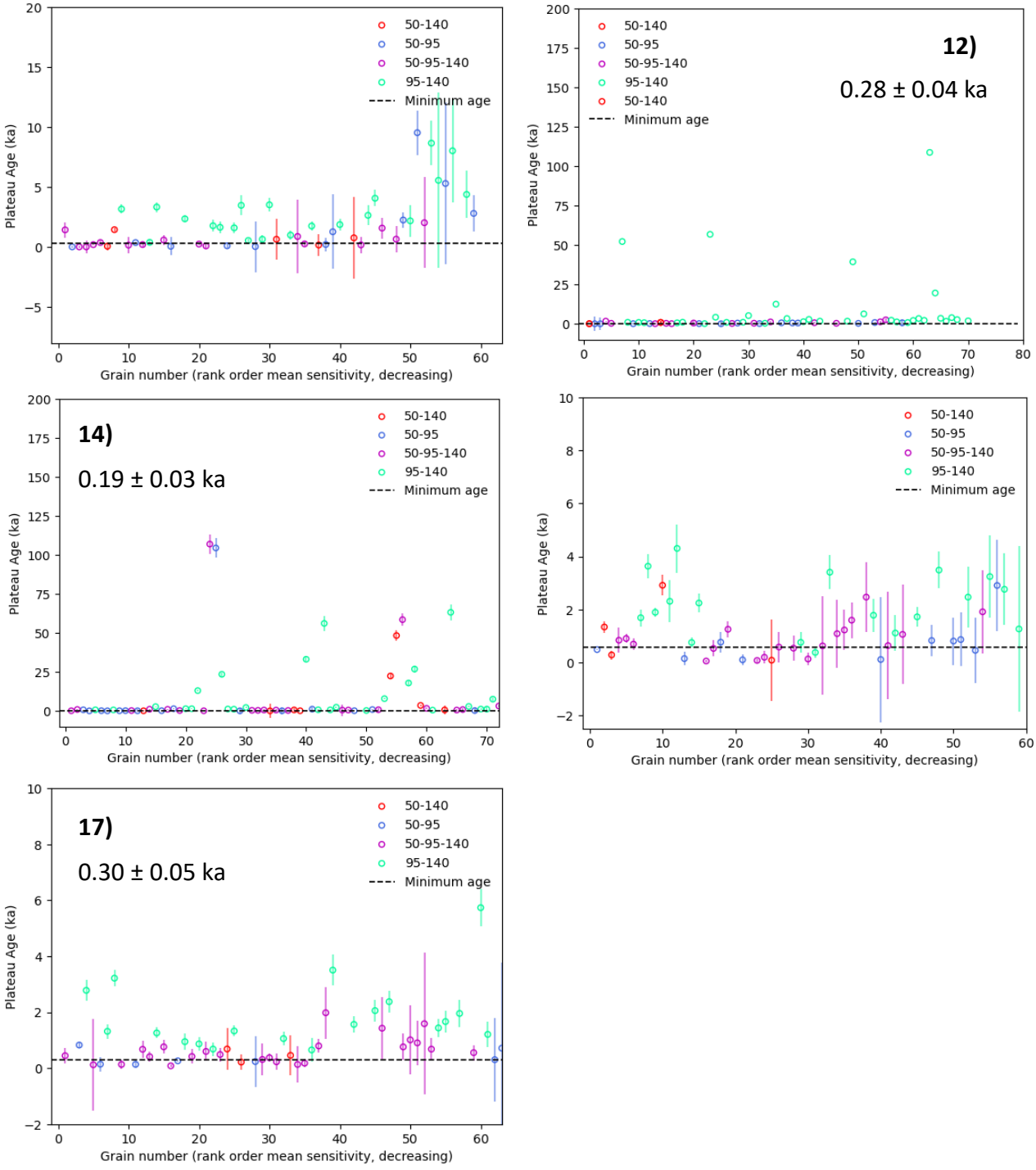

Figure 4.17. *Single grain plateau ages for a subset of samples 22187, 22188, 22189, 22191, and 22190. Coloured points indicate plateau age and type for individual grains. Minimum age calculated from plateau ages is shown on each subplot and is indicated by the black dashed line. The bold numbers on each subplot represent the relative locations of these sample*

This section has presented the analysis MET-IRSL data for samples from the Allt Dubhaig using several different methods including: combined signals apparent age, plateau age, single grain apparent age, equivalent dose, sensitivity and burial-bleach distributions, and the plateau ages and types of individual grains. Each method of analysis contributes a different type of information to the storage

and transport story for the Allt Dubhaig. The following section will discuss what can be learnt from several of the MET-IRSL analysis methods presented here, and the degree to which each contributes to a consistent history in the context of the study site.

4.5. Discussion

This section is structured based on the type of sediment transport and storage information it is possible to elucidate from the data presented in Section 4.4 into three categories. These are:

1) Light exposure regime. Bleaching extent prior to burial can be assessed by interrogating plateau ages and plateau types of single grains. The downstream evolution of the relative frequency of different plateau types is quantified, what can be learnt from this about potential sources of sediment to the main channel is discussed.
2) Storage and transport chronology. ILT-3ET signal ratios of combined signals used to identify the degree to which non-equilibrium bleaching conditions are observed in each sample. A potential method for quantifying minimum light exposure and storage times between sample locations is proposed.
3) Intra channel grain population characteristics. The degree to which distinct populations of grains can be identified within a single sample is assessed with the use of a Gaussian mixture model. The downstream evolution of potential distinct grain populations is discussed.

The final part of this section presents the application of a burial-bleach model described and discussed in Section 3.5.1.2 to the downstream profile of combined ILT-3ET signals of samples from the Allt Dubhaig. Several approaches to fitting the model to these data are explored. The resulting average burial and bleach times that grains are subject to over the time they spend in this system are used in a proposed method for estimating virtual velocity.

4.5.1. Light exposure regime

What is meant by the term ‘light exposure regime’ is the amount, timing, and number of light exposure events that sediment is subject to in a reach of a fluvial system. This can include light exposure during transport or following deposition on a point bar or other feature. Broadly, there are two idealised types of system behaviour in terms of light exposure: 1) bleaching in transport; and 2) bleaching following temporary deposition (Gray *et al.,* 2018; Guyez *et al.,* 2023). In reality, the majority of fluvial systems will exhibit both dynamics in some proportion and may also alternate between which is dominant through time and space. For simplicity, it is assumed that for the Allt Dubhaig, bleaching is dominant. Based on the overall trend of ILT-3ET signal decrease over the study reach, with small sections of

increase, it appears that the Allt Dubhaig exhibits storage and bleaching behaviour consistent with Conceptual model (3) (Figure 1.8) (Section 1.5), which is shown in Figure 4.18.

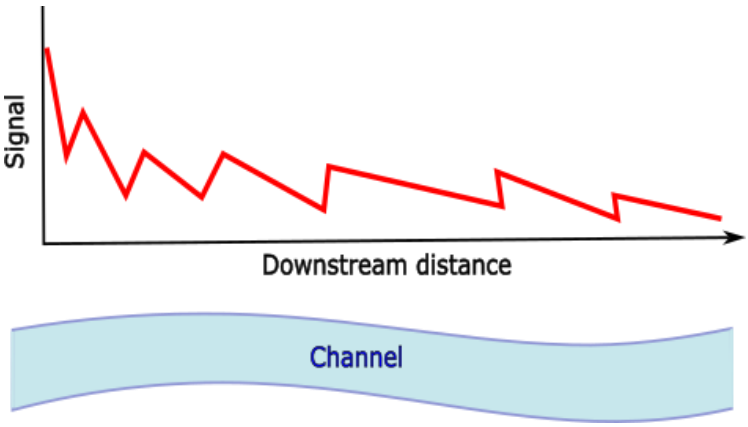

Figure 4.18. *Conceptual model of an idealised channel whereby as grains are transported through the system (left to right), they are subject to both storage and light exposure, but the amount of time exposed to light is sufficient, relative to the time spent in storage, to cause an overall decrease in IRSL signal with downstream distance (from Section 1.4).*

The identification of plateaus between ILT-3ET signals allows assessment of bleaching extent prior to burial. This section explores whether the proportions of plateau types observed in a single sample can be used to identify the different pathways grains in that sample may have taken to enter the channel. Specifically, grains that were entrained from the moraine, and grains that entered the channel upstream of the study reach from elsewhere in the valley. Using the ILT-3ET protocol, there are four possible plateau types outlined by Ivester *et al.* (2022):

1) Three-temperature (3T) plateau indicates sufficient light exposure to reset all three signals.
2) Low temperature plateau (LT) between the IR_{50} and the IR_{95} implies partial bleaching insufficient to reset the slow-bleaching IR_{140}.
3) High temperature plateau (HT) between the IR_{95} and the IR_{140} indicates a short light exposure event that causes reduction or resetting of the IR_{50}, but not the IR_{95} and the IR_{140}, a HT plateau also suggests that the penultimate light exposure event was sufficient to reset the IR_{95} and the IR_{140}.
4) A plateau between the IR_{50} and IR_{140}. This is a potentially anomalous response where ILT-3ET age estimates are not in the 'right' order (Rhodes & Leathard, 2022).

Figure 4.19 shows the frequencies of different plateau types for each sample in Figure 4.15. Starting with the samples in the upper reach of the site, we see the highest number of HT plateaus in sample 22181, which is the first sample downstream from the moraine. It is suggested that this reflects grains that have been eroded from the moraine base, and immediately subject to light exposure on entry to the in-channel flux. Simultaneously, we see a reduction in LT plateaus and an increase in 3T plateaus for

samples 18031, 22181 and 22180. These could be grains that originated upstream of the moraine that have spent sufficient time in transport for all three ILT-3ET signals to be reset. This may indicate that prior to the perturbation to the in-channel sediment flux caused by input of glacial sediments, grains are getting increasingly well-bleached before entering storage are exposed to more light during a typical transport cycle as they travel downstream.

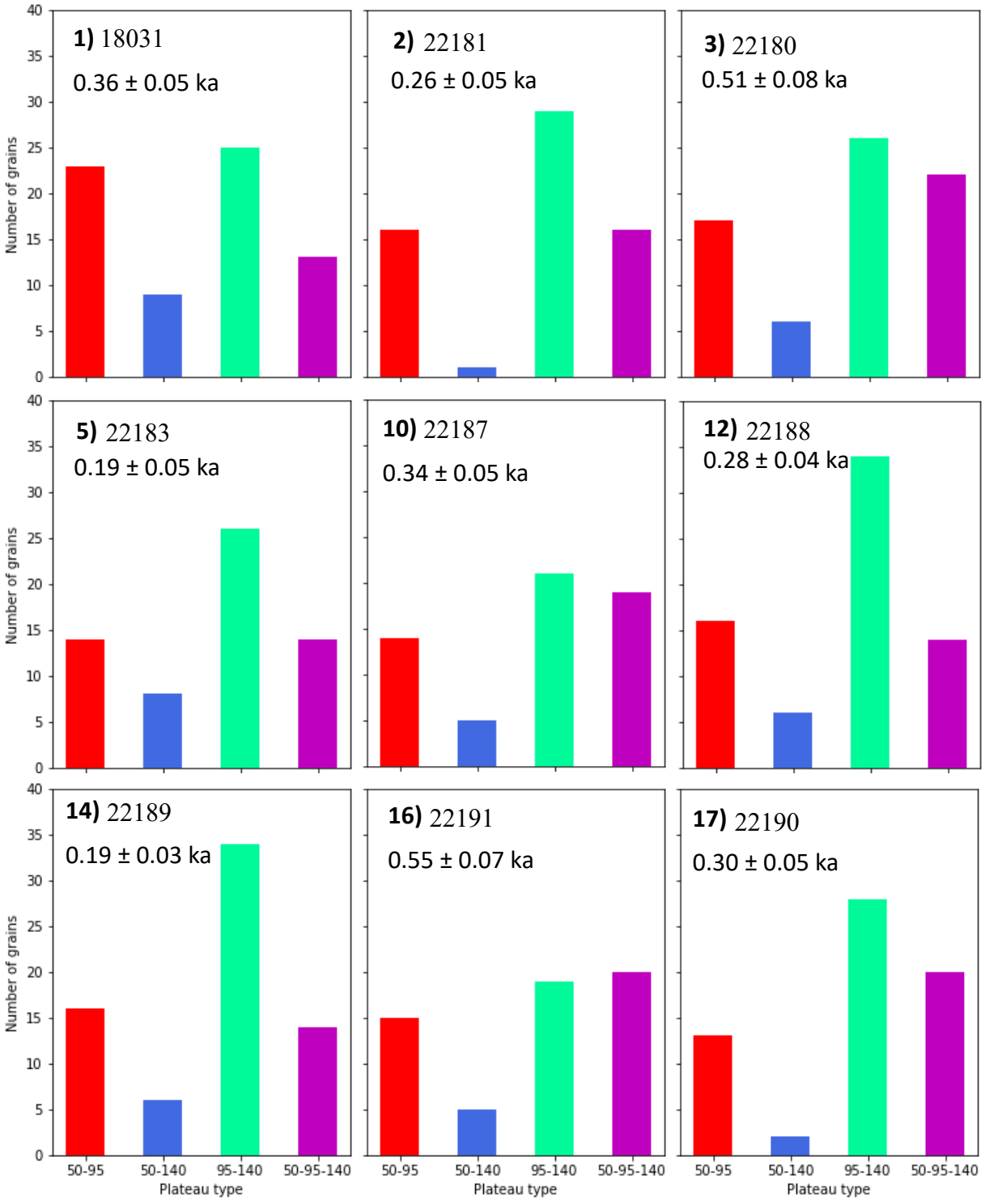

Figure 4.19. *Frequency of different plateau types. It is possible to observe four types of plateaus using the ILT-3ET measurement protocol.*

Moving towards the middle reach, we see a reduction in HT plateaus and an increase in 3T plateaus in samples 22183 and 22187. We also observe a rapid reduction in SSA apparent age and fraction of saturation over this ~ 1 km stretch (Figure 4.8). This combination suggests, over this section of the stream, grains are being flushed through on relatively short timescales and the dominance of bleaching in transport is in fact observed. Further, between samples 22183 and 22191, there is a gradual increase in 3T plateaus. This may indicate the 'resident' population of grains that originate upstream of the moraine and are subject to increasing light exposure as they travel down this ~ 800 m stretch. The flattening of age profiles throughout this section is interpreted to mean that grains begin to move increasingly slowly through this section and are being bleached for longer durations as they do so.

In samples 22188 and 22189, we observe a significant increase in HT plateaus combined with a gradual increase in SSA apparent age (Figure 4.8) ~ 2 km downstream of our most upstream sampling location. However, an increase in minimum plateau age is not observed. This could suggest input of new, poorly bleached older material.

There are two potential explanations for this. First, between sample 22187 and 22188 a small tributary, meets the main channel. The tributary, shown in Figure 4.20, flows through the floodplain, adjacent to the Allt Dubhaig to the east. Grains that comprise the sediment load of this tributary will have had different transport-storage histories owing to its smaller size. In addition, the eastern valley wall is considerably further from the tributary than the western wall is to the main channel. Thus, the main channel is more likely to be supplied with sediments from the valley sides, from sources such as the moraine in the upper section of the alluvial reach. The ages, bleaching and bleaching status of grains transported by the tributary will likely differ from those of the main channel, thus perturbing the signal. An alterative interpretation follows from the observation of Ferguson & Ashworth (1991), that the lateral activity of the Allt Dubhaig increases further downstream of the alluvial section. Thus, sufficient new material to cause an increase in apparent age could be supplied by bank erosion of flood plain sediments. Making the assumption that floodplain sediments were fluvially transported in the main channel prior to deposition and burial, this could account for the poorly bleached status of potential input of new material and the older age. The age of the source of this new material is not inferred directly from these data. However, an increase in apparent age with downstream distance tells us that new material is older than the resident material of the main channel. Both scenarios contradict our expectations of minimal lateral input of sediment to the Allt Dubhaig.

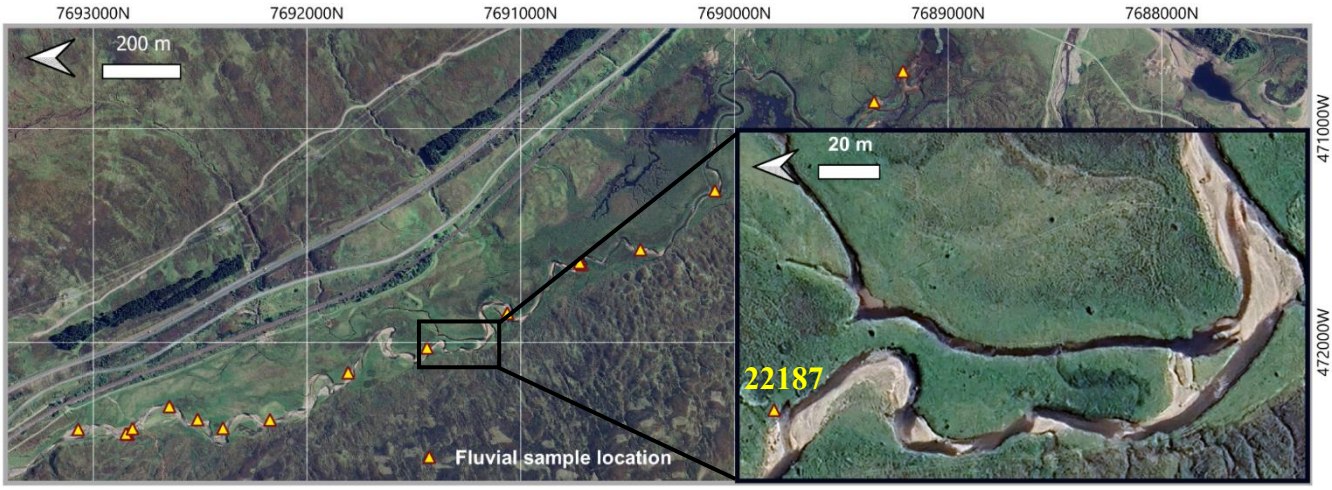

***Figure 4.20**. The location of the confluence between the main channel of The Allt Dubhaig and a small tributary that joins between the locations of sample 22187 and 22188.*

The ability to identify plateau ages is unique to MET-IRSL. Inspection of the downstream evolution of plateau type frequencies has provided insight into the timings and locations of potential perturbation to the idealised pattern of Conceptual model 3 shown in Figure 4.19. Two potential mechanisms of lateral input of sediment have been identified: 1) in the upper section, likely from the moraine and 2) in the middle-lower section, either from tributary input or significant variation in rates of erosion of floodplain sediments, or a combination of these processes. It is suggested that the case of variable rates of bank erosion of floodplain sediments is perhaps most consistent with the observations presented here and those of other studies (e.g. Ferguson & Ashworth, 1991).

4.5.2. Grain storage and transport chronology

This section will inspect signal ratios of combined signals used to identify the degree to which non-equilibrium bleaching conditions are observed in each sample and explore a method for quantifying minimum light exposure and storage times between sample locations.

By applying the concept of equilibrium and non-equilibrium bleaching introduced in Section 3.5.1.1 in Chapter 3, the extent of light exposure prior to burial, for the total signal, can be determined. Here, equilibrium bleaching parameters measured for sample 22181 (the second sample along the downstream profile) were used to forward model bleaching rates of ILT-3ET signals with increasing prior light exposure (Figure 4.21). This forward model predicts the reduction in bleaching rate with increasing prior light exposure, shows this effect is more pronounced at the lower measurement temperatures, as observed in Experiments 3.4.1.1 and 3.4.1.2, Chapter 3. The black line in the plots shown in Figure 4.21 represents an equilibrium bleach.

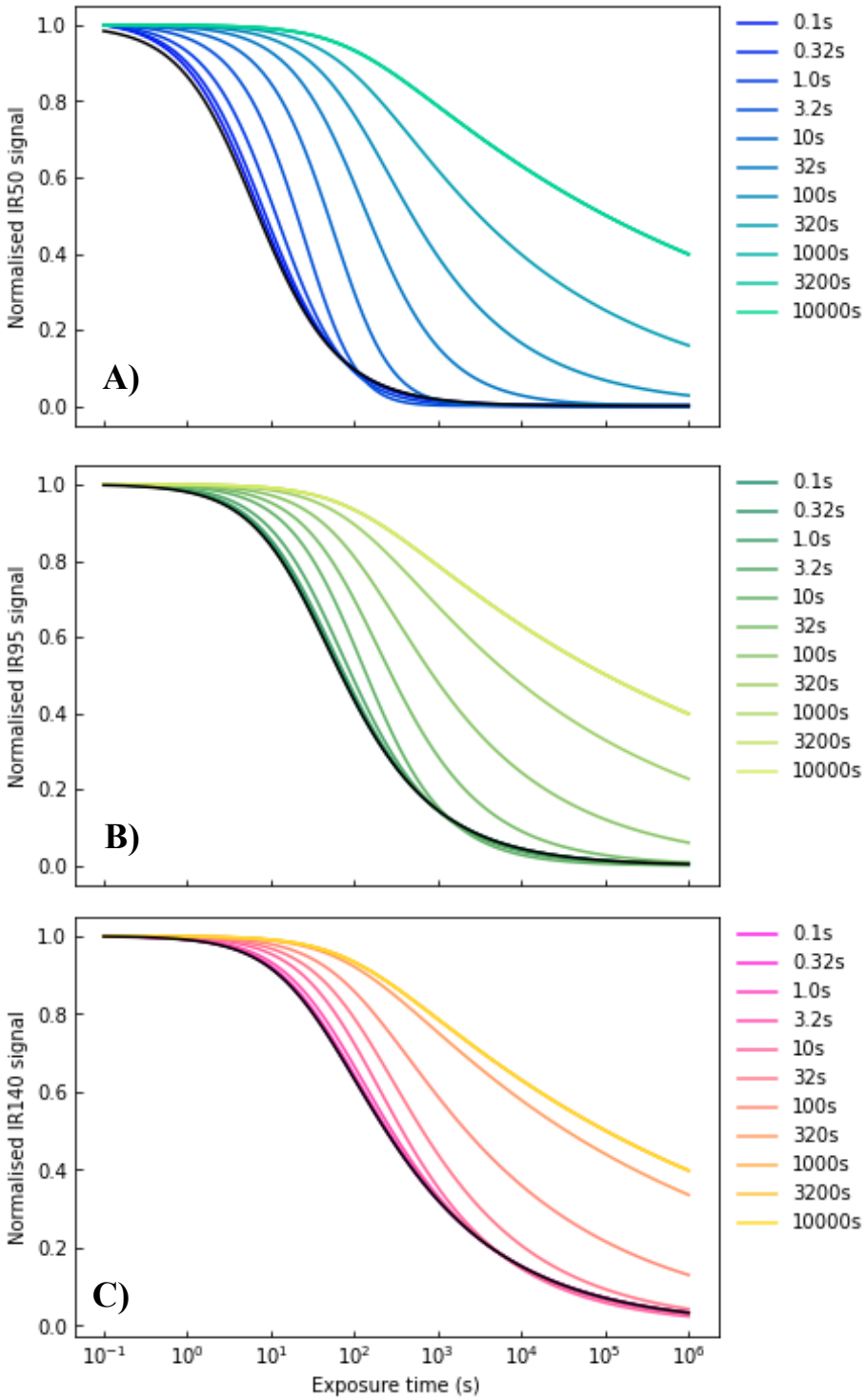

Figure 4.21. *Measured equilibrium and modelled non-equilibrium blue light bleach curves for combined signals of sample 22181 expressed as a fraction of the unbleached signal for the IR_{50} (**A**), IR_{95} (**B**) and IR_{140} (**C**). The bold black line in each panel is a fit to equilibrium blue light bleaching measurements. The coloured lines are forward modelled non-equilibrium bleach curves with increasing lengths of prior blue light exposure.*

Signal ratios for the modelled decays in Figure 4.21 were calculated by dividing the IR_{50} decays by the IR_{95} decays and dividing the IR_{95} decays by the IR_{140} decays. These are shown by the coloured lines in Figure 4.22 below, with observed signal ratios from the suite of 17 fluvial samples from the Allt Dubhaig (black circles). Signal ratios of observed samples were calculated using fraction of saturation

In Figure 4.21, the y-axis is the signal ratio; the x-axis is an estimated light exposure time. For the observed fluvial signals, an estimated fraction of saturation light exposure equivalent was calculated by using Eq. 1.3, Chapter 1, which is the bleaching function of (Bailiff & Barnet, 1994), rearranged in terms of time, t with I_0 as the observed fraction of saturation. Estimated light exposure equivalent is herein denoted as $t \approx FoS$. Non-equilibrium bleaching is assumed because, looking at Figure 4.8 agreement between ILT-3ET signals is not observed, which suggests signals were not reset prior to burial. Therefore, parameters a, and b are the corresponding non-equilibrium bleaching parameters from the fits shown in Figure 4.21 above. Each sample was assigned a pair of non-equilibrium parameters, depending on its signal ratio.

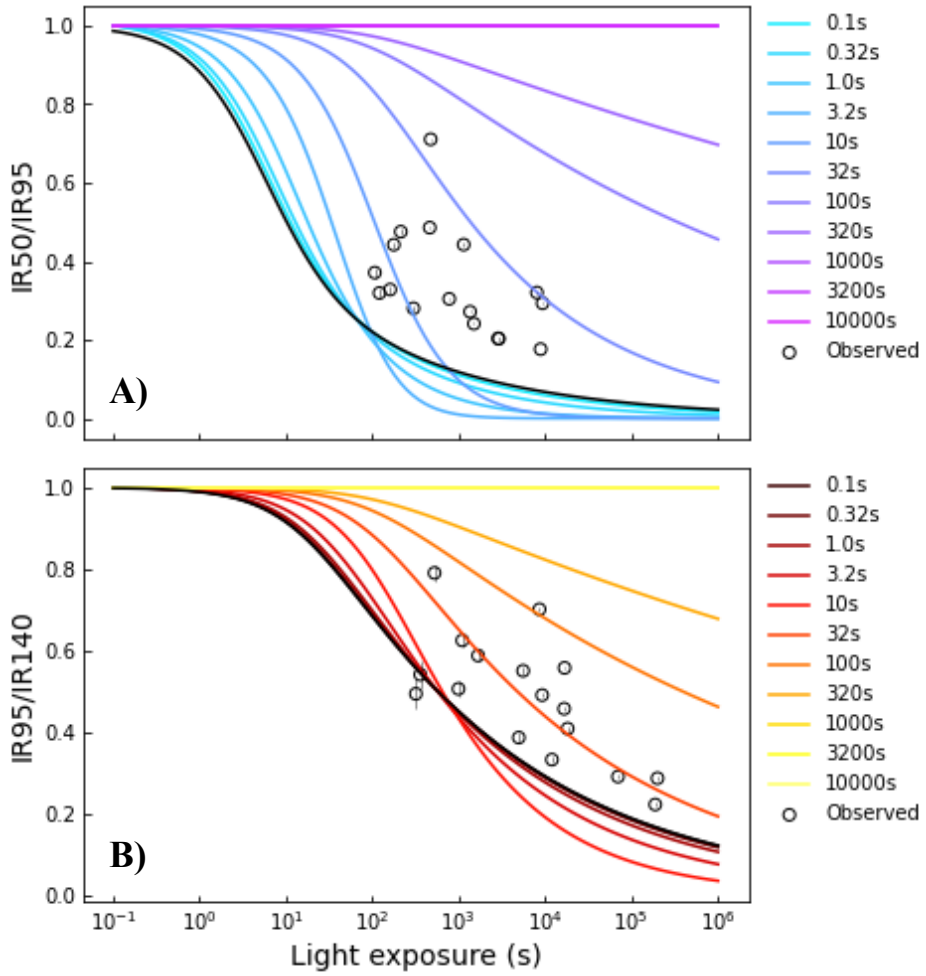

Figure 4.22. *Ratios of measured equilibrium (black line) and modelled non-equilibrium (coloured lines) blue light bleach curves of sample 22181.* ***A)*** *ratios of the IR_{50} to the IR_{95} signals.* ***B)*** *Ratios of the IR_{95} to the IR_{140} signals. The black circles represent ratios of measured signals of the fluvial samples, for these data x-axis values were calculated by converting fraction of saturation to estimated light exposure equivalent using the bleaching function of (Bailiff & Barnet, 1994), rearranged in terms of time, t.*

By estimating the degree of departure along the x-axis of the observed signal ratios (black circles in Figure 4.22) from the equilibrium line (black line in Figure 4.22), using linear interpolation, it is possible to estimate light exposure prior to burial, t_{prior} for that sample accounting for the necessary increase in signal of the following sample. A minimum length of past light exposure is estimated using the signal ratios of the IR_{50} and the IR_{95}, and a maximum exposure time using the signal ratios of the IR_{95} and the IR_{140}. These values are converted to a fraction of saturation equivalent, ΔFoS, which represents the change in fraction of saturation as a result of estimated light exposure prior to burial. This can be expressed as:

$$t_{prior} = t_{eq} - t_O \tag{4.1}$$

$$\Delta FoS = \frac{FoS_O}{(1 + a * t_{prior})^b} \tag{4.2}$$

where $t_O$is light exposure in seconds when y is equal to observed fraction of saturation, t_{eq} is light exposure in seconds when the equilibrium ratio is equal to observed fraction of saturation, FoS_O is observed fraction of saturation for a given ILT-3ET signal for a given sample, a is bleachability from equilibrium fits shown in Figure 4.5.3 above, b is order from fits the equilibrium fits shown in Figure 4.21 above. Figure 4.23 shows ΔFoS subtracted from FoS_O plotted with downstream distance for the three ILT-3ET signals.

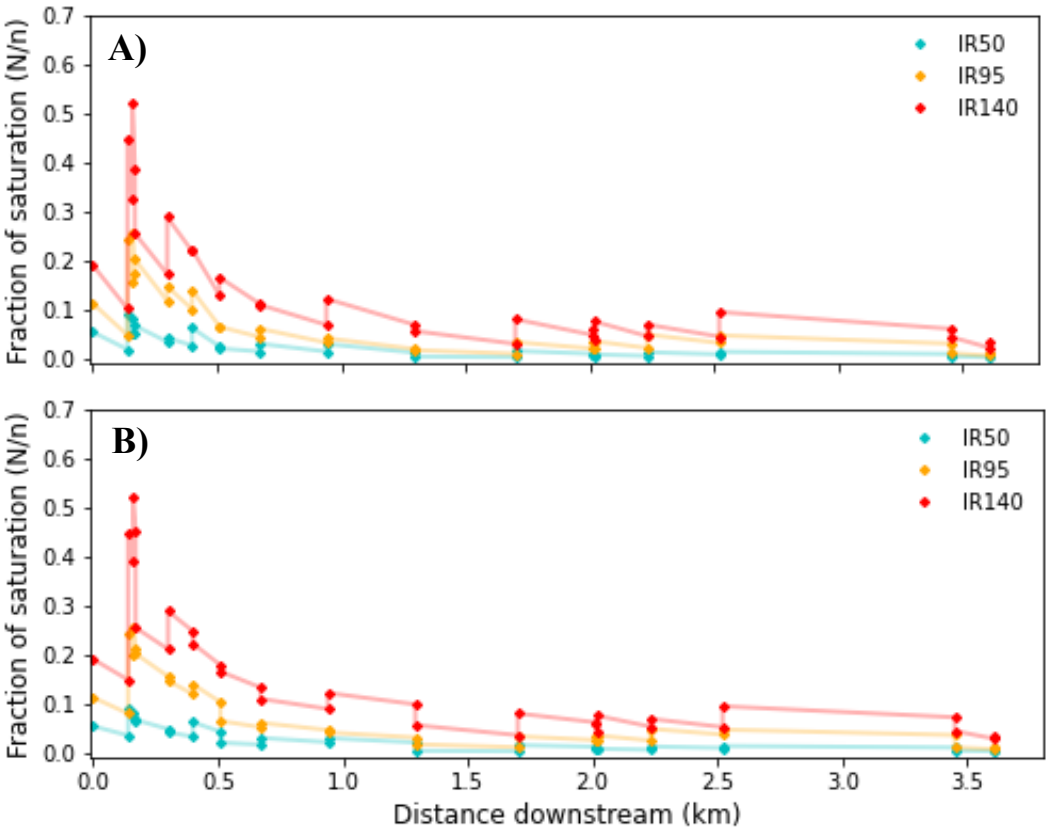

Figure 4.23. *FoS_O with ΔFoS subtracted from FoS_O for each sample location. FoS_O is simply observed fraction of saturation., ΔFoS is calculated as the degree of departure of the observed signal ratios from measured equilibrium ratios converted into fraction of saturation. ΔFoS is calculated using the corresponding non-equilibrium bleaching parameters.* ***A)*** *A minimum ΔFoS is calculated using IR50 to IR95 signal ratios.* ***B)*** *A maximum ΔFoS is calculated using IR95 to IR140 signal ratios*

Figure 4.23 shows that in the upstream section, where a rapid decrease in fraction of saturation is observed, longer bleach times, which produce larger values for ΔFoS, prior to burial are necessary to achieve this rate of signal reduction. Whereas downstream, shorter bleach times are observed. Figure 4.24 shows minimum and maximum estimates of light exposure equivalent, $t \approx FoS$. In contrast to what is observed in Figure 4.23, minimum and maximum estimates of $t \approx FoS$ increases significantly downstream (Figure 4.24)

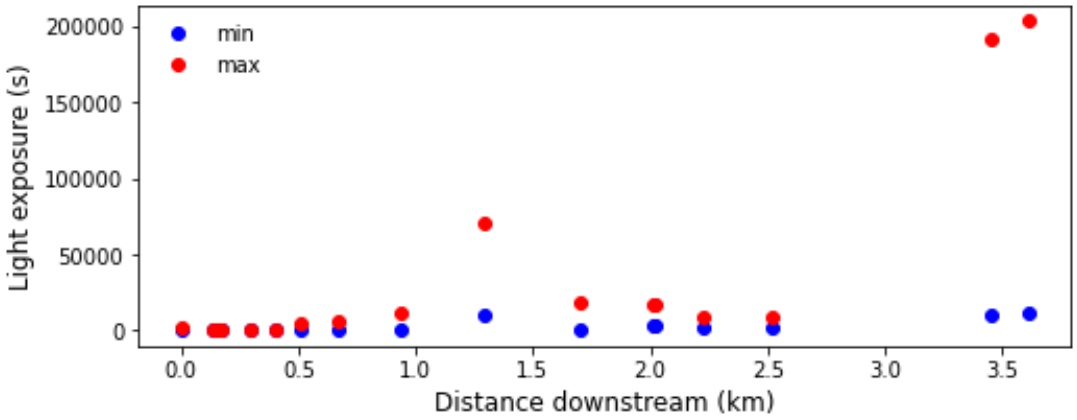

***Figure 4.24**. Minimum and maximum light exposure equivalent, $t \approx FoS$ of combined ILT-3ET signals plotted with downstream distance. It appears light exposure prior to the most recent burial increases downstream.*

This suggests some mechanism that causes and increase in fraction of saturation, and apparent age, despite increasing light exposure prior to burial downstream, and that does not cause our three signals to depart from each other significantly. It is suggested that this mechanism is the entrainment of floodplain material eroded from the banks, the signal of which may also have been observed in single grain plateau type variability presented in Section 4.19. Further, the input of this new material does not cause significant perturbation to the relative difference between the three signals. Therefore, it is suggested that the ILT-3ET signals of these flood plain sediments could be in similar ratios to those that we observe in our samples from the main channel. In turn, this may indicate that these sediments were previously transported under a transport regime similar to that we observe in the present day.

4.5.3. Intra-channel grain population characteristics

This section discusses the potential of single grain distributions to provide a finer resolution insight into the diversity of grain histories in the system, and isolate distinct groups of grains with shared histories. The real power behind this concept stems from the fact that a single grain is the smallest measurable unit of transport and storage. A single grain has been subject to the same dose and light exposure history. Additional power comes from the ability to curate hundreds of observations from a single sample, which allows for assessment of the probabilities of different transport and storage histories.

A gaussian mixture model is fit to $\log_n$ single grain equivalent dose distributions for all 17 of the samples collected from the active channel of the Allt Dubhaig. These include all grains that provided an equivalent dose and therefore contain information from partially bleached grains as well as well-bleached grains. Each sample was fit with one through six components and Akaike Information

Criterion applied to determine the number of components that produced an optimal fit. Optimal fits are displayed in Figures 4.25-28 for equivalent doses determined from the IR_{50}, IR_{95} and IR_{140} signal.

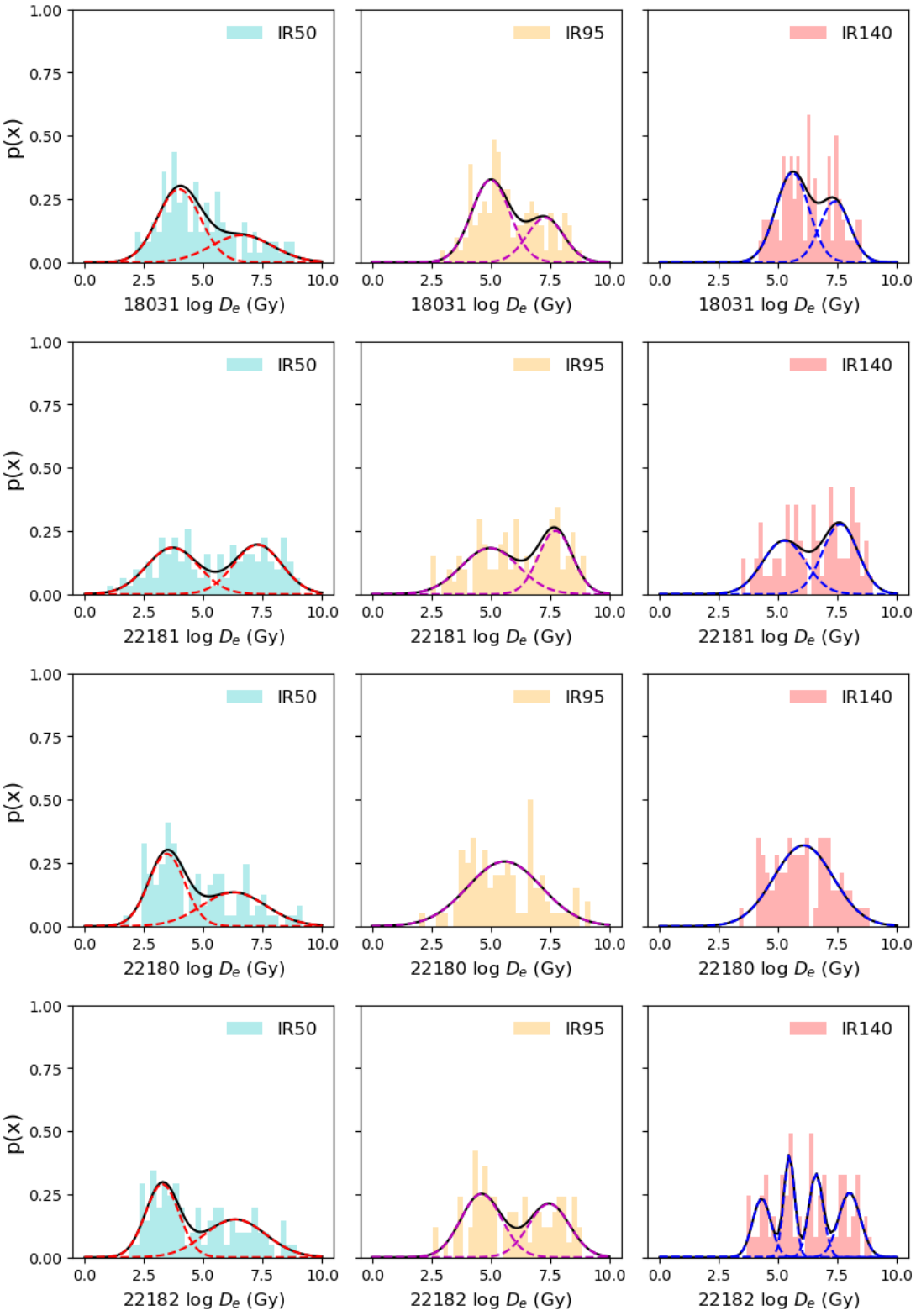

***Figure 4.25**. Optimal fits of a gaussian mixture model to log equivalent dose distributions estimated for the IR_{50}, IR_{95} and IR_{140} signals. Black lines represent the best fit probability density function, coloured dashed lines represent best fit component probability density functions. Samples shown here are 18031, 22181, 22180, 22182, in downstream order*

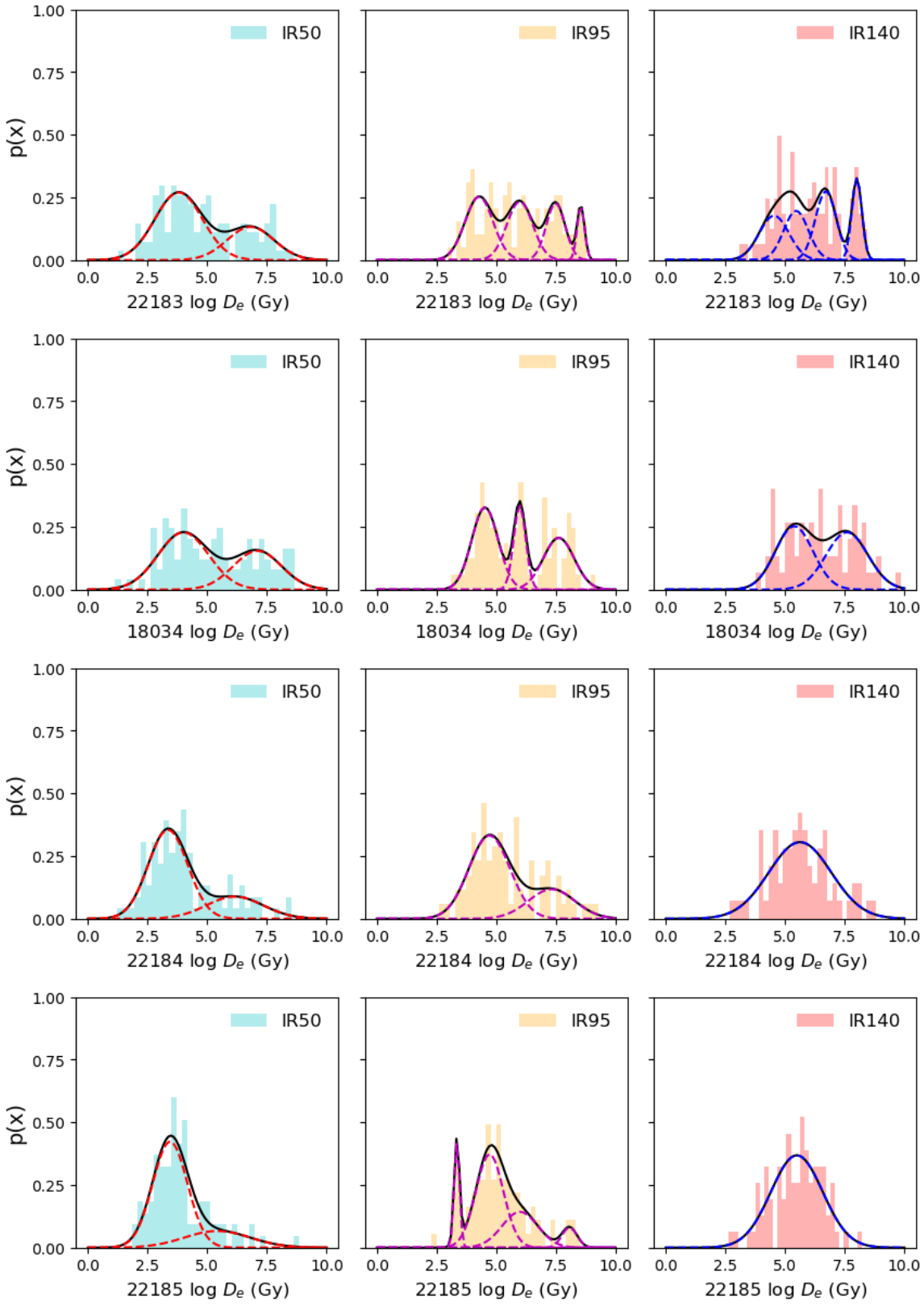

***Figure 4.26**. Optimal fits of a gaussian mixture model to log equivalent dose distributions estimated for the IR_{50}, IR_{95} and IR_{140} signals. Black lines represent the best fit probability density function, coloured dashed lines represent best fit component probability density functions. Samples shown here are 22183, 18034, 22184, 22185, in downstream order.*

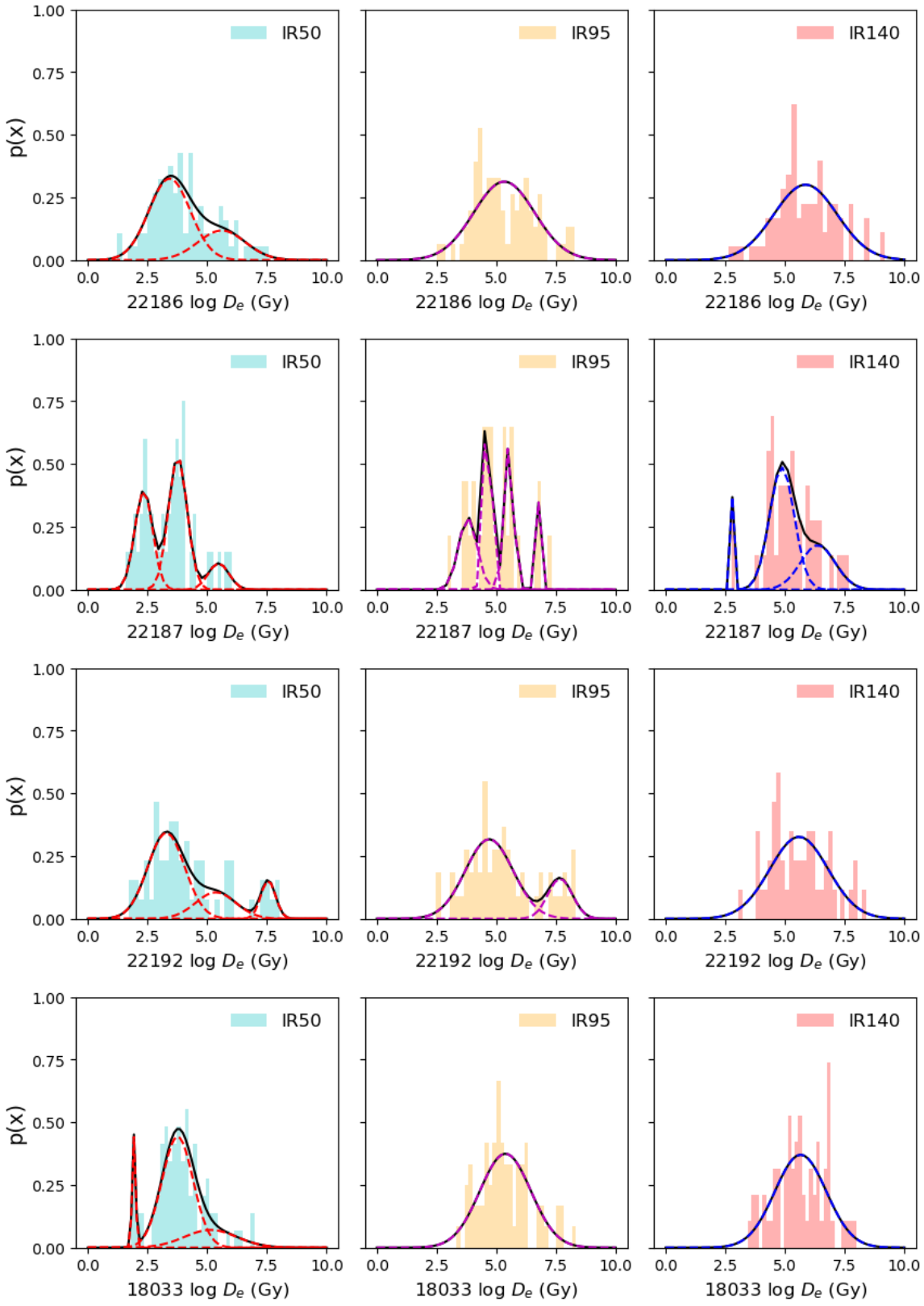

Figure 4.27. *Optimal fits of a gaussian mixture model to log equivalent dose distributions estimated for the IR_{50}, IR_{95} and IR_{140} signals. Black lines represent the best fit probability density function, coloured dashed lines represent best fit component probability density functions. Samples shown here are 22186, 22187, 22192, 18033 in downstream order.*

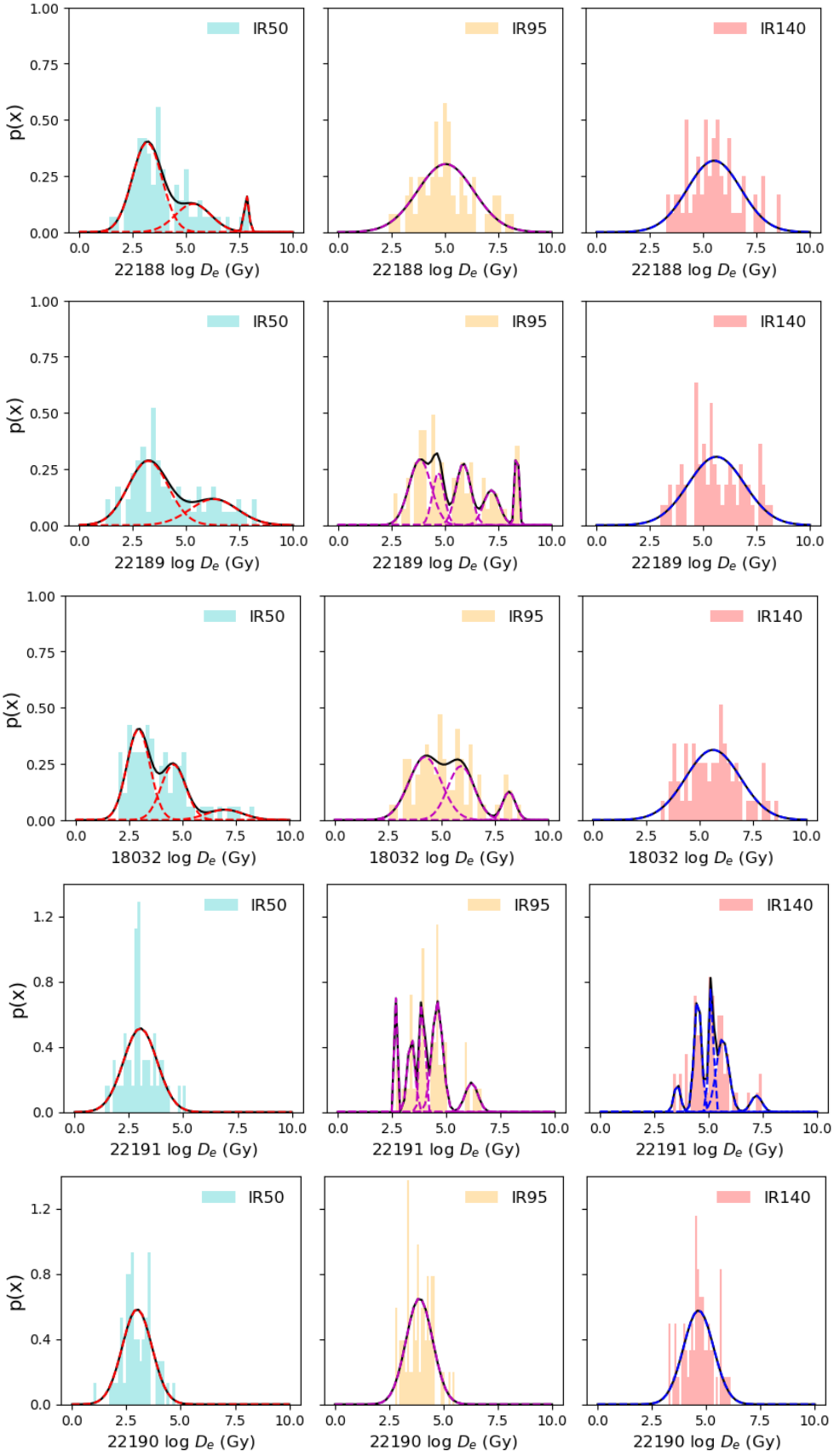

Figure 4.28. *Optimal fits of a gaussian mixture model to log equivalent dose distributions estimated for the IR_{50}, IR_{95} and IR_{140} signals. Black lines represent the best fit probability density function, coloured dashed lines represent best fit component probability density functions. Samples shown here are 22188, 22189, 18032, 22191, 22190 in downstream order.*

Using this procedure, two gaussians provide an optimal fit for the three most upstream samples, and this is consistent for all three measurement temperatures, apart from the IR_{140} and IR_{95} for sample 22180. Continuing downstream, IR_{50} distributions remain best fit by two components, with an increasingly greater probability of grains belonging to the younger component population, until the tenth sample downstream, 22192. The IR_{95} distributions of samples 22183 and 18034, the fifth and sixth samples downstream, are best fit by four and three components respectively. The IR_{140} for these samples is best fit by three and two components. Downstream from this, IR_{140} equivalent dose distributions are best fit by a single gaussian and the optimal fit for the IR_{95} fluctuates between two and three components. Yet further downstream, at sample 22189 and 22191, the IR_{95} is best fit with five components, however this complexity is not detected by this procedure in the distributions of the IR_{50} and IR_{140}.

The same procedure was applied to equivalent dose distributions of sample 22178, taken from the moraine sediments, with results visible in Figure 4.29. The plateau age of this sample was measured to be 14.9 ± 2.6 ka. The moraine sediments are largely comprised of two main components, with grains much more likely to be from the older population. The older grains are likely pre-glacial sediments, perhaps deposited fluvially or comprising soil cover.

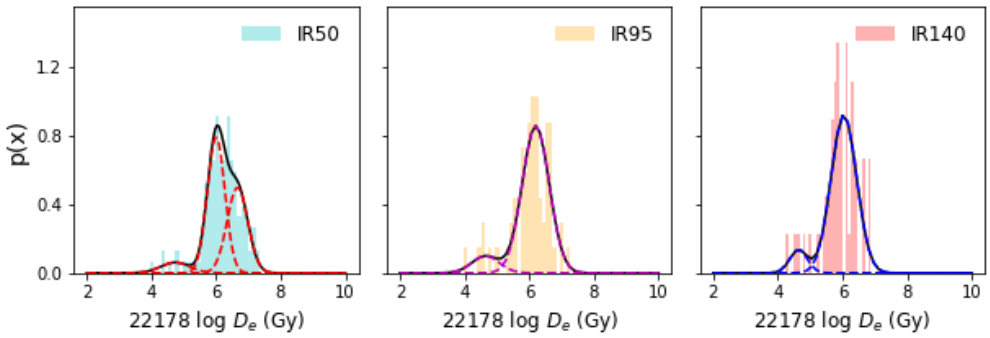

Figure 4.29. *Optimal fits of a gaussian mixture model to log equivalent dose distributions estimated for the IR_{50}, IR_{95} and IR_{140} signals for sample 22178, which was taken from the moraine. Black lines represent the best fit probability density function, coloured dashed lines represent best fit component probability density functions.*

For the fluvial samples, the probabilities of grains belonging to either of the two populations within each of the four most upstream samples appear to be of a more similar size, compared to the moraine sample shown in Figure 4.29. One explanation for this is that the younger population is comprised of fluvial sediments transported from elsewhere in the catchment, and that the older population is comprised of glacial sediments entrained from the moraine in the upstream section of the study site. With four components providing a best fit, the IR_{140} distribution of sample 22180 suggests comparable likelihoods of finding grains of four different ages. This is not in agreement with the IR_{50} or the IR_{95}, and could be the product of the low bleachability of the IR_{140}. It is possible that as grains are entrained

from the moraine, the IR_{50} and IR_{95} are bleached rapidly and that their distributions more closely reflect the transport regime of the stream. In this scenario, the IR_{140} may reflect the various bleaching histories of the grains that comprise the moraine sediments.

There is consistent homogeneity of the IR_{140} downstream of sample 18034, whereas the IR_{50} and IR_{95} distributions display greater complexity. An explanation for this behaviour could be related to the concept of equilibrium and non-equilibrium bleaching. As well as a slow bleaching rate, the IR_{140} is also characterised by a slower departure from equilibrium bleaching conditions (Figure 4.5.3). The forward model of bleaching rate following variable lengths of past light exposure in Section 4.5.3.2 predicts that the IR_{140} requires ~ 5 minutes of prior blue light exposure in laboratory conditions to display significant departure from equilibrium bleaching behaviour. In nature, there are several factors that could lengthen the time necessary for this to occur in this setting, such as cloud cover and turbidity. Thus, it is suggested that the complexity of the IR_{50} and IR_{95} relative to the IR140, may reflect populations of grains in various degrees of disequilibrium, which are a product of different light exposure and transport histories.

4.5.4. Burial-bleach model development for transport rate estimation

This section discusses the application of the burial-bleach model described in Section 3.5.1.2, Chapter 3 to the downstream profile of combined signals. A detailed description parameters can be found in 3.5.1, Chapter 3. In this preliminary modelling study, the burial-bleach model was fit to the fluvial dataset by minimising the sum of the squared difference between the most upstream data point and the most downstream data point. In Section 5.5 some of the results shown below are compared to those obtained through modelling the histories of individual grains.

Model parameters include: number of burial-bleach cycles, bleach time per cycle, burial time per cycle, bleaching acceleration and burial acceleration. The number of cycles simulated was varied between 5 and 15, burial time was varied between 200 and 2000 years, and both bleaching and burial acceleration was varied between 0.5 and 2.5. Parameter space was explored for bleach time per cycle to experiment with scenarios where either bleaching or storage dominates luminescence behaviour of the in-channel sediment. Each parameter was sampled at 10 equal steps and each model run was comprised of 100,000 simulations. The application of the burial-bleach model to this dataset provides an estimate of average bleaching and burial times for each cycle of transport and storage, and an estimate of the number of cycles a grain or group of grains will undergo between the most upstream sampling location and the most downstream sampling location.

The model was fit to the data using three approaches to assess its explanatory power for the behaviour of this system. These approaches are: 1) using the entire suite of 17 fluvial samples collected in 2018

and 2022) using the dataset of the 13 samples collected in 2022 only (this dataset does not include the sample upstream of the moraine); and 3) by separating the 2022 dataset into an upstream section where rapid reduction in signals is observed and a downstream where gradual increase in signal is observed and fitting these individually.

All model fits used bleaching and growth parameters from direct measurements of sample 22181 (the third sample downstream). For the first approach, bleach time per cycle was varied between 10 and 60 seconds. These values were selected based on the decay of the fastest bleaching signal, the IR_{50} observed for sample 22181. The best fit returned eight cycles of bleaching and burial; 40 seconds of bleaching per cycle; 200 years of burial per cycle; a bleaching acceleration factor of 2.05, and a burial acceleration factor of 1.16. A visual representation of this model output is shown in Figure 4.30. This simulation predicts that, on average, bleaching and storage times increase by 105% and 16% each cycle respectively. Applying the method of transport rate estimation outlined by Conceptual model 1 (Figure 4.30), whereby a virtual velocity can be calculated using the sum of estimated storage times per cycle (Section 1.5), virtual velocity is estimated at 1.26 m yr^{-1} over ~3.5 km.

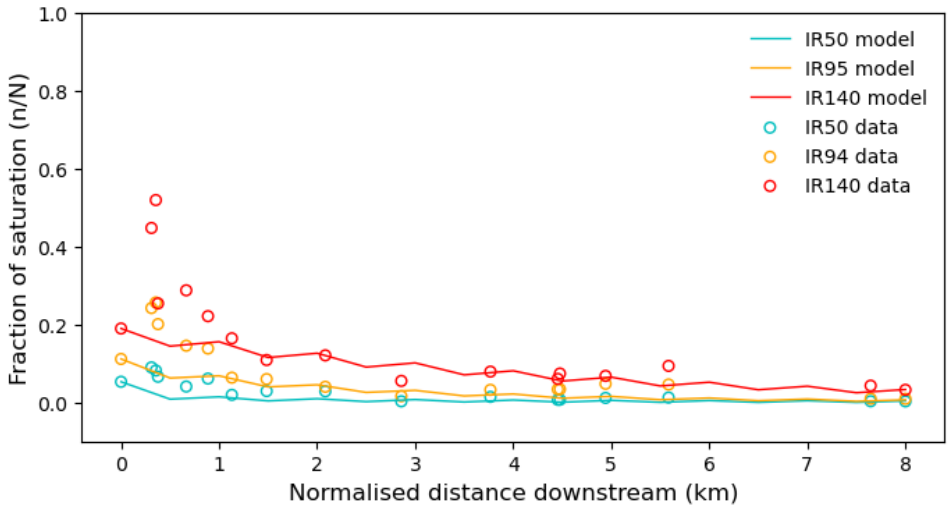

Figure 4.30. *Visualisation of the best fit of the burial bleach model to the entire fluvial dataset from 100,000 simulations using approach 1). The number of cycles simulated was varied between 5 and 15, bleach time was varied between 10 and 60s, burial time was varied between 200 and 2000 years, and both bleaching and burial acceleration was varied between 0.5 and 2.5.*

There is a clear departure of the data from the model at ~0.75 km, which is where it is suggested that the erosion of moraine sediments causes an elevation of the in-channel sediment flux luminescence signal, most notable for the IR_{140}. Downstream from here, the model performs well at estimating the downstream behaviour of the IR_{50} and IR_{95}. Allowing for longer bleach times, between 100 and 1000 seconds per cycle did not improve the fit for this approach.

The second approach simulates bleaching and burial from the first sampling location downstream from the moraine, with a much higher initial fraction of saturation, and starts by varying bleach time per cycles between 10 and 60 seconds. Using the second approach (Figure 4.31), the optimal fit returned 13 cycles of bleaching and burial, 43 seconds of bleaching per cycle, 1200 years of burial per cycle, a bleaching acceleration factor of 2.27, and a burial acceleration factor of 0.94. Here, the model predicts that, on average, bleach time is increasing by 127% every cycle, whereas storage times are decreasing by 6%. These parameter values produce a virtual velocity estimate of 0.31 m yr^{-1}, much slower than that estimated using the first approach. In addition, the model is unsuccessful at capturing the rate of decrease in IR_{140} signal.

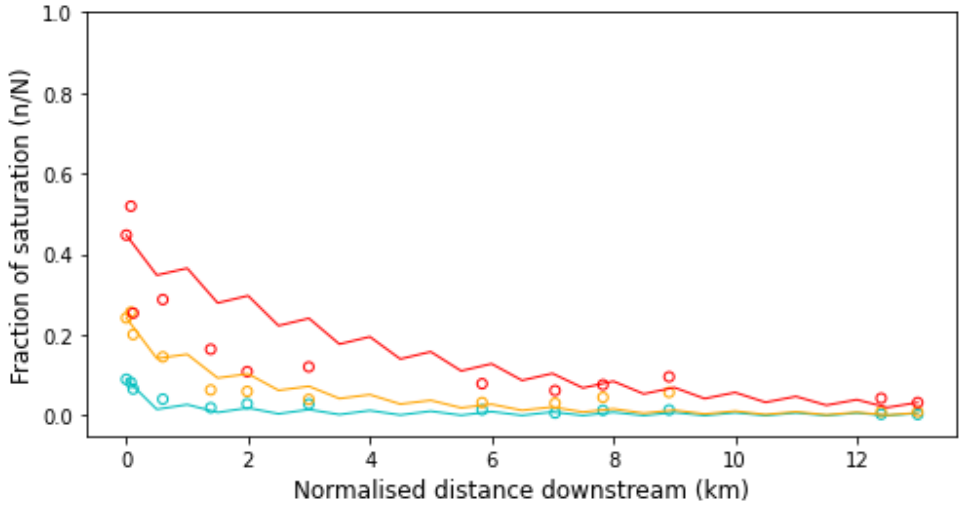

Figure 4.31. *Visualisation of an optimal fit of the burial bleach model to the 2022 dataset from 100 000 simulations. The number of cycles simulated was varied between 5 and 15, bleach time was varied between 10 and 60s, burial time was varied between 200 and 2000 years, and both bleaching and burial acceleration was varied between 0.5 and 2.5*

The discrepancy in estimated transport rates between first and second approaches appears to be caused by the much longer average storage times predicted by the second approach. Subsequently, the parameter space for bleach time per cycle was further explored. By varying bleach times between 1000 and 10000 seconds, the following optimal fit was produced (Figure 4.32).

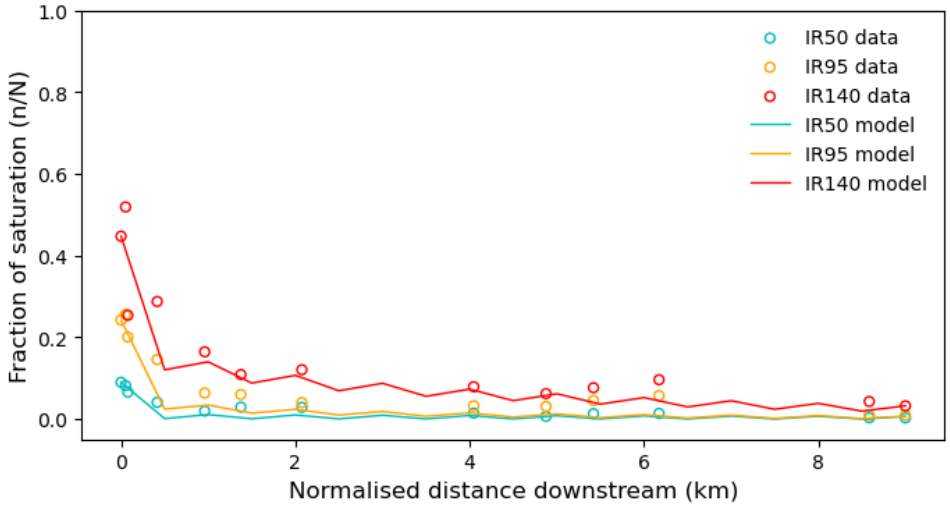

***Figure 4.32**. Visualisation of an optimal fit of the burial bleach model to the 2022 dataset from 100 000 simulations. The number of cycles simulated was varied between 5 and 15, bleach time was varied between 100 and 10000s, burial time was varied between 200 and 2000 years, and both bleaching and burial acceleration was varied between 0.5 and 2.5.*

With alternative bleach time parameter space, the model predicts 9 cycles of bleaching and burial; 4450 seconds of bleaching per cycle; 1000 years of burial per cycle; a bleaching acceleration factor of 1.83, and a burial acceleration factor of 0.94. Here, the model predicts that, on average, bleach time is increasing by 83% every cycle, whereas storage times are decreasing by 6%. This produces a virtual velocity estimate of 0.38 m yr^{-1}.

Figure 4.32 above displays an improved model fit for the 2022 dataset, where the most upstream sample is located downstream from the moraine and thus, an elevated fraction of saturation is observed. At this location elevated luminescence signals in the active channel indicate input of material (moraine sediments) with different signal magnitudes, rather than a variable transport rate or conditions. It is possible a variation in transport style is observed further downstream, where apparent age begins to gradually increase in the first four downstream samples. Downstream signal profiles (e.g. Figure 4.8) combined with results from Section 4.5.2 and Section 4.5.3 support this notion and suggest that the system may undergo a transport regime shift between the rapid signal reduction upstream section and the gradually increasing signal in the downstream section.

The possibility of an apparent shift in transport style was explored by applying the model to the 2022 dataset where the ~1.5 km upstream reach and the ~2 km downstream reach were treated in isolation (Figure 4.33). Bleach times were varied between 100 and 1000 seconds. For simulation of the upstream section, the optimal number of cycles was seven, bleach time per cycle was 230 seconds with an acceleration factor of 2.27, burial time per cycle was 200 years, with an acceleration factor of 1.16. Using these parameter values, estimated virtual velocity is calculated at 0.5 m yr^{-1}. Simulation of the

downstream section yielded an optimal number of cycles of five bleach time per cycle was 560 seconds with an acceleration factor of 1.16, burial time per cycle was 200 years, with an acceleration factor of 1.16. These parameter values produce a virtual velocity estimate of 1.39 m yr^{-1}. The key differences in model output for upstream and downstream is the bleach time per cycle and bleaching acceleration factor, as well as the number of burial-bleach cycles. The virtual velocity estimates differ by ~0.9 m yr^{-1}, with faster average transport in the downstream reach.

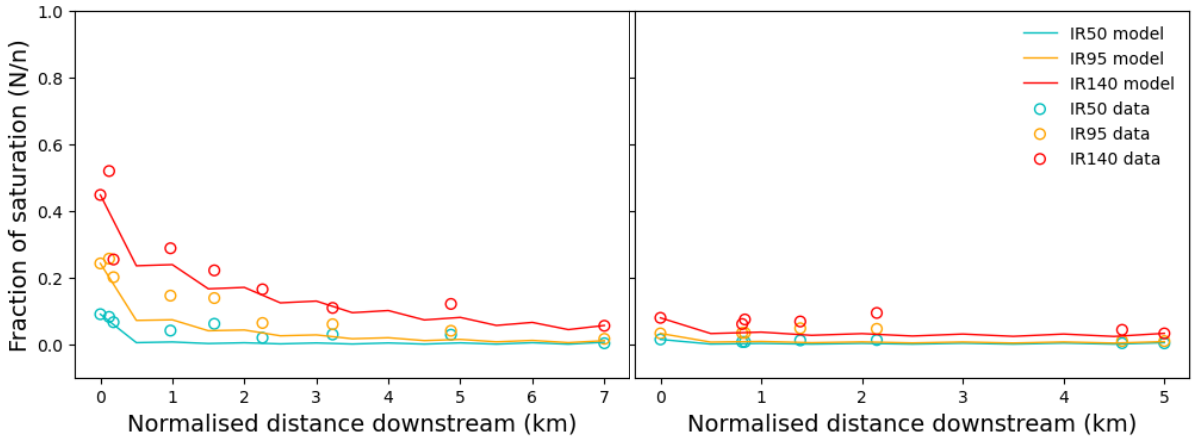

Figure 4.33. *Burial-bleach model applied to upstream and downstream sections of the Allt Dubhaig in isolation. Left panel: visualisation of an optimal fit of the burial bleach model to the upstream section of the 2022 dataset from 100 000 simulations. Right panel: visualisation of an optimal fit of the burial bleach model to the downstream section of the 2022 dataset from 100 000 simulations. The number of cycles simulated was varied between 5 and 15, bleach time was varied between 1000 and 10000s burial time was varied between 200 and 2000 years, and both bleaching and burial acceleration was varied between 0.5 and 2.5.*

Upstream, this devolved approach improves the fit for the IR_{140}, but is not as successful for the lower temperature signals. Downstream, the IR_{140} and IR_{95} are slightly underestimated, similarly to the first two approaches. Estimated virtual velocity for the downstream reach is just 0.13 m yr^{-1} above virtual velocity derived using the first approach, which fits the model to the 2018 and 2022 datasets combined, and includes a data point upstream of the moraine. This suggests that perturbation to the in-channel signals caused by the addition of moraine sediments is relatively short-lived, as the system bleaches away the luminescence signature of these grains over ~0.5 km. In turn, this may indicate that the rate of erosion of moraine sediments is such that the volume of sediment entrained is small relative to the in-channel flux.

Longer bleach times in the downstream section are consistent with the findings of Section 4.5.2 (e.g. Figure 4.24). There is an abrupt change in channel gradient reported by Ferguson *et al.*, (1991) (from 0.02˚ to 0.00015˚), which occurs between 2 and 2.5 km downstream from the first sample location of this study. As a result, longer light exposure times would be expected as grains remain on the bed or

travelling slowly because of the significant reduction in bed shear stress (100 Pa to 30 Pa) associated with the change in gradient (Ferguson *et al*., 1996). However, an elevated transport rate is not expected in these conditions. Thus, in this case, the model is underestimating the number of times grains are subject to a cycle of transport and storage in the downstream reach. This illustrates that different systems will be sensitive to perturbation of different parameters (e.g. bleaching and burial) dependent on whether transport or storage dominates the luminescence behaviour of the in-channel sediment. A robust statistical study of model sensitivity to parameter variability is required to address this. In addition, further model development to simulate lateral input of new material represents a crucial next step for MET-IRSL based sediment transport models.

4.6. Conclusions

Samples were collected from the active channel of a small gravel bed river, the Allt Dubhaig in Scotland and measured using the ILT-3ET protocol, a low-three-temperature MET-IRSL protocol adapted from the protocols of Ivester *et al.,* 2022 and Rhodes & Leathard (2022). Downstream profiles of MET-IRSL signals were presented using a range of approaches, single grain distributions of apparent age, sensitivity and burial-bleach ratios were presented and clear downstream trends in single grain distributions were identified. Notably, it was observed that single grain distributions narrowed with downstream distance and that there was increasing dominance of light exposure over storage with downstream distance. It was interpreted that this was an indication that the system bleaching and burial characteristics of the Allt Dubhaig were most aligned with Conceptual model 3 (Section 1.5) where the length of light exposure to which grains are subject to during transport is sufficient to cause an overall decrease all MET-IRSL signals with downstream distance despite evidence of storage.

Prior to sample measurement, it was expected that the Allt Dubhaig would display ‘flume-like’ behaviour based on evidence presented in the literature (e.g. Ferguson & Ashworth, 1991; Hoey & Ferguson, 1994, Ferguson & Wathen, 1998; Ferguson *et al*., 2002). However, multiple lateral inputs were identified through interrogating plateau ages and plateau type variability of single grains (Section 4.5.1), quantification of non-equilibrium bleaching conditions (Section 4.5.2), and examining intra-channel grain population characteristics to identify distinct groups of grains with shared histories (Section 4.5.3). It was interpreted that the sources of lateral input are glacial sediments from a moraine in the upstream section of the study site, and elevated rates of erosion of flood plain sediments through bank erosion. Moraine input was initially revealed by a significant increase in MET-IRSL signals in samples immediately downstream from the location of the moraine. Further, moraine sediments were dated using single grain ILT-3ET (~15 ka) and plateau ages were identified. Subsequently, the signatures of these grains were detected through inspecting the variability of single grain distributions and single grain plateau ages in downstream samples. Elevated levels of entrainment of floodplain

sediments were investigated due to an observed zones of gradual downstream increase in MET-IRSL ages of combined signals in the middle and lower sections of the study site. An alternative process causing this increase was hypothesised to be input from a small tributary ~2 km downstream. It was concluded that entrainment of flood plain sediments was the more credible source of input responsible for downstream increases through inspection of signal ratios, which revealed that the older input did not cause significant perturbation to the ratios of signals of samples from the main channel. Therefore, it was interpretated that this indicated that grains comprising input at these locations were transported under similar conditions to those observed in the present day.

A burial-bleach model was applied to the Allt Dubhaig dataset using several approaches. One approach, which fitted the model to a subset of 13 samples that were collected in 2022, estimated that grains in this system were subject to nine cycles of storage and transports over the length of the study reach and that, on average, cycles comprised of 4450 seconds of bleaching and 1000 years of burial per cycle, but also that light exposure increased by 83% every cycle, and that storage times decreased by 6%. Estimates of average storage times were used to produce a virtual velocity estimate of 0.38 m yr^{-1} over ~ 3 km. Using another approach, the model was fitted to the ~1.5 km upstream reach and the ~2 km downstream reach in isolation to explore the possibility of a shift in transport regime, and how transport rates may vary over the length of the study site. Upstream, the model fitted seven cycles of bleaching and burial comprised of 230 seconds of light exposure and 200 years of burial which increase by 120% and 15% each cycle respectively. Downstream, the model fitted five cycles of bleaching and burial comprising of 560 seconds of bleaching and 200 years of burial, which both increased by 15% each cycle. This devolved approach produced slower transport for the upstream reach, and faster for the downstream reach at 0.5 m yr^{-1} and 1.39 m yr^{-1} respectively. Overall, MET-IRSL analysis and modelling of signal was able to reveal the Allt Dubhaig is a more complex system than is suggested by existing literature e.g. Ferguson & Ashworth (1991); Hoey & Ferguson (1994), Ferguson & Wathen (1998); Ferguson *et al*., (2002); Hodge *et al*., (2011).

5.0. Chapter 5 Application of MET-IRSL to large-scale fluvial systems and a model to reconstruct the transport histories

5.1. Introduction

This chapter applies some of the techniques presented in Chapter 4 to MET-IRSL data from two fluvial systems in different geomorphic settings. The Solimões River is usually considered the main strand of the Amazon system. The Solimões flows ~1600 km from the Peruvian border to the confluence of the Rio Negro, ~75 km east of Manaus. The headwaters of the Santa Clara River River are located ~50 km north of Central Los Angeles. From here it flows ~130 km to the Pacific Ocean coast just south of the city of Ventura. This chapter tests the utility of MET-IRSL as tool to extract information of sediment transport for systems with potentially more complex dynamics, and MET-IRSL signal behaviour, than that of the Allt Dubhaig, Scotland presented in Chapter 4.

The final section of this chapter (Section 5.5) presents an approach to modelling the bleaching and burial histories of individual grains for three samples (two from the Allt Dubhaig and one from the Solimões) by adapting the burial-bleach model that was introduced in Section 3.5.1.2 in Chapter 3. It is demonstrated that the signal ratios of individual grains are directly related to whether grains have been bleached in an equilibrium or non-equilibrium state and that these ratios can be reproduced for each grain using this approach. Subpopulations of grains with shared histories are identified and it is suggested that grains preserve a memory of upstream bleaching and burial conditions at downstream locations. It is shown that transport rates can be derived from single grain measurements through the application of this modelling approach.

5.2. Methods

5.2.1. The Solimões River, Brazil

The Solimões is the name given to the main strand of the Amazon River and flows ~ 1600 km east from where the borders of Colombia, Peru and Brazil meet to Manaus where it is joined by the Rio Negro. The Solimões drains an area of 2,150,000 km^2 with a mean discharge of 102,800 m^3 s-1 (Meade, 1994). The rivers that comprise the Amazon system fall into three categories based on their biogeochemistry (Sioli, 1984): whitewater, blackwater and clearwater rivers. The Solimões is a whitewater river, which means carries a high load of nutrient-rich suspended sediments (Furch, 1984).

5.2.1.1. Study site and sampling strategy

The Solimões samples presented in this chapter were collected from the riverbed by Andre Sawakuchi in 2010-11. This was achieved from a boat with a light-proof tent constructed around the centreboard, which is like a retractable keel that allows access to the water so a grab could be lowered down to the riverbed to obtain a sample. Twelve samples were collected from the Solimões and one from the Rio Negro (lab code L0610). The locations of these samples are shown in Figure 5.1. The depth and distance downstream for each sample is shown in Table 5.1. The environmental dose rate used for age estimation of these samples is 2.0 Gy/ka, based on measurements from other samples in the Amazon system (e.g. Sawakuchi *et al.,* 2018).

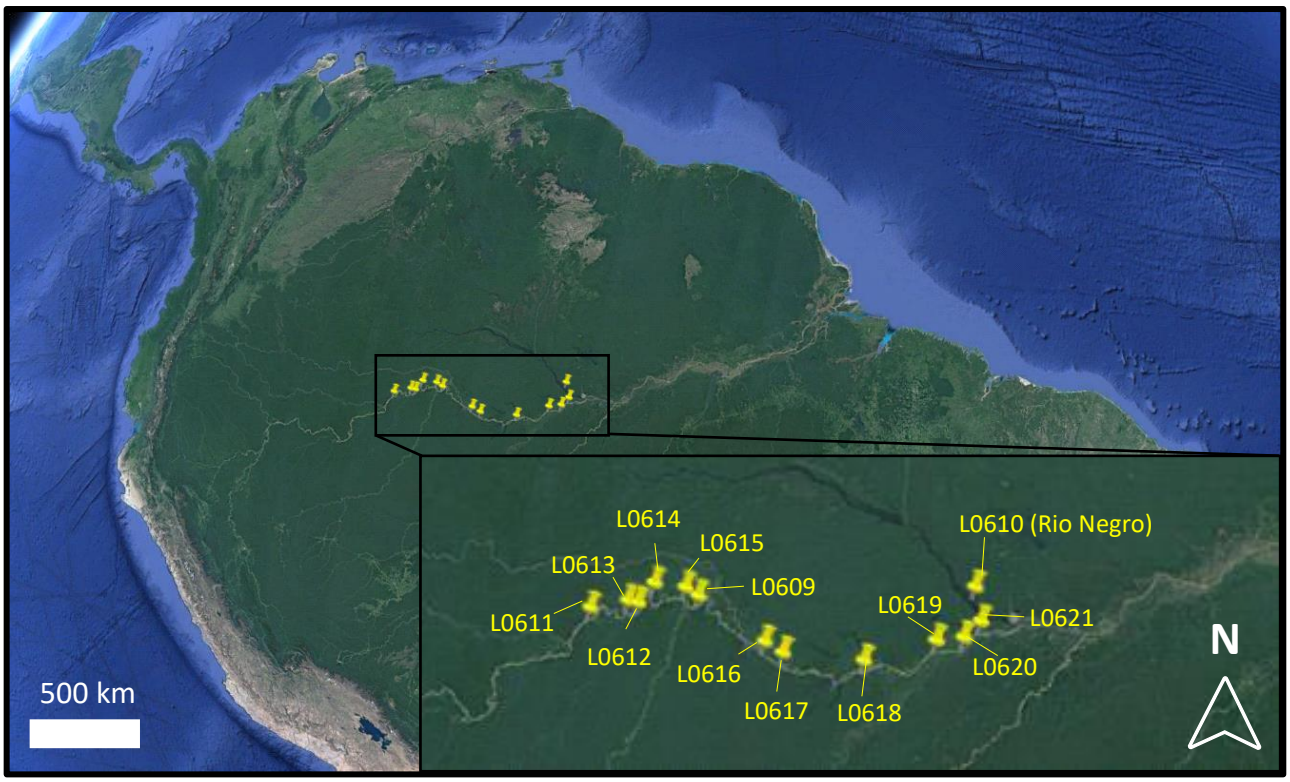

Figure 5.1*. Locations of samples collected from the bed of the Solimões by Andre Sawakuchi in 2010-11 and their lab codes. Note one sample (L0610) was collected from the Rio Negro just upstream of where it joins the Solimões. This sample is not included in the results and analysis presented in this chapter because here the focus is on the evolution of MET-IRSL signals in the main channel of the Solimões.*

Table 5.1. *The depth below the surface and distance downstream for each sample collected from the Solimões*

Lab code	Distance downstream (km)	Depth below surface (m)
L0611	0	27
L0613	78	7
L0612	98	16
L0614	156	19
L0615	219	20
L0609	253	14
L0616	414	20
L0617	455	14
L0618	617	15
L0619	762	25
L0620	815	30
L0621	859	7.7

5.2.1.2. Sample measurement

Single grains were measured using the METx protocol, a five temperature MET-IRSL protocol adapted from the protocol of McGuire & Rhodes (2015a). Adaptations were made following the advice of Colarossi *et al.,* (2018) including the use of a larger test dose (20 Gy) and a warm bleach at 250˚C for 100 seconds prior to the test dose. Two discs comprised of approximately 100 grains were measured for each sample. A more detailed explanation of sample measurement and the METx protocol can be found in Section 2.2.2.1 in Chapter 2. The METx protocol is summarised in Table 5.2. Felspar samples were prepared and sieved at 180-250µm by Andre Sawakuchi in Brazil and sent to the University of Sheffield where they were re-sieved to 180-212 µm.

Table 5.2. *The METx protocol used to measure single grains for each of the Solimões samples*

Natural or beta dose
Preheat 60s 250°C 5°Cs^{-1}
IRSL 50°C 2.5s 90% power
IRSL 95°C 2.5s 90% power
IRSL 140°C 2.5s 90% power
IRSL 185°C 2.5s 90% power
IRSL 230°C 2.5s 90% power
IRSL warm bleach 250°C 100s 90%
Beta test dose 20 Gy
Preheat 60s 250°C 5°Cs^{-1}
IRSL 50°C 2.5s 90% power
IRSL 95°C 2.5s 90% power
IRSL 140°C 2.5s 90% power
IRSL 185°C 2.5s 90% power
IRSL 230°C 2.5s 90% power
IRSL hot bleach 290°C 100s 90%

5.2.2. The Santa Clara River, southern California

The headwaters of the Santa Clara River in the San Gabriel mountains in the Western Transverse Ranges of California, from here it flows ~ 130 km west until it meets the Pacific Ocean just south of the city of Ventura. The Santa Clara River drains an area of 4200 km^2 its annual streamflow is highly variable in association with the El Niño Southern Oscillation (e.g. Andrews et al., 2004). The northeast of the catchment is bounded by the San Andreas Fault zone and within the catchment are several smaller faults including the Ventura fault located just ~ 5 km north of the estuary of the Santa Clara River. In a highly tectonically active region also prone to wildfires, rates of sediment supply to the Santa Clara River are high, varying between 2-10 times higher in the Western Transverse Ranges compared to the surrounding areas (Warrick and Mertes, 2009).

5.2.2.1. Study site and sampling strategy

Samples were collected from the active channel of the Santa Clara River by Chris McGuire in 2011-12. The environmental dose rate was measured in situ at each sample location with a gamma spectrometer. The locations of these samples are shown in Figure 5.2. The distance downstream for each sample is shown in Table 5.3.

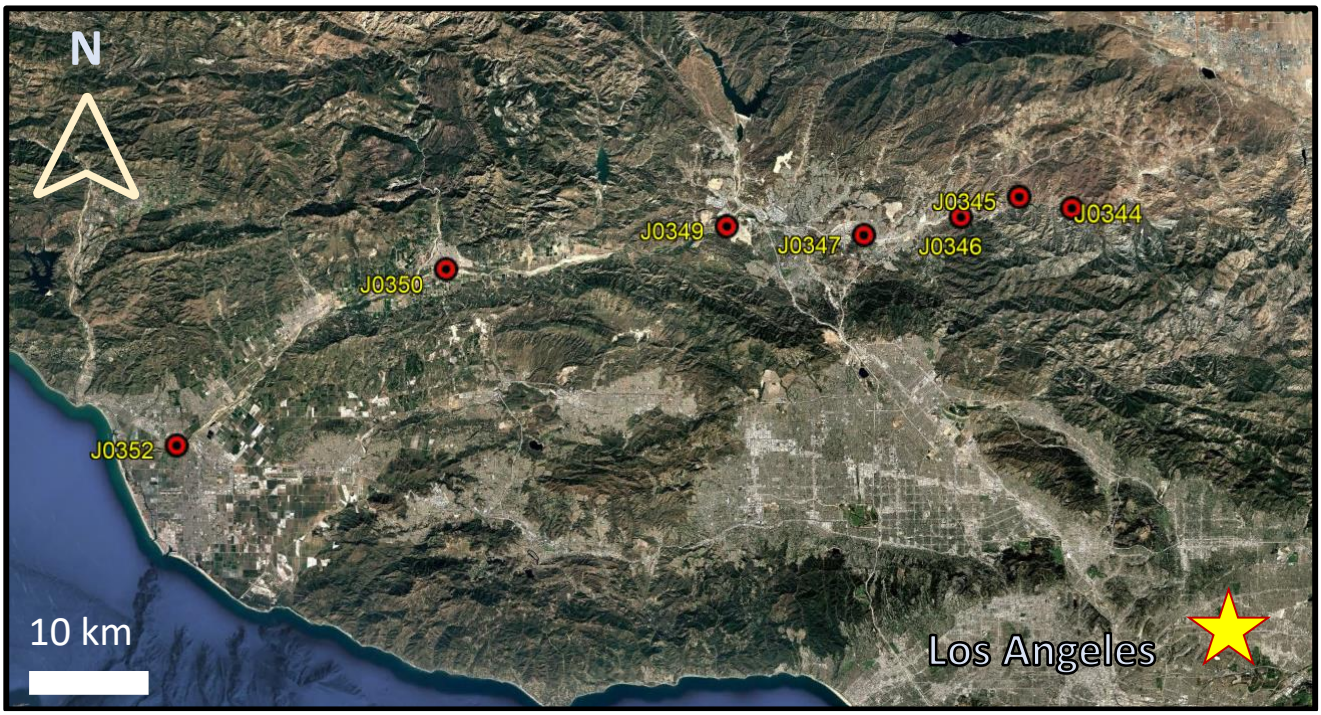

***Figure 5.2**. Locations of samples collected along the Santa Clara River by Chris Mc Guire in 2011-12. Lab codes in downstream order are J0344, J0345, J0346, J0347, J0349, J0350 and J0352.*

Table 5.3. *Samples collected from the Santa Clara River and distances downstream.*

Lab code	Distance downstream (km)
J0344	0
J0345	6.7
J0346	13.4
J0347	24
J0349	40.5
J0350	71.4
J0352	105.2

5.2.2.2. Sample measurement

Single grains were measured using the METx protocol in the same manner as the Solimões samples (Table 5.2, Section 5.2.1.2). These samples were prepared at the University of California, Los Angeles by Chris McGuire in 2012-13.

5.3. Results

5.3.1. The Solimões River, Brazil

This section first presents downstream profiles of METx signals for the Solimões and discusses how expression of downstream METx signals can stimulate different avenues for interpretation and research.

5.3.1.1. Downstream MET-IRSL signal profiles

Downstream profiles of super synthetic aliquot (SSA) apparent age (ka) (Figure 5.3) and mean apparent age (ka) (Figure 5.4) reveal quite different downstream trends. Figure 5.3a shows the downstream evolution of all five METx signals, whereas Figure 5.3b shows only the IR_{50}, IR_{95} and IR_{140} to display these three signals in more detail.

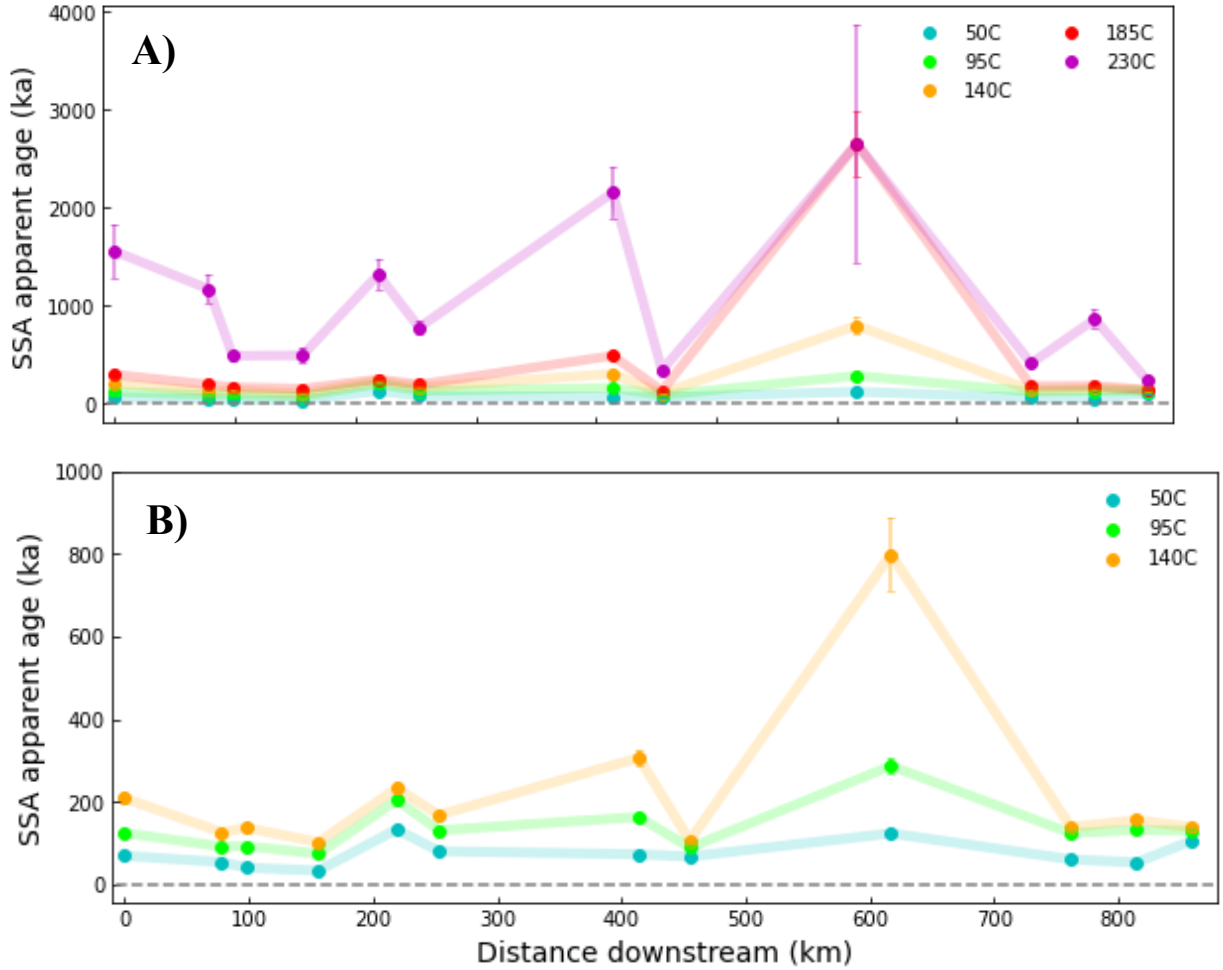

***Figure 5.3**. Downstream profile of super synthetic aliquot apparent age, for the Solimões. Super synthetic aliquot apparent age is also referred to as combined signal. **A)** Combined signals of all five METx temperatures. **B)** Combined signals of just the lowest three METx temperatures, to illustrate variability in these signals more clearly.*

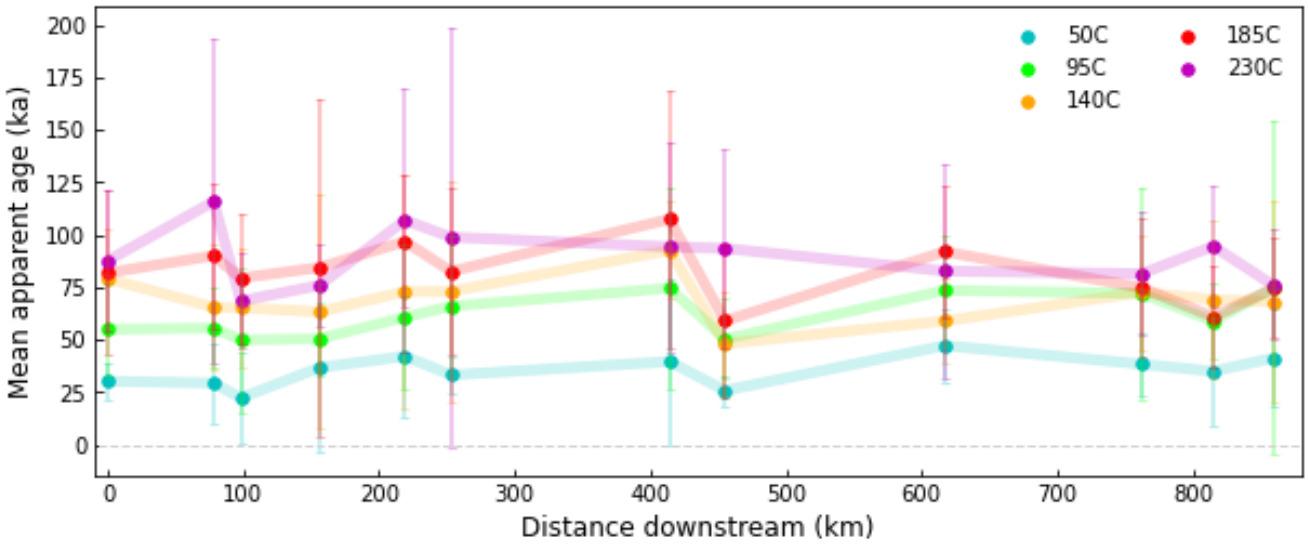

Figure 5.4. *Downstream profile of METx mean apparent ages of the Solimões samples. Includes all grains that provided an equivalent dose estimate.*

In Figure 5.3 showing SSA apparent age with downstream distance, an increase in all five METx signals is observed ~600 km downstream from the first sampling location, although this is less pronounced for the IR_{50}. Over the length of the profile, these signals display four other smaller peaks, including the most upstream datapoint. There is strong coherence between signals. In contrast, this dramatic fluctuation in signal is not captured by mean apparent age (Figure 5.4). Rather, there is an increase in the IR_{50} and IR_{95} signals by ~10 and 20 ka respectively over the ~900 km study reach. Note that at the first sample location, the IR_{140}, IR_{185}, and IR_{230} mean apparent ages are within 10 ka of each other, whereas the IR_{50} and IR_{95} give rise to much younger ages (Figure 5.4). There is some coherence between METx mean apparent ages until ~700 km downstream, with the exception of the IR_{230}.

Figure 5.5 shows downstream trends in SSA fraction of saturation (N/n). Here, it appears that the slowest bleaching IR_{230} remains close to saturation over the course of the study reach, although these signals have large errors. The other four signals, display downstream fluctuations closely resembling those of SSA apparent age. The IR_{185} approaches saturation ~250 km downstream, where it remains for ~ 150km. With the exception of the IR_{230}, METx fraction of saturation decrease between ~410 km and ~460 km downstream, and then rise over the next ~150 km. Over the last ~100 km of the study reach, the IR_{50}, IR_{95} and IR_{140} signals display an increase in fraction of saturation, whereas the IR_{185} decreases.

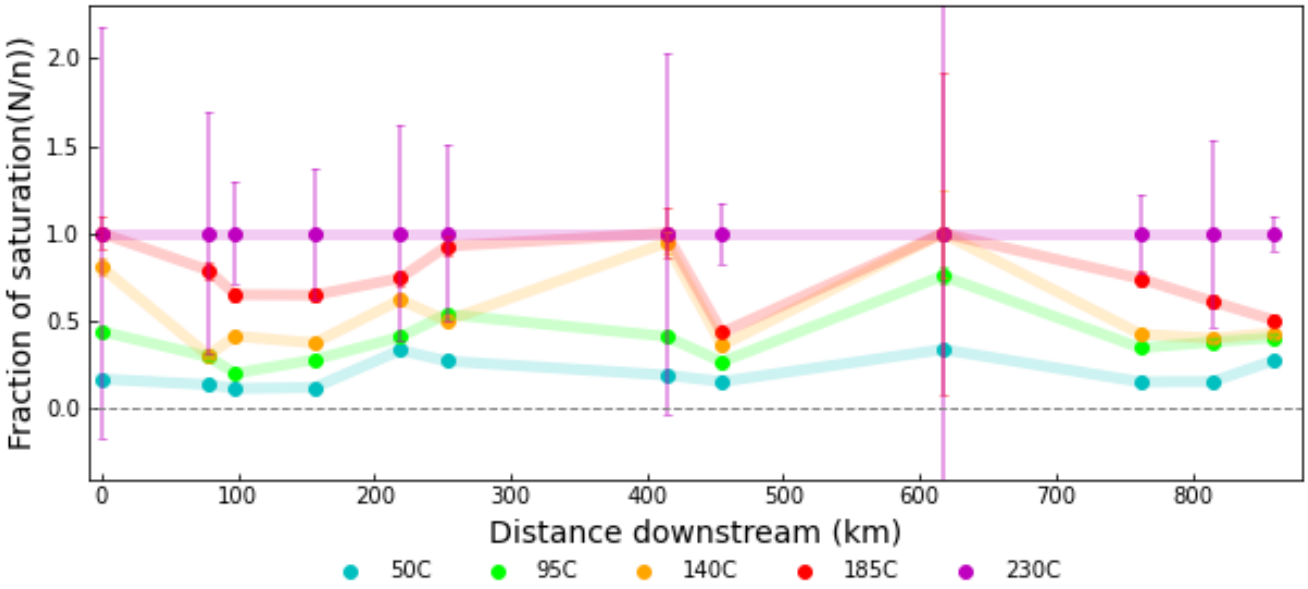

***Figure 5.5**. Downstream profile of super synthetic aliquot METx fraction of saturation of the Solimões samples.*

Figure 5.6 displays the downstream evolution of plateau age (ka). The method for estimating minimum age of Ivester *et al.,* (2022) is described in Chapter 2, Section 2.5. These minimum age estimates are calculated using only the signals of the well bleached grains, whereas signals expressed as SSA apparent age, mean apparent age, and fraction of saturation (Figures 5.3, 5.4, 5.5 respectively), contain information from grains that may have been partially bleached prior to burial and storage. The ages of the well bleached grains in Figure 5.6 reveal a somewhat different downstream trend. The early peak in signal ~100 km downstream is consistent with a rise in mean apparent age signals at this location, however, this is not observed for SSA apparent age or fraction of saturation. Over the next ~150 km there is a general trend of decrease in minimum age. This decrease is observed only for the IR_{50} SSA apparent age and the IR_{50}, IR_{95} and IR_{185} fraction of saturation. Another difference worth noting is that the large increase in SSA apparent age ~600 km downstream for all five METx signals is absent from the downstream profile of minimum age. Rather, there is a ~7 ka increase in minimum age ~450 km downstream, which is this is far less dramatic than that observed in Figure 5.3a, 5.3b.

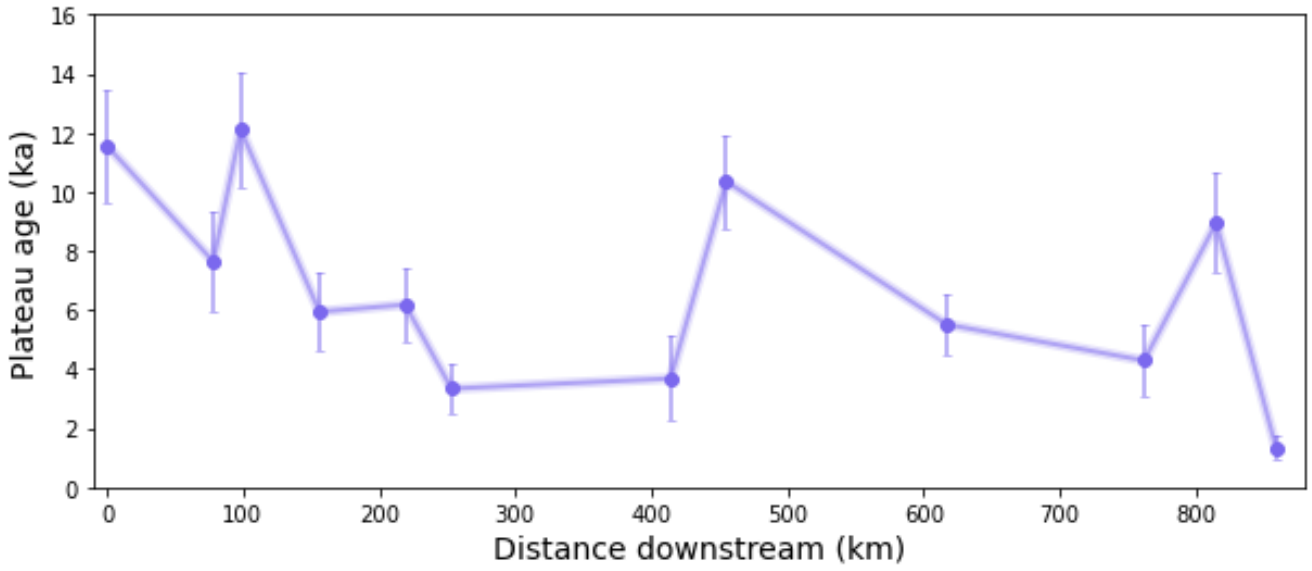

***Figure 5.6**. Downstream profile of minimum METx plateau ages of the Solimões samples. Note plateau ages are calculated from well-bleached grains.*

For these samples, the total signal, which includes the signals of partially bleached grains, provides information on sediment transport and system dynamics that can be lost in a simple arithmetic mean signal from the same grains. At least for the IR_{140}, IR_{185} and IR_{230}, downstream trends in total signal reveal a large increase in SSA apparent age ~600 km downstream (Figure 5.3a). Since this increase is not as marked in the downstream profile of mean apparent age (Figure 5.4), this suggests that these are large signals coming from a few grains. Nonetheless, an increase in mean apparent age for the IR_{50}, IR_{95}, IR_{140} and IR_{185} signals is observed at this location. In contrast, this is not observed when looking at just the well bleached grains that provide a minimum age (Figure 5.6). From this, it is suggested that the large increase in total signal ~600 km downstream reflects input of older, poorly bleached material at some location between ~450 and ~600km. This could reflect grains coming out of storage, or from geologic sources not attributable to palaeo-Solimões deposition.

As discussed in Chapter 4, well bleached and partially bleached grains can be identified through the measuring of multiple IRSL signals at a series of elevated temperatures. Here, it is suggested that both types of grains provide information that could be valuable for determining sediment transport dynamics. For the partially bleached grains, even where there are no apparent age estimates in agreement, the relative differences between multiple signals contains information on the transport conditions for these grains (e.g. the 'burial-bleach ratio' of Rhodes & Leathard, 2023 discussed in Chapter 4), whereas plateau ages and plateau types of the well bleached grains can provide information on duration of past light exposure and storage times (insights into the light exposure history of individual grains from plateau age and plateau type are presented and discussed in the following section). Differences in downstream behaviour indicate it may be valuable to utilise multiple means of

signal expression, such as total signal, average signal and minimum age, when using IRSL as a tool to investigate fluvial sediment transport and storage histories.

5.3.1.2. Single grain plateaus

Figures 5.7 and 5.8 show the plateau ages for all grains that provided plateau ages, including those that did not contribute to the minimum age estimate for that sample. Figure 5.7 displays these results for samples L0611, 613, 612, 614¸615, 609, in downstream order. Figure 5.8 shows samples L0616, 617, 618, 619¸620, 621, in downstream order. The different coloured points in Figures 5.7 and 5.8 correspond to the number of METx signals that form the plateau. When using the METx measurement protocol, there are 26 possible types of plateaus. At first order, the age of the plateau provides constraint on the timing of a bleaching event at deposition. At second order, the degree to which high temperatures form a plateau, the better bleached a grain was before it was buried. In more detail, plateau 'depth', which relates to the highest temperature plateau-forming METx signal, may provide information on the minimum extent of past light exposure for multiple events. Thus, downstream variability in the relative proportions of different plateau types can be interpreted to indicate changes in bleaching conditions, and therefore potentially relate to transport conditions through time.

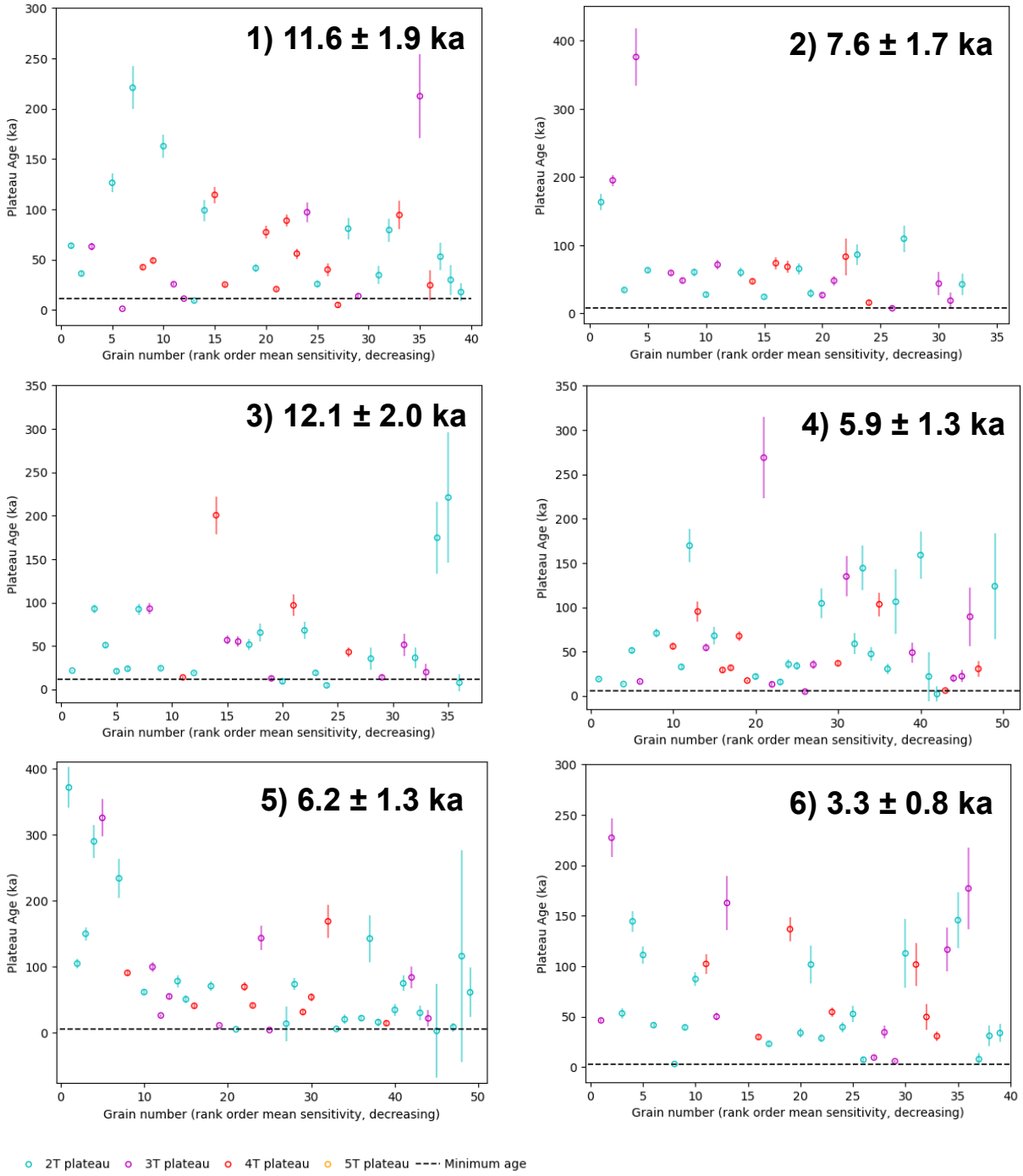

Figure 5.7. *Single grain plateau ages for the first six Solimões samples. Lab codes: 1) L0611, 2) L0613, 3) L0612, 4) L0614, 5) L0615, 6) L0609. Data points are coloured in accordance with the number of METx temperatures that form a plateau. Two-temperature plateaus are blue, three temperature plateaus are purple, four-temperature plateaus are red, five-temperature plateaus are yellow. Minimum age calculated from plateau ages is shown on each subplot and is indicated by the black dashed line. The numbers on each subplot represent the relative locations of these samples*

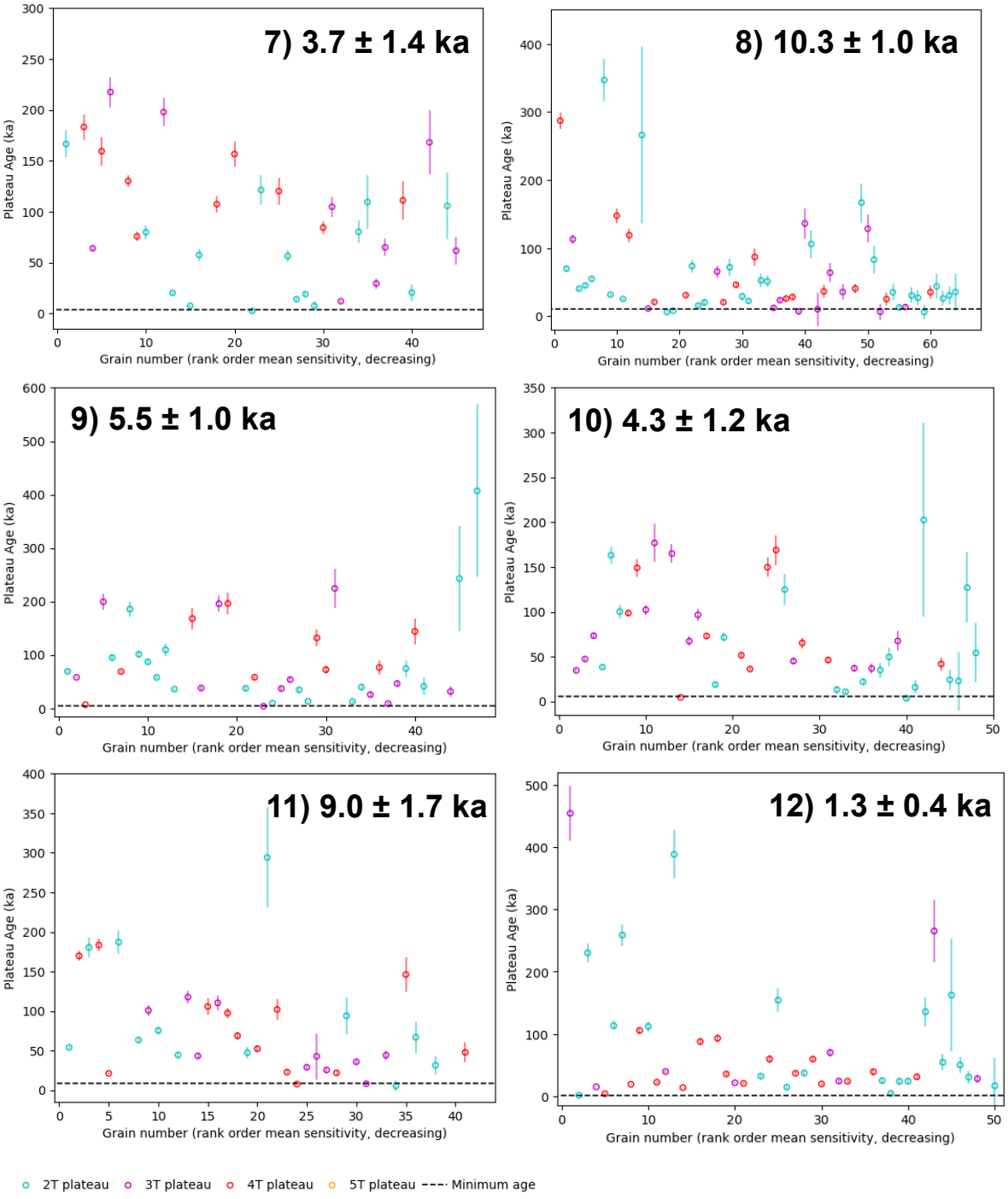

Figure 5.8. *Single grain plateau ages for the last six Solimões samples. Lab codes: 7) L0616, 8) L0617, 9) L0618, 10) L0619, 11) L0620, 12) L0621. Data points are coloured in accordance with the number of METx temperatures that form a plateau. Two-temperature plateaus are blue, three temperature plateaus are purple, four-temperature plateaus are red, five-temperature plateaus are yellow. Minimum age calculated from plateau ages is shown on each subplot and is indicated by the black dashed line. The numbers on each subplot represent the relative locations of these samples.*

Figures 5.7 and 5.8 show a relatively high variability of plateau ages within each sample, and that this is consistent over the ~900 km study reach. This consistent variability is particularly high compared to that observed in the Allt Dubhaig samples in Figure 4.4.9. It also appears that for the majority of samples, two-temperature plateaus are most abundant (Figure 5.7, 5.8). This is with the exception of three samples at 78 km, 414 km and 815 km downstream. These samples have a higher proportion of three-temperature plateaus, to which IR_{95}-IR_{140}-IR_{185} plateaus are the largest contributors. For these grains, a possible interpretation of their light exposure history is as follows, in chronological order: 1) Most recent bleach event: prior to the most recent burial, grains were bleached for a short time that allowed the IR_{50} signal to begin to decay, but not long enough for the IR_{95} to start decaying at a rate that caused its departure from the IR_{140} and IR_{185}, 2) Penultimate bleach event: a much longer light exposure event, grains were bleached for sufficient time to allow all METx signals to reset, apart from the slowest bleaching IR_{230}, the timing of this event is described by the plateau age.

Figure 5.9 shows downstream variability of the relative proportions of two-, three-, and four-temperature plateaus. As mentioned above, two-temperature plateaus are most abundant other than at three locations. Looking at four-temperature plateaus, after an initial reduction over the first ~100 km, there is a gradual, but clear increase in the relative proportion of four-temperature plateaus with downstream distance. With METx, there are five possible four-temperature plateaus. The simplest to interpret are IR_{50}-IR_{95}-IR_{140}-IR_{185} and IR_{95}-IR_{140}-IR_{185}-IR_{230} plateaus, which herein will be referred to as 'low' or 'high' four-temperature plateaus respectively (L4T and H4T plateaus).

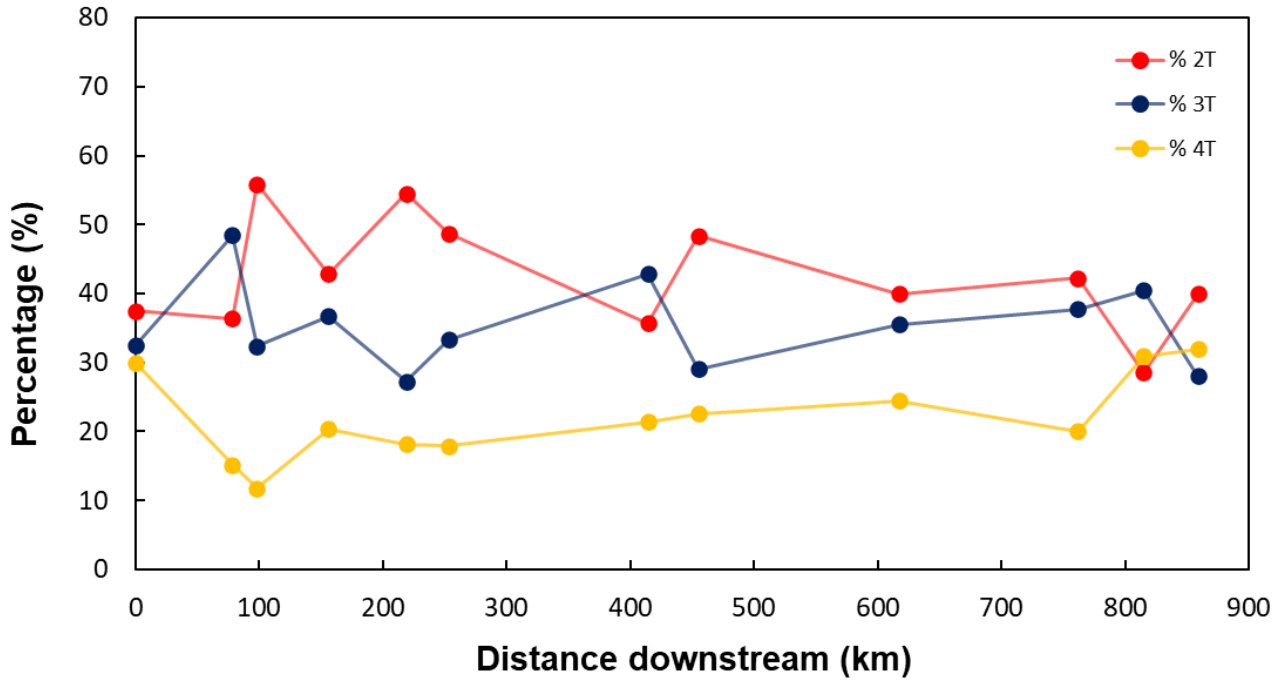

Figure 5.9. Downstream variability in the proportions of two-, three- and four-temperature plateaus from single grain measurements of the Solimões samples.

Both types of four-temperature plateaus indicate grains were well-bleached during the event to which the plateau age corresponds. L4T plateaus suggest extensive bleaching prior to the most recent burial, whereas H4T plateaus indicate a much shorter bleaching event prior to the most recent burial (or fading of the IR_{50} signal), preceded by a much longer bleaching event, sufficient to reset all METx signals. However, it should be considered that the IR_{50} signal may suffer from anomalous fading, which could cause its departure from the other METx signals. Whether or not this is the case, the downstream increase in four-temperature plateaus in Figure 5.9 suggests that grains are subject to longer durations of light exposure prior to entering storage as they travel downstream.

To further investigate the chronology of potentially variable bleaching conditions, grains were assigned a 'bleach index', which corresponds to extent of light exposure prior to burial based on plateau type in a similar fashion to Rhodes & Leathard (2022) (Table 5.3). A summary of bleaching index assignment is shown in Table 5.3. Grains with one of nine, of the possible 26, METx plateau types were assigned a bleach index and were included in the following analysis. The nine plateau types were selected because they do not have any 'missing' temperatures, in part for simplicity but also because it is possible to be more confident in the signals of these grains, where METx apparent ages are in agreement, or increase monotonically with measurement temperature.

Each grain was also given an overall 'bleach score', calculated by multiplying an estimate of the duration of past light exposure during the event to which the plateau age refers by the bleaching index. Past light exposure duration is estimated using Eq. 1.3 rearranged in terms of time, t. from Chapter 3, which is the bleaching function of (McGuire & Rhodes, 2015a) written in terms of time, t, with I_0 as observed fraction of saturation, much like in Section 4.5.3.2. The reason for multiplying estimated past light exposure by bleaching index (Table 5.3) is to account for different grains bleaching at different rates due to factors unrelated to transport history such as their geology. Figure 5.10 shows plateau age plotted over bleach score, with data points coloured based on their bleach index. This allows visualisation of the relationship between plateau age, duration of past light exposure, and how well-bleached grains were during this light exposure event. The grey lines in each subplot of Figure 5.10. indicate median plateau age and bleach score, dividing each subplot into four divisions.

***Table 5.3**. Summary of bleaching index assignment based on plateau type.*

METx signals in plateau	Plateau type	Bleach index
185-230	High two-temperature	5
140-185-230	High three-temperature	5
95-140-185-230	High four-temperature	5
140-185	Medium-high two-temperature	4
50-95	Low two-temperature	2
50-95-140	Low three-temperature	3
50-95-140-185	Low-four-temperature	4
95-140	Medium-low two-temperature	3
95-140-185	Medium three-temperature	4

In the majority of cases, grains close to median plateau age and median bleach score are well-bleached, indicated by the presence of pink and purple data points surrounding the intersection of the median plateau age and median bleach score. Other similarities between samples include the tendency for grains above median age to be relatively poorly bleached, indicated by the presence of blue data points in the top left division of each subplot. Grains below median age tend to be well-bleached, indicated by the pink and purple points in the bottom right division of each subplot. These patterns could suggest that two broad populations of grains are observed within each of these samples: older, poorly bleached grains, and younger well-bleached grains. Reasons for the presence of potentially distinct grain populations are not immediately clear from these data. However, it appears that the in-channel sediment in this reach of the Solimões is comprised of grains that share one of two histories, broadly speaking.

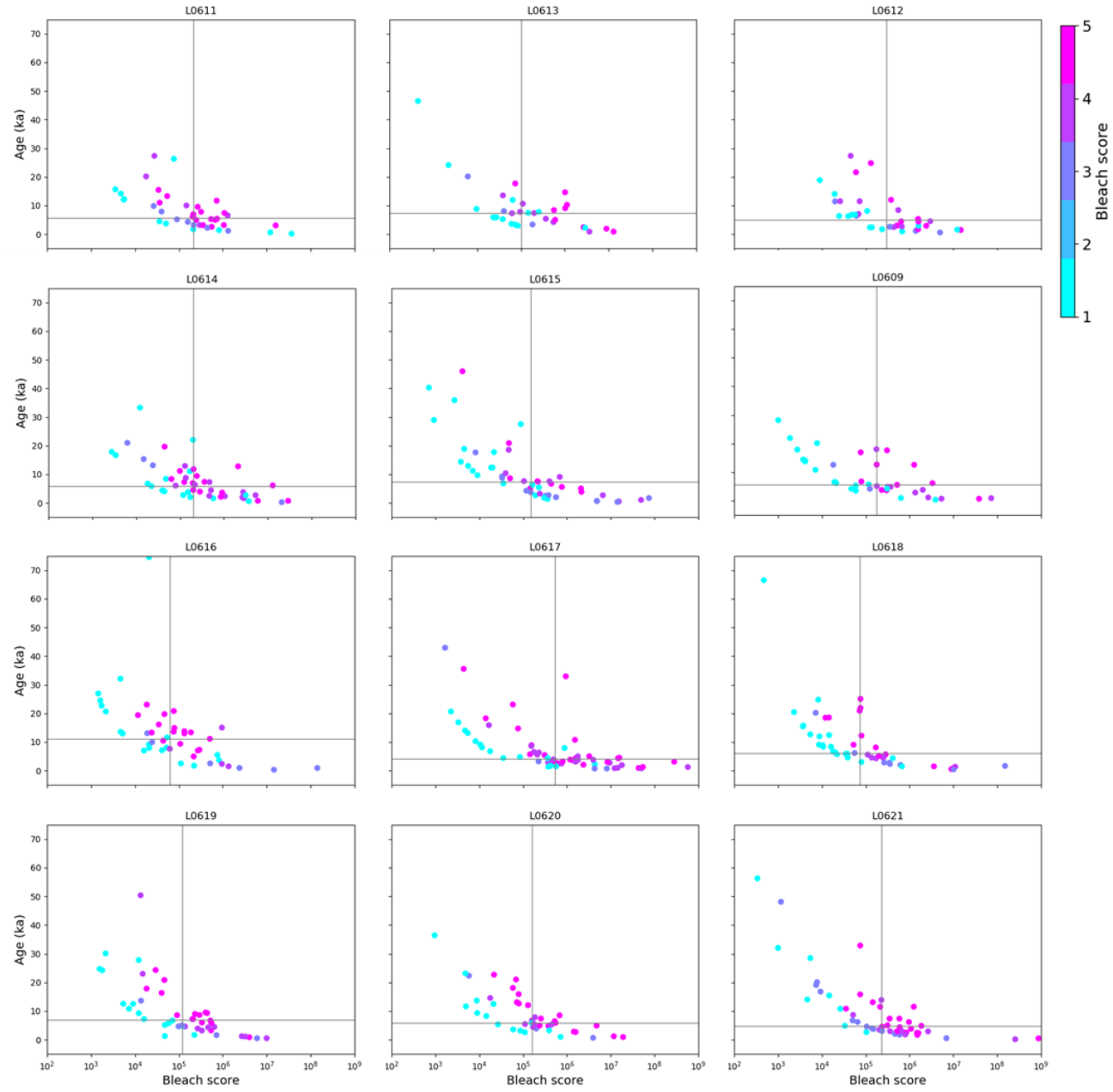

Figure 5.10. *Plateau ages of single grains plotted against 'bleach score', which is a metric containing information on length of past light exposure (see text for details). Grains are coloured based on 'bleaching index', which contains information on the METx temperatures that form the plateau of each grain. The grey lines indicate the median value for bleach score (x-axis) and plateau age (y-axis), dividing each subplot into four divisions. In a clockwise direction starting from the top left division, these represent: older-poorly-bleached, older-well-bleached, younger-well-bleached, and younger-poorly-bleached grains.*

5.3.1.3. Single grain distributions

5.3.1.3.1. Burial-bleach ratios

Distributions of single grain log_{10} burial-bleach ratios in downstream order are shown in Figure 5.11. The burial-bleach ratio, defined by Rhodes & Leathard (2022), relates to the ratio of storage to light exposure. A more detailed explanation of this parameter can be found in Section 1.3. In Figure 5.11, low log_{10} burial-bleach ratios reflect a low ratio of storage to light exposure, whereas higher values typically reflect higher ratios. Samples L0611, 613, 612 and 614 record a larger proportion of high burial-bleach ratios relative to low burial-bleach ratios. Moving downstream, distributions appear to approach a normal distribution (i.e. lognormal this is a log scale), perhaps with the exception of samples L017 and L0620. This may indicate that the length of time grains spend in storage, relative to the length of time they are exposed to light, increases with downstream distance.

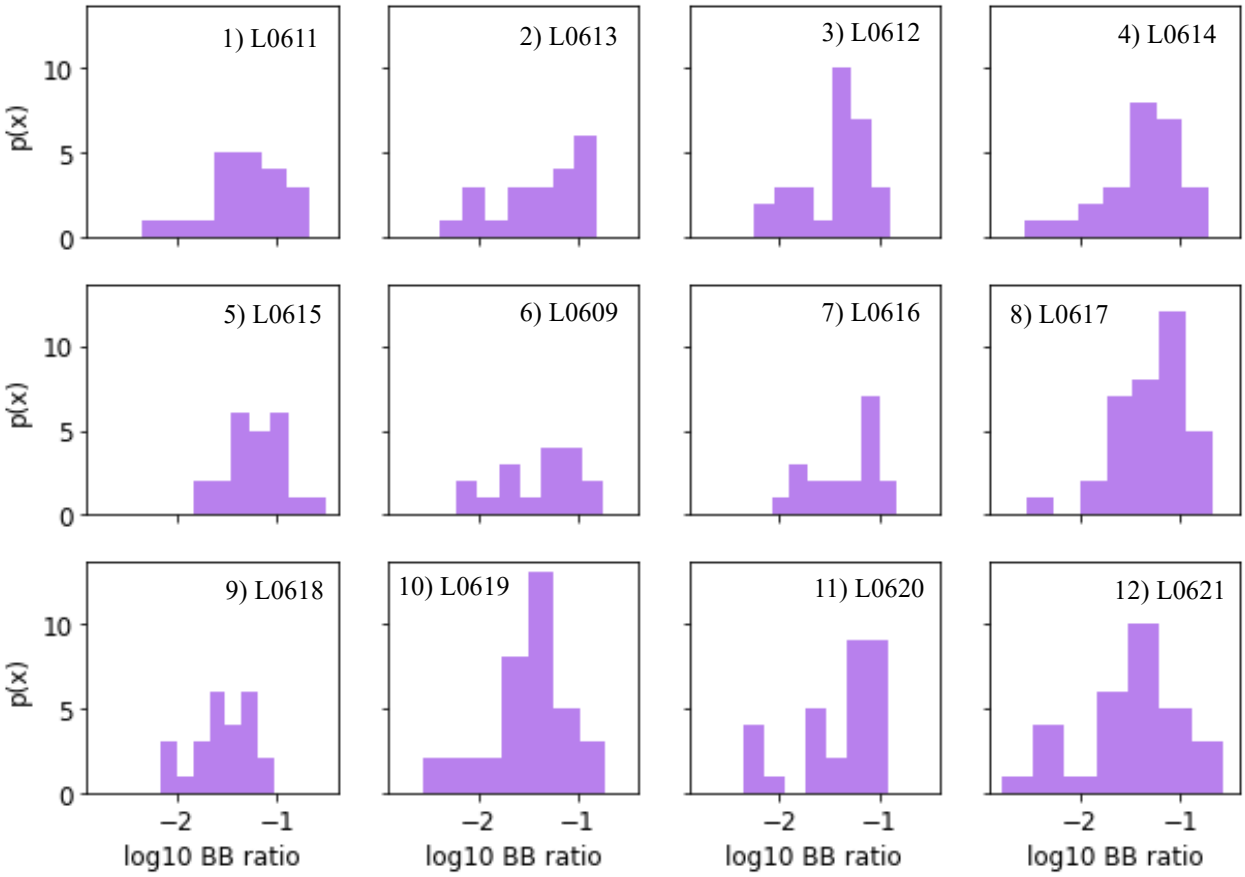

Figure 5.11. *Distributions of single grain log_{10} burial-bleach ratios calculated using the approach of Rhodes & Leathard (2022) for each of the Solimões samples. The numbers that precede the sample codes on the top right corner of each plot represents the relative location of the sample downstream.*

5.3.1.3.2. Equivalent dose

This section applies the gaussian mixture model described in Section 4.5.3 to the log equivalent dose distributions of the Solimões samples. Figures 5.13 and 5.14 display optimal fits for each METx signal (different colours) in order of downstream distance. This section assesses the utility of this approach for identifying potential distinct grain populations for these samples. It is suggested in Section 4.5.3.3 that distinct equivalent dose populations may arise due to the concept of equilibrium and non-equilibrium bleaching. According to the concept of equilibrium bleaching introduced in Section 3.5.1.1 in Chapter 3, MET-IRSL signals of grains that have been subject to different lengths of prior light exposure, and perhaps owing to transport histories, are characterised by different bleaching behaviours, namely a reduction in bleaching rate as a function of past light exposure duration. Here, a gaussian mixing model is applied to all five METx signals, and it is discussed whether this approach contributes additional insight into transport dynamics for the Solimões.

In Figures 5.13 and 5.14 it is observed that with increasing measurement temperature, log equivalent dose distributions become narrower, and higher equivalent dose values are recorded. Narrowing distributions indicates increasing homogeneity of signals as grains that comprise the main channel flux are transported downstream. The rate and extent of this process could be related to the characteristic hydraulic and transport regime of the system. In other words, it appears that the longer grains spend in the channel, the more that their luminescence characteristics will reflect the system's fluvial dynamics, as opposed to the conditions where grains entered the channel.

Samples that are best fit by multiple component gaussians across more than one measurement temperature include L0611, 614, 609, 617, 618, 619, 620. Downstream trends in distribution characteristics are perhaps more apparent for the Allt Dubhaig samples presented in Section 4.5.3.3; the downstream profile of the Allt Dubhaig samples (e.g. Figure 4.4.2.) more closely resembles an exponential decay in age, whereas the ages of the Solimões samples presented here display greater fluctuation downstream, and when expressed as a mean, exhibit a pattern of gradual increase over the ~900 km study reach. This suggests that, in the Solimões, storage dominates downstream signal characteristics, rather than bleaching. Therefore, it may be that the downstream evolution of MET-IRSL signals in Solimões is somewhat consistent with Conceptual model 4 (Section 1.5) (Figure 5.12):

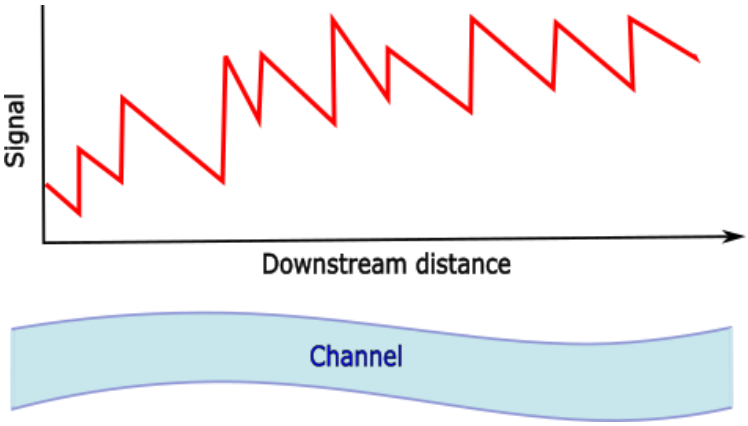

Figure 5.12. *Conceptual model of an idealised channel whereby as grains are transported through the system (left to right), they are subject to both storage and light exposure, but the amount of time exposed to light is insufficient, relative to the time spent in storage, to cause an overall decrease in IRSL signal with downstream distance*

A reason for the type of signal behaviour illustrated by Conceptual model 4 in Figure 5.12 above is likely the very low light conditions in this deep (up to 30 m), sediment-laden channel. In contrast, in the Allt Dubhaig, at least in the upstream section, bleaching dominates the downstream evolution of ILT-3ET signals in the clear, gravel bed channel. This is evidenced by the initial rapid reduction in signal over just ~0.5 km (e.g. Figure 4.9.). Thus, if in a bleaching-dominated system, distinct grain populations do in fact arise due to the degree to which past light exposure has caused MET-IRSL signals to depart from equilibrium, in a storage-dominated system, one may expect distinct grain populations to arise as grains enter the channel, coming out of storage centres with variable characteristic resident times. Subsequently, it is possible that locations where log equivalent dose distributions are best fit by multiple components, are close to storage centres that supplies the main channel with sediment under certain conditions.

Future work could be directed towards distinguishing the population of grains that enter and exit the study reach as part of the main channel flux and have a METx signal 'signature' characteristic of the system's sediment transport regime, from grains that enter the main channel as lateral input for large, more complex systems such as the Solimões. At the Allt Dubhaig site, it was possible to measure the signal characteristics of individual grains from a location that is potentially one source of sediment to the main channel, the moraine on the western bank of the river (Section 4.4.1). With single grain measurements and plateau age estimation, it was observed that the scatter of plateau ages of fluvial samples just downstream from the moraine closely resembled that of this potential sediment source, whereas this pattern was not observed upstream from this location. For the Solimões, a main channel that is typically ~2 km in width, and has an average depth of ~18 m, the identification of potential

sources of sediment is more complex. As mentioned above, it is possible that these locations are indicated by dose distributions fitted by multiple component gaussians, and perhaps where we see large increases in SSA apparent age in Figure 5.3.

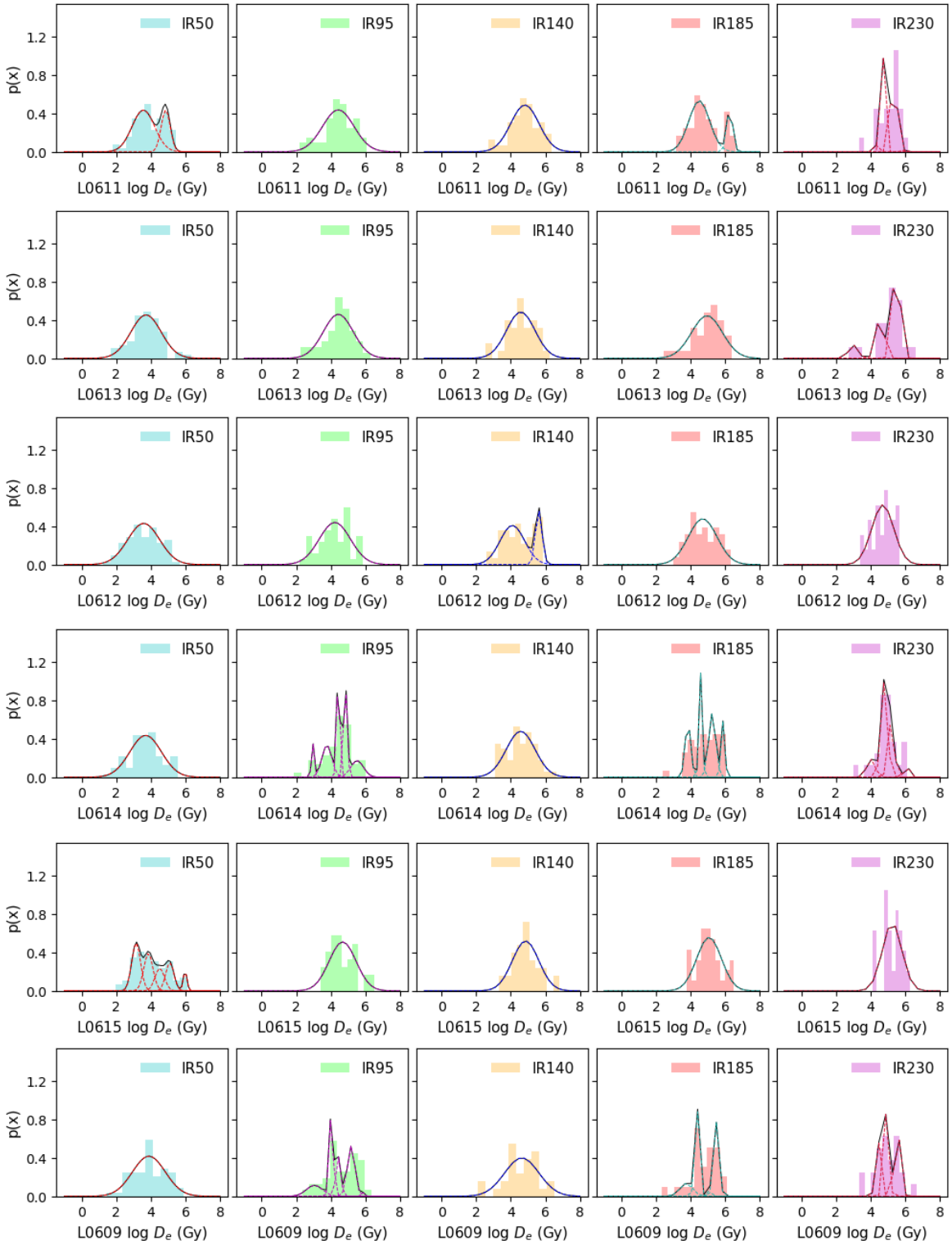

***Figure 5.13**. Optimal fits of a gaussian mixture model to log equivalent dose distributions estimated for the IR_{50}, IR_{95} and IR_{140}, IR_{185} and IR_{230} signals. Black lines represent the best fit probability density function, coloured dashed lines represent best fit component probability density functions. Samples shown here are L0611, L0613, L0612, L0614, L0614 and L0609, in downstream order.*

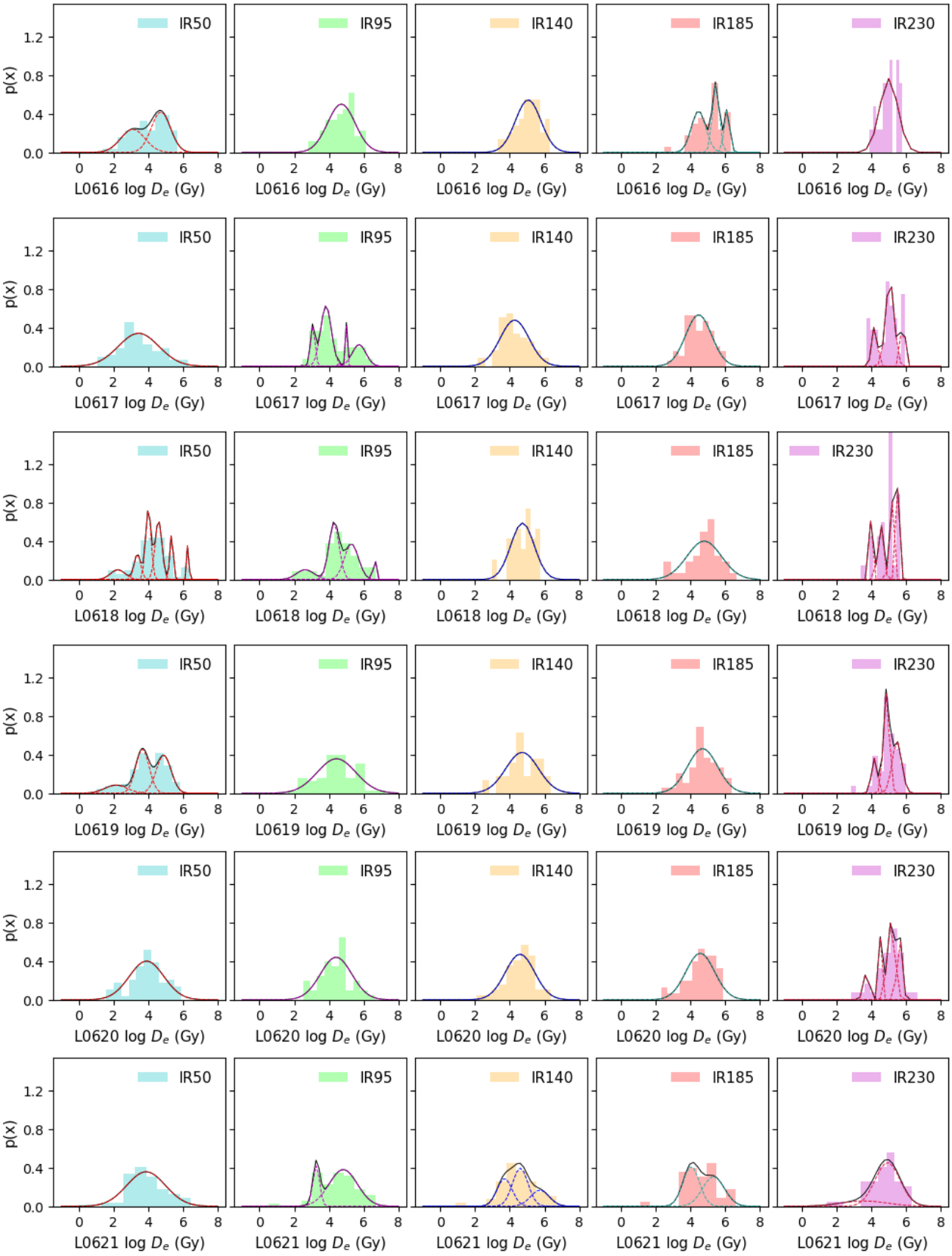

Figure 5.14. *Optimal fits of a gaussian mixture model to log equivalent dose distributions estimated for the IR_{50}, IR_{95} and IR_{140}, IR_{185} and IR_{230} signals. Black lines represent the best fit probability density function, coloured dashed lines represent best fit component probability density functions. Samples shown here are L0616, L0617, L0618, L0619, L0620 and L0620, in downstream order.*

5.3.2. The Santa Clara River

5.3.2.1. Downstream MET-IRSL signal profiles

Downstream profiles of super synthetic aliquot (SSA) apparent age (ka) and mean apparent age (ka) are shown in Figures 5.15 and 5.16. respectively. In Figure 5.15, super synthetic aliquot apparent age remains at a constant low level until ~ 20 km downstream, where a significant increase is observed for all five METx signals at ~ 40 km. This increase is most pronounced for the IR_{230}. Moving downstream to the location at ~70 km downstream, the IR_{95}, IR_{140}, IR_{185} continue to increase, particularly the IR140 and IR185. At this location the IR_{50} and IR_{230} decrease, at by ~ 120 and ~ 150 ka respectively. At the most downstream location, all signals decrease in apparent age. This decrease is increasingly dramatic with increasing measurement temperature, with the IR230 dropping by close to 600 ka over ~30 km.

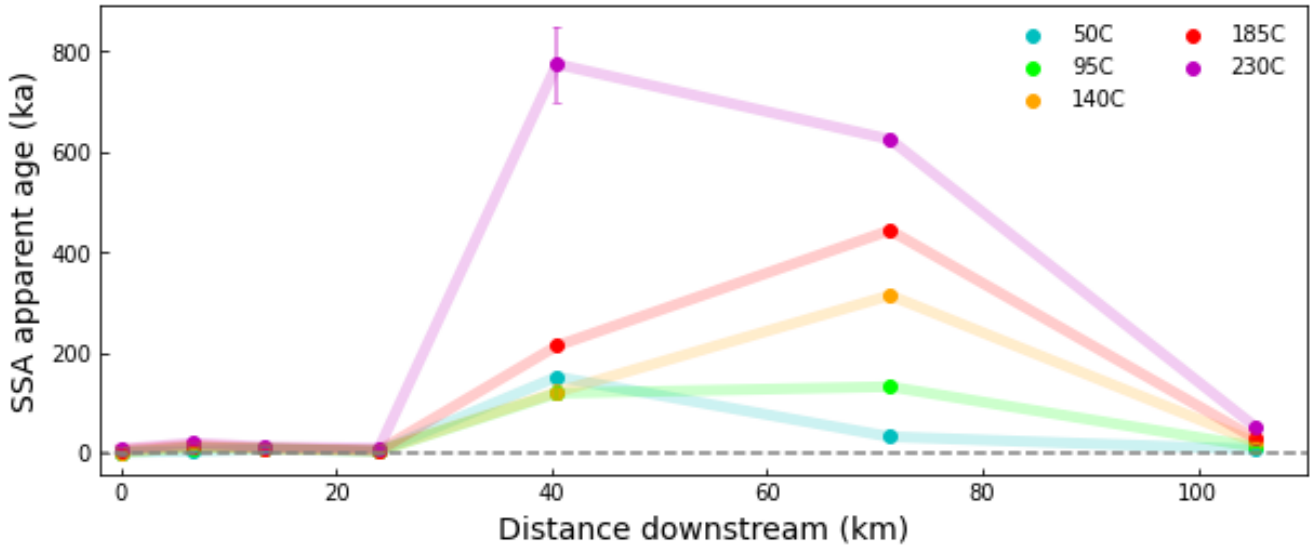

Figure 5.15. *Downstream profile of super synthetic aliquot apparent age, for the Santa Clara River. Super synthetic aliquot apparent age is also referred to as combined signal*

The downstream evolution of METx mean apparent ages captures a somewhat different trend (Figure 5.16. There is considerably more fluctuation of the IR_{140}, and IR_{230} over the first ~20 km of the study reach, compared to that displayed in Figure 5.15. The IR_{185} displays continuous increase over this section, and the IR_{50} and IR_{95} remain at a constant lower level. The five signals exhibit little change in mean apparent age over the middle ~30 km. Yet, unlike the pattern captured by super synthetic aliquot apparent age, it appears all five METx signals increase over the last ~30 km (Figure 5.16), with the IR_{185} and IR_{230} displaying a more rapid increase in age than the other three signals.

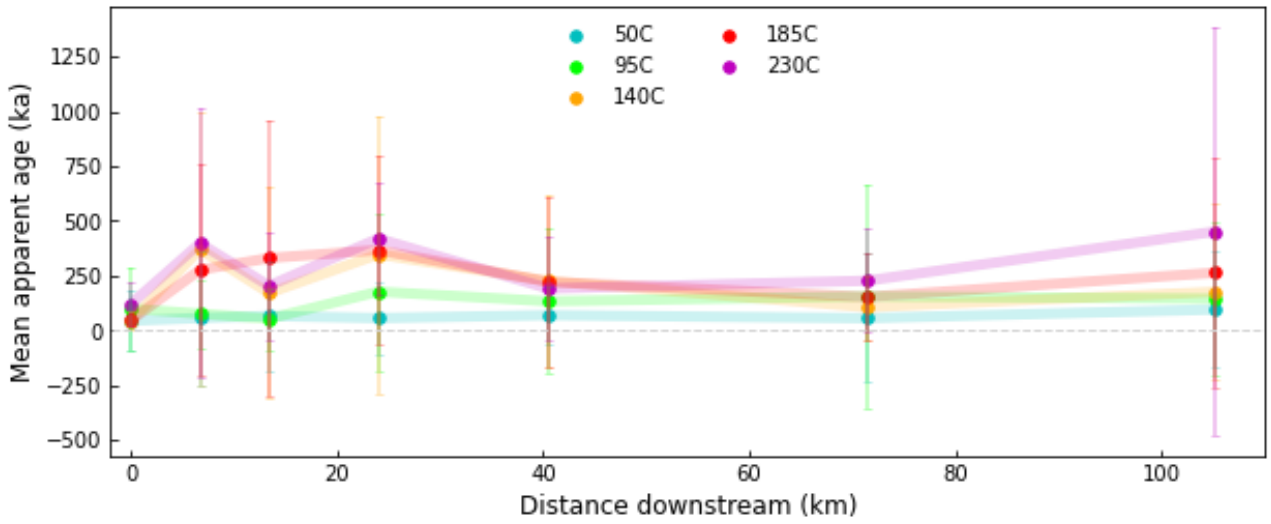

Figure 5.16. *Downstream profile of METx mean apparent ages of the Santa Clara River samples. Includes all grains that provided an equivalent dose estimate.*

Figure 5.17. shows the downstream trend of minimum plateau age (ka). These minimum age estimates are calculated using the plateau method outlined in Ivester *et al.,* (2022) and Rhodes & Leathard (2022) is described in Chapter 2, Section 2.5. By using grains where two or more METx signals are in agreement within their uncertainties, the minimum plateau ages in Figure 5.17 represent grains that were well bleached prior to burial. The signals of these grains exhibit an initial decrease from ~0.8 ka to close to zero age, followed by an increase to ~0.5 ka with change over the next ~30 km. An increase to ~1.4 ka is observed ~70 km downstream. The downstream evolution of minimum age also follows a different pattern, as do SSA apparent age and mean apparent age.

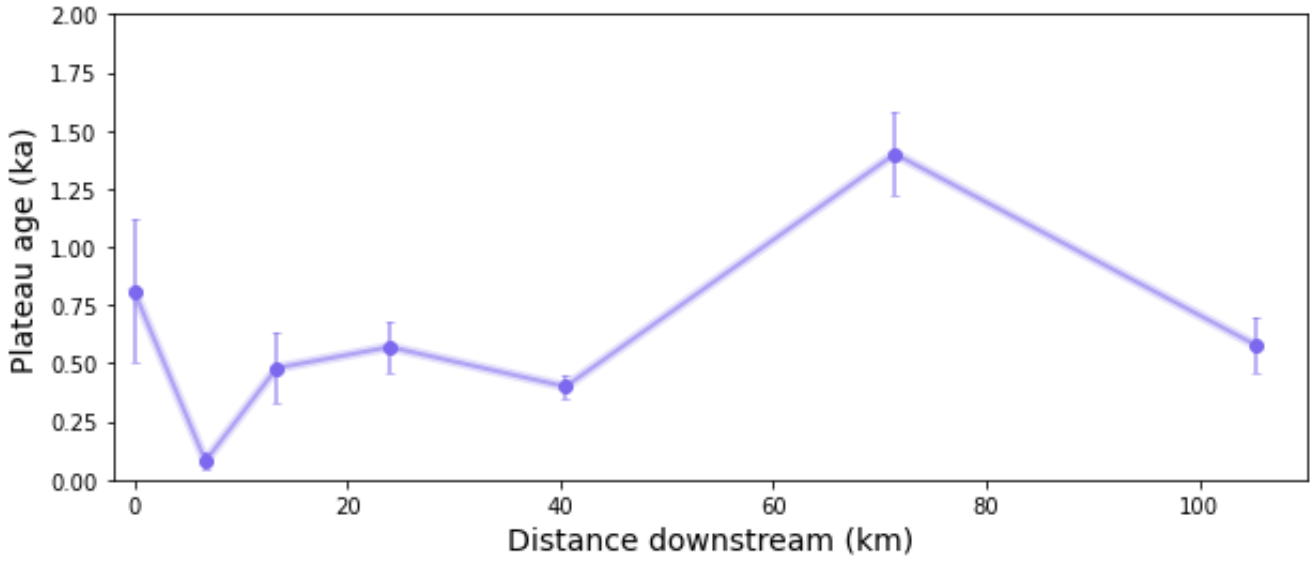

Figure 5.17. *Downstream profile of minimum METx plateau ages of the Santa Clara Rivers samples. Note plateau ages are calculated from just the well-bleached grains.*

Similarly to in Figures 5.3-5.6 in Section 5.3.1 displaying the downstream trend of METx expressed in multiple ways for the Solimões samples (specifically, signals super synthetic aliquot apparent age, mean apparent age, fraction of saturation, and minimum plateau age), the downstream evolution of METx signals in the Santa Clara River varies significantly when presenting MET-IRSL signal in different ways (super synthetic aliquot apparent age, mean apparent age and minimum plateau age). This is highlighted to emphasise an advantage of single grain MET-IRSL, which is that signals can be analysed in multiple ways to provide more than one result for a given sample, each of which can provide a different insight into grain population characteristics. What can be specifically learnt from presenting downstream signals in different ways (i.e. super synthetic aliquot apparent age, mean apparent age, minimum plateau age) will be discussed throughout this chapter, largely in Section 5.4. However, here there is a need to take some caution when determining what specific information is provided by a given signal, or type of signal. Geomorphic and geologic context should also be taken into consideration when making these types of interpretations.

The zones of significant increase in SSA apparent age, and minimum plateau age suggest there is some process that causes significant perturbation to the METx signals of grains in the main channel the Santa Clara River. For SSA an increase in all five signals occurs ~40 km downstream, and in the IR95, IR140 and IR185 at ~70 km. An increase in minimum plateau age is observed ~70 km downstream. For mean apparent age, a small increase in IR_{140}, IR_{185} and IR_{230} is observed at ~7 km and ~25 km. It is acknowledged that for each form of signal expression, and indeed each METx signal, extent and rate of the aforementioned increases in age do vary. This poses the question of whether expressing the signal in multiple ways provides information on different sediment transport processes, or if one process is captured by different signals at different stages.

5.3.2.2. Single grain plateau ages

Figure 5.18 shows the plateau ages for all grains that provided plateau age estimates, including those that did not contribute to the minimum age for that sample, in downstream order. As in Section 5.3.1.2, different coloured points in Figures 5.18 correspond to the number of METx signals that form the plateau. Compared to the Solimões samples in Section 5.3.1.2, in samples J0344, J0345, J0346, J0347, and J0349 there are relatively few grains that were subject to sufficient bleaching prior to burial to form a plateau age. These samples are from the first, second, third, fourth and fifth locations downstream (0, 7, 13, 24 and 41 km). In contrast, J0350 and J0352, at 71 and 105 km downstream, display considerably more plateau ages. This could be the result of several processes including a shift in bleaching conditions, or input of new material with, perhaps with different bleaching properties. Further, the Santa Clara River is located in a highly tectonically active area (Keller *et al.,* 1982). The

impact of tectonic activity on erosion rates may be reflected in the luminescence characteristics of the main channel sediment flux. This will be discussed further in Section 5.4.

To draw another comparison with the Solimões samples displayed in Figures 5.7 and 5.8, there are also very few grains, from the samples displayed in Figure 5.18 below, with plateau ages considerably older than the minimum age estimate. This could suggest relatively low levels of reworking of palaeo-channel and terrace sediments. In addition, the relative lack of grains with older plateau ages may indicate that extended light exposure events are infrequent for grains in the main channel of Santa Clara River. In the context of the Santa Clara River, significant transport events occur during storm events which transport large volumes of sediment resulting in highly turbid water (Downs *et al.,* 2013) where little bleaching can take place.

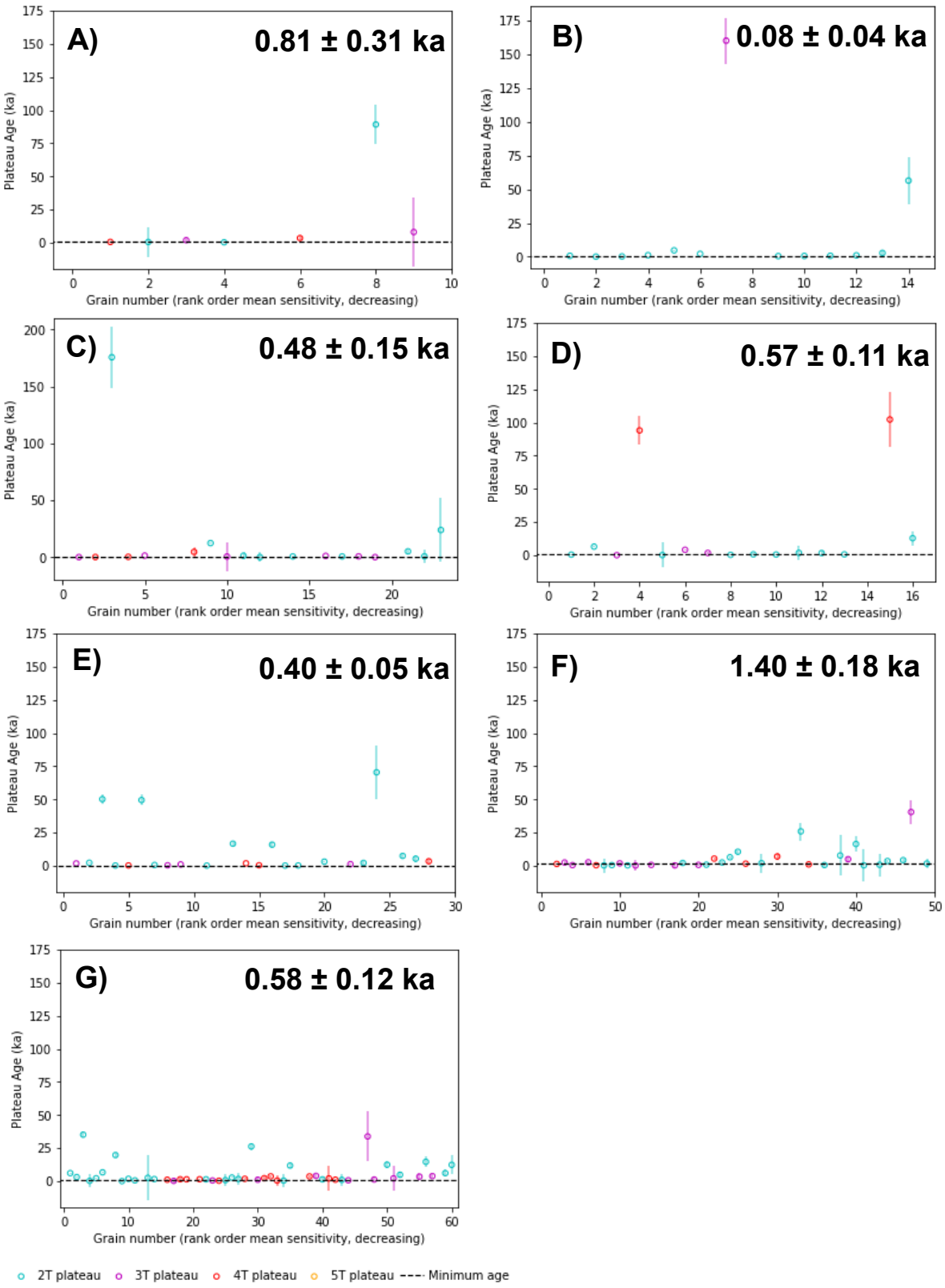

Figure 5.18. *Single grain plateau ages for the Santa Clara samples. Lab codes: A) J0344, B) J0345, C) J0346, D) J0347, E) J0349, F) J0350, G) J0352. Data points are coloured in accordance with the number of METx temperatures that form a plateau. Two-temperature plateaus are blue, three temperature plateaus are purple, four-temperature plateaus are red, five-temperature plateaus are yellow. Minimum age calculated from plateau ages is shown on each subplot and is indicated by the black dashed line. The numbers on each subplot represent the relative locations of these samples.*

Using the same approach outlined in Section 5.3.1.2, all grains that provided plateau ages were assigned a ‘bleach index’ and a ‘bleach score’, and the fraction of saturation of every grain was converted to a ‘light exposure equivalent’ (Figure 5.19). An explanation of the method used to estimate past light exposure can be found in Section 4.5.3.2. Much like in Figure 5.9 in the previous section, the grey lines in each subplot of Figure 5.19 indicate median plateau age and bleach score, dividing each subplot into four divisions. Again, for samples J0344, J0345, J0346, J0347, and J0349, rather few grains provide plateau age estimates that deviate significantly from the median plateau age. However, for the more downstream samples J0350 and J0352, more plateau ages are observed and there is more variability in bleach score, which relates to the bleaching conditions recorded by these grains. There is also a higher occurrence of grains in the top left division, which is indicative of older, more poorly bleached grains. Grains in this category from the most downstream sample, J0352, generally record poorer bleaching conditions, indicated by the presence of blue data points in the top left division.

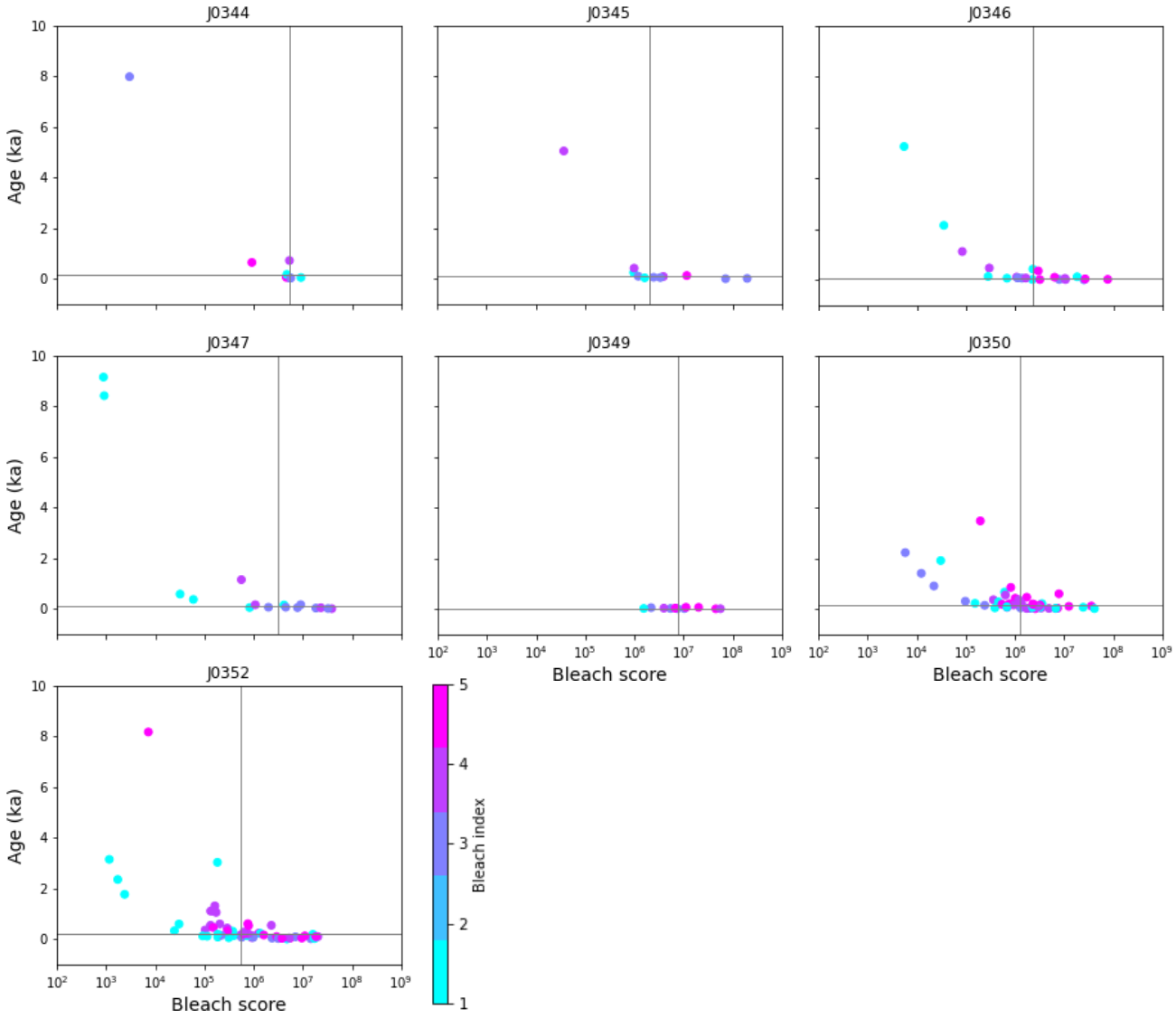

Figure 5.19. *Plateau ages of single grains plotted against 'bleach score', which is a metric containing information on length of past light exposure (see text for details). Grains are coloured based on 'bleaching index', which contains information on the METx temperatures that form the plateau of each grain. The grey lines indicate the median value for bleach score (x-axis) and plateau age (y-axis), dividing each subplot into four divisions. In a clockwise direction starting from the top left division, these represent: older-poorly-bleached, older-well-bleached, younger-well-bleached, and younger-poorly-bleached grains.*

5.4. Discussion

5.4.1. Introduction

This section proposes potential sediment transport scenarios for the Solimões and the Santa Clara River, based on the METx measurements and analysis presented in Section 5.3. Secondly, considerations for applying MET-IRSL as a tool for determining sediment transport in large, complex fluvial systems, such as those presented in this chapter, is discussed. Finally, this section presents a model for reconstructing the histories of individual grains and deriving virtual velocities. This model is applied to two samples from the Allt Dubhaig, and one sample from both the Solimões and the Santa Clara River. Virtual velocities estimated by modelling the histories of individual grains from these samples are compared to those derived using multiple grain signals to assess the potential for calculating sediment transport rates from single grain MET-IRSL data.

5.4.2. The Solimões

The downstream profile of mean apparent age suggests an overall increase in the ages all five METx signals over the ~ 900 km study reach (Figure 5.3). Further, there is strong coherence between zones of signal growth and reduction in downstream profiles of mean apparent age and SSA apparent age, yet the rate of increase varies between METx signals (Figure 5.3, Figure 5.4).

An overall increase in all METx signals with downstream distance is a clear indication that grains are subject to significant storage time as they move through this system. It is inferred that grains are also subject to light exposure due to the variable rates of signal growth observed. An example of this is illustrated in Figure 5.20 below, which is Figure 5.3 with one example of variable rates of METx signal increase indicated by the black box. As discussed in Section 3.5, Chapter 3, whilst buried and subject to radiation, IRSL signals measured at different temperatures grow (in age) at the same rate, but the trapped charge population bleaches at different rates. Thus, it is suggested that variable rates of age increase observed in fluvial systems, such as those highlighted in Figure 5.20, indicate light exposure.

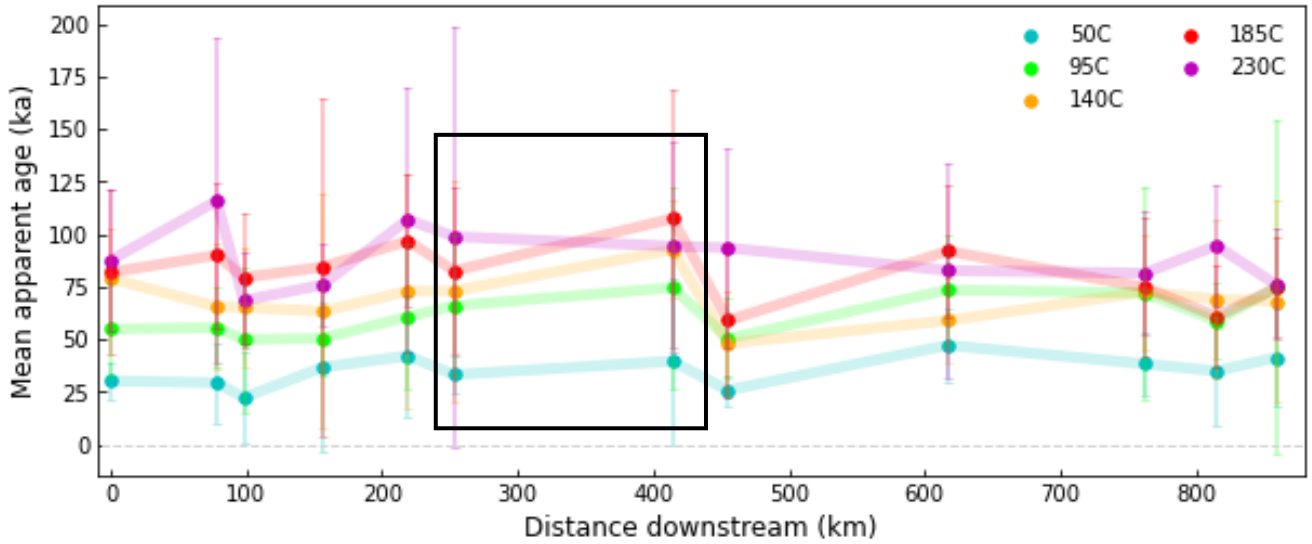

Figure 5.20. *A stretch of the Solimões where the METx signals appear to increase at different rates, excluding the IR_{230}. Note the IR_{230} uncertainties are particularly large perhaps because it is close to saturation.*

It is proposed the downstream evolution of METx signals indicate the Solimões is characterised by both storage and bleaching, with storage exerting a dominant effect on the downstream evolution of luminescence signals. With reference to the idealised conceptual models presented in Section 1.5 of Chapter 1, it is possible that a sediment transport rate can be estimated for the ~ 900 km study reach using the approach outlined in Conceptual model 4, also shown in Figure 5.12.

In Conceptual model 4 presented in Section 1.5 there is an overall increase in apparent age over the distance that grains are transported, and grains are also subject to light exposure. Transport rate estimation using this model exploits the assumptions that during storage, signal takes place at the same rate for all METx signals. In contrast, when grains are exposed to light, METx signals bleach at different rates. Therefore, the differences in overall increase in age over the study reach, observed for the IR_{50} and IR_{95} in Figure 5.21, can be accounted for by light exposure. This allows the construction of a pair of parallel equations that produce estimates of average total storage time (ka) and average age reduction due to light exposure (ka) over the study reach.

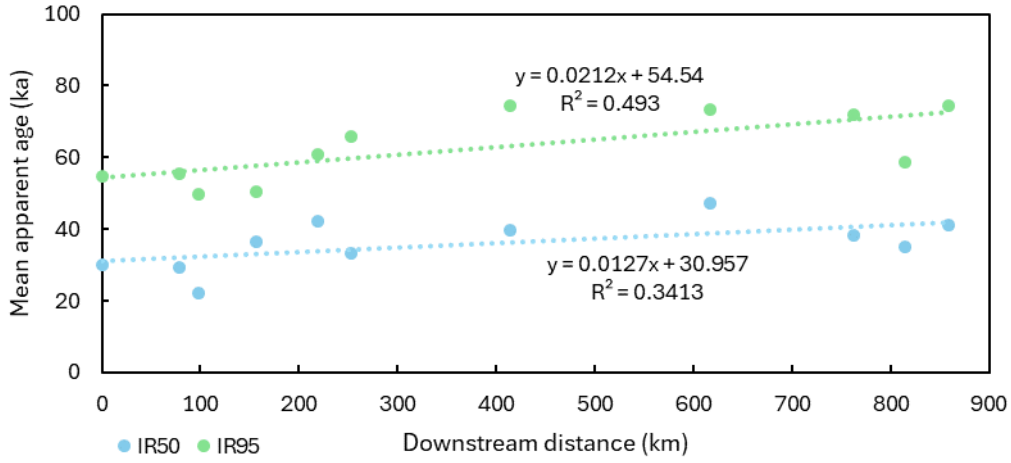

Figure 5.21. *Least squares linear fits to the downstream profile of IR_{50} (blue) and IR_{95} (green) mean apparent ages for the Solimões. Note the difference in slope gradients between the two signals.*

The total difference in age over the length of the study reach, ΔAge is calculated by subtracting the age of the most downstream sample from the age of the most upstream sample. ΔAge is calculated for both the IR_{50} and the IR_{95} to -11.1 ka and -14 ka respectively. are inserted into the parallel equations. These are expressed as:

$$\Delta Age_{\,IR50} + t_{storage} = t_{bleach} \tag{5.1}$$

$$\Delta Age_{\,IR95} + t_{storage} = 0.2t_{bleach} \tag{5.2}$$

where $\Delta Age_{\,IR50}$ (is the total increase in apparent age between 0 km and the most downstream location (859 km) for the IR50 signal and $\Delta Age_{\,IR95}$ is the total increase in apparent age between 0 km and the most downstream location for the IR95 signal. In Eq. 5.2, t_{bleach} is multiplied by 0.2 to reflect the IR_{95} bleaching at approximately one fifth of the rate of the IR_{50} according to multiple grain bleaching measurements of feldspar standard sample MJ39. By solving these equations, average storage time, $t_{storage}$ is estimated at 21.6 ka and average age reduction by light exposure, t_{bleach} is estimated to be 10.5 ka. A reduction of 10.5 ka is equivalent to just ~ 20 seconds of sunlight exposure. This light exposure time is negligible relative to a storage time of 21.6 ka. Therefore, taking 21.6 ka as a transit time and dividing this by a distance of 859 km, an average transport rate of ~ 40 m yr^{-1} is approximated for this reach of the Solimões. After fading corrections were applied to the IR_{50} and IR_{95}, the derived average storage time and transport rate did not change significantly and were calculated at 25.0 ka and ~ 34 m yr^{-1} respectively.

This approach was also applied using the IR_{50} signal paired with the IR_{140} and IR_{185} signals over the first ~ 400 km of the study reach, since these signals also display an overall trend of increase over this section (Figure 5.22, Figure 5.23). These results are summarised in Table 5.4.

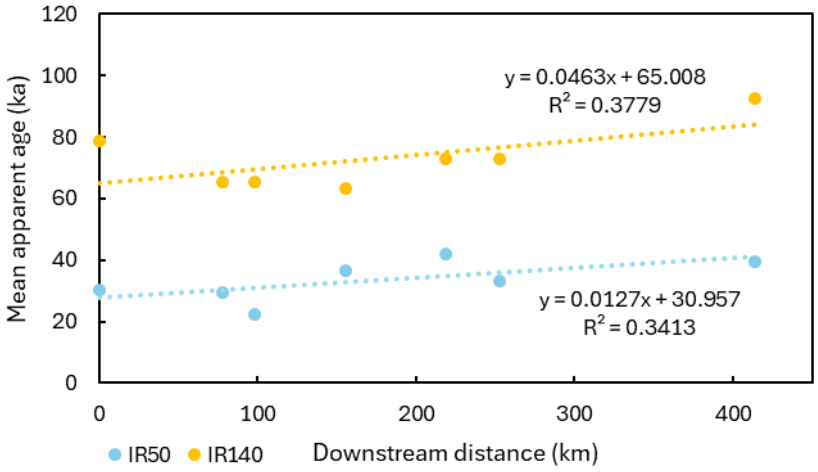

***Figure 5.22**. Least squares linear fits to the downstream profile of IR_{50} (blue) and IR_{140} (yellow) mean apparent ages for the Solimões. Note the difference in slope gradients between the two signals.*

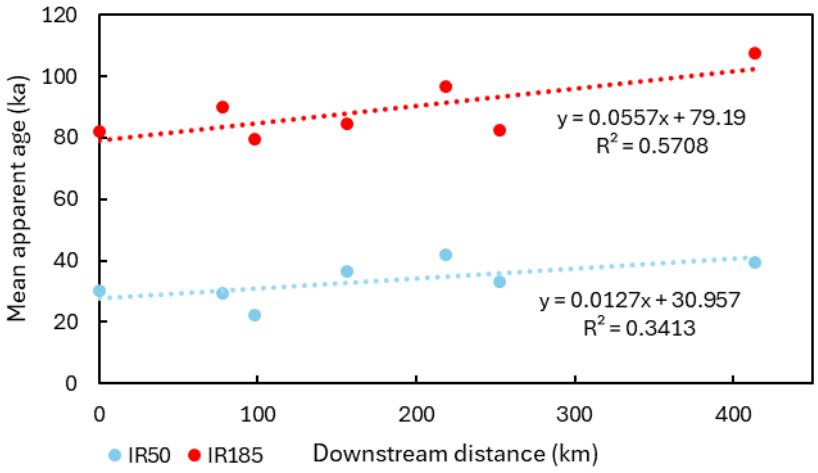

***Figure 5.23.** Least squares linear fits to the downstream profile of IR_{50} (blue) and IR_{185} (red) mean apparent ages for the Solimões. Note the difference in slope gradients between the two signals.*

Table 5.4. *Comparison of average storage times, average bleach times, and average transport rates for the Solimões when using different pairs of METx signals to solve Equations 5.1 and 5.2 (see text for details).*

METx signal pair	$t_{storage}$ **(ka)**	t_{bleach} **(ka)**	**Transport rate (m yr^{-1})**
IR50-IR95	21.6	10.5	40
IR50-IR140	14.3	5.0	30
IR50-IR185	189.3	17.8	15

The transport rates estimated using different pairs of METx signals appear to vary, decreasing with increasing measurement temperature. Since a single grain has been subject to the same light exposure and storage, it cannot be the case that different METx signals of an individual grain record different lengths of light exposure. Subsequently, there could be several reasons for the different results shown in Table 5.4 such as: 1) transport rates are actually the same, with increasingly large uncertainties on the higher values, or 2) the IR_{140} and IR_{185} in fact approach saturation over ~ 400 km of transport in the Solimões.

5.4.3. The Santa Clara

Downstream profiles of SSA apparent age (Figure 5.15) and minimum plateau age (Figure 5.17) clearly indicate significant perturbation to the in-channel sediment flux of the Santa Clara River. It is suggested that in this case, the significant increase in SSA apparent age is the result of lateral input of material with a high fraction of saturation. It appears that this input occurs ~ 40 km downstream (sample J0349), as indicated by the first major increase in SSA apparent age (Figure 5.15). Minimum plateau age of J0349 does not capture the input of such unbleached material at the ~ 40 km mark because as the new material enters the channel, it is not subject to sufficient light exposure for METx signals to form plateaus. There is however, a ~1 ka increase in minimum age a further ~ 30 km downstream. Applying the principle of time-space equivalency outlined in Section 1.5, Chapter 1, it is suggested that this increase reflects the distance travelled by the unbleached grains that entered the channel at ~ 40 km by the time they have been subject to sufficient light exposure for multiple METx signals to be reset and form plateaus before entering storage at some stage downstream. However, this alone does not indicate whether these grains have been subject to multiple cycles of transport and storage over this ~ 30 km stretch.

The downstream profile of mean apparent age also provides insight into the nature of lateral input at ~ 40 km downstream. The absence of a significant increase in the METx mean apparent ages of J0349 suggests the volume of this input is small relative to the volume of the in-channel sediment flux. Taking the IR_{185} and IR_{230} signals, 15% out of a total of 26 grains and 21% and out of a total of 19 grains that gave equivalent dose estimates were greater than three sigma above the mean ages of these signals respectively. Out of the total 200 positions measured, this is potentially as low as 2% of grains. Nonetheless it is also important to note that single grain analysis of these samples yielded far fewer results than for the Solimões and the Allt Dubhaig. This could mean that actual proportion of input material that to the in-channel flux in these samples could be much lower, and suggests clarity could be gained by measuring an additional 200 grains in the future.

5.4.3.2. Bleach-burial model application

This section discusses the extent to which application of the burial-bleach model provides additional insight to the volume or age of the lateral input material using multiple grain signals, and whether with this knowledge, it is possible to estimate an average sediment transport rate for the study reach.

Firstly, a simple, first order approach is proposed for estimating the age contribution of the input material to the in-channel sediment by calculating the degree of departure of the data from model predictions of the downstream evolution of METx signal fraction of saturation. A conceptual model of

this approach is shown in Figure 5.24, whereby α, expected signal, is subtracted from β, the observed signal to estimate the age contribution of the input material to the in-channel sediment flux (ΔAge_{in}).

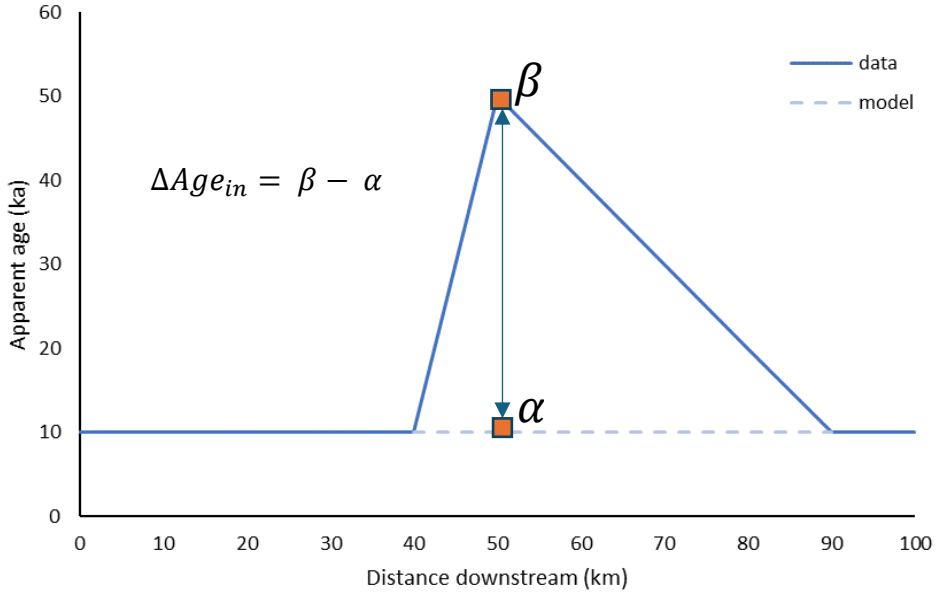

Figure 5.24. *Schematic diagram outlining the approach to calculating the degree of departure of the data from the model to estimate the age contribution of potential new input to the sediment flux of the main channel of the Santa Clara River.*

A burial-bleach model is fit for the IR_{50}, IR_{95}, IR_{140} and IR_{185} signals. The IR_{230} is omitted from the model fit because it has observed fraction of saturation of ~ 0.8 at the most downstream location whilst the IR_{50}, IR_{95}, IR_{140} and IR_{185} signals are significantly lower and appear to be in approximately equal ratios with respect to each other. This suggests the IR_{230} maintains the signature of the upstream input of new material at the most downstream location.

The model was fit to the Santa Clara River dataset using the approach outlined in Section 4.5.4, Chapter 4. Figure 5.25 displays the best fit model, which gives a least squares value of 3.09×10^4. This simulation used an average bleach cycle length of 100, and an average storage time of 0.5 ka multiplied by their respective acceleration factors for each bleach-burial cycle. The model also fitted bleaching and burial acceleration factors of 1.27 and 0.83 respectively, indicating that bleach cycle length increases with downstream distance and burial cycle length decreases with downstream distance.

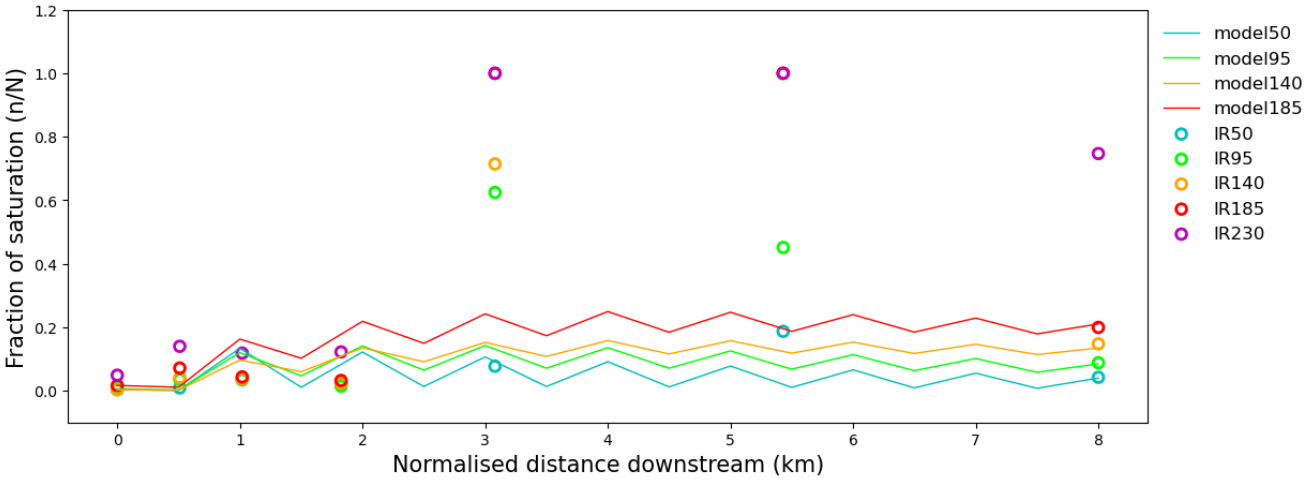

Figure 5.25. *A visualisation of the best fit of the burial bleach model presented in Chapter 3 to the Santa Clara River dataset to estimate the degree of departure of the data from the model in order to characterise the lateral input of that is potentially causing such elevated METx signals ~ 40 km downstream.*

As outlined in Section 3.5.2.1, Chapter 3, one bleach-burial cycle is comprised of a period of bleaching followed by a period of burial. One of the challenges of simulating average cyclical bleaching and burial between locations in a dataset such as this, is that there is uncertainty surrounding at what stage of a bleach-burial cycle, or transport and storage cycle, grains were when they were sampled from the channel. The apparent age of a sample can provide some constraint here, since from this one can interpret the timing of burial following deposition. However, it should be noted that the bleach-burial model presented here simulates average transport and storage behaviour, rather than individual transport and storage events. For the purpose of characterising the input of material that causes such a significant increase in signal at sample J0349 at ~ 40 km downstream, a minimum and maximum expected fraction of saturation (signal) is taken for the IR_{95}, IR_{140} and IR_{185} by extracting the start and end values for the bleach-burial cycle simulated at this location in order to estimate the degree of departure of the data from the model. Using the method outlined in Figure 5.24, the minimum and maximum estimates of ΔAge_{in} for the IR_{95}, IR_{140} and IR_{185} signals of sample J0349 is estimated to be 80-106 ka, 77-104 ka, and 87-125 ka respectively. These results are summarised in Table 5.5.

Table 5.5*. Minimum and maximum age contributions of lateral input ~ 40 km downstream to the main channel sediment flux of the Santa Clara River.*

Temperature (˚C)	Min. ΔAge_{in} (ka)	Max. ΔAge_{in} (ka)
95	80	106
140	77	104
185	87	125

There is broad agreement in a ΔAge_{in} estimate of ~ 90-100 ka across the three signals included in this analysis. This indicates the input material was bleached sufficiently to reset each of these signals prior to its storage. The location and what constitutes the source of this material remains an open question. The Santa Clara River is located in a highly tectonically active area, which means the river is supplied with a significant volume of sediment (Warrick and Mertes, 2009). Tectonic processes could cause an influx of material of an age inconsistent with those of sediments that comprise the main channel flux. It should also be considered that the catchment of the Santa Clara River houses extensive urban development, and its channel, banks and tributaries have been subject to over a century of anthropogenic modification. At ~ 40 km downstream, sample J0349 is located where the city of Santa Clarita extends either side of the channel. Thus, it is possible input of highly unbleached material to the main channel at this location is the result of human activity. For example, Figure 5.26 compares Google Earth imagery from 2018 to that of the present day for the area immediately surrounding sample J0352 at ~ 40 km downstream, where a significant increase in METx signals is observed and reveals significant construction work over this period. A large housing estate has been constructed on the south bank of the Santa Clara River at this location, which may be at least partly responsible for the production of material that potentially caused a significant increase in METx signals at this location.

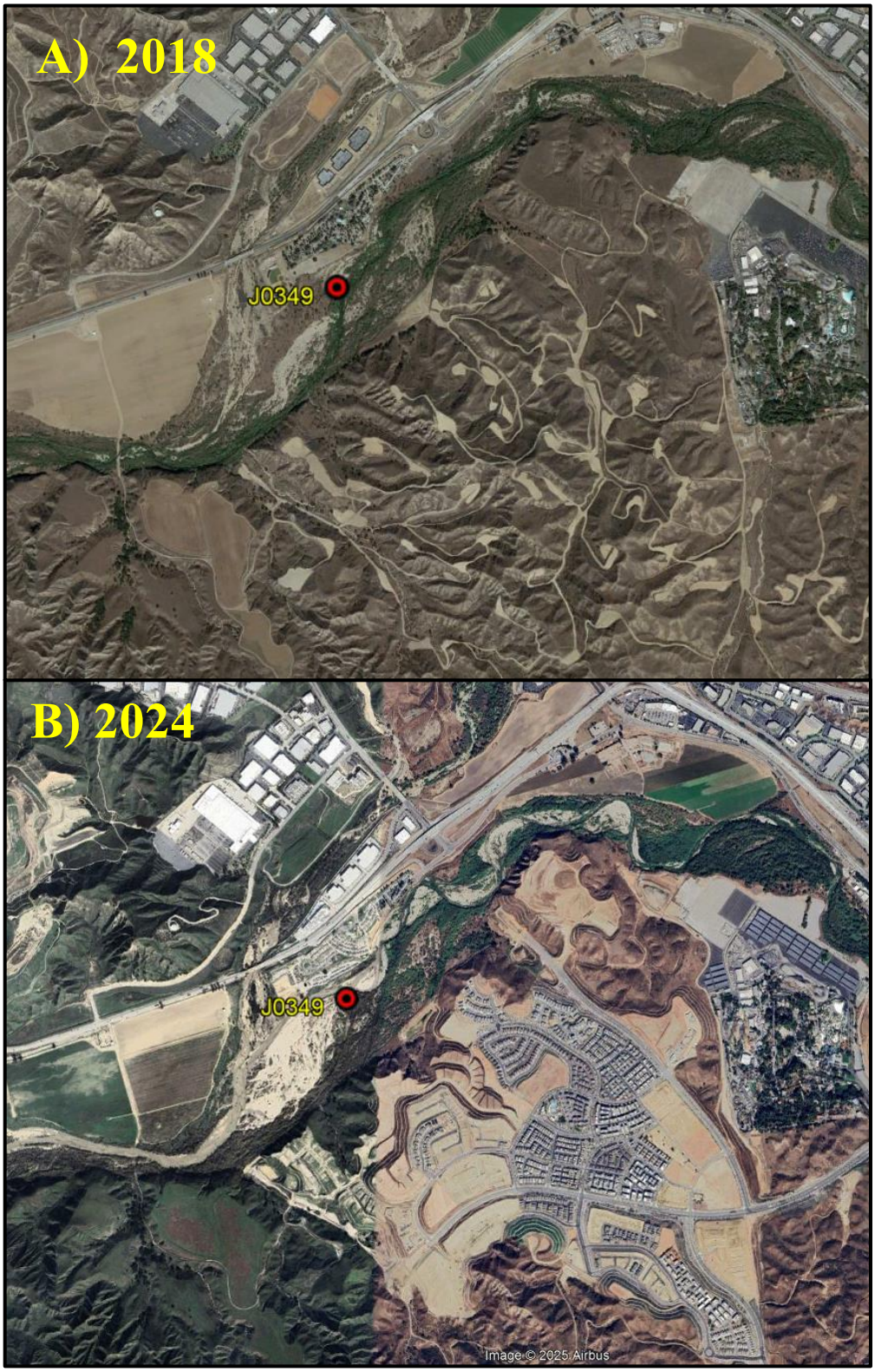

Figure 5.26. *Comparison of historic Google Earth Imagery with the present day for the area surrounding sample J0349 ~ 40 km downstream. Note the construction of a large residential estate between 2018 and the present day.*

5.5. Modelling the histories of single grains

This section presents results and discussion of an approach to modelling the bleaching and burial histories of individual grains for four samples using the burial-bleach model that was introduced in Section 3.5.1.2, Chapter 3 and applied to multiple grain datasets from the Allt Dubhaig in Chapter 4 and the Santa Clara River in Chapter 5. This modelling study uses ILT-3ET single grain fraction of saturation from sample 22181 (upstream) and 22190 (downstream) from the Allt Dubhaig, METx single grain fraction of saturation from sample L0620 from the Solimões, and METx fraction of saturation from sample J0352 from the Santa Clara River. Virtual velocities from these single grain data are calculated, single grain virtual velocities of the Allt Dubhaig samples are compared to those derived from multiple grain signals presented in Sections 4.5.4. The advantages and potential power of reconstructing single grain histories, compared to the traditional multiple grain approach of McGuire & Rhodes (2015a), are discussed.

Bleaching and growth parameters input to the model were derived directly from super synthetic aliquot measurements for each sample. This is in part for practicality reasons, and also because, as demonstrated in the bleach recovery experiment in Section 3.4.2, Chapter 3, the use of single grain bleaching parameters can introduce a lot noise. Bleach recovery was successful using average bleaching parameters within uncertainties. The bleaching recovery experiment in Section 3.4.2, Chapter 3 did also demonstrate successful light exposure recovery using the fitted parameters of each individual grain when recovered values were weighted by their uncertainties, so it would be worthwhile exploring this option for model input in the future once an method for uncertainty estimation and dealing with high levels of noise is defined (discussed in Section 3.5.1.4, Chapter 3). I_{max} as fraction of saturation was set to 1 for all grains thus, these model fits simulate the entire history of a grain since it was last saturated. Burial times were subject to constraint between 10^{-2} and 10^{7} years, bleach times were subject to constraint between 10^{-2} and 10^{7} seconds. The number of bleach-burial cycles simulated was fixed to five cycles. Estimated average burial and bleach times per cycle were found for each grain using least squares optimisation between model predictions of ILT-3ET fraction of saturation, and observed ILT-3ET fraction of saturation. For samples 22181 and 22190 the grains used in this study were only those that provided a result for all three measurement temperatures. For these grains, the burial bleach model essentially finds optimal burial and bleach times to reproduce the observed ratios of ILT-3ET signals.

Figure 5.27 shows $\log_{10}$ optimal burial times plotted against $\log_{10}$ optimal bleach times for the individual grains of each sample. Firstly, Figure 5.27a and Figure 5.27b, which display results from grains of upstream and downstream Allt Dubhaig respectively, will be discussed. Initially striking is the emergence of subpopulations, which are tentatively highlighted in each subplot of Figure 5.27. In

Figure 5.27a, there is a group of grains for which the model fitted very low burial times (pink circle), which suggests zero storage. This indicates that the signal ratios of these grains can be reproduced by the model with a single bleach time, which varies between 10^0 and 10^7s seconds. This may represent grains that entered the channel from of glacial deposits where they were essentially saturated, since it is unlikely they were subject to significant light exposure prior to burial during glaciation. Once in the channel, these grains were subject to various lengths of light exposure prior to storage, but according to the model, the signal ratios of these grains do not require cyclical burial and bleaching. The second subpopulation is a cluster of grains with estimated average storage times approximately between 100 and 100,000 years per cycle. The model required cyclical bleaching and burial to reproduce the signal ratios of these grains. Average bleaching and burial times for this sample, including those with zero storage, are 109,320 seconds and 2290 years of storage respectively, since saturation.

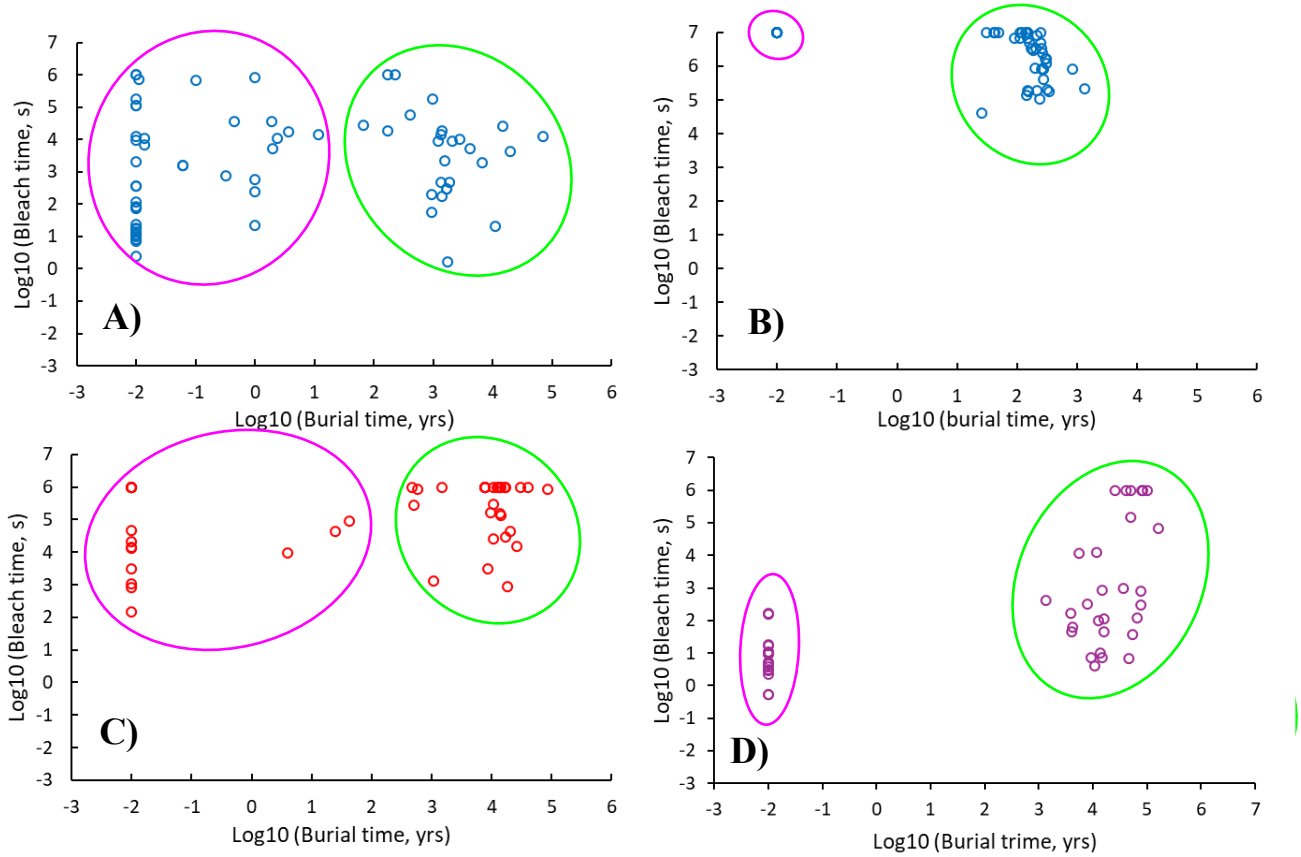

Figure 5.27. *Log10 estimated burial time against log10 bleach time for individual grains for samples* ***A)*** *22181, ~0.15 km downstream from the first sample location in the Allt Dubhaig,* ***B)*** *22190, ~3.6 km downstream from the first sample location in the Allt Dubhaig (most downstream location),* ***C)*** *L0620 from the Solimões River (second to most downstream location),* ***D)*** *J0352 from the Santa Clara River (most downstream location). Grains for which very short burial times (<10 years) are fit are circled in pink, and those for which substantial burial times (>10 years) are fit are circled in green.*

Inspection of Figure 5.27b also reveals two distinctive subpopulations of grains, comparable to those observed in Figure 5.27a. This sample, 22190, is ~3.35 km downstream from 22181 in Figure 5.27a. At this location, it appears that the bleach-burial signature of grains circled in green in Figure 5.27a has been preserved throughout the length of the system. In Figure 5.27b, grains circled in green cluster around approximately 10^2-10^4 years of burial 10^5 and $>10^7$ seconds of bleaching per cycle. There is greater homogeneity in burial-bleach ratios of these grains, which is consistent with the hypothesis that the longer grains spend in a system, the more that their signal ratios will reflect characteristic transport and storage dynamics, rather than perhaps heterogenous sources of input. The average burial time for grains in this sample, including those with zero storage is 934 years over the five cycles simulated, which can be used to estimate a virtual velocity of 3.9 m yr^{-1}. This differs from the virtual velocity estimated for the downstream section of the Allt Dubhaig using the combined signal approach of 1.39 m yr^{-1} by 2.5 m yr^{-1} (see Section 4.5.4, Chapter 4). Nonetheless, these estimates are firmly within the same order of magnitude.

Application of the model to grains from sample L0620 from the Solimões produces somewhat surprising results (Figure 5.27c). Similarly to the Allt Dubhaig samples in Figure 5.a and 5.b, subpopulations can be identified, but perhaps most surprising is the number of grains that do not require storage to reproduce METx ratios, and the number of grains that require very long bleach times. Downstream profiles of combined signals (e.g. Figure 5.2, 5.3) indicate a strong storage signal for this system relative to bleaching, with increases in apparent age. Using parallel equations Eq. 5.1 and Eq. 5.2, average light exposure over the 959 km study reach was estimated to be just 6.9 seconds, whereas the single grains in Figure 5.c, the model fits the majority of grains with $< 10^3$ seconds of bleaching per cycle. Average storage time per cycle estimated from sample L0620 is 9770 years and average bleach time is 512,190 seconds. As discussed, this average bleach time is significantly higher than estimates derived from the combined signals for the study reach of the Solimões. However, since the model presented here uses an I_{max} input value of 1, it is possible longer bleach times are observed because, few grains entered the channel of the Solimões close to saturation, perhaps excluding the IR_{230} signal. Thus, the modelled average bleach and burial times presented here, may reflect storage and transport over a much larger reach of the Amazon. Taking 3000 km as an approximate length for the Amazon system, single grain derived storage times provide a virtual velocity of 61 m yr^{-1}, there is strong potential that this rate lies within the uncertainties of transport rates estimated from combined signals.

In the Santa Clara River, application of the model to sample J0352 also reveals distinct subpopulations of grains (Figure 5.27d). It is perhaps surprising that there are so few grains with average storages times less than 1000 years (note this does not necessarily correspond to older ages), and that many of

these are poorly bleached. Nonetheless, at least for the well-bleached this could be consistent with the relative lack of grains with older plateau ages, since this observation may indicate that extended light exposure events are infrequent for grains in the main channel of Santa Clara River (Figure 5.27) The storage times modelled and presented in Figure 5.27d can be used to estimate a virtual velocity of 0.9 m yr^{-1} for the Santa Clara River.

This modelling study has demonstrated that the signal ratios of individual grains is directly related to whether grains have been bleached in an equilibrium or non-equilibrium state and that these ratios can be reproduced for each grain using this approach. Reconstruction of single grain sediment transport and storage using a burial-bleach model that simulates non-equilibrium bleaching single grains allows the identification of which specific grains have equilibrium bleaching histories, and which have non-equilibrium histories. The modelling results for Allt Dubhaig samples 22181 and 22190, suggest that grains at downstream locations may preserve a memory of upstream bleaching and burial. Further, the consistency of the virtual velocity estimate derived from estimated average storage for sample 22190 (2.3 m yr^{-1}) with the combined signal virtual velocity (1.39 m yr^{-1}) is a promising indication that the MET-IRSL signals of single grains record a transport-storage history that is coherent with the history provided by combined signals for at least some systems.

These results presented here suggest huge potential for reconstructing the histories of individual grains, and for deriving virtual velocities from single grain MET-IRSL data. In the future, the fine resolution insight into system dynamics gained through the ability to identify subpopulations of grains with shared transport-storage histories could make significant contributions to addressing issues of particulate organic carbon (POC) transport, biodegradation, capture and export, particularly if successfully applied to large scale systems, such as the Amazon Basin. Current models of carbon transport in fluvial systems are relatively sophisticated (e.g. Torres *et al.,* 2017) but often estimate transport at the catchment scale and lack site-specific estimations of storage times at an adequate temporal scale (Bertassoli Jr. *et al.*, 2017). A study by Respasch *et al.* (2021) documents POC transport, and several other variables important to carbon cycling in the Rio Bermejo in the Amazon Basin in Argentina. This comprehensive study includes dating of sediment cores using quartz OSL and a transport rate estimation using ^{10}Be. Respasch *et al.* (2021) construct a model to make a basin-wide estimate of the proportion of POC lost through process of oxidation using the catchment-wide transport rate of Dosseto *et al.* (2006). However, estimates at such a large spatial scale may mask site-specific dynamics that could significantly alter estimated loss of POC. Single grain storage and transport reconstruction has the potential to address these challenges to accurate modelling of carbon transport, storage, capture and export through the ability to identify multiple sediment transport pathways and potentially transport rates within a single reach.

6.0. Chapter 6 Conclusions

The transfer of sediment across the Earth shapes both the human and physical world. Sediment transport is both a driver of and responder to landscape evolution over geological time scales, inextricably linked to climate processes and tectonic activity (Anderson & Anderson, 2010). The movement of sediment enriches the soils we rely on for food production and drives land degradation, threatening the livelihoods of many (Burbank & Anderson, 2009). A quantitative understanding sediment transport is a key to sustainable development, yet current methods for measuring and modelling these processes are highly inefficient and often lack the spatial-temporal resolution to account for localised effects. The overall aim of this thesis was to develop feldspar MET-IRSL as a tool to provide information on sediment storage times and transport rates that is capable of circumventing some of these challenges posed by traditional sediment tracing techniques. This section lists the four objectives that were set to achieve this aim, and details how they were addressed.

Objective 1: Investigate feldspar MET-IRSL bleaching to determine an ideal function with which to model the bleaching process for grains in fluvial transport.

A series of bleaching experiments were conducted to contribute to understanding of the IRSL bleaching process (Chapter 3). It was identified that MET-IRSL bleaching form has a dependency on length of prior light exposure, providing MET-IRSL signals have not been saturated or reset. It was observed in Experiments 3.4.1.1 and 3.4.1.2 that MET-IRSL bleaching rate decreases with increasing lengths of prior light exposure. The terms ‘equilibrium bleaching and ‘non-equilibrium bleaching’ were introduced to describe this effect on MET-IRSL decay. The term ‘equilibrium bleaching’ describes how MET-IRSL decay proceeds following saturation of the signal, or when signals have been reset prior to receiving a dose. ‘Non-equilibrium bleaching’ refers to the reduced rate of MET-IRSL decay following partial bleaching. During an equilibrium bleach, MET-IRSL signals of a single grain will remain in distinct, measurable ratios. During a non-equilibrium bleach, owing to the different bleaching rates of MET-IRSL signals, signal ratios depart from an equilibrium state. Subsequently, quantification of departure from equilibrium for grains from fluvial systems allowed the identification of subpopulations of grains with shared bleaching and burial histories.

A known light exposure time was successfully recovered from single grain MET-IRSL measurements using bleaching parameters estimated from direct measurements of individual grains (Experiment 3.4.2, Chapter 3). Three approaches to achieving light exposure recovery were explored and it was determined that two of these approaches demonstrated reasonable success (Section 3.5.2). One approach used average bleaching parameter values calculated from the parameter estimates of grains grains that provided fractional uncertainties below 0.5. Another successful approach used the

individual bleaching parameter values for each grain weighted by their respective uncertainties to calculate a weighted mean recovered light exposure time. Since some recovered light exposure times produced rather large uncertainties, it is suggested that perhaps a combined approach whereby for the brightest grains with low bleaching parameter uncertainties their individually fitted parameters are used in light exposure recovery, but for dimmer grains with large bleaching parameter uncertainties, average parameter values are used could reduce the high levels of noise introduced by single grain measurements.

Based on laboratory measurements of samples collected from the Allt Dubhaig, Scotland (Chapter 4), and numerical modelling studies (Chapter 3, 4, 5) it was confirmed that to reconstruct the bleaching and burial histories of grains that have been fluvially transported, it is necessary to account for equilibrium and non-equilibrium bleaching conditions to construct accurate sediment transport models. This is a key way in which the burial-bleach model presented in this thesis differs from current luminescence-based sediment transport models. Based on the research described here, this model was published in Rhodes *et al.* (2024)

Objective 2: Develop optimal methods for analysing MET-IRSL data to determine fluvial sediment transport dynamics and assess the success of the burial-bleach model.

Samples were collected from the active channel of a small gravel bed river, the Allt Dubhaig in Scotland and measured using the ILT-3ET protocol, a low-three-temperature MET-IRSL protocol adapted from the protocols of Ivester *et al.,* 2022 and Rhodes & Leathard (2022) (Chapter 4). Single grain and multiple grain (combined) signals revealed complementary information on the sediment transport dynamics of the Allt Dubhaig. Downstream profiles of combined signals revealed an overall trend of decrease in apparent ages with some zones of signal increase. It was observed that single grain apparent age distributions narrowed with downstream distance and that there was increasing dominance of light exposure over storage with downstream distance despite zones of increase in combined signal apparent age. It was interpreted that this was an indication that the resident population of grains in the channel recorded dominance of bleaching over storage, and that some mechanism was causing lateral input of new material

Prior to sample measurement, it was expected that the Allt Dubhaig would display ‘flume-like’ behaviour based on evidence presented in the literature (e.g. Ferguson & Ashworth, 1991; Hoey & Ferguson, 1994, Ferguson & Wathen, 1998; Ferguson *et al*., 2002). However, multiple lateral inputs were identified through interrogating plateau ages and plateau type variability of single grains (Section 4.5.1), quantification of non-equilibrium bleaching conditions (Section 4.5.2), and by examining intra-channel grain population characteristics to identify distinct groups of grains with shared histories

(Section 4.5.3). It was interpreted that the sources of lateral input are glacial sediments from a moraine in the upstream section of the study site, and elevated rates of erosion of flood plain sediments through bank erosion, which is consistent with increased channel sinuosity reported in the literature (Hoey & Ferguson, 1994) and also in the field and by remote sensing.

A burial-bleach model was applied to the Allt Dubhaig dataset using several approaches to estimate virtual velocity. One approach, which fitted the model to a subset of 13 samples that were collected in 2022, produced a virtual velocity estimate of 0.38 m yr^{-1} over ~ 3 km. Using another approach, the model was fitted to the ~1.5 km upstream reach and the ~2 km downstream reach isolation, which produced virtual velocities of 0.5 m yr^{-1} and 1.39 m yr^{-1} respectively. Overall, MET-IRSL analysis and modelling of MET-IRSL signals was able to reveal the Allt Dubhaig is a more complex system than is suggested by existing literature.

Objective 3: Test and apply methods developed in achieving Objective 2 to elucidate sediment transport information for more complex systems with multiple potential lateral inputs.

In Chapter 5, the techniques presented in Chapter 4 were applied to MET-IRSL data from two fluvial systems in contrasting geomorphic settings: the Solimões River, considered the main strand of the Amazon, in Brazil, and the Santa Clara River in southern California.

In contrast to the Allt Dubhaig, combined MET-IRSL age (expressed as a mean of single grains) displayed a trend of overall increase over the ~900 km study reach of the Solimões River. This was interpreted as an indication that grains are subject to significant storage time as they move through this system. The downstream profile of combined ages also revealed zones of increase in apparent age where the MET-IRSL increased at different rates. This was attributed to the light exposure grains are subject to in this system because IRSL signals measured at different temperatures grow at the same rate, but the trapped charge population bleaches at different rates, this to variable rates of increase of in apparent age of MET-IRSL signals with downstream distance. Downstream patterns displayed by MET-IRSL signals indicated the Solimões is characterised by both storage and bleaching, with storage exerting a dominant effect on the downstream evolution of luminescence signals. Light exposure is thought to be minimal due to the very low light conditions in this deep (up to 30 m), sediment-laden channel.

The variable rates of signal increase over the length of the Solimões was exploited to estimate average storage times and virtual velocities for grains that move through this system. Pairs of combined METx signals were used to construct parallel equations, which could be solved to calculate average storage times and degree of age reduction by light exposure. Using different pairs of signals, average storage times ranged from 25-190 ka after fading correction of the IR_{50} and IR_{95} signals. Despite this large

range, each pair of signals produced a virtual velocity in the range of 15-34 m yr^{-1}. Nonetheless, this did highlight some methodological considerations. For example, it is possible that the observed variation in virtual velocity are related to increasingly large uncertainties on the higher values.The MET-IRSL derived storage time is consistent with that of Wittman *et al.,* (2015) who estimate residence times of ~29 ka in the Amazon Basin. The MET-IRSL derived transport rate is lower than the estimate of Dosseto *et al*. (2006) of 210 m yr^{-1} for the entire Amazon Basin, potentially highlighting the importance of determining sediment transport rates at smaller spatial scales for identifying localised variability.

Downstream profiles from samples from the Santa Clara River indicated significant perturbation to the in-channel sediment flux, which is suggested to be caused by lateral input of new material. Single grain analysis revealed this input comprises a relatively small number of grains with very large signals, potentially as low as 2% of the 200 grains measured for this sample. The ability to quantify the relative contribution of these grains to the main channel sediment flux is unique to single grain approaches, and may prove beneficial to studies interested in quantifying the relative input of potentially contaminated sediments to water resources that see considerable human use.

In addition, the potential age contribution of this lateral input to the combined age of the main channel sediment flux was determined through application of the burial-bleach model to the Santa Clara River dataset. The downstream evolution of METx signals in the Santa Clara River was simulated in order to quantify the degree of departure of the data from the model, or 'expected' signal where significant increase in combined age is observed. There was broad agreement in estimates of the age contribution of the new material to the main channel sediment flux across METx temperatures, calculated at ~ 90-100 ka. It was interpreted that agreement between signals indicates the new material was bleached sufficiently to reset each of these signals prior to its storage. Although the precise location of the source of this material remains an open question, it was considered that areas surrounding the Santa Clara River are highly urbanised and have been developed extensively over the past decade. Therefore, significant construction work may have produced the material that caused a significant increase in combined signals. Furthermore, the Santa Clara River is also located in a highly tectonically active region. Tectonic processes mean the river is supplied with very large volumes of sediment and could cause an influx of material of an age inconsistent with those of sediments that comprise the main channel flux.

Objective 4: Reconstruct transport histories using single grains to identify multiple pathways of transport within a single sample.

The burial-bleach model was adapted to reconstruct the histories of individual grains to estimate storage times and virtual velocities independently of the combined signals. The model used average bleaching and growth parameters from the sensitive grains of a given sample derived from direct measurements. This was demonstrated to be a successful approach based on the results of the bleach recovery experiment (Experiment 3.4.2). The model was fitted the observed ratios of MET-IRSL signals of individual grains to estimate average bleach and burial times for each grain since it was last saturated. For each sample, this resulted in the emergence of subpopulations of grains with shared bleaching and burial histories. It was possible to distinguish specific grains with equilibrium bleaching histories from those with non-equilibrium histories. This revealed multiple potential transport pathways for grains within one sample: one where grains enter the channel and are flushed through the system until they enter storage at some stage (equilibrium grains), and one where grains enter the channel and are subject to multiple cycles of bleaching and burial, causing the departure of their signal ratios from equilibrium (non-equilibrium grains). Modelling the histories of single grains produced a virtual velocity of 3.9 m yr^{-1} for the Allt Dubhaig, which is of the same order of magnitude as that of the combined signals. Application of the same model to the Solimões River produces a virtual velocity estimate of 61 m yr^{-1}, which also highly likely to be within the uncertainty estimates of the transport rate derived from combined MET-IRSL signals. This demonstrates the ability of single grains to independently contribute bleaching and storage histories to a transport rate that is coherent with the information provided by the combined signals, which has huge potential for determining localised variability of sediment transport rates and pathways.

References

Abia, A.L.K., Ubomba-Jaswa, E. and Momba, M.N.B., 2017. Riverbed sediments as reservoirs of multiple vibrio cholerae virulence-associated genes: a potential trigger for cholera outbreaks in developing countries. Journal of Environmental and Public Health, 2017

Aitken, M.J., 1985. Thermoluminescence dating: past progress and future trends. *Nuclear Tracks and Radiation Measurements (1982)*, *10*(1-2), pp.3-6.

Aitken, M.J. and Valladas, H., 1992. Luminescence dating relevant to human origins. *Philosophical Transactions of the Royal Society of London. Series B: Biological Sciences*, *337*(1280), pp.139-144.

Aitken, Martin Jim. (1998). Introduction to optical dating: the dating of Quaternary sediments by the use of photon-stimulated luminescence. Clarendon Press

Anderson, R. S., & Anderson, S. P. (2010). Geomorphology: The mechanics and chemistry of landscapes. Cambridge: Cambridge University Press.

Andrews, E.D., Antweiler, R.C., Neiman, P.J. and Ralph, F.M., 2004. Influence of ENSO on flood frequency along the California coast. *Journal of Climate*, *17*(2), pp.337-348.

Armitage, S.J. and King, G.E., 2013. Optically stimulated luminescence dating of hearths from the Fazzan Basin, Libya: a tool for determining the timing and pattern of Holocene occupation of the Sahara. *Quaternary Geochronology*, *15*, pp.88-97.

Ashworth, P.J., 1987. Bedload transport and channel change in gravel-bed rivers.

Auclair, M., Lamothe, M. and Huot, S., 2003. Measurement of anomalous fading for feldspar IRSL using SAR. *Radiation measurements*, *37*(4-5), pp.487-492.

Bateman, M.D., Swift, D.A., Piotrowski, J.A., Rhodes, E.J. and Damsgaard, A., 2018. Can glacial shearing of sediment reset the signal used for luminescence dating?. *Geomorphology*, *306*, pp.90-101.

Bateman, M.D., Kinnaird, T.C., Hill, J., Ashurst, R.A., Mohan, J., Bateman, R.B. and Robinson, R., 2021. Detailing the impact of the Storegga Tsunami at Montrose, Scotland. *Boreas*, *50*(4), pp.1059-1078.

Bailiff, I.K. and Barnett, S.M., 1994. Characteristics of infrared-stimulated luminescence from a feldspar at low temperatures. *Radiation Measurements*, *23*(2-3), pp.541-545.

Berger, G.W. (1990). Effectiveness of natural zeroing of the thermoluminescence in sediment. Journal of Geophysical Research, 95, 12,375-12,397

Berger, G.W. and Luternauer, J.J., 1987. Preliminary field work for thermoluminescence dating studies at the Fraser River delta, British Columbia. *Geological Survey of Canada Paper*, *87*, pp.901-904.

Bertassoli Jr, D.J., Sawakuchi, A.O., Sawakuchi, H.O., Pupim, F.N., Hartmann, G.A., McGlue, M.M., Chiessi, C.M., Zabel, M., Schefuß, E., Pereira, T.S. and Santos, R.A., 2017. The fate of carbon in sediments of the Xingu and Tapajós clearwater rivers, Eastern Amazon. *Frontiers in Marine Science*, *4*, p.44.

Bøtter-Jensen, L., Bulur, E., Duller, G.A.T. and Murray, A.S., 2000. Advances in luminescence instrument systems. *Radiation Measurements*, *32*(5-6), pp.523-528.

Brown, A.G., Rhodes, E.J., Davis, S., Zhang, Y., Pears, B., Whitehouse, N.J., Bradley, C., Bennett, J., Schwenninger, J.-L. Firth, A., Firth, E., Hughes, P., Walling, D., (2021) Late Quaternary evolution of a lowland anastomosing river system: Geological-topographic inheritance, non-uniformity and implications for biodiversity and management. Quat. Sci. Rev. 260, 106929, https://doi.org/10.1016/j.quascirev.2021.106929

Brown, N.D., Rhodes, E.J., (2017). Thermoluminescence measurements of trap depth in alkali feldspars extracted from bedrock samples. Radiation Measurements 96, 53-61, http://dx.doi.org/10.1016/ j.radmeas.2016.11.011

Brown, N.D., Rhodes, E.J., Harrison, T.M., 2017. Using thermoluminescence signals from K-feldspars for low-temperature thermochronology. Quaternary Geochronology 41, 31-41. https://doi.org/10.1016/j.quageo.2017.07.006

Brown, N.D., Rhodes, E.J., Antinao, J.L., McDonald, E.V. 2015 Single-grain post-IR IRSL signals of K-feldspars from alluvial fan deposits in Baja California Sur, Mexico. Quaternary International 362, 132-138, http://dx.doi.org/10.1016/j.quaint.2014.10.024

Brown, N. D. (2020). Which geomorphic processes can be informed by luminescence measurements? Geomorphology, 367, 107296. https://doi.org/10.1016/j.geomorph.2020.107296

Burbank, D. W., & Anderson, R. S. (2009). Tectonic geomorphology. Malden, MA: John Wiley & Sons

Buylaert, J.P., Murray, A.S., Thomsen, K.J. and Jain, M., 2009. Testing the potential of an elevated temperature IRSL signal from K-feldspar. *Radiation measurements*, *44*(5-6), pp.560-565.

Buylaert, J.P., Jain, M., Murray, A.S., Thomsen, K.J., Thiel, C. and Sohbati, R., 2012. A robust feldspar luminescence dating method for Middle and Late P leistocene sediments. *Boreas*, *41*(3), pp.435-451.

Chamberlain, E. L., & Reimann, T. (2021). A case against subtracting a laboratory residual dose for feldspar singlegrain luminescence dating, Ancient TL, Vol. 39, No. S, 2021 – Special Issue - LED2021 Abstracts.

Colarossi, D., Duller, G.A.T., Roberts, H.M., Tooth, S. and Lyons, R., 2015. Comparison of paired quartz OSL and feldspar post-IR IRSL dose distributions in poorly bleached fluvial sediments from South Africa. *Quaternary Geochronology*, *30*, pp.233-238.

Colarossi, D., Duller, G.A. and Roberts, H.M., 2018. Exploring the behaviour of luminescence signals from feldspars: implications for the single aliquot regenerative dose protocol. *Radiation Measurements*, *109*, pp.35-44.

Craig, D.L., Fallowfield, H.J. and Cromar, N.J., 2004. Use of microcosms to determine persistence of Escherichia coli in recreational coastal water and sediment and validation with in situ measurements. *Journal of Applied Microbiology*, *96*(5), pp.922-930.

Daniels, J.T., 2016. *Mineralogic controls on the infrared stimulated luminescence of feldspars: An exploratory study of the effects of Al, Si order and composition on the behavior of a modified post-IR IRSL signal*. University of California, Los Angeles.

Davies, C.M., Long, J.A., Donald, M. and Ashbolt, N.J., 1995. Survival of fecal microorganisms in marine and freshwater sediments. *Applied and Environmental Microbiology*, *61*(5), pp.1888-1896.

Dosseto, A., Bourdon, B., Gaillardet, J., Allègre, C.J. and Filizola, N., 2006. Time scale and conditions of weathering under tropical climate: Study of the Amazon basin with U-series. *Geochimica et Cosmochimica Acta*, *70*(1), pp.71-89.

Dosseto, A., Bourdon, B. and Turner, S.P., 2008. Uranium-series isotopes in river materials: Insights into the timescales of erosion and sediment transport. *Earth and Planetary Science Letters*, *265*(1-2), pp.1-17.

Downs, P.W., Dusterhoff, S.R. and Sears, W.A., 2013. Reach-scale channel sensitivity to multiple human activities and natural events: Lower Santa Clara River, California, USA. *Geomorphology*, *189*, pp.121-134.

Duller, G.A.T., 1995. Luminescence dating using single aliquots: methods and applications. *Radiation Measurements*, *24*(3), pp.217-226.

Duller, G.A., 2008. Luminescence Dating: guidelines on using luminescence dating in archaeology.

Duller, G.A.T., 2015. The Analyst software package for luminescence data: overview and recent improvements. *Ancient TL*, *33*(1), pp.35-42.

Duller, G.A.T. and Bøtter-Jensen, L., 1993. Luminescence from potassium feldspars stimulated by infrared and green light. *Radiation Protection Dosimetry*, *47*(1-4), pp.683-688.

Fu, X. and Li, S.H., 2013. A modified multi-elevated-temperature post-IR IRSL protocol for dating Holocene sediments using K-feldspar. *Quaternary Geochronology*, *17*, pp.44-54.

Ferguson, R. and Ashworth, P., 1991. Slope-induced changes in channel character along a gravel-bed stream: the Allt Dubhaig, Scotland. *Earth surface processes and landforms*, *16*(1), pp.65-82.

Ferguson, R.I., Cudden, J.R., Hoey, T.B. and Rice, S.P., 2006. River system discontinuities due to lateral inputs: generic styles and controls. *Earth Surface Processes and Landforms: The Journal of the British Geomorphological Research Group*, *31*(9), pp.1149-1166.

Ferguson, R., Hoey, T., Wathen, S. and Werritty, A., 1996. Field evidence for rapid downstream fining of river gravels through selective transport. *Geology*, *24*(2), pp.179-182.

Ferguson, R.I. and Wathen, S.J., 1998. Tracer-pebble movement along a concave river profile: Virtual velocity in relation to grain size and shear stress. *Water Resources Research*, *34*(8), pp.2031-2038.

Ferguson, R.I., Bloomer, D.J., Hoey, T.B. and Werritty, A., 2002. Mobility of river tracer pebbles over different timescales. *Water Resources Research*, *38*(5), pp.3-1.

Fu, X., Li, B. & Li, S., 2012. Testing a multi-step post-IR IRSL dating method using polymineral fine grains from Chinese loess. Quaternary Geochronology 10, 8-15.

Furch, K. (1984). “Water chemistry of the Amazon basin: the distribution of chemical elements among freshwaters,” in The Amazon: Limnology and Landscape Ecology of a Mighty Tropical River and its Basin, ed. H. Sioli (Berlin: Springer), 167–199. doi: 10.1007/978-94-009-6542-3_6

Hilton, R.G. and West, A.J., 2020. Mountains, erosion and the carbon cycle. *Nature Reviews Earth & Environment*, *1*(6), pp.284-299.

Hodge, R.A., Hoey, T.B. and Sklar, L.S., 2011. Bed load transport in bedrock rivers: The role of sediment cover in grain entrainment, translation, and deposition. *Journal of Geophysical Research: Earth Surface*, *116*(F4).

Hoey, T.B. and Ferguson, R., 1994. Numerical simulation of downstream fining by selective transport in gravel bed rivers: Model development and illustration. *Water resources research*, *30*(7), pp.2251-2260.

Gardade, L. and Khandeparker, L., 2017. Spatio-temporal variations in pathogenic bacteria in the surface sediments of the Zuari estuary, Goa, India. *Current Science*, pp.1729-1738.

Gemmell, A.M.D., (1985). Zeroing of the TL signal of sediment undergoing fluvial transportation: a laboratory experiment. Nuclear Tracks and Radiation Measurements 10, 695-702.

Gemmell, A.M.D., (1999). IRSL from fine-grained glacifluvial sediment. Quaternary Geochronology, 18, 207–215.

Godfrey-Smith, D.I., Huntley, D.J. and Chen, W.H., 1988. Optical dating studies of quartz and feldspar sediment extracts. *Quaternary Science Reviews*, *7*(3-4), pp.373-380.

Gray, H.J., Tucker, G.E., Mahan, S.A., McGuire, C. and Rhodes, E.J., 2017. On extracting sediment transport information from measurements of luminescence in river sediment. *Journal of Geophysical Research: Earth Surface*, *122*(3), pp.654-677.

Gray, Harrison J., Gregory E. Tucker, and Shannon A. Mahan. "Application of a luminescence-based sediment transport model." *Geophysical Research Letters* 45, no. 12 (2018): 6071-6080.

Gray, H.J., Jain, M., Sawakuchi, A.O., Mahan, S.A. and Tucker, G.E., 2019. Luminescence as a sediment tracer and provenance tool. *Reviews of Geophysics*, *57*(3), pp.987-1017.

Guyez, A., Bonnet, S., Reimann, T., Carretier, S., Norton, K. and Wallinga, J., 2023, May. Feldspar luminescence signal of modern fluvial sediments as a proxy for erosion rates?. In *EGU General Assembly Conference Abstracts* (pp. EGU-3135).

Guzmán, G., Quinton, J.N., Nearing, M.A., Mabit, L. and Gómez, J.A., 2013. Sediment tracers in water erosion studies: current approaches and challenges. *Journal of Soils and Sediments*, *13*, pp.816-833.

Hassan, M.A. and Ergenzinger, P., 2003. Use of tracers in fluvial geomorphology. *Tools in fluvial geomorphology*, pp.397-423.

Hodge, R.A., Hoey, T.B. and Sklar, L.S., 2011. Bed load transport in bedrock rivers: The role of sediment cover in grain entrainment, translation, and deposition. *Journal of Geophysical Research: Earth Surface*, *116*(F4).

Huntley, D.J., 2006. An explanation of the power-law decay of luminescence. *Journal of Physics: Condensed Matter*, *18*(4), p.1359.

Huntley, D.J., Godfrey-Smith, D.I. and Thewalt, M.L., 1985. Optical dating of sediments. *Nature*, *313*(5998), pp.105-107.

Huntley, D.J. and Lamothe, M., 2001. Ubiquity of anomalous fading in K-feldspars and the measurement and correction for it in optical dating. *Canadian Journal of Earth Sciences*, *38*(7), pp.1093-1106.

Hütt, G., Jaek, I., & Tchonka, J. (1988). Optical dating: K-feldspars optical response stimulation spectra. Quaternary Science Reviews, 7(3–4), 381–385.

Ivester, A.H., Rhodes, E.J., Dolan, J.F., Van Dissen, R.J., Gauriau, J., Little, T., and McGill, S.F., 2022. A method to evaluate the degree of bleaching of IRSL signals in feldspar: The 3ET method. *Quaternary Geochronology*, *72*, p.101346.

Jain, M., Murray, A. S. & Bøtter-Jensen, L. (2004). Optically stimulated luminescence dating: how significant is incomplete light exposure in fluvial environments? Quaternaire 15, 143–157.

Jain, M., Murray, A.S., Bøtter-Jensen, L. and Wintle, A.G., 2005. A single-aliquot regenerative-dose method based on IR (1.49 eV) bleaching of the fast OSL component in quartz. *Radiation Measurements*, *39*(3), pp.309-318.

Jain, M., Sohbati, R., Guralnik, B., Murray, A.S., Kook, M., Lapp, T., Prasad, A.K., Thomsen, K.J. and Buylaert, J.P., 2015. Kinetics of infrared stimulated luminescence from feldspars. *Radiation Measurements*, *81*, pp.242-250.

Jain, M. and Ankjærgaard, C., 2011. Towards a non-fading signal in feldspar: insight into charge transport and tunnelling from time-resolved optically stimulated luminescence. *Radiation Measurements*, *46*(3), pp.292-309.

Keller, E.A., Johnson, D.L., Clark, M.N. and Rockwell, T.K., 1982. *Tectonic geomorphology and earthquake hazard, north flank, central Ventura Basin, California* (No. 81-376). US Geological Survey.

Kars, R.H., Reimann, T., Ankjærgaard, C. and Wallinga, J., 2014. Bleaching of the post-IR IRSL signal: new insights for feldspar luminescence dating. *Boreas*, *43*(4), pp.780-791.

Lawson, M.J., Daniels, J.T. and Rhodes, E.J., 2015. Assessing Optically Stimulated Luminescence (OSL) signal contamination within small aliquots and single grain measurements utilizing the composition test. *Quaternary International*, *362*, pp.34-41.

Li, B. and Li, S.H., 2011. Luminescence dating of K-feldspar from sediments: a protocol without anomalous fading correction. *Quaternary Geochronology*, *6*(5), pp.468-479.

Lowick, S.E., Buechi, M.W., Gaar, D., Graf, H.R. and Preusser, F., 2015. Luminescence dating of M iddle P leistocene proglacial deposits from northern S witzerland: methodological aspects and stratigraphical conclusions. *Boreas*, *44*(3), pp.459-482.

McGuire, C. and Rhodes, E.J., 2015a. Downstream MET-IRSL single-grain distributions in the Mojave River, southern California: Testing assumptions of a virtual velocity model. *Quaternary Geochronology*, *30*, pp.239-244.

McGuire, C. and Rhodes, E.J., 2015b. Downstream MET-IRSL single-grain distributions in the Mojave River, southern California: Testing assumptions of a virtual velocity model. *Quaternary Geochronology*, *30*, pp.239-244.

Meade, R.H., 1994. Suspended sediments of the modern Amazon and Orinoco rivers. □ˏˏ Quaternary International 21, 29-39.

Milan, D.J. and Large, A.R., 2014. Magnetic tracing of fine-sediment over pool-riffle morphology. *Catena*, *115*, pp.134-149.

Murray, A.S. and Roberts, R.G., 1997. Determining the burial time of single grains of quartz using optically stimulated luminescence. *Earth and Planetary Science Letters*, *152*(1-4), pp.163-180.

Murray, A.S. and Wintle, A.G., 2003. The single aliquot regenerative dose protocol: potential for improvements in reliability. *Radiation measurements*, *37*(4-5), pp.377-381.

Murray, A.S., Thomsen, K.J., Masuda, N., Buylaert, J.P. and Jain, M., 2012. Identifying well-bleached quartz using the different bleaching rates of quartz and feldspar luminescence signals. *Radiation measurements*, *47*(9), pp.688-695.

Nathan, R.P., Thomas, P.J., Jain, M., Murray, A.S. and Rhodes, E.J., 2003. Environmental dose rate heterogeneity of beta radiation and its implications for luminescence dating: Monte Carlo modelling and experimental validation. *Radiation Measurements*, *37*(4-5), pp.305-313.

Nottebaum, V., Stauch, G., Kai, H., Zhang, J. R., and Lehmkuhl, F. (2015). Unmixed loess grain size populations along the northern Qilian Shan (China): Relationships between geomorphologic, sedimentologic and climatic controls. Quat. Int. 372, 151–166. doi:10.1016/j.quaint.2014.12.071

Ollerhead, J., and Huntley, D. J. (2011). Optical dating of young feldspars: The zeroing questions. Anc. TL 29, 59–63

Pagonis, V., Ankjærgaard, C., Jain, M. and Chithambo, M.L., 2016. Quantitative analysis of time-resolved infrared stimulated luminescence in feldspars. *Physica B: Condensed Matter*, *497*, pp.78-85.

Perkins, T.L., Clements, K., Baas, J.H., Jago, C.F., Jones, D.L., Malham, S.K. and McDonald, J.E., 2014. Sediment composition influences spatial variation in the abundance of human pathogen indicator bacteria within an estuarine environment. *PloS one*, *9*(11), p.e112951.

Pizzuto, J., Schenk, E.R., Hupp, C.R., Gellis, A., Noe, G., Williamson, E., Karwan, D.L., O'Neal, M., Marquard, J., Aalto, R. and Newbold, D., 2014. Characteristic length scales and time-averaged transport velocities of suspended sediment in the mid-Atlantic Region, USA. *Water Resources Research*, *50*(2), pp.790-805.

Poolton, N.R.J., Kars, R.H., Wallinga, J. and Bos, A.J.J., 2009. Direct evidence for the participation of band-tails and excited-state tunnelling in theluminescence of irradiated feldspars. *Journal of Physics: Condensed Matter*, *21*(48), p.485505.

Poolton, N.R.J., Wallinga, J., Murray, A.S., Bulur, E.N.V.E.R. and Bøtter-Jensen, L., 2002a. Electrons in feldspar I: on the wavefunction of electrons trapped at simple lattice defects. *Physics and Chemistry of Minerals*, *29*, pp.210-216.

Poolton, N.R.J., Ozanyan, K.B., Wallinga, J., Murray, A.S. and Bøtter-Jensen, L., 2002b. Electrons in feldspar II: a consideration of the influence of conduction band-tail states on luminescence processes. *Physics and Chemistry of Minerals*, *29*, pp.217-225.

Preusser, F., Degering, D., Fuchs, M., Hilgers, A., Kadereit, A., Klasen, N., Krbetschek, M., Richter, D. and Spencer, J.Q., 2008. Luminescence dating: basics, methods and applications. *E&G Quaternary Science Journal*, *57*(1/2), pp.95-149.

Rendell, H.M., Webster, S.E. and Sheffer, N.L., 1994. Underwater bleaching of signals from sediment grains: new experimental data. *Quaternary Science Reviews*, *13*(5-7), pp.433-435.

Repasch, M., Scheingross, J. S., Hovius, N., Lupker, M., Wittmann, H., et al., (2021). Fluvial organic carbon cycling regulated by sediment transit time and mineral protection. Nature Geoscience 14, 842–848, https://doi.org/10.1038/s41561-021-00845-7.

Reimann, T., Notenboom, P. D., De Schipper, M. A., and Wallinga, J. (2015). Testing for sufficient signal resetting during sediment transport using a polymineral multiple-signal luminescence approach. Quat. Geochronol. 25, 26–36. doi:10.1016/j. quageo.2014.09.002

Rhodes, E.J., 2000. Observations of thermal transfer OSL signals in glacigenic quartz. *Radiation Measurements*, *32*(5-6), pp.595-602.

Rhodes, E.J., 2015. Dating sediments using potassium feldspar single-grain IRSL: initial methodological considerations. *Quaternary International*, *362*, pp.14-22.

Rhodes, E.J., Ramsey, C.B., Outram, Z., Batt, C., Willis, L., Dockrill, S. and Bond, J., 2003. Bayesian methods applied to the interpretation of multiple OSL dates: high precision sediment ages from Old Scatness Broch excavations, Shetland Isles. *Quaternary Science Reviews*, *22*(10-13), pp.1231-1244.

Rhodes, E.J., Singarayer, J.S., Raynal, J.-P., Westaway, K.E., Sbihi-Alaoui, F.Z. (2006). New age estimates for the Palaeolithic assemblages and Pleistocene succession of Casablanca, Morocco. Quaternary Science Reviews 25, 2569-2585.

Rhodes, E., 2007. Quartz single grain OSL sensitivity distributions: implications for multiple grain single aliquot dating. *Geochronometria*, *26*(1), pp.19-29.

Rhodes, E.J., 2011. Optically stimulated luminescence dating of sediments over the past 200,000 years. *Annual Review of Earth and Planetary Sciences*, *39*(1), pp.461-488.

Rhodes, E.J. and Bailey, R.M., 1997. The effect of thermal transfer on the zeroing of the luminescence of quartz from recent glaciofluvial sediments. *Quaternary Science Reviews*, *16*(3-5), pp.291-298.

Rhodes, E.J. and Leathard, J.A., 2022. MET-IRSL used to track pre-depositional sediment transport history. *Quaternary Geochronology*, *70*, p.101294.

Rhodes, E.J., Spano, T.M., Hodge, R.A., Sawakuchi, A.O. and Bertassoli Jr, D.J., 2024. Single grain K-feldspar MET-IRSL sediment transport determination: bleaching patterns and rates. *Quaternary Geochronology*, *85*, p.101626.

Sanderson, D.C.W., 1988. Fading of thermoluminescence in feldspars: characteristics and corrections. *International Journal of Radiation Applications and Instrumentation. Part D. Nuclear Tracks and Radiation Measurements*, *14*(1-2), pp.155-161.

Sanderson, D.C., Bishop, P., Stark, M., Alexander, S. and Penny, D., 2007. Luminescence dating of canal sediments from Angkor Borei, Mekong Delta, southern Cambodia. *Quaternary Geochronology*, *2*(1-4), pp.322-329.

Sawakuchi, H.O., Neu, V., Ward, N.D., Barros, M.D.L.C., Valerio, A.M., Gagne-Maynard, W., Cunha, A.C., Less, D.F., Diniz, J.E., Brito, D.C. and Krusche, A.V., 2017. Carbon dioxide emissions along the lower Amazon River. *Frontiers in Marine Science*, *4*, p.76.

Sawakuchi, A.O., Jain, M., Mineli, T.D., Nogueira, L., Bertassoli Jr, D.J., Häggi, C., Sawakuchi, H.O., Pupim, F.D.N., Grohmann, C.H., Chiessi, C.M. and Zabel, M., 2018. Luminescence of quartz and feldspar fingerprints provenance and correlates with the source area denudation in the Amazon River basin. *Earth and Planetary Science Letters*, *492*, pp.152-162.

Schroder, D.K., 1998. New life in detecting defects. *IEEE circuits and devices magazine*, *14*(6), pp.14-20.

Sioli H., 1984. The Amazon and its main affluents: Hydrography, morphology of the river, courses, and river types. In: Sioli H. (eds). The Amazon. Monographiae Biologicae vol 56, Springer, Dordrecht.

Siqueira-Souza, F.K., Hurd, L.E., Yamamoto, K.C., Soares, M.G.M., Cooper, G.J., Kahn, J.R. and Freitas, C.E., 2021. Patterns of pelagic fish diversity in floodplain lakes of whitewater and blackwater

Sissons, J.B., 1974. A Late-glacial ice cap in the central Grampians, Scotland. *Transactions of the Institute of British Geographers*, pp.95-114.

Smedley, R.K., Duller, G.A., Pearce, N.J.G. and Roberts, H.M., 2012. Determining the K-content of single-grains of feldspar for luminescence dating. *Radiation Measurements*, *47*(9), pp.790-796. drainage systems within the central Amazon River basin of Brazil. *Frontiers in Ecology and Evolution*, *9*, p.602895.

Smedley, R.K., Duller, G.A.T. and Roberts, H.M., 2015. Bleaching of the post-IR IRSL signal from individual grains of K-feldspar: Implications for single-grain dating. *Radiation Measurements*, *79*, pp.33-42.

Smedley, Rachel K., & Skirrow, G. K. (2020). Luminescence dating in fluvial settings: overcoming the challenge of partial bleaching. In Palaeohydrology (pp. 155–168). Springer.

Sohbati, R. (2013). “Luminescence, rock surfaces,” in Encyclopedia of scientific dating methods. Editors W. J. Rink and J. Thompson (Berlin, Germany: Springer), 7.

Sohbati, R., Murray, A.S., Chapot, M.S., Jain, M., Pederson, J., 2012. Optically stimulated luminescence (OSL) as a chronometer for surface exposure dating. J. Geophys. Res.117, B09202. https://doi .org /10 .1029 /2012JB009383.

Spooner, N. A. (1992). Optical dating: Preliminary results on the anomalous fading of luminescence from feldspars. Quaternary Science Reviews, 11(1), 139–145. https://doi.org/10.1016/0277-3791(92)90055-D

Spooner, N. A. (1994). The anomalous fading of infrared-stimulated luminescence from feldspars. Radiation Measurements, 23(2), 625–632. https://doi.org/10.1016/1350-4487(94)90111-2

Stokes, S., Bray, H. E., & Blum, M. D. (2001). Optical resetting in large drainage basins: Tests of zeroing assumptions using single-aliquot procedures. Quaternary Science Reviews, 20(5), 879–885.

Stone, A.E., Bateman, M.D. and Thomas, D.S., 2015. Rapid age assessment in the Namib Sand Sea using a portable luminescence reader. *Quaternary geochronology*, *30*, pp.134-140.

Sun, D., Bloemendal, J., Rea, D.K., Vandenberghe, J., Jiang, F., An, Z., Su, R., (2002). Grain-size distribution function of polymodal sediments in hydraulic and aeolian environments, and numerical partitioning of the sedimentary components. Sedimentary geology, 152(3-4), pp.263-277.

Thomsen, K.J., Murray, A. S., & Bøtter-Jensen, L. (2005). Sources of variability in OSL dose measurements using single grains of quartz. Radiation Measurements, 39(1), 47–61. https://doi.org/10.1016/j.radmeas.2004.01.039 Thomsen, Kristina Jørkov, Murray, A. S., Jain, M., & Bøtter-Jensen, L. (2008). Laboratory fading rates of various luminescence signals from feldspar-rich sediment extracts. Radiation Measurements, 43(9–10), 1474– 1486.

Thomsen, K.J., Murray, A.S. and Jain, M., 2011. Stability of IRSL signals from sedimentary K-feldspar samples. *Geochronometria*, *38*, pp.1-13.

Torres, M. A., Limaye, A. B., Ganti, V., Lamb, M. P., West, A. J., Fischer, W. W. (2017). Model predictions of long-lived storage of organic carbon in river deposits. Earth Surface Dynamics, 5(4), 711–730. https://doi.org/10.5194/esurf-5-711-2017.

Walling, D.E., 2013. Beryllium-7: The Cinderella of fallout radionuclide sediment tracers?. *Hydrological Processes*, *27*(6), pp.830-844.

Warrick, J.A. and Mertes, L.A., 2009. Sediment yield from the tectonically active semiarid Western Transverse Ranges of California. *Geological Society of America Bulletin*, *121*(7-8), pp.1054-1070.

Wintle, A. G. (1973). Anomalous Fading of Thermo-luminescence in Mineral Samples. Nature, 245(5421), 143– 144. https://doi.org/10.1038/245143a0 Wintle, Ann G. (1997). Luminescence dating: laboratory procedures and protocols. Radiation Measurements, 27(5–6), 769–817.

Wintle, A.G., 1973. Anomalous fading of thermo-luminescence in mineral samples. *Nature*, *245*(5421), pp.143-144.

Wintle, A.G. and Murray, A.S., 2006. A review of quartz optically stimulated luminescence characteristics and their relevance in single-aliquot regeneration dating protocols. *Radiation measurements*, *41*(4), pp.369-391.

Wittmann, H., von Blanckenburg, F., Dannhaus, N., Bouchez, J., Gaillardet, J.,Guyot, J.L., Maurice, L., Roig, H., Filizola, N., Christl, M., (2015). A test of thecosmogenic10Be(meteoric)/9Be proxy for simultaneously determining basin-wide erosion rates, denudation rates, and the degree of weathering in the Amazon basin. J. Geophys. Res. Earth Surf.,120, 2498–2528, doi:10.1002/2015JF003581.

Wynants, M., Munishi, L., Mtei, K., Bodé, S., Patrick, A., Taylor, A., Gilvear, D., Ndakidemi, P., Blake, W.H. and Boeckx, P., 2021. Soil erosion and sediment transport in Tanzania: Part I–sediment source tracing in three neighbouring river catchments. *Earth Surface Processes and Landforms*, *46*(15), pp.3096-3111.

Yi, S., Buylaert, J.P., Murray, A.S., Lu, H., Thiel, C. and Zeng, L., 2016. A detailed post-IR IRSL dating study of the Niuyangzigou loess site in northeastern China. *Boreas*, *45*(4), pp.644-657.

Yi, S., Li, X., Han, Z., Lu, H., Liu, J. and Wu, J., 2018. High resolution luminescence chronology for Xiashu Loess deposits of Southeastern China. *Journal of Asian Earth Sciences*, *155*, pp.188-197.

Zhang, J., Tsukamoto, S., Nottebaum, V., Lehmkuhl, F. and Frechen, M., 2015a. De plateau and its implications for post-IR IRSL dating of polymineral fine grains. *Quaternary Geochronology*, *30*, pp.147-153

Zhang, J., Nottebaum, V., Tsukamoto, S., Lehmkuhl, F. and Frechen, M., 2015b. Late Pleistocene and Holocene loess sedimentation in central and western Qilian Shan (China) revealed by OSL dating. *Quaternary International*, *372*, pp.120-129.

Zhang, J., Guralnik, B., Tsukamoto, S., Ankjærgaard, C. and Reimann, T., 2023. The bleaching limits of IRSL signals at various stimulation temperatures and their potential inference of the pre-burial light exposure duration. *Frontiers in Earth Science*, *10*, p.933131.

Zhang, J., Tsukamoto, S. and Long, H., 2023. Testing the potential of pulsed post-IR IRSL dating on Chinese loess deposits. *Quaternary Geochronology*, *78*, p.101469.